

*Acyl pyrazolones & their structural analogues:
Synthesis, characterization, crystal structure and studies
on their bio-active metal complexes*

Thesis submitted to

The Maharaja Sayajirao University of Baroda

For the degree of

DOCTOR OF PHILOSOPHY

In

CHEMISTRY

Submitted by

Ms. Komal M. Vyas



**Department of Chemistry
Faculty of Science
The Maharaja Sayajirao University of Baroda
Vadodara- 390 002
Gujarat (INDIA)**

September-2012

*Acyl pyrazolones & their structural analogues:
Synthesis, characterization, crystal structure and studies
on their bio-active metal complexes*

Thesis submitted to

The Maharaja Sayajirao University of Baroda

For the degree of

DOCTOR OF PHILOSOPHY

In

CHEMISTRY

Submitted by

Ms. Komal M. Vyas



**Department of Chemistry
Faculty of Science
The Maharaja Sayajirao University of Baroda
Vadodara- 390 002
Gujarat (INDIA)**

September-2012

*In the name of lord
“Ganesha”.....*



*Dedicated to my parents
and grand parents*

Dr. R. N. Jadeja
Assistant Professor
Department of Chemistry
Faculty of Science
The M. S. University of Baroda
Vadodara-390 002



Department of Chemistry
Centre of Advanced Studies in Chemistry
& DST-FIST sponsored Department
Faculty of Science, Vadodara 390 002
India
Tel: +91-265-2795552

The Maharaja Sayajirao University of Baroda

CERTIFICATE

This is to certify that the work presented in the thesis entitled “Acyl pyrazolones & their structural analogues: Synthesis, characterization, crystal structure and studies on their bio-active metal complexes” submitted by Ms. Komal M. Vyas for the award of the degree of **Doctor of Philosophy in Chemistry** is the authentic and original research work carried out by her under my guidance and supervision in the Department of Chemistry, Faculty of Science, The Maharaja Sayajirao University of Baroda, Vadodara - 390002 India.

Dr. R. N. Jadeja
(Research Supervisor)
Department of Chemistry

Prof. B. V. Kamath
(Head)
Department of Chemistry
HEAD,
CHEMISTRY DEPARTMENT
FACULTY OF SCIENCE
M. S. UNIVERSITY OF BARODA
VADODARA - 390 002.

Prof. Nikhil Desai
(Dean)
Faculty of Science
DEAN,
FACULTY OF SCIENCE
M. S. UNIVERSITY OF BARODA
VADODARA - 390 002.

Declaration

I hereby declare that this thesis entitled “Acyl pyrazolones & their structural analogues: Synthesis, characterization, crystal structure and studies on their bio-active metal complexes” is my own work conducted under the supervision of Dr. R. N. Jadeja, in Department of Chemistry, The Maharaja Sayajirao University of Baroda, Vadodara (Gujarat)-390002 India and to the best of my knowledge it contains no material previously published by another person, nor material which to a substantial extent has been accepted for the award of any degree or diploma at any other educational institution, except where due acknowledgement is made in the thesis. Any contribution made to the research by anyone, with whom I have worked, during my candidature, is fully acknowledged.

I also declare that the intellectual content of this thesis is the product of my own work, except to the extent that assistance from others in the project's design and conception or in style, presentation and linguistic expression is acknowledged.

Date: 25/09/2012

Place: Vadodara


(Komal M. Vyas)

ACKNOWLEDGEMENTS

"Oum Shree Ganeshay Namah"

Before presenting this thesis, I remember with great gratitude, the people who were to me a constant source of encouragement and help throughout my work.

I am very much grateful to the universal and invincible God, the King of kings and the Lord of lords, the glorious fountain and continuous source of inspirations! I offer salutations to him and my head bows with dedication from within my heart, to the Lord "Ganesh" for enabling me to complete this work.

*It is my privilege to express my sincere thanks to my co-traveller, my research supervisor, **Dr. R. N. Jadeja**, Assistant Professor, Department of Chemistry, Faculty of Science, The Maharaja Sayajirao University of Baroda, Vadodara, for offering me such an exciting field of research. I express my deep gratitude to him, who has enlightened my ideas and who have been highly concerned about the progress of my work and without whom this work could not have reached to the present stage. I am thankful to him for his invaluable help, thought-provoking guidance, encouraging attitude and pleasant behaviour throughout this study, which always inspired me in heading rapidly towards my goal and helped me achieving the aim of my present task very speedily. The confidence and courage I obtained from him promote me to pursue more goals and dreams that are laid ahead in my life.*

I am also grateful to Prof. B. V. Kamath, Head, Department of Chemistry, Faculty of Science, The Maharaja Sayajirao University of Baroda, Vadodara, for providing me with necessary facilities and constant support whenever needed throughout my research work. My sincere thanks are also due to Prof. N. D. Desai, Dean, Faculty of Science, The Maharaja Sayajirao University of Baroda, Vadodara, for the immense help I received from him.

I am also grateful to Prof. V. K. Gupta, Post-Graduate Department of Physics & Electronics, University of Jammu, Jammu Tawi, India, for his constant help for X-ray crystallography. I am very much thankful to him for his immediate help and co-operation I received from him. I am also thankful to the other members of his group.

I wish to express my sincere thanks to Dr. R. V. Devkar, Division of Phytotherapeutics and Metabolic Endocrinology, Faculty of Science, The M. S.

University of Baroda, Vadodara, for giving me the opportunity to work on Anti-cancer studies. I am thankful to Mr. Dipak Patel for doing all the Anti-cancer studies.

I also offer my sincere thanks to Dr. C. Ratna Prabha and Mr. Rushikesh Joshi, Department of Biochemistry, Faculty of Science, The M. S. University of Baroda, Vadodara, for their help in starting the other biological studies. I am also thankful to the other members of this group for their help.

My sincere thanks to Dr. K. R. Surti, Department of Chemistry, Sardar Patel University, Vallabhvidyanagar, for helping me in the interpretation of Thermal studies. I would like to thank Dr. Ganpati, The M. S. University of Baroda, Vadodara, for helping me in the TGA measurements.

I am thankful to the University Grant Commissions, Alembic Research Fellowship and University Research Fellowship for financial support.

I am very much thankful to Nutan Dye Chem., Sachin, Surat, for providing me the starting materials (pyrazolones) as free gift samples for my research work. I am also thankful to Shiva Pharmachem. Ltd., Baroda and S. D. Fine Chemicals, Mumbai, for providing the acyl chlorides as free gift samples for carrying out my research.

I express my sincere thanks to my Ph. D. Coursework Co-ordinators, Prof. R. G. Kothari, Prof. N. D. Kulkarni, Dr. D. Chakraborty, Dr. P. Sudhakar, Dr. V. K. Singh and Dr. Sujit Kumar for their help in completing my course work for the degree.

I would like to thank all the incharge teachers of the different instruments for their constant help. I am also thankful to all the instrument operators mainly Harishbhai, Harnish Soni, Nilesh Jain, Hemant Mande, Akeelbhai, Dimple Shah, Rahul Kadu, Sanjay Verma and all other members.

I gratefully acknowledge the most willing help and co-operation shown by SPARK-Baroda and Alembic-Baroda for providing facilities for NMR and C, H, N studies. I am thankful to CDRI Lucknow, SAIF-Chandigarh and SAIF-IIT-Bombay for spectral studies.

I feel lucky and very proud to have intimate friends like Harnish, Puran, Sanjay (my colleague), Nishant, Rama and Kushan, who have been always participating with my problems and disappointments and rebuilt my confidence at appropriate stages and also were ready to help me throughout the study. Thanks to Kushan for giving me the Camera for the photography.

I am thankful to all teaching staff of the department. I am thankful to all non-teaching staff of my department mainly Ms. Revathi Ganesh, Mr. Rawal, Mr. Bhrambhatt, Mr. D. R. Bhavsar, Mr. Kalpesh Bhavsar and Mr. Rane. I am thankful to Mr. Yogesh (Aum Copy Point) for printing my thesis.

I would like to thank my other seniors and friends and colleagues, Mayur, Shardul, Zala, Jigar, Ketan, Shilpi, Umesh, Priyanka, Namrata, Harsha, Varsha, Soyeb, Krupa, Arti, Rinky, Vishwanath, Ageethadidi, Ashokbhai, Mitesh, Rahul, Ronak, Mr. Joseph, Dr. Jignesh and Sadhu. I would also like to thank our dissertation students Vrunda, Ravindra, Naresh, Maitry and Deepika.

*Who in this world can entirely and adequately thank the parents who have given us everything that we possess in this life? The life itself is their gift to us, so I am at loss of words in which to own my most esteemed father (my friend) **Shri Maheshbhai Vyas** and My loving mother **Smt. Yoginaben** and most venerated late grand fathers **Shri Arvindlal and Shri Nathalal**, late grandmother **Padmaben** and also to my grandmother **Ramilaben**. I would like to acknowledge my beloved brother **Jaimin**, who has also helped me whenever I needed. I also like to remember here, my doggi, **Rani**, who is also a part of my family. I have no words to acknowledge the sacrifices efforts, lot of prayers, support, encouragement and firm dedication and devotion of my parents. Their endless prayers contributed a lot towards successful completion of this research project. Words become meaningless when I look at them as icons of strength for being what I am today. Had my father not been there as pillar of strength, this building of my achievement would never have stood. I just dedicated this thesis to them.*

The constraint of time and space will only permit me to show appreciation to a handful of people and organizations: my school teachers, my graduate and post-graduate teachers for their contribution to my life and career. A long list of friends, colleagues, mentors, benefactors and formators which cannot be contained in this I say a big thank you.

Throughout the course of my Ph.D. I have had help from numerous people. I have tried to thank everybody but if I've missed someone I'm sorry and it's just down to my forgetfulness.

Komal M. Vyas

Content

Chapter-1. Synthesis, characterization and crystal structures of 4-acyl pyrazolones based metal complexes

1.1. Introduction	(1-16)
1.1.1. 4-acyl pyrazolones as ligands	3
1.1.2. Metal complexes of 4-acyl pyrazolones	7
1.1.2.1. Transition metal complexes of 4-acyl pyrazolones	7
1.2. Experimental	(17-18)
1.2.1. Materials	17
1.2.2. Single crystal X-ray structure determination	17
1.3. Syntheses of ligands	(18-23)
1.3.1. Syntheses of 4-toluoyl pyrazolones	(18-21)
1.3.1.1. 3-methyl-4-(4-methylbenzoyl)-1-phenyl-1H-pyrazol-5(4H)-one [TPMP]	18
1.3.1.2. 1-(3-chlorophenyl)-3-methyl-4-(4-methylbenzoyl)-1H-pyrazol-5(4H)-one [TMCPMP]	19
1.3.1.3. 3-methyl-4-(4-methylbenzoyl)-1- <i>p</i> -tolyl-1H-pyrazol-5(4H)-one [TPTMP]	20
1.3.2. Syntheses of 4-propionyl pyrazolones	(21-23)
1.3.2.1. 3-methyl-1-phenyl-4-propionyl-1H-pyrazol-5(4H)-one [PPMP]	21
1.3.2.2. 1-(3-chlorophenyl)-3-methyl-4-propionyl-1H-pyrazol-5(4H)-one [PMCPMP]	22
1.3.2.3. 3-methyl-4-propionyl-1- <i>p</i> -tolyl-1H-pyrazol-5(4H)-one [PPTMP]	23
1.4. Characterization of 4-acyl pyrazolone ligands	(23-33)
1.4.1. Physicochemical properties	23
1.4.2. IR spectral studies	24
1.4.3. NMR spectral studies	(24-30)
1.4.3.1. ¹ H NMR spectral studies	(24-27)
1.4.3.1.1. ¹ H NMR spectral studies of 4-propionyl pyrazolones	27
1.4.3.1.2. ¹ H NMR spectral studies of 4-toluoyl pyrazolones	27
1.4.3.2. ¹³ C NMR spectral studies	(27-30)
1.4.3.2.1. ¹³ C NMR spectral studies of 4-propionyl pyrazolones	27
1.4.3.2.2. ¹³ C NMR spectral studies of 4-toluoyl pyrazolones	29
1.4.4. Mass spectral studies	(30-33)

1.4.4.1. Mass spectral studies of 4-propionyl pyrazolone ligands	30
1.4.4.2. Mass spectral studies of 4-toluoyl pyrazolone ligands	31
1.5. Syntheses of Cu(II) complexes of 4-acyl pyrazolones	(33-41)
1.5.1. Syntheses of binary complexes of 4-acyl pyrazolones	(33-35)
1.5.1.1. Cu(TPMP) ₂ (1)	33
1.5.1.2. Cu(TMCPMP) ₂ (2)	34
1.5.1.3. Cu(TPTPMP) ₂ (3)	35
1.5.2. Syntheses of ternary complexes	(35-41)
1.5.2.1. Syntheses of ternary complexes of 4-propionyl pyrazolones	(35-38)
1.5.2.1.1. [Cu(PPMP)(Phen)NCS] (4)	35
1.5.2.1.2. [Cu(PPMP)(Bipy)NCS] (5)	36
1.5.2.1.3. [Cu(PMCPMP)(Phen)NCS] (6)	37
1.5.2.1.4. [Cu(PMCPMP)(Bipy)NCS] (7)	37
1.5.2.1.5. [Cu(PPTPMP)(Phen)NCS] (8)	38
1.5.2.1.6. [Cu(PPTPMP)(Bipy)NCS] (9)	38
1.5.2.2. Syntheses of ternary complexes of 4-toluoyl pyrazolones	(39-41)
1.5.2.2.1. [Cu(TPMP)(Phen)NCS] (10)	39
1.5.2.2.2. [Cu(TPMP)(Bipy)NCS] (11)	39
1.5.2.2.3. [Cu(TMCPMP)(Phen)NCS] (12)	40
1.5.2.2.4. [Cu(TMCPMP)(Bipy)NCS] (13)	40
1.5.2.2.5. [Cu(TPTPMP)(Phen)NCS] (14)	41
1.5.2.2.6. [Cu(TPTPMP)(Bipy)NCS] (15)	41
1.6. Characterization of Cu(II) complexes of 4-acyl pyrazolones	(42-73)
1.6.1. Physicochemical properties of the synthesized complexes	42
1.6.2. Crystal structure description	(44-59)
1.6.2.1. Crystal structure description of binary complexes	(44-49)
1.6.2.1.1. Intermediate [Ca(TPMP) ₂ (EtOH) ₂]	44
1.6.2.1.2. Complex 1	48
1.6.2.2. Crystal structure description of ternary complexes	(49-59)
1.6.2.2.1. Ternary complexes containing 4-propionyl pyrazolones	(50-54)
1.6.2.2.1.1. Complex 5	50
1.6.2.2.1.2. Complex 9	53
1.6.2.2.2. Ternary complexes containing 4-toluoyl pyrazolones	(54-59)
1.6.2.2.2.1. Complex 10	54
1.6.2.2.2.2. Complex 11	56
1.6.2.2.2.3. Complex 13	57
1.6.3. IR spectral studies	(59-62)
1.6.3.1. IR spectral studies of binary complexes	60
1.6.3.2. IR spectral studies of ternary complexes	60

1.6.4. Mass spectral studies	(62-66)
1.6.4.1. Mass spectral studies of binary complexes	62
1.6.4.2. Mass spectral studies of ternary complexes	63
1.6.5. Electronic spectral studies	(66-68)
1.6.5.1. Electronic spectral studies of binary complexes	66
1.6.5.2. Electronic spectral studies of ternary complexes	66
1.6.6. Thermal studies	(68-70)
1.6.6.1. Thermal studies of binary complexes	68
1.6.6.2. Thermal studies of ternary complexes	69
1.6.7. Magnetic measurement studies	70
1.6.8. ESR studies	(71-73)
1.6.8.1. ESR studies of binary complexes	71
1.6.8.2. ESR studies of ternary complexes	72
Conclusions	73
Literature cited.	(74-80)

Chapter-2. Synthesis, characterization and crystal structure of metal complexes containing pyrazolone based thio-semicarbazones

2.1. Introduction	(81-87)
2.1.1. Thiosemicarbazones of 4-acyl pyrazolones	81
2.1.2. Metal complexes of thiosemicarbazones	84
2.1.3. Metal complexes of pyrazolone based thiosemicarbazones	85
2.2. Experimental	(87-88)
2.2.1. Materials	87
2.2.2. Single crystal X-ray structure determination	88
2.3. Syntheses of thiosemicarbazone ligands	(88-90)
2.3.1. (Z)-2-((1-(3-chlorophenyl)-3-methyl-5-oxo-4,5-dihydro-1H-pyrazol-4-yl)(p-tolyl)methylene)hydrazinecarbothioamide [TMCPMP-TS]	88
2.3.2. (Z)-2-((3-methyl-5-oxo-1-p-tolyl-4,5-dihydro-1H-pyrazol-4-yl)(p-tolyl)methylene)hydrazinecarbothioamide [TPTPMP-TS]	89
2.4. Characterization of thiosemicarbazones	(90-98)
2.4.1. Physicochemical properties	90
2.4.2. IR spectral studies	90
2.4.3. NMR spectral studies	(91-92)
2.4.3.1. ¹ H NMR spectral studies	91
2.4.3.2. ¹³ C NMR spectral studies	92
2.4.4. Mass spectral studies	(93-95)
2.4.5. Molecular structure of ligand TMCPMP-TS	(95-98)

3.1.2.1. 4-alkyl(or aryl)aminomethylidene-5-pyrazolones with (-C4 C-N(H)-C-) unit	127
3.1.2.2. 4-Hydrazone-5-pyrazolones (-C4-C=N-N-C- unit)	128
3.1.2.2.1. Schiff bases containing salicylidenehydrazones	128
3.1.2.2.2. Schiff bases containing acylhydrazones	130
3.1.2.3. Bis-5-pyrazolones	131
3.1.3. Tautomerism in pyrazolone containing Schiff base ligands	132
3.1.4. Metal complexes of pyrazolone Schiff bases	(133-140)
3.1.4.1. Metal complexes containing 4-alkyl(or aryl)aminomethylidene-5-pyrazolones	133
3.1.4.2. Metal complexes containing salicylidenehydrazones	135
3.1.4.3. Metal complexes containing Acylhydrazones	137
3.1.4.4. Metal complexes containing bis-pyrazolones	138
3.2. Experimental	141
3.2.1. Materials	141
3.2.2. Single crystal X-ray structure determination	141
3.3. Syntheses of Schiff base ligands	(141-145)
3.3.1. Syntheses of Schiff base ligands of 4-toluoyl pyrazolones	(141-144)
3.3.1.1. 5-methyl-2-phenyl-4-(<i>p</i> -tolyl- <i>p</i> -tolylimino-methyl)-2,4- dihydro-pyrazol-3-one [TPMP-T]	141
3.3.1.2. 4-[(4-bromo-phenylimino)- <i>p</i> -tolyl-methyl]-5-methyl-2- phenyl-2,4- dihydro-pyrazol-3-one [TPMP-BA]	142
3.3.1.3. 2-(3-chloro-phenyl)-5-methyl-4-(<i>p</i> -tolyl- <i>p</i> -tolylimino- methyl)-2,4-dihydro-pyrazol-3-one [TMCPMP-T]	143
3.3.1.4. 4-[(4-bromo-phenylimino)- <i>p</i> -tolyl-methyl]-2-(3-chloro- phenyl)-5-methyl-2-phenyl-2,4-dihydro-pyrazol-3-one [TMCPMP-BA]	143
3.3.1.5. 5-methyl-2- <i>p</i> -tolyl-4-(<i>p</i> -tolyl- <i>p</i> -tolylimino-methyl)-2,4- dihydro-pyrazol-3-one [TPTMP-T]	144
3.3.1.6. 4-[(4-bromo-phenylimino)- <i>p</i> -tolyl-methyl]-5-methyl-2- <i>p</i> -tolyl-2,4-dihydro-pyrazol-3-one [TPTMP-BA]	144
3.3.2. Syntheses of Schiff base ligands of 4-propionyl pyrazolones	145
3.3.2.1. 5-methyl-2- <i>p</i> -tolyl-4-(1- <i>p</i> -tolylimino-propyl)-2H- pyrazol-3-one [PPTMP-T]	145
3.3.2.2. 2-(3-chloro-phenyl)-5-methyl-4-(1- <i>p</i> -tolylimino- propyl)-2H-pyrazol-3-one [PMCPMP-T]	145
3.4. Characterization of Schiff base ligands	(146-160)
3.4.1. Physicochemical properties of the Schiff base ligands	146
3.4.2. IR spectral studies	146
3.4.3. NMR spectral studies	(147-152)
3.4.3.1. ¹ H NMR spectral studies	(147-150)
3.4.3.1.1. ¹ H NMR spectral studies of 4-toluoyl pyrazolone based Schiff bases	147

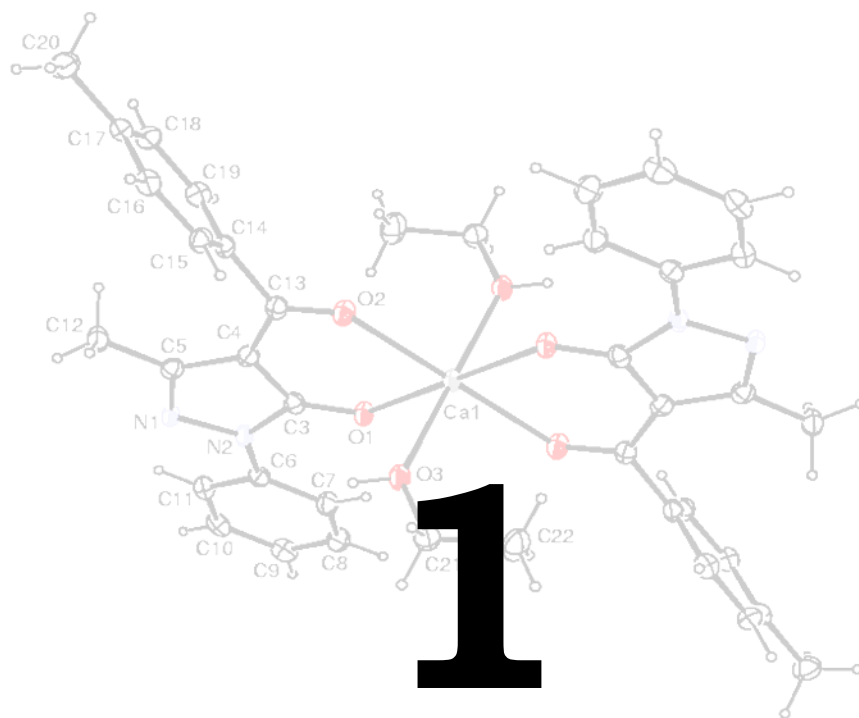
3.4.3.1.2. ^1H NMR spectral studies of 4-propionyl pyrazolone based Schiff bases	150
3.4.3.2. ^{13}C NMR spectral studies	(150-152)
3.4.3.2.1. ^{13}C NMR spectral studies of 4-toluoyl pyrazolone based Schiff bases	150
3.4.3.2.2. ^{13}C NMR spectral studies of 4-propionyl pyrazolone based Schiff bases	151
3.4.4. Mass spectral studies	(152-156)
3.4.4.1. Mass spectral studies of 4-toluoyl pyrazolone based Schiff base ligands	152
3.4.4.2. Mass spectral studies of 4-propionyl pyrazolone based Schiff base ligands	154
3.4.5. Molecular structure of ligands	(156-160)
3.5. Syntheses of Cu(II) complexes	(161-165)
3.5.1. $[\text{Cu}(\text{TPMP-T})_2(\text{H}_2\text{O})_2]$ (24)	161
3.5.2. $[\text{Cu}(\text{TPMP-BA})_2(\text{H}_2\text{O})_2]$ (25)	162
3.5.3. $[\text{Cu}(\text{TMCPMP-T})_2(\text{H}_2\text{O})_2]$ (26)	162
3.5.4. $[\text{Cu}(\text{TMCPMP-BA})_2(\text{H}_2\text{O})_2]$ (27)	162
3.5.5. $[\text{Cu}(\text{TPTPMP-T})_2(\text{H}_2\text{O})_2]$ (28)	163
3.5.6. $[\text{Cu}(\text{TPTPMP-BA})_2(\text{H}_2\text{O})_2]$ (29)	163
3.6. Syntheses of Ni(II) complexes	(164-165)
3.6.1. $[\text{Ni}(\text{PPTPMP-T})_2(\text{H}_2\text{O})_2]$ (30)	164
3.6.2. $[\text{Ni}(\text{PMCPMP-T})_2(\text{H}_2\text{O})_2]$ (31)	164
3.7. Characterization of metal(II) complexes	(165-182)
3.7.1. Physicochemical properties of the synthesized complexes	165
3.7.2. IR spectral studies	(167-168)
3.7.3. Mass spectral studies	(168-171)
3.7.4. Electronic spectral studies	(171-173)
3.7.5. Thermal studies	(173-176)
3.7.5.1. Thermal studies of Cu(II) complexes	173
3.7.5.2. Thermal studies of Ni(II) complexes	176
3.7.6. Magnetic measurement studies	(176-177)
3.7.6.1. Magnetic measurement studies of Cu(II) complexes	177
3.7.6.2. Magnetic measurement studies of Ni(II) complexes	177
3.7.7. ESR studies	(178-179)
3.8. Modified synthesis in comparison with previous synthesis of Cu(II) complex $[\text{Cu}(\text{TPMP-BA})_2]$ (32)	(179-180)
3.8.1. Molecular structure of $[\text{Cu}(\text{TPMP-BA})_2]$	(180-182)
Conclusions	183
Literature cited.	(184-187)

Chapter-4. DNA binding, cleavage and Anti cancer activities of many of the synthesized metal complexes

4.1. Introduction	(188-207)
4.1.1. A structural introduction to DNA	191
4.1.2. Binding to DNA	194
4.1.3. Interest of binding drugs to DNA	194
4.1.4. DNA Binding Modes	(195-197)
4.1.4.1. Intercalative binding	195
4.1.4.2. Groove binding	196
4.1.4.3. External binding	196
4.1.5. Drugs which bind to DNA	(197-198)
4.1.6. DNA Cleavage	(198-199)
4.1.7. Binding with Serum Albumins	199
4.1.8. Anti-cancer studies	(200-206)
4.1.8.1. Cell viability (MTT) assay	200
4.1.8.1.1. Significance of MTT Assay	201
4.1.8.2. LDH Release Assay	202
4.1.8.3. Intracellular ROS generation (DCFDA staining)	202
4.1.8.4. Mitochondrial Membrane Potential	203
4.1.8.5. Nuclear morphology assay (DAPI staining)	204
4.1.8.6. AO/EB staining	204
4.1.8.7. Cell cycle analysis & FITC Annexin-V/PI Staining	204
4.1.9. Metal complexes against different diseases	207
4.2. Experimental	(207-213)
4.2.1. Materials	207
4.2.2. DNA binding studies	207
4.2.3. Tryptophan Quenching Studies	210
4.2.4. Anticancer activity	(210-213)
4.2.4.1. Cell culture	210
4.2.4.2. Cell viability (MTT) assay	211
4.2.4.3. Cellular integrity (LDH release) assay	211
4.2.4.4. Intracellular ROS generation (DCFDA staining)	211
4.2.4.5. Mitochondrial Membrane Potential	211
4.2.4.6. Nuclear morphology assay (DAPI staining)	211
4.2.4.7. AO/EB staining	212
4.2.4.8. Cell cycle analysis	212
4.2.4.9. FITC Annexin- V/PI Staining	212
4.2.4.10. Statistical analysis	213
4.3. DNA binding activities of the compounds under investigation	(213-223)
4.3.1. Electronic absorption titration	213
4.3.1.1. Absorption spectral studies of 4-acyl pyrazolone based complexes	214

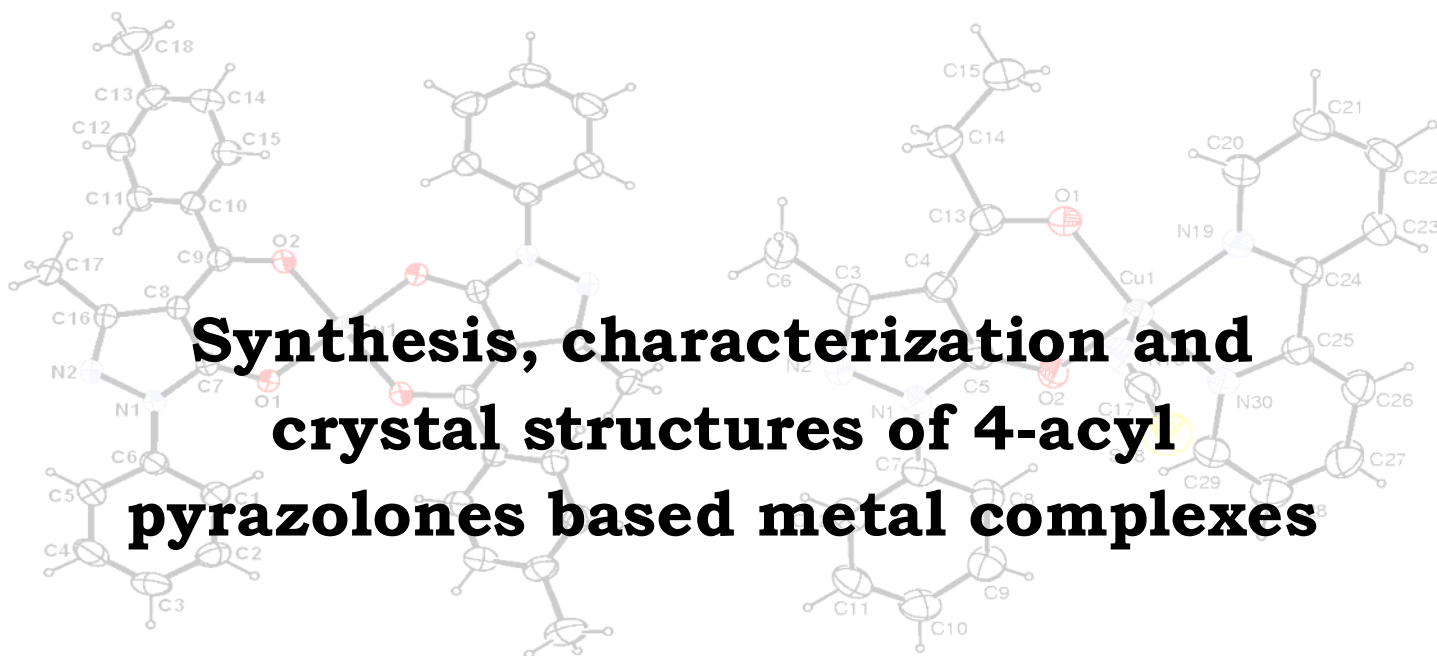
4.3.1.2. Absorption spectral studies of thiosemaicarbazone based complexes	215
4.3.1.2.1. Simple complexes	215
4.3.1.2.2. Ternary complexes	216
4.3.2. Ethidium Bromide Displacement Assay	216
4.3.3. Viscosity measurements	220
4.3.3.1. Viscosity measurements for binary complexes containing 4-toluoyl pyrazolones	221
4.3.3.2. Viscosity measurements for simple complexes containing pyrazolone based thiosemicarbazone	222
4.4. DNA cleavage activities of the compounds under investigation	(223-230)
4.4.1. Hydrolytic cleavage	224
4.4.2. Oxidative cleavage	226
4.4.2.1. Oxidative cleavage by binary complexes of 4-toluoyl pyrazolones	226
4.4.2.2. Oxidative cleavage by binary complexes of 4-toluoyl pyrazolones based thiosemicarbazone	228
4.5. Protein binding studies	(230-233)
4.6. Anti cancer studies of the synthesized complexes	(233-246)
4.6.1. MTT Assay	233
4.6.2. LDH Release Assay	235
4.6.3. Measurement of Mitochondrial Membrane Potential	236
4.6.4. Intracellular ROS generation (DCFDA staining)	239
4.6.5. AO/EB staining	241
4.6.6. Nuclear morphology assay (DAPI staining)	241
4.6.7. Cell cycle analysis	243
4.6.8. FITC Annexin- V/PI Staining	245
Conclusions	247
Literature cited.	(249-254)
<i>Publications</i>	<i>I</i>
<i>Participation in Seminars/Conferences</i>	<i>II</i>

CHAPTER



1

**Synthesis, characterization and
crystal structures of 4-acyl
pyrazolones based metal complexes**

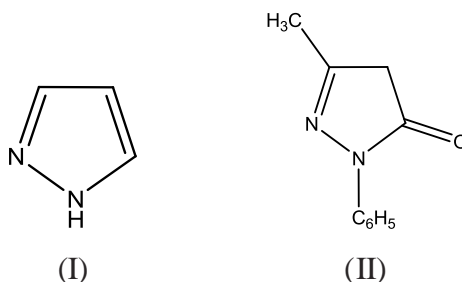


1.1. Introduction

Nitrogen heterocycles are of special interest because they constitute an important class of natural and synthetic products, many of which exhibit useful biological activities and unique electrical and optical properties [1, 2]. Oxazolone, pyrazolone and pyrazoline derivatives are in general well-known five-membered nitrogen-containing heterocyclic compounds. We are interested in only pyrazolone derivatives due to their variety of applications.

What are pyrazolones???????

The pyrazole ring system (I) consists of a doubly unsaturated five membered ring containing two adjacent nitrogen atoms. Knorr [3, 4] first synthesized a compound containing this system in 1883 by the reaction of ethylacetoacetate with phenyl hydrazine which yielded in 1-phenyl-3-methyl-5-pyrazolone (II).



Knorr [5] introduced the name pyrazolone for these compounds to denote that the nucleus derived from pyrrole by replacement of carbon by nitrogen; since many drugs and dyes contain the pyrazole nucleus, the class has been widely studied and the field continue to be active today even though antipyrine and related medicine no longer in common use. Pyrazolone dyes are especially important in colour photography.

History of pyrazolones.....

Since the synthesis of antipyrine (2, 3-dimethyl-1-phenyl-5-pyrazolone) by Knorr [6, 7], a great deal of attention has been paid to the analgesic and antipyretic properties of these compounds. The discovery of these properties prompted the search for other pyrazolones with similar behaviour but with a better therapeutic action. As a

result of this interest, aminoantipyrine (the 4-amino-antipyrine) was synthesized [8] and incorporated into the pharmacopoeia as an antipyretic and later on, as an analgesic and anti-inflammatory agent. Nevertheless, the use of these compounds in the treatment of human declined significantly after their toxicity for bone marrow was discovered. A new advance in this field occurred in 1949 when H. Stenzl synthesized phenylbutazone [9], a product for the treatment of rheumatoid arthritis. Once again, the high toxicity of these compounds in human beings has restricted their use, which is currently limited to the veterinary field. Since these first historical moments, the synthesis of pyrazolones has remained to a large extent focused on the search for less toxic new anti-inflammatory drugs [10] or the preparation of new compounds with antifungal [11], antitumor [12] and antihyperglycemic [13] activities.

Although the use of pyrazolones as drugs has warranted significant attention, many more applications have been devised for this group of molecules outside the pharmaceutical field. For example, they have been applied to the solvent extraction of metal ions [14], for analytical purposes [15], in the preparation of azo colourants [16], as ligands in complexes with catalytic activity [17] and in the synthesis of rare earth metal complexes with interesting photophysical properties [18].

4-acyl pyrazolones in brief.....

Acylation is one of the fundamental reactions in organic chemistry and can be carried out by wide variety of reagents. Pyrazolone-5 derivatives, especially 4-acyl pyrazolone form an important class of organic compounds and their derivatives represent a big scientific and applied interest in analytical applications, catalysis, dye and extraction metallurgy, etc. [19–21] because they display several different coordination modes, with respect to classical β -diketonate. Furthermore, 4-acyl pyrazolone derivatives have the potential to form different types of coordination compounds due to the several electron-rich donor centers [22].

Acyipyrazolones are an interesting class of β -diketones, containing a pyrazole fused to a chelating arm. The first synthesis of an acyipyrazolone appeared at the end of the XIX century [23]. However, it was only in 1959 that Jensen reported an

advantageous method of preparation of 1-phenyl-3-methyl-4-acylpyrazol-5-ones [24]. Pyrazolone and its derivatives form an important class of compounds and have attracted considerable scientific and applied interest. Pyrazolones, especially 4-acylpyrazolone, display several different coordination modes with respect to classical β -diketonates [19, 25].

1.1.1. 4-acyl pyrazolones as ligands

F. Marchetti *et al.* have reported a review on the coordination chemistry of β -diketones, a part of which was focused on relevant results in the field of 4-acylpyrazolones [26]. He has also reported a review with more detailed description of 4-acylpyrazolones coordination chemistry, which has greatly increased in the last decades [27]. The literature is so wide that it is not possible to cover each and every report in this chapter. Therefore, the introduction part is limited to a brief discussion on the 4-acylpyrazolone and their metal complexes.

In the classical method of synthesis of 4-acyl pyrazolones (HL), the reactants are the corresponding acyl chlorides and 1-phenyl-3-methylpyrazol-5-one, easily obtained from condensation between phenylhydrazine and ethyl acetoacetate. Acylation easily occurs at C-4 position of the pyrazole ring in basic (calcium hydroxide) dioxane or THF at reflux. Subsequent treatment with acid aqueous solution affords the HL in high yield as a solid powder insoluble in water (Fig. 1.1).

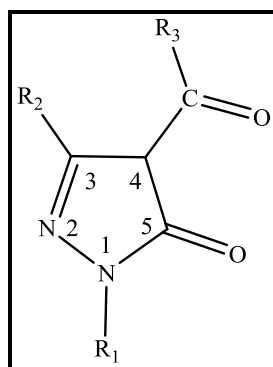


Fig. 1.1. General structure of 4-acyl pyrazolone

The classical method of synthesis varies when the acyl group is trifluoromethyl $-\text{CF}_3$ or heptafluoropropyl $-\text{CF}_2\text{CF}_2\text{CF}_3$: the reaction is performed at 0° in pyridine, which acts as solvent and base and 1-phenyl-3-methylpyrazol-5-one reacts with fluorinated anhydrides. Addition of aqueous solution of HCl again provokes formation and precipitation of HL [28, 29]. The peripheral positions R_1 , R_2 and R_3 can be easily changed in order to vary the electronic and steric features of HL ligands. Other groups different to phenyl ring have been introduced in N1 position, by using different starting hydrazines in the preparation of 1- R_1 -3-methylpyrazol-5-one ($\text{R}_1 = \text{CH}_3, \text{C}_6\text{H}_4\text{NO}_2, \text{C}_6\text{H}_4\text{CF}_3, \text{C}_5\text{H}_4\text{N}$) [30–33]. Among them it is worth mentioning the introduction of a pyridine ring, which increases the number of donor atoms in HL, a ligand potentially O_2, N_2 -tetradentate, with two different chelating moieties placed in opposite faces of the pyrazole ring (Fig. 1.2) [33].

It is also possible to substitute the methyl in C-3 position, for example with a phenyl one, by using ethyl benzoylacetate in the preparation of the reactant 1- R_1 -3- R_2 -pyrazol-5-one [34, 35]. Also, a vinyl group can be introduced in R_2 , the corresponding HL ligands being only used in organic synthesis to form pyranopyrazolones and not in the interaction with metal acceptors [36]. However, acyl substitution has been much more explored, where a large number of groups, from alkyl to aryls, have been introduced by simply choosing different acyl chlorides. Heteroatoms in the acyl position have also been introduced, i.e. heteroaromatic rings such as thienyl and furyl groups (Fig. 1.3), but to date these ligands have not displayed any coordination through the additional O- and S donor atoms [37, 38]. A work on lanthanide derivatives reported the use of HL ligands containing OEt, NMe_2 or NPh_2 groups in the acyl position [29]. Alkoxy groups $-\text{OR}$ in the acyl moiety HL by substitution of the CCl_3 with an $-\text{OR}$ group when the reactions have been reported in alcoholic ROH solvents ($\text{R} = \text{Me}, \text{Et}, i\text{Pr}, \text{Bn}$) (Fig. 1.4) [39, 40].

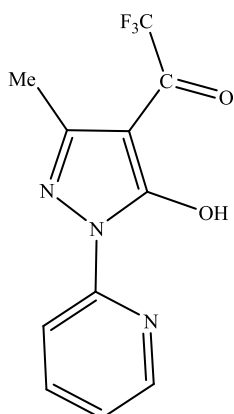


Fig. 1.2. Acyl pyrazolone containing CF_3 .

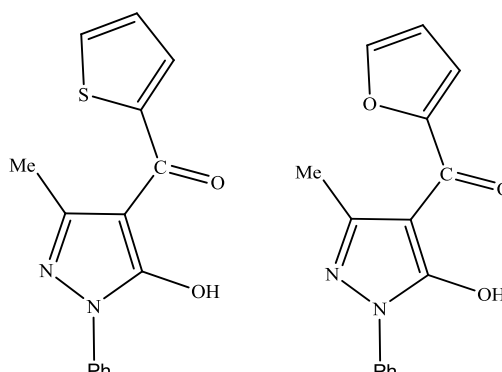


Fig. 1.3. Acyl pyrazolones containing thienyl and furyl groups

Fusion of 5-pyrazolone with AcNH_2 followed by the alkaline hydrolysis affords 4-acetyl-3-methyl-1-phenyl-2-pyrazolin-5-one, which undergoes condensation with RCHO ($\text{R} = \text{phenyl, furyl, } p\text{-Me}_2\text{NC}_6\text{H}_4, p\text{-MeC}_6\text{H}_4, p\text{-MeOC}_6\text{H}_4, p\text{-HOC}_6\text{H}_4, p\text{-O}_2\text{NC}_6\text{H}_4$), affording HL ligands containing a $\text{C}=\text{C}$ double bond in α -position to the chain $\text{C}=\text{O}$ (Fig. 1.5) [41].

An exotic variation in acyl moiety is represented by a $\text{CH}_2\text{C}(\text{O})\text{CH}_3$ group, to form a 1-phenyl-3-methyl-4-acetoacetyl-5-pyrazolone [42] which has been characterized also by X-ray studies (Fig. 1.6) showing the molecule to exist in a tautomeric form containing two intramolecular H-bonds [43].

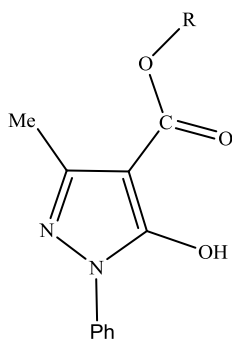


Fig. 1.4. Acyl pyrazolone containing -OR group

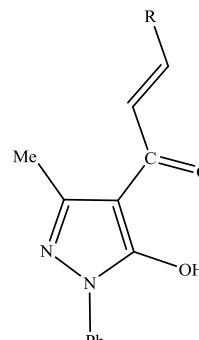


Fig. 1.5. Acyl pyrazolone containing $\text{C}=\text{C}$ in α position to the carbonyl chain

Another interesting variation is represented by bisacyl pyrazolone ligands where two acylpyrazolone units are linked to each other through a polymethylene chain of variable length ($n = 0-8, 10, 20$) (Fig. 1.7). They are potentially tetradentate bis-chelating donors that can be synthesized by using the appropriate diacyl chloride [44].

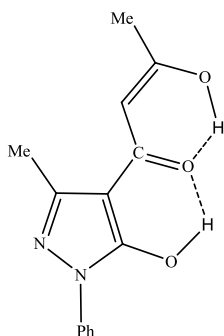


Fig. 1.6. Acyl pyrazolone containing $\text{CH}_2\text{C}(\text{O})\text{CH}_3$ group

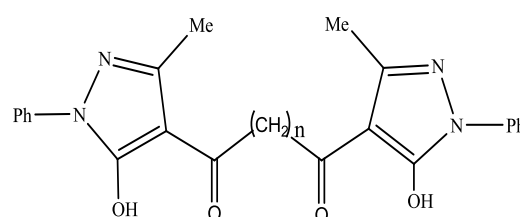


Fig. 1.7. Bis acylpyrazolones containing polymethylene chain

Similarly, a phenyl group can be introduced between the two acylpyrazolone moieties, by using the appropriate benzenedicarbonyl chlorides, as in the tetradentate donors ligands (*o/m/p*) (Fig. 1.8) [20].

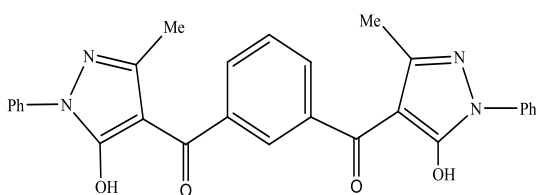


Fig. 1.8. Bis acylpyrazolone containing *m*-phenyl group

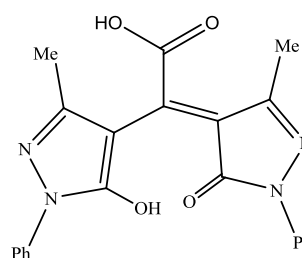


Fig. 1.9. Different bisacyl pyrazolone

F. Marchetti *et al.* have reported the synthesis of the hypothetical ligand, following Yoshikuni method from phthaloyl chloride and 1-phenyl-3-methylpyrazol-5-one in anhydrous dioxane, afforded a completely different species than bis(acylpyrazolone) [45] (Fig. 1.9). Moreover, the spectral data of this ligand are in accordance with those reported by Yoshikuni [20].

A polydentate O4, N-donor ligand (Fig. 1.10), has been synthesized by using the corresponding pyridine-2,6-dicarbonyl chloride and 1-phenyl-3-methyl-5-pyrazolone [46]. A potentially hexadentate trischelating donor ligand has been synthesized (Fig. 1.11) starting from 1,3,5-benzene tricarbonyl trichloride and 1-phenyl-3-methylpyrazol-5-one [47, 48].

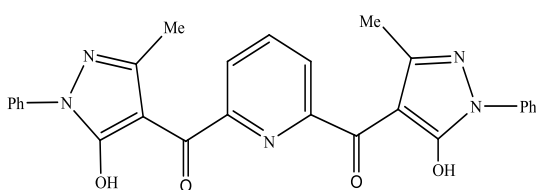


Fig. 1.10. Bis-acyl pyrazolone containing pyridine ring

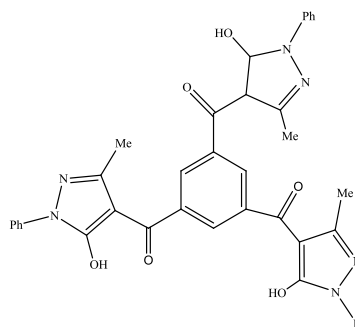


Fig. 1.11. Trisacyl pyrazolone

1.1.2. Metal complexes of 4-acyl pyrazolones

4-acyl pyrazolones can form complexes with many metal ions including transition metal ions, alkali metals, alkaline earth metals, lanthanides, actinides, etc. There is a wide range of complexes derived from acyl pyrazolones and transition metal ions in the literature, but here we have included only few examples.

1.1.2.1. Transition metal complexes of 4-acyl pyrazolones

The first Ti acylpyrazolonates, $[\text{Ti}(\text{OR})_{4-n}(\text{HL})_n]$ and $[\text{TiCl}_{4-n}(\text{HL})_n]$ ($n=1, 2$; $\text{R}=\text{Et}, i\text{Pr}$), were described in 1982 [49]. After this, many mononuclear (Fig. 1.12) and dinuclear (Fig. 1.13) complexes have been reported till now [49, 50]. The dinuclear species contain $\eta^1: \eta^5$ -bridged cyclopentadienyl groups. Whereas the another complex (Fig. 1.14) was obtained from interaction of CpTiCl_3 and HL [50].

The insecticidal activity of some of these compounds against *Trogoderma granarium* was tested [51]. Other studies on the insecticidal activity of dinuclear Ti acylpyrazolones toward *Periplaneta americana* (a household pest), *Trogoderma*

granarium and *Tribolium castaneum* (stored product pests), and the larvae of *Aedes aegypti* (an insect pest of medical importance) have been reported, assessing their potentials with respect to Cp_2MCl_2 ($\text{M}=\text{Ti}$) or HL alone [52]. A decades later a cyclo-tetranuclear $[\text{Ti}(\eta^2\text{-O})(\text{L})_2]_4$ (Fig. 1.15) derivative has been synthesised and fully characterized also by X-ray diffraction methods [12].

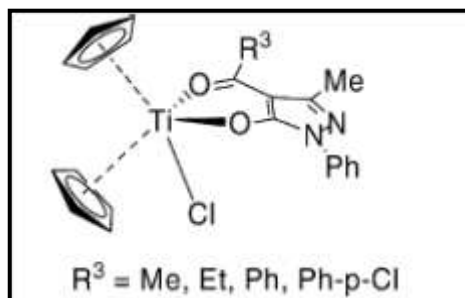


Fig. 1.12. Mononuclear Ti complex

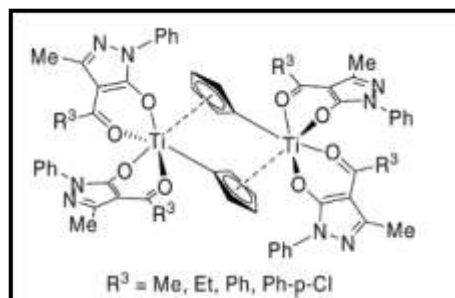


Fig. 1.13. Dinuclear Ti complex

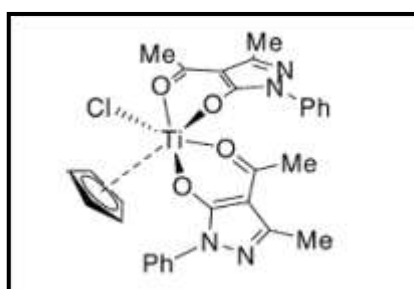


Fig. 1.14. Mononuclear Ti complex with two acyl pyrazolones

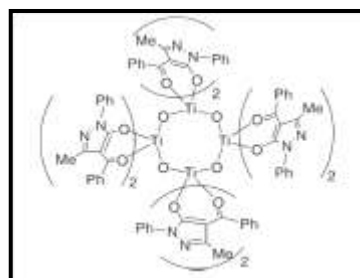


Fig. 1.15. Tetranuclear Ti complex

The first vanadium(IV) acylpyrazolonate derivatives appeared in 1976, when an oxovanadium(IV) $[\text{VO}(\text{HL})_2]$ compound, synthesized from interaction between $\text{VOSO}_4 \cdot 5\text{H}_2\text{O}$ and HL in the presence of NaOAc in EtOH, has been characterized spectroscopically and magnetically [53]. A series of dioxovanadium(V) derivatives was synthesized from interaction of an ethanol solution of HL and aqueous solution of NH_4VO_3 acidified with HCl. The acylpyrazolonates coordinate both in the anionic L and neutral keto–enol monodentate HL forms. IR studies show that $\text{O}=\text{V}=\text{O}$ system is likely to be bent in a trigonal bipyramidal environment (Fig. 1.16) [54]. Square pyramidal oxovanadium(IV) compounds were prepared by mixing an ethanolic solution of HL with a $\text{H}_2\text{O}/\text{EtOH}$ solution of V_2O_5 acidified with HCl (Fig. 1.17) [55].

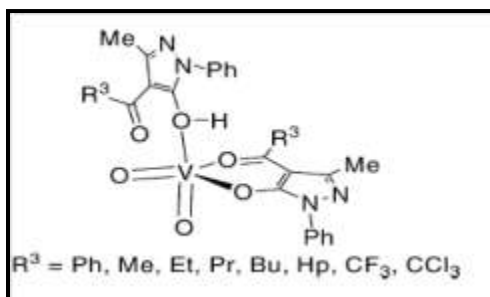


Fig. 1.16. Oxovanadium complex with TBP environment

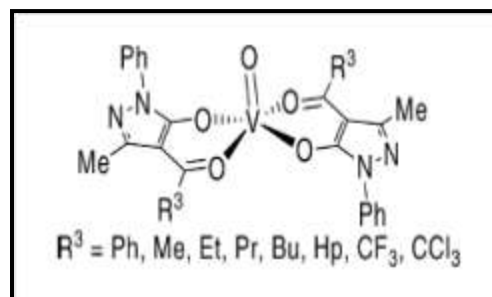


Fig. 1.17. Oxovanadium complex with square pyramidal environment

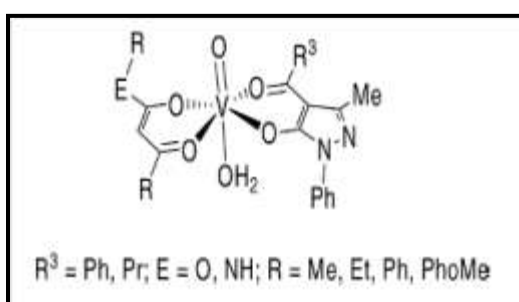


Fig. 1.18. Oxovanadium complex with linear O=V-OH₂

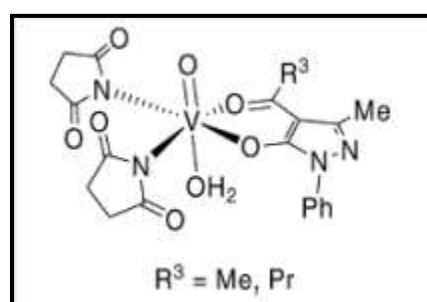


Fig. 1.19. Oxovanadium complex with octahedral environment

Mixed-ligand complexes of oxovanadium(IV) have been synthesized by interaction of $\text{VOSO}_4 \cdot 5\text{H}_2\text{O}$ with HL in aqueous ethanol medium [56, 57]. The three dimensional molecular modelling and analysis on some of these compounds indicates an octahedral environment on V with a linear $\text{O}=\text{V}-\text{OH}_2$ moiety (Fig. 1.18) [56, 57]. Similar mixed-ligand complexes have been obtained and characterized by magnetic measurements, ESR, electronic and IR spectral studies, indicating octahedral geometries for these derivatives (Fig. 1.19) [58]. Recently, our group has also reported the oxovanadium(IV) complex with octahedral environment. It has been characterized by X-ray crystallography and it is found to be good Heterogeneous Catalyst for the Oxidation of Styrene under Mild Conditions [59].

Monomeric derivatives, containing the bis(acylpyrazolone) ligands in the monoanionic form and acting as η^3 -tridentate O-donors, have been reported and characterized [60]. IR spectra showed that $\text{O}=\text{V}=\text{O}$ species exist as the *cis* form in the

complexes [60]. Some ionic oxoniobium(V) acylpyrazolone derivatives have been spectroscopically and magnetically characterized [61].

The complex containing an octahedrally six-coordinated chromium, has been reported. It is a paramagnetic compound with μ_{eff} 4.00 BM, typical of octahedral Cr complexes [62]. Some cyanonitrosyl chromium derivatives were synthesized. Analytical and spectral studies suggest a six-coordination on Cr atom, with CN ligands and O atoms of L in equatorial plane as well as NO and H₂O *trans* to each other, in axial positions (Fig. 1.20). Two different $\nu(\text{C}=\text{O})$ absorption bands have been detected in their IR spectra, the lower one for cyclic and higher one for exocyclic carbonyl groups [63, 64]. Magnetic ESR studies suggest they are low-spin d^5 complexes, with μ_{eff} 1.72–1.75 BM [63, 64]. Thermal studies were reported [65] together with the separation and identification of its two geometric isomers [66].

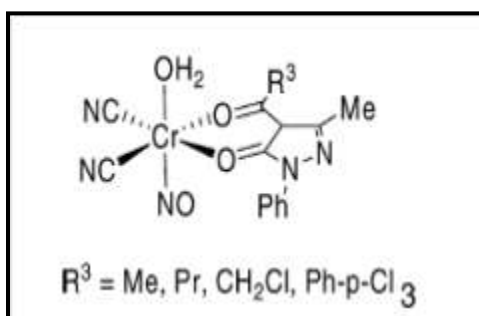


Fig. 1.20. Mononuclear Cr complex

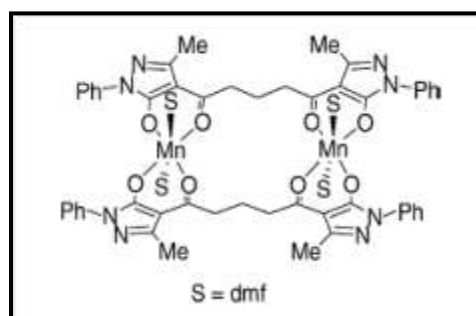


Fig. 1.21. Dinuclear Mn complex

Mn acylpyrazolonates of formula $[\text{Mn}(\text{HL})_2(\text{H}_2\text{O})_2]$ were synthesized. Replacement of a Me by a Ph group in the 4-acyl moiety decreases the C=O, C=C, and M=O stretching frequencies. Substitution of a Me group by CF₃ increases the C=O and C=C bond strengths and decreases M=O bond strength [67–69]. Also, some Mn(II) derivatives were fully characterized and the crystal structure of the latter resolved (Fig. 1.21), which is a dimeric compound containing bridging tetradentate ligands connecting two Mn atoms [70, 71]. These compounds are in a distorted octahedral environment with DMF molecules in *trans* positions. They are high-spin paramagnetic d^5 derivatives. A variable temperature magnetic susceptibility study showed that a weak antiferromagnetic exchange interaction exists between the metal centres in the complexes [70, 71].

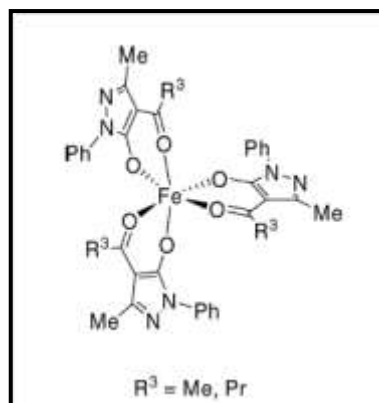


Fig. 1.22. Mononuclear Fe(III) complex with octahedral environment

Derivatives of Co and Ni have been hypothesized to exist in an octahedral geometry with *trans* H₂O ligands [28, 67, 68, 72]. Trivalent Fe and Co complexes were reported [69, 73] and spectroscopic [74] and thermal studies [65] of Fe complexes have been reported. Several aspects of the triplet state ketone-sensitized photoreduction of Ni complexes were studied. The sensitized reduction was much more efficient than direct photolysis in H-donating solvents and the reaction products were identified as the metal in (0) oxidation state, the free protonated ligand and oxidation products derived from the solvents [75]. Derivatives of Fe were synthesized HL in the presence of HCl. They were spectroscopically characterized and are high-spin octahedral complexes [76, 77]. Crystal structures of Fe derivatives were reported, showing they crystallize as *fac*-isomeric octahedral species (Fig. 1.22) [78]. Cobalt(II) derivatives were synthesized and characterized by interaction of Co(OAc)₂ with HL [79]. In some Fe derivatives, the ligand forms a dimeric species whereas in some case it forms a monomeric compound [80]. The anhydrous compounds of Co(II) or Ni(II) have been prepared by an electrochemical method [81]. The derivatives of Co and Ni are dinuclear with bridging tetradentate ligands [70].

The first report on copper acylpyrazolonates was on the [Cu(L)₂] compound, synthesized by mixing Cu(OAc)₂·H₂O and HL [82]. The derivatives [Cu(L)₂(H₂O)₂] were prepared similarly and a detailed IR study was performed [28, 67-69, 72]. Electronic and infrared studies of several Cu(II) derivatives of acylpyrazolonates,

containing a 4-acyl moiety of variable chain length, show bathochromic shift of the L absorptions upon coordination [83]. The stability of the C=O bond of the CO-Cu bonding system decreases while that of the Cu-O bond in the same system increases as the carbon chain of the 4-acyl substituent in L increases [83]. The triplet state ketone-sensitized photoreduction was investigated and shown to be much more efficient than direct photolysis in H-donating solvents [75]. The reaction products were identified as the metal in 0 oxidation state, the free protonated ligands and oxidation products derived from the solvents [75].

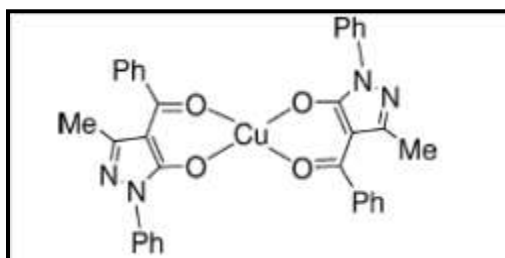


Fig. 1.23. Mononuclear Cu(II) complex with square planar environment

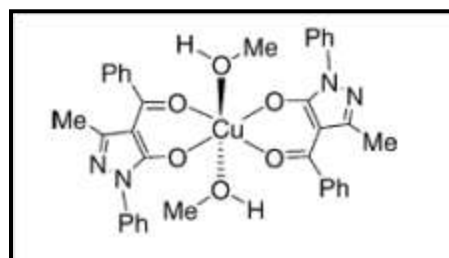


Fig. 1.24. Mononuclear Cu(II) complex with octahedral environment

Derivatives $[\text{Cu}(\text{L})_2]$ (Fig. 1.23) and $[\text{Cu}(\text{L})_2(\text{MeOH})_2]$ (Fig. 1.24) have been also structurally investigated [84]. The coordination geometry around Cu(II) in the former is slightly distorted square-planar, while the geometry around Cu(II) in the latter is distorted octahedral with four oxygen atoms of two L ligand occupying the equatorial positions and two methanol molecules occupying the axial positions [84].

A number of binary and mixed ligand complexes were reported [85-87]. In $[\text{Cu}(\text{L})_2(\text{EtOH})]$ type of complexes, the additional donor atoms of heterocycles in 4-acyl moiety has virtually no effect on the structure and composition of the complexes formed and coordination happens through always both carbonyl arms of L ligands [85]. When $[\text{Cu}(\text{L})_2]$ interact with an excess of PR_3 , reduction from Cu(II) to Cu(I) was observed and $[\text{Cu}(\text{L})(\text{PR}_3)_2]$ (R= Ph, Cy, Bn, Ph-*p*-Me) complexes were synthesized (Fig. 1.25) [86]. The X-ray crystal structures of this type of complexes [86, 87] shows a strongly distorted tetrahedral coordination environment of Cu, where

distortion increases as steric hindrance in 4-acyl moiety of L and mainly as phosphine substituents increase. The P-Cu-P bond angles vary from 127° to 140° [86, 87].

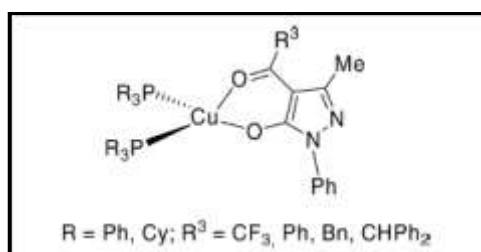


Fig. 1.25. Mixed ligand Cu(II) complex with $-\text{PR}_3$

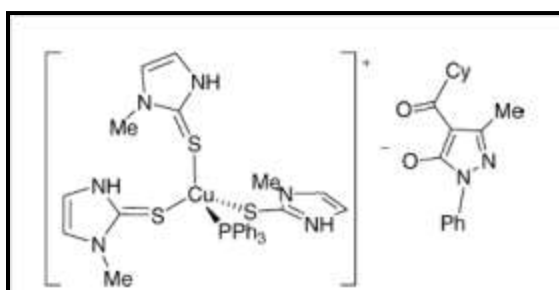


Fig. 1.26. Mixed ligand Cu(II) complex with Hmimt

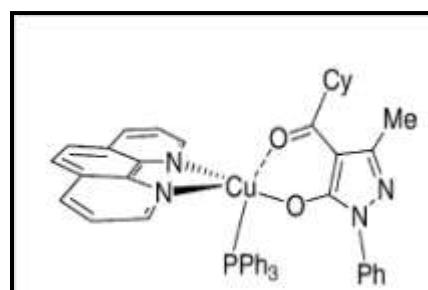


Fig. 1.27. Mixed ligand Cu(II) complex with Phen

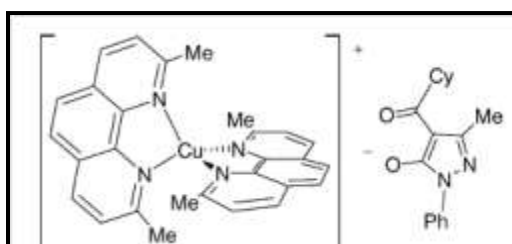


Fig. 1.28. Mixed ligand Cu(II) complex with cupr

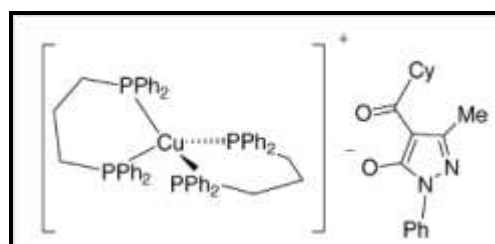


Fig. 1.29. Mixed ligand Cu(II) complex with dppp

$[\text{Cu}(\text{L})(\text{PPh}_3)_2]$ reacts with 1-m thylimidazoline- 2-thione (Hmimt), with 1,10-phenanthroline (phen), with 2,9-dimethyl-1,10-phenanthroline (cupr) and with bis(diphenylphosphino)propane (dppp), yielding the mixed ligand compounds $[\text{Cu}(\text{PPh}_3)(\text{Hmimt})_3](\text{L})$ (Fig. 1.26), $[\text{Cu}(\text{L})(\text{PPh}_3)(\text{phen})]$ (Fig. 1.27), $[\text{Cu}(\text{cupr})_2](\text{L})$ (Fig. 1.28) and $[\text{Cu}(\text{dppp})_2](\text{L})$ (Fig. 1.29), respectively [87].

The crystal structures of $[\text{Cu}(\text{L})_2(\text{bipy})] \cdot 1.5(\text{acetone})$ and $[\text{Cu}(\text{L})_2(\text{phen})] \cdot \text{EtOH}$ were detected, showing the Cu atom in a tetragonally distorted octahedral arrangement of the four O-atoms of HL with N_2 -donor ligand in equatorial position [88]. Two sets of Cu-O distances, the longer being in axial positions were found [88].

Volatility studies, electro spray mass spectra and IR in vapour phase were carried out for Cu(I) and Cu(II) L complexes. These compounds showed volatility in a narrow range of temperature and their use as molecular precursors in CVD explored [88, 89]. Studies on thermal decomposition of a number of $[\text{Cu}(\text{L})_2]$ compounds showed the melting points decreasing linearly by increasing the molecular weight of the complexes [90]. The crystal structure of $[\text{Cu}(\text{L})_2(\text{H}_2\text{O})]$ (Fig. 1.30) shows a square-pyramidal structure with L ligands arranged in an *anti* configuration to each other and with H_2O at the apex of polyhedron [91]. Both hydrogen atoms of H_2O are involved in an intermolecular H-bonding network with pyridinic nitrogen atoms of L-donors belonging to two neighbouring complexes [91]. Mixed ligand complexes of these derivatives have also been reported [91].

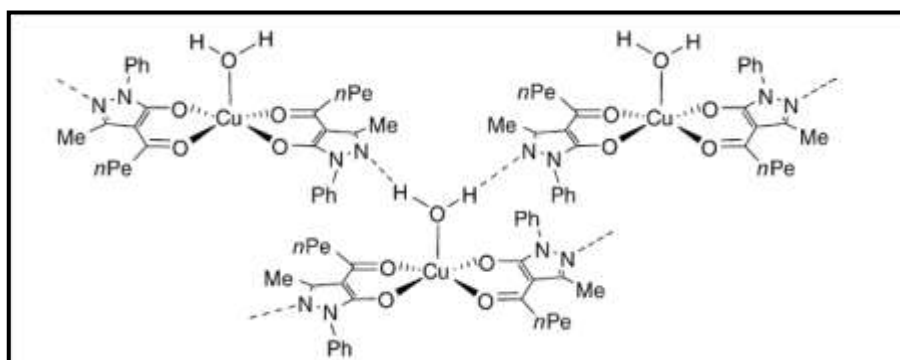


Fig. 1.30. Mononuclear Cu(II) complex $[\text{Cu}(\text{L})_2(\text{H}_2\text{O})]$

Dinuclear mixed-ligand complexes containing 2-hydroxyacetophenonato (haph) and neutral HL have been synthesized by reaction between $[\text{Cu}(\text{haph})_2(\text{H}_2\text{O})]$ and HL [92]. Octahedral geometries on copper atoms have been proposed, based on magnetic measurements, EPR, electronic and IR studies, and HL likely act as bridging bidentate neutral donor ligands [92].

The complexation of Cu(II) with potentially tetradentate ligands was investigated. Complex structure and stoichiometry are affected by the polymethylene chain length, through a steric effect [71, 44]. They are dimeric species (Fig. 1.31) as well as they are monomers (Fig. 1.32) [71, 44].

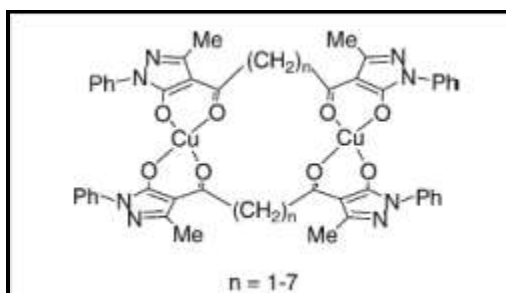


Fig. 1.31. Dinuclear Cu(II) complex

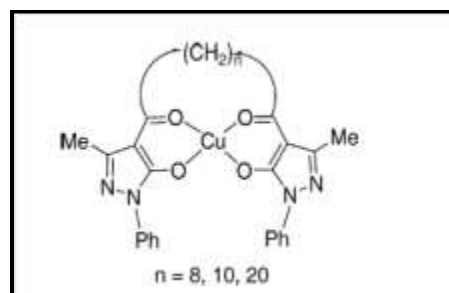


Fig. 1.32. Monomeric Cu(II) complex

The Cu(II) complex has also been prepared by an electrochemical method which generates the dianion that reacts with $\text{Cu}(\text{SO}_3\text{CF}_3)_2$ [81]. The crystal structure consists of two types of mononuclear units, characterized by different conformations of the polymethylene chain [93]. Both molecules contain a Cu atom in an almost square-planar environment of O atoms and all L moieties are planar [93].

The compounds $[\text{Zn}(\text{L})_2(\text{H}_2\text{O})_2]$ were synthesized by reaction of $\text{Zn}(\text{OAc})_2$ and HL [28, 67, 68, 74]. They were hypothesized to be six-coordinate by O_2 -bidentate chelating L-donors and two water molecules in the metal coordination sphere [28, 67, 68, 73]. Compounds $[\text{Zn}(\text{L})_2(\text{EtOH})_x(\text{H}_2\text{O})_y]$ ($x = 0-2$; $y=0, 2$) were reported together with a detailed analytical and spectroscopic characterization, a decades later [94].

The crystal structure of $[\text{Zn}(\text{L})_2(\text{H}_2\text{O})]$ (Fig. 1.33) shows a five-coordinate Zn, in a square-pyramidal environment, which is realized by the coordination of one molecule of H_2O in the apical position and two O_2 -chelating L ligands in the equatorial plane [95]. The coordination polyhedron is significantly distorted towards a trigonal-bipyramidal arrangement [95].

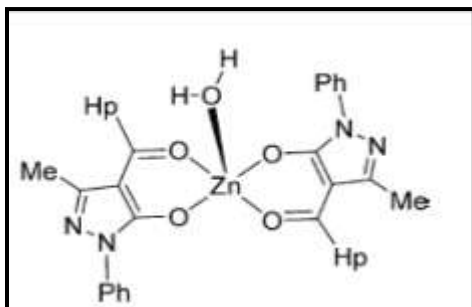


Fig. 1.33. Mononuclear Zn(II) complex with square pyramidal environment

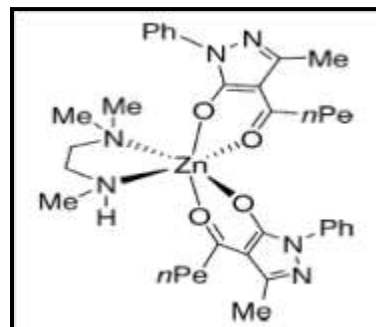


Fig. 1.34. Mononuclear Zn(II) complex with octahedral environment

The compound $[\text{Zn}(\text{L})_2(\text{DMF})_2]$ has been prepared and fully characterized [96]. The L ligand is bidentate with coordination through the two oxygen atoms and the zinc atom displays an octahedral coordination geometry with *trans* DMF molecules [96]. The crystal structure of $[\text{Zn}(\text{L})_2]$ shows a slightly distorted square-planar geometry around zinc [84].

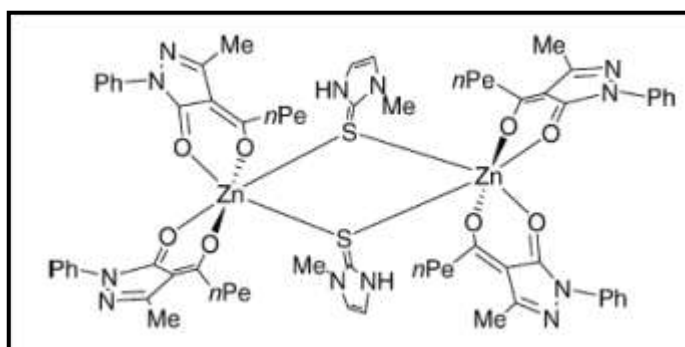


Fig. 1.35. Dinuclear Zn(II) complex

Zinc derivatives $[\text{Zn}(\text{L})_2(\text{S})_n]$ ($n = 1$; $\text{S} = \text{MeOH}$, $n = 2$) react with N-donors L' ($\text{L}' = \text{phen}$, bipy , trime , tmeda) yielding $[\text{Zn}(\text{L})_2(\text{L}')]$ [97]. The X-ray structure of derivative $[\text{Zn}(\text{L})_2(\text{trime})]$ (Fig. 1.34) shows a six-coordinate zinc in a slightly distorted octahedral environment [97]. Reaction of $[\text{Zn}(\text{L})_2(\text{MeOH})_2]$ with L' ($\text{L}' = \text{imH}$, Meim , NHEt_2) affords monomeric derivatives $[\text{Zn}(\text{L})_2(\text{L}')]$, whereas by interaction with Hmimt the dinuclear compound $[\text{Zn}(\text{L})_2(\text{Hmimt})]_2$ has been obtained, containing bridging η^2 -sulphur donor Hmimt (Fig. 1.35) [97].

1.2. Experimental

1.2.1. Materials

The compound 3-methyl-1-phenyl-1H-pyrazol-5(4H)-one (PMP), 1-(3-chlorophenyl)-3-methyl-1H-pyrazol-5(4H)-one (MCPMP) and 3-methyl-1-p-tolyl-1H-pyrazol-5(4H)-one (PTPMP) were obtained from Nutan Dye Chem., Sachin, Surat, India as free gift samples. Dioxane was obtained from E. Merck (India) Ltd. *p*-toluoyl chloride (Shiva Pharmachem. Ltd., Baroda) and propionyl chloride (S. D. Fine Chemicals, Mumbai) were obtained from as free gift samples. Calcium hydroxide, $\text{Cu}(\text{OAc})_2 \cdot \text{H}_2\text{O}$, $\text{Cu}(\text{NO}_3)_2 \cdot 3\text{H}_2\text{O}$, ammonium thiocyanate, 1, 10 phenanthroline and 2, 2' bipyridyl were obtained from LOBA Chem. Pvt. Ltd., Mumbai and used as supplied. Absolute alcohol was obtained from Baroda Chem. Industry Ltd. and was used after distillation. Methanol was obtained from Spectrochem., Mumbai, India. All the chemicals used were of AR grade. Solvents used in this study were purified and dried following the standard procedures wherever required [98].

1.2.2. Single crystal X-ray structure determination

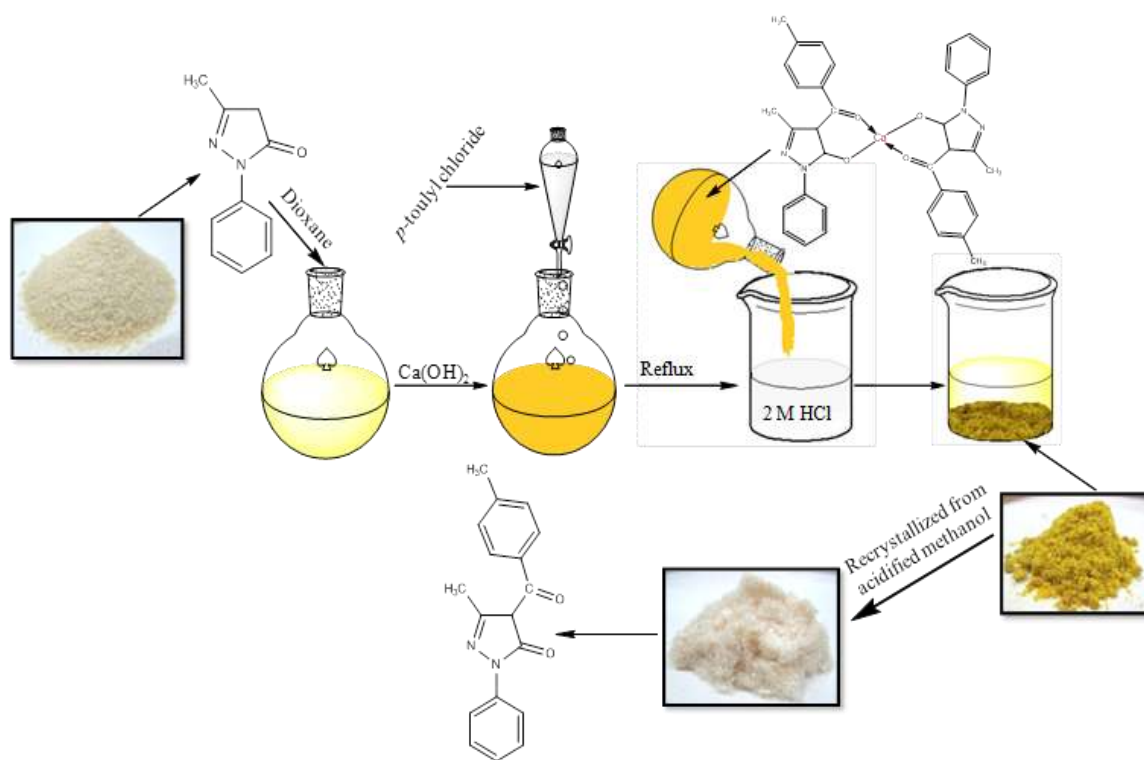
Crystals having good morphology were chosen for three-dimensional intensity data collection. X-ray intensity data of some of the complexes were collected at room temperature on Bruker CCD area-detector diffractometer equipped with graphite monochromated $\text{MoK}\alpha$ radiation ($\alpha=0.71073 \text{ \AA}$). The crystals used for data collection was of suitable dimensions. The unit cell parameters were determined by least-square refinements of all reflections in both cases. All the structures were solved by direct method and refined by full-matrix least squares on F^2 . Data were corrected for Lorentz, polarization and multi-scan absorption correction [99]. The structures were solved by direct methods using SHELXS97 [100]. All non-hydrogen atoms of the molecule were located in the best E-map. Full-matrix least-squares refinement was carried out using SHELXL97 [100]. Hydrogen atoms were placed at geometrically fixed positions and allowed to ride on the corresponding non-H atoms with C-H = 0.93-0.96 \AA , and $U_{\text{iso}}=1.5 U_{\text{eq}}$ of the attached C atom for methyl H atoms and 1.2 U_{eq} for other H atoms. Atomic scattering factors were taken from International

Tables for X-ray Crystallography (1992, Vol. C, Tables 4.2.6.8 and 6.1.1.4). An ORTEP [101] view of the both the complexes with atomic labelling are shown in further section. The geometry of the molecule has been calculated using the software PLATON [102] and PARST [103].

1.3. Syntheses of ligands

1.3.1. Syntheses of 4-toluoyl pyrazolones

1.3.1.1. 3-methyl-4-(4-methylbenzoyl)-1-phenyl-1H-pyrazol-5(4H)-one [TPMP]:



Scheme 1.1. Synthesis of TPMP

3-methyl-1-phenyl-1H-pyrazol-5(4H)-one (17.4 g, 0.1 mol) was dissolved in hot dioxane (80 cm³) in a flask equipped with a stirrer, separating funnel and reflux condenser. Calcium hydroxide (14.81 g, 0.2 mol) was added to this solution, followed by *p*-toluoyl chloride (15.4 g, 0.1 mol) added drop wise with precaution, as this reaction was exothermic. During this addition the whole mass was converted into a

thick paste. After the complete addition, the reaction mixture was refluxed for half an hour and then it was poured into dilute hydrochloric acid (200 cm³, 2 M). The colored crystals (TPMP) thus obtained were separated by filtration and recrystallized from an acidified methanol–water mixture (HCl:MeOH:H₂O = 1:80:19).

TPMP is cream crystals. Yield 80.85 % m.p. 120°C Anal. calc. for C₁₈H₁₆N₂O₂ M.W.: 292.33, C(73.95%), H(5.52%), N(9.52%), found: C(73.68%), H(5.21%), N(9.51%); ¹H NMR (CDCl₃): δ ppm 2.16 (s, 3H, PZ C-CH₃), 2.47 (s, 3H, N-TL C-CH₃), 7.28-7.46(m, 5H, Ph), 7.49-7.59(m, 4H, TL), 7.88-7.90 (s, 2H, PZ ring). IR (KBr, cm⁻¹): 1598(s) (C=N, cyclic), 1641(m) (C=O, pyrazolone ring); ¹³C NMR (CDCl₃) δ ppm: 16.04 [C-CH₃, PZ], 21.70 [C-CH₃, TL], 103.56 [C=O], 120.72-142.73 [substituted benzene rings]; MS: *m/z* = 292.07 [C₁₈H₁₆N₂O]⁺, 214.05 [C₁₂H₁₁N₂O₂]⁺, 200.03 [C₁₁H₉N₂O₂]⁺, 119.04 [C₈H₇O]⁺, 91.06 [C₇H₇]⁺.

1.3.1.2. 1-(3-chlorophenyl)-3-methyl-4-(4-methylbenzoyl)-1H-pyrazol-5(4H)-one [TMCPMP]:



Scheme 1.2. Synthesis of TMCPMP

It was prepared analogously from 1-(3-chlorophenyl)-3-methyl-1H-pyrazol-5(4H)-one and *p*-toluoyl chloride. The colored crystals (TMCPMP) thus obtained were separated by filtration and recrystallized.

TMCPMP is brown crystals. Yield 81.20 % m.p. 100°C Anal. calc. for

$C_{18}H_{15}N_2O_2Cl$ M.W.: 326.78, C(66.16%), H(4.63%), N(8.57%), found: C(66.20%), H(4.52 %), N(8.51%); 1H NMR ($CDCl_3$): δ ppm 2.15 (s, 3H, PZ C-CH₃), 2.47 (s, 3H, N-TL C-CH₃), 7.25-7.41(m, 4H, Ph), 7.56-7.85 (m, 4H, TL), 7.87-7.98 (s, 2H, PZ ring). IR (KBr, cm^{-1}): 1580(s) (C=N, cyclic), 1635(m) (C=O, pyrazolone ring); ^{13}C NMR ($CDCl_3$): δ ppm 16.13 [C-CH₃, PZ], 21.72 [C-CH₃, TL], 103.59 [C=O], 118.14-143.00 [substituted benzene ring], 162.90 [C-Cl]; MS: m/z = 326.03 [$C_{18}H_{15}N_2O_2Cl$]⁺, 290.53 [$C_{18}H_{15}N_2O_2$]⁺, 214.07 [$C_{11}H_8N_2O_2Cl$]⁺, 200.05 [$C_{11}H_9N_2O_2$]⁺, 119.05 [C_8H_7O]⁺, 91.07 [C_7H_7]⁺.

1.3.1.3. 3-methyl-4-(4-methylbenzoyl)-1-*p*-tolyl-1H-pyrazol-5(4H)-one [TPTPMP]:

It was prepared analogously from 3-methyl-1-*p*-tolyl-1H-pyrazol-5(4H)-one and *p*-toluoyl chloride. The colored crystals (TPTPMP) thus obtained were separated by filtration and recrystallized.



Scheme 1.3. Synthesis of TPTPMP

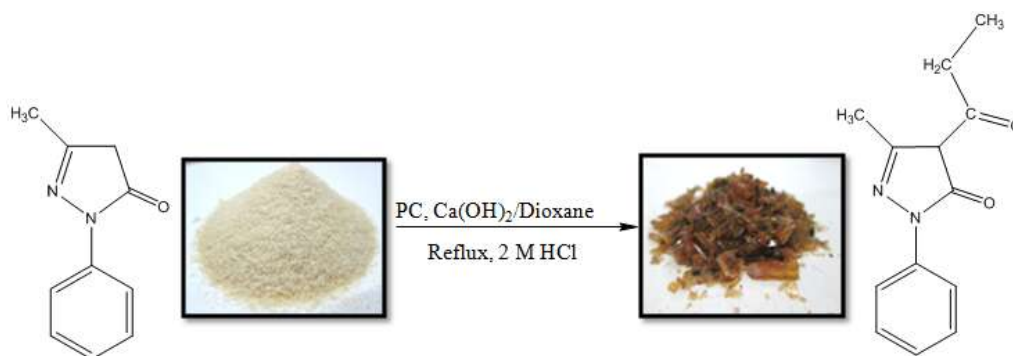
TPTPMP is yellow crystals. Yield 80.25 % m.p. 150°C Anal. calc. for $C_{19}H_{18}N_2O_2$ M.W.: 306.36, C(74.49%), H(5.92%), N(9.14%), found: C(74.39%), H(5.87%), N(9.03%); 1H NMR ($CDCl_3$): δ ppm 2.15 (s, 3H, PZ C-CH₃), 2.40 (s, 3H, TL C-CH₃), 2.46 (s, 3H, N-TL C-CH₃), 7.27-7.33(m, 4H, Ph), 7.56-7.76 (m, 4H, TL); IR (KBr, cm^{-1}): 1543(s) (C=N, cyclic), 1630(m) (C=O, pyrazolone ring),

1 2 2 2 (s) (C=N, azomethane); ^{13}C NMR (CDCl_3): δ ppm 16.00 [C-CH₃, PZ], 21.08 [C-CH₃, TL], 21.69 [C-CH₃, TL], 103.56 [C=O], 120.73-142.60 [substituted benzene rings]; MS: m/z = 306.08 [$\text{C}_{19}\text{H}_{18}\text{N}_2\text{O}_2$]⁺, 214.95 [$\text{C}_{12}\text{H}_{11}\text{N}_2\text{O}_2$]⁺, 185.12 [$\text{C}_{11}\text{H}_{11}\text{N}_2\text{O}$]⁺, 123.82 [$\text{C}_5\text{H}_4\text{N}_2\text{O}_2$]⁺, 119.05 [$\text{C}_8\text{H}_7\text{O}$]⁺, 91.04 [C_7H_7]⁺.

1.3.2. Syntheses of 4-propionyl pyrazolones

1.3.2.1. 3-methyl-1-phenyl-4-propionyl-1H-pyrazol-5(4H)-one [PPMP]:

It was prepared analogously from 3-methyl-1-phenyl-1H-pyrazol-5(4H)-one and propionyl chloride. The colored crystals (PPMP) thus obtained were separated by filtration and recrystallized.

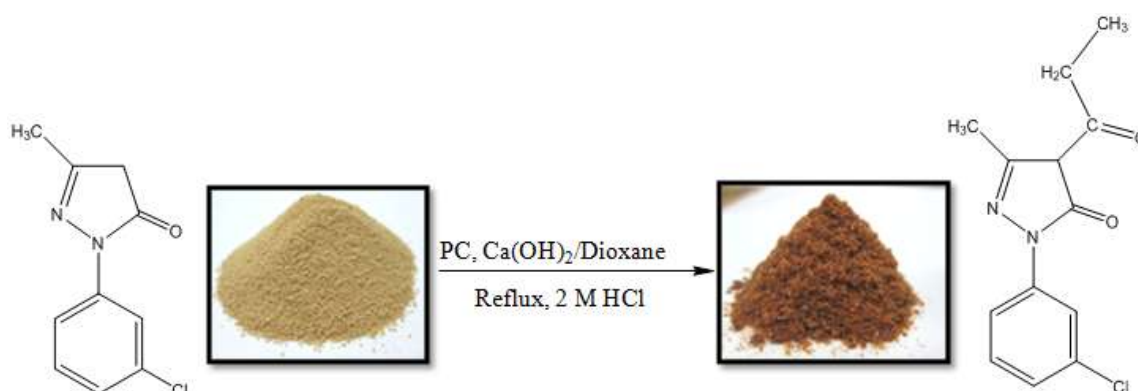


Scheme 1.4. Synthesis of PPMP

PPMP is brown crystals. Yield 80.85 % m.p. 90°C Anal. calc. for $\text{C}_{13}\text{H}_{14}\text{N}_2\text{O}_2$ M.W.: 230.26, C(67.81%), H(6.13%), N(12.17%), found: C(68.12%), H(6.06%), N(12.25%); ^1H NMR (CDCl_3): δ ppm 1.24-1.28 (t, 3H, Propionyl C-CH₃), 2.486 (s, 3H, PZ C-CH₃), 2.77-2.82 (q, 2H, Propionyl -CH₂-), 7.27-7.85 (m, 5H, Ph). IR (KBr, cm^{-1}): 1563(s) (C=N, cyclic), 1635(m) (C=O, pyrazolone ring), 1651(m) (C=O, propionyl group); ^{13}C NMR (CDCl_3) δ ppm: 8.15 [C-CH₃, Propionyl], 15.72 [C-CH₃, PZ], 32.47 [-CH₂-, Propionyl], 160.29 [C=O, PZ], 120.61-137.29 [substituted benzene ring], 198.20 [C=O, Propionyl], 103.43 [>C-N-, PZ]; MS: m/z = 230.02 [$\text{C}_{13}\text{H}_{14}\text{N}_2\text{O}_2$, MIP]⁺, 231.26 [$\text{C}_{13}\text{H}_{14}\text{N}_2\text{O}_2$, (m+1) peak]⁺, [$\text{C}_{13}\text{H}_{14}\text{N}_2\text{O}_2$, (m-1) peak]⁺, 200.62 [$\text{C}_{11}\text{H}_8\text{N}_2\text{O}_2$, Base peak]⁺, 201.31 [$\text{C}_{11}\text{H}_9\text{N}_2\text{O}_2$]⁺, 82.70 [$\text{C}_3\text{H}_3\text{N}_2\text{O}$]⁺, 137.20 [$\text{C}_7\text{H}_{10}\text{N}_2\text{O}$]⁺, 68.90 [C_5H_8]⁺, 56.99 [C_4H_8]⁺.

1.3.2.2. 1-(3-chlorophenyl)-3-methyl-4-propionyl-1H-pyrazol-5(4H)-one [PMCPMP]:

It was prepared analogously from 1-(3-chlorophenyl)-3-methyl-1H-pyrazol-5(4H)-one and propionyl chloride. The colored crystals (PMCPMP) thus obtained were separated by filtration and recrystallized.

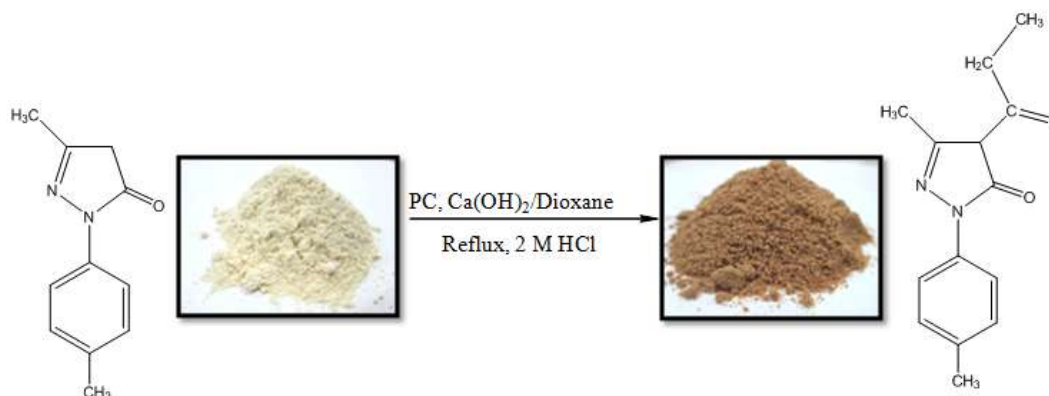


Scheme 1.5. Synthesis of PMCPMP

PMCPMP is brown crystals. Yield 69.6 % m.p. 86°C Anal. calc. for C₁₃H₁₃ClN₂O₂ M.W.: 264.71, C(58.99%), H(4.95%), N(10.58%), found: C(60.01%), H(4.86 %), N(10.54%); ¹HNMR (CDCl₃): δ ppm 1.25-1.29 (t, 3H, Propionyl C-CH₃), 2.48 (s, 3H, PZ C-CH₃), 2.77-2.82 (q, 2H, Propionyl -CH₂-), 7.24-7.93 (m, 4H, Ph); IR (KBr, cm⁻¹): 1585(s) (C=N, cyclic), 1634(m) (C=O, pyrazolone ring); ¹³C NMR (CDCl₃) δ ppm: 8.32 [C-CH₃, Propionyl], 15.79 [C-CH₃, PZ], 32.13 [-CH₂-, Propionyl], 161.18 [C=O, PZ], 118.13-138.39 [substituted benzene ring], 197.48 [C=O, Propionyl], 103.64 [>C-N-, PZ]; MS: m/z = 264.08 [C₁₃H₁₃ClN₂O₂, MIP]⁺, 266.08 [C₁₃H₁₃ClN₂O₂, (m+2) peak]⁺, 263 [C₁₃H₁₃ClN₂O₂, (m-1) peak]⁺, 236.15 [C₁₁H₉ClN₂O₂]⁺, 85.07 [C₃H₄N₂O]⁺, 96.81 [C₄H₄N₂O]⁺, 68.93 [C₅H₈]⁺, 219.21 [C₁₂H₁₄N₂O₂]⁺, 56.92 [C₄H₈, Base peak]⁺, 138.17 [C₁₁H₉ClN₂O₂]⁺, 125.16 [C₆H₈N₂O]⁺, 42.96 [C₃H₆]⁺.

1.3.2.3. 3-methyl-4-propionyl-1-*p*-tolyl-1H-pyrazol-5(4H)-one [PPTPMP]:

It was prepared analogously from 3-methyl-1-*p*-tolyl-1H-pyrazol-5(4H)-one and propionyl chloride. The colored crystals (PPTPMP) thus obtained were separated by filtration and recrystallized.



Scheme 1.6. Synthesis of PPTPMP

PPTPMP is brown crystals. Yield 70.5 % m.p. 100°C Anal. calc. for C₁₄H₁₆N₂O₂ M.W.: 244.29, C(68.83%), H(6.60%), N(11.47%), found: C(68.75%), H(6.43%), N(11.49%); ¹HNMR (CDCl₃): δ ppm 1.23-1.27 (t, 3H, Propionyl C-CH₃), 2.38 (s, 3H, TL C-CH₃), 2.47 (s, 3H, PZ C-CH₃), 2.76-2.81 (q, 2H, Propionyl -CH₂-), 7.24-7.70 (m, 4H, Ph); IR (KBr, cm⁻¹): 1547(s) (C=N, cyclic), 1626(m) (C=O, pyrazolone ring); ¹³C NMR (CDCl₃) δ: 8.13 [C-CH₃, Propionyl], 15.72 [C-CH₃, PZ], 21.02 [C-CH₃, TL], 32.61 [-CH₂-, Propionyl], 159.81 [C=O, PZ], 120.68-136.43 [substituted benzene rings], 198.43 [C=O, Propionyl], 103.31 [>C-N-, PZ]; MS: *m/z* = 244.33 [C₁₄H₁₆N₂O₂, MIP]⁺, 245.28 [C₁₄H₁₆N₂O₂, (m+1) peak]⁺, 243.57 [C₁₄H₁₆N₂O₂, (m-1) peak]⁺, 216.36 [C₁₂H₁₂N₂O₂]⁺, 214.56 [C₁₂H₁₀N₂O₂, Base peak]⁺, 215.32 [C₁₂H₁₁N₂O₂]⁺, 79.05 [C₆H₆]⁺, 90.90 [C₇H₇]⁺, 68.93 [C₅H₈]⁺, 56.98 [C₄H₈]⁺.

1.4. Characterization of 4-acyl pyrazolone ligands

1.4.1. Physicochemical properties

All these compounds are intensively coloured, air and moisture free crystalline solids. They are highly soluble in common organic solvents. Physicochemical data of

ligands are listed in section 1.3. The structure of the ligands can be confirmed from these data along with spectroscopic evidence discussed later. The elemental analysis matches well with the empirical formula of the ligands.

1.4.2. IR spectral studies

The IR spectra of 4-acyl pyrazolones have been studied extensively [104]. The differences in IR spectra between the two tautomers of 4-acyl pyrazolones have also been reported [105]. However, assignment of all the bands in the IR spectra of all the ligands is not straightforward due to overlapping bands. The IR spectrum of ligands itself has broad ill-defined features in the regions 3500-2000 and 1700-1000 cm^{-1} making C=O, C=N and aromatic stretching frequency assignments very difficult. The most important IR absorption bands of the ligands are presented in section 1.3.

There are two peaks attributed by the carbonyl groups for the keto form. The reason is that there are two types of carbonyl groups in the keto form: one is the free carbonyl in the toluoyl ring and the other is the hydrogen bonded carbonyl in the pyrazolone ring, based on the information obtained from ^1H and ^{13}C NMR studies in solution state (discussed later). The strong bands around 1630 and 1650 cm^{-1} range are assigned to $\nu_{\text{C=O}}$ of the pyrazolone-ring and $\nu_{\text{C=O}}$ of the toluoyl ring, respectively [106]. The strong band at 1500-1595 cm^{-1} is observed in all ligands, is assigned to $\nu_{\text{C=N}}$ of the pyrazolone ring, which also suggests that ligands exist as the keto form in solid state, consisting with the keto form. Several other definite IR peaks are also observed. All these suggest that structure of the ligands in the solid state is the keto form.

1.4.3. NMR spectral studies

The NMR spectra of all the ligands were recorded in CDCl_3 at room temperature. The NMR spectral data with their assignments are given in section 1.3.

1.4.3.1. ^1H NMR spectral studies

The proton NMR spectra of two of the ligands (PMCPMP & TPMP) are shown in Figs. 1.36 & 1.37, respectively. In both the spectra, the integral intensities of

each signal were found to agree with the number of different types of protons present. The much downfield signal observed in some of the ligands at $\sim \delta$ 11.6 ppm is characteristic of intramolecular H-bonded –OH/-NH proton.

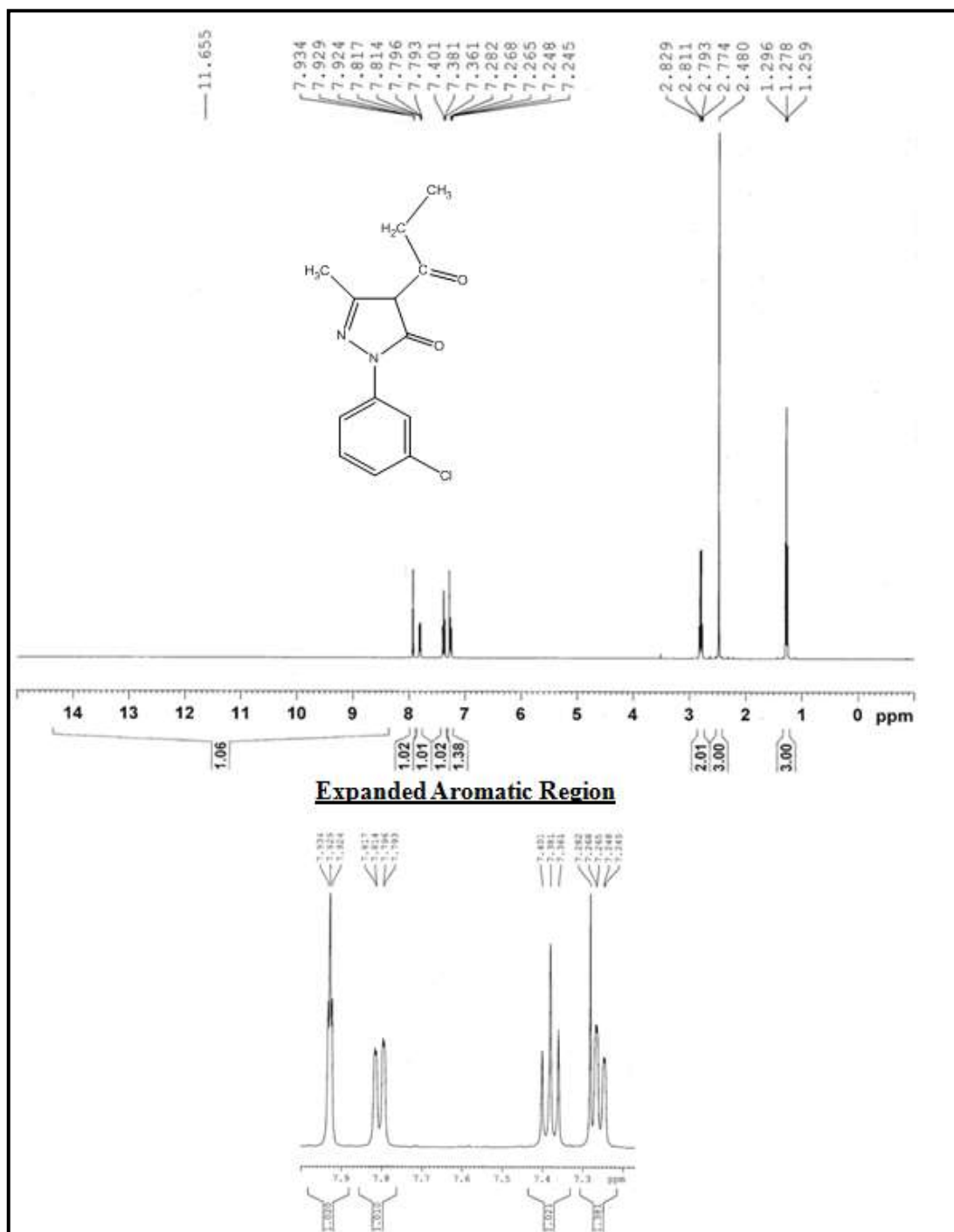


Fig. 1.36. ^1H NMR spectrum of the ligand PMCPMP

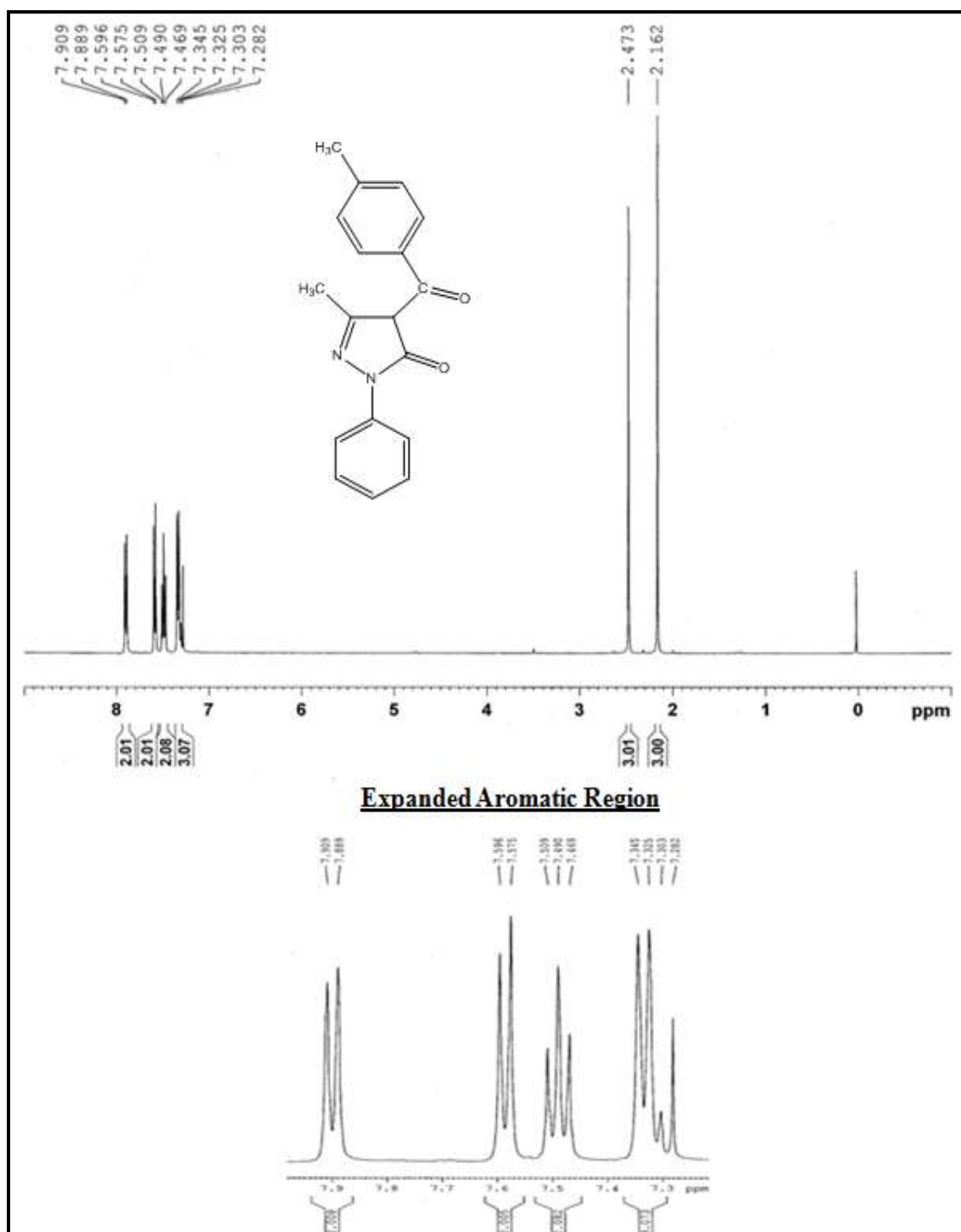


Fig. 1.37. ^1H NMR spectrum of the ligand TPMP

1.4.3.1.1. ^1H NMR spectral studies of 4-propionyl pyrazolones

In the aliphatic region, triplets corresponding to methyl protons of 4-propionyl group are observed in the range of δ 1.24-1.29 ppm. The methylene protons appear as a quartet in the range of δ 2.76-2.82 ppm in the spectra of both the ligands. 5-methyl protons of pyrazolone ring resonate at $\sim \delta$ 2.45 ppm [107]. The signal due to methyl group of pyrazolone ring is observed at $\sim \delta$ 2.48 ppm as singlet in the spectra of all the ligands. The signal due to *p*-substituted methyl group of ligand appears at $\sim \delta$ 2.38 ppm as a singlet in the NMR spectrum of PPTPMP. In the aromatic region, the aryl protons of two benzene rings resonate in the range of δ 7.24-7.93 ppm as multiplets.

1.4.3.1.2. ^1H NMR spectral studies of 4-toluoyl pyrazolones

In the aliphatic region, triplet corresponding to methyl protons of pyrazolone ring is observed in the range of δ 2.15-1.19 ppm. The methyl protons of toluoyl ring (one in case of TPMP and TMCPMP, two in case of TPTPMP) appeared as a singlet in the range of δ 2.40-2.47 ppm. In the aromatic region, a few doublets and in few cases some overlapping doublets/multiplets are observed in the range δ 7.28-7.98 ppm. These doublets/multiplets are due to aryl protons of three benzene rings.

1.4.3.2. ^{13}C NMR spectral studies

^{13}C NMR spectral data of the ligands (recorded in CDCl_3) are presented in section 1.3. The ^{13}C NMR spectra of ligands PPMP and TPMP are shown in Figs. 1.38 & 1.39, respectively.

1.4.3.2.1. ^{13}C NMR spectral studies of 4-propionyl pyrazolones

In the ^{13}C NMR spectra the carbon atoms of the methyl group of propionyl chain appear in the range δ 8.13–8.32 ppm in the spectra of all ligands. The carbon atoms of the methyl group of pyrazolone ring appear in the range 15.72-15.79 ppm in all the spectra. Similarly, in the spectra of all ligands, the signal due to methylene carbon of the propionyl group appears in the range 32.13-32.61 ppm. The carbon atom

of methyl group of toluoyl ring appears at δ 21.02 ppm in the case of PPTPMP. The singlet appearing for all ligands at $\delta \sim 103$ ppm is assigned to the carbon atom of the >C-N- moiety, the significant upfield shift is due to the electron-donating methyl group attached to it.

The carbon atoms of one benzene ring exhibit signals in the range δ 118.13-138.39 ppm and the number of signals vary from four to six. Four signals were observed for PPTPMP, as expected for the *p*-substituted benzene rings because of symmetry. However, PMCPMP shows six signals, as all carbon atoms are different due to the presence of -Cl. The PPMP also shows four signals.

In the low field region, three signals were observed around δ 147 and 160, which are associated with the carbon atoms of the heterocyclic ring. The most deshielded signal ($\delta \sim 198$ ppm) can be assigned to >C=O attached to the propionyl group.

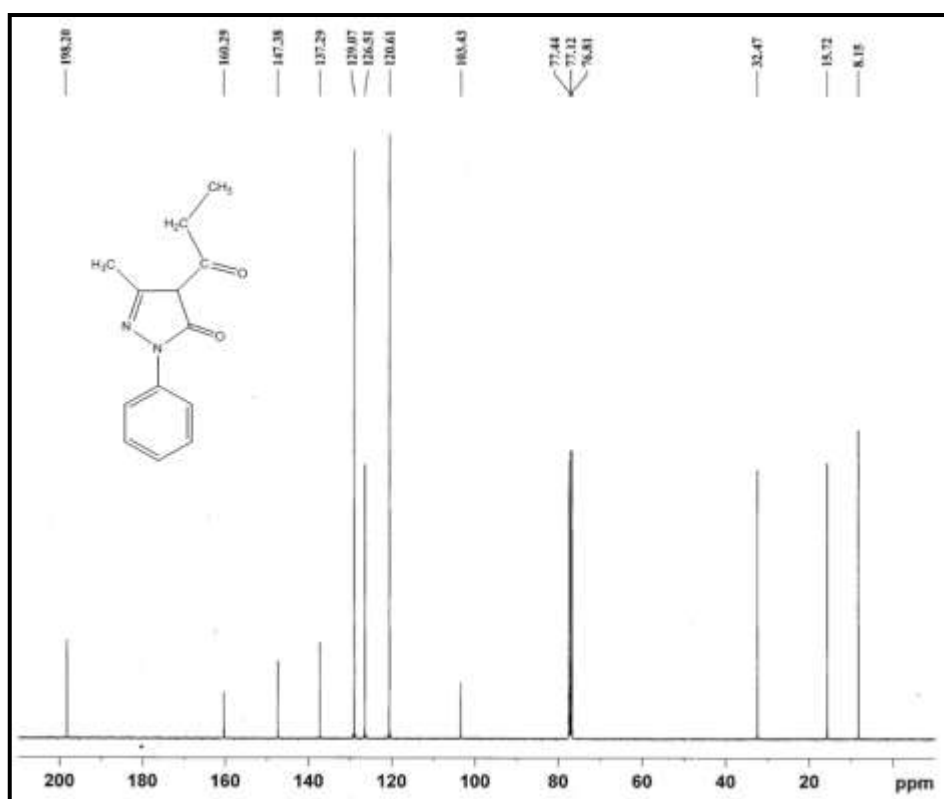


Fig. 1.38. ^{13}C NMR spectrum of PPMP

deshielded signal ($\delta \sim 191$ ppm) can be assigned to $>C=O$ attached to the toluoyl group.

1.4.4. Mass spectral studies

The mass spectral data of all the ligands with their tentative assignments are described in section 1.3. The mass spectra of two ligands PPMP and TPMP are shown in Figs. 1.40 & 1.41, respectively.

1.4.4.1. Mass spectral studies of 4-propionyl pyrazolone ligands

The mass spectra of the ligands are in good agreement with proposed structures. The electronic impact mass spectrum of PPMP is shown in (Fig. 1.40). It shows a molecular ion peak at m/z 230.02 with a relative intensity near to 70%, which is equivalent to its molecular weight.

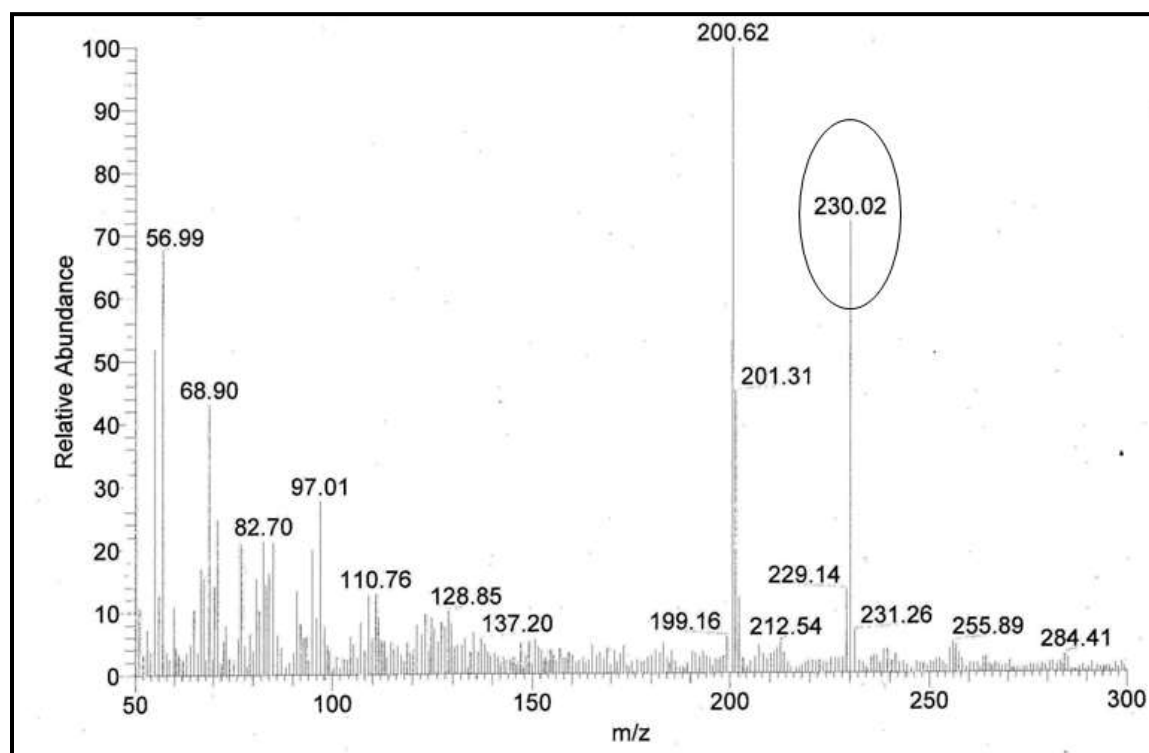


Fig. 1.40. The Mass spectrum of the PPMP

The mass spectra of the ligands revealed the molecular ion peak at m/z **230.02** (PPMP), m/z **264.08** (PMCPMP) and **244.33** (PPTPMP), which coincident with the formula weight (230.26) for PPMP, (264.71) for PMCPMP and (244.29) for PPTPMP support the identity of the proposed structures.

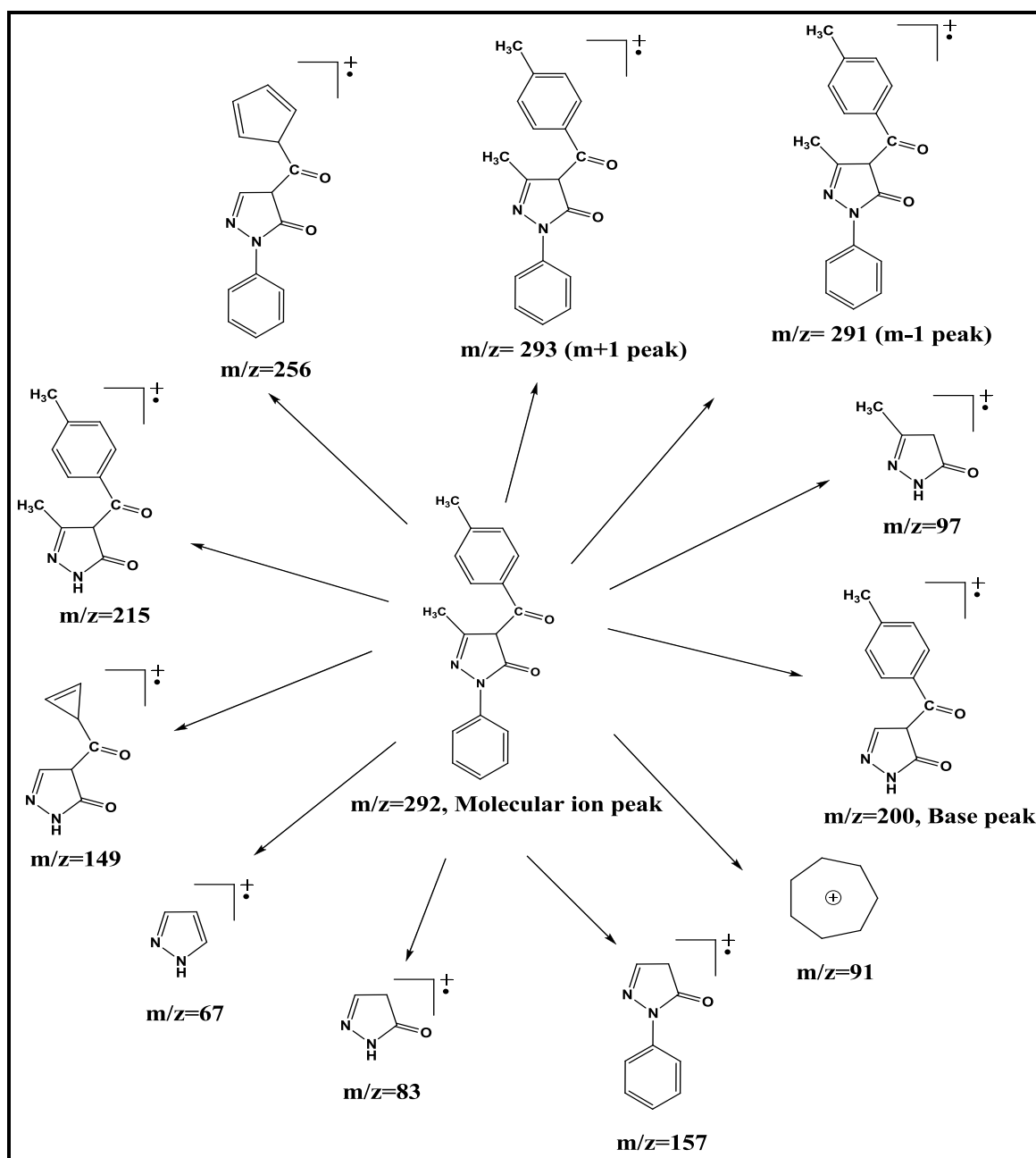
A peak corresponding to substituted pyrazolone can be observed at m/z (**200**) in the mass spectrum of PPMP, which itself is a base peak with 100% relative abundance, whereas in case of PMCPMP and PPTPMP, peaks at m/z 56.92 and 214.56 are the base peaks, respectively. Besides this, the (m+1), (m+2) and (m-1) peaks were observed in all the acylpyrazolone ligands.

1.4.4.2. Mass spectral studies of 4-toluoyl pyrazolone ligands

Fragmentation patterns of the ligands were obtained by mass spectrometry which is coupled with GC component as mentioned above. Normally the mass spectral fragmentation of the compound is found to give a characteristic pattern. Each kind of fragment has a particular ratio of mass to charge, or m/z value. For most ions, the charge is 1, so that m/z is simply the mass of the fragment. Thus, for ligand **TPMP** it exhibited a systematic fragmentation pattern (Scheme 1.7). The electronic impact mass spectrum of TPMP ligand is shown in (Fig. 1.43). It gave a molecular ion peak of m/z **292.07**, which is in good agreement with the molecular weight.

The mass spectra of the ligands revealed the molecular ion peak at m/z **292.07** of the TPMP, m/z **326.03** for the TMCPMP and m/z **306.08** for the TPTPMP, which coincident with the formula weight (292) for the TPMP, (326) for the TMCPMP and (306) for the TPTPMP support the identity of the proposed structures.

A peak corresponding to the 5 member pyrazolone ring with toluyl ring only can be observed at around m/z (**200**) in the mass spectra of all ligands, which is the base peak with 100% abundance. A peak corresponding to the substituted pyrazolone ring can also be observed at m/z (**214**) in the mass spectra of all ligands. A peak corresponding to the tropylium ion can be observed at m/z (**91**) in the mass spectra of all three ligands.



Scheme 1.7. Fragmentation pattern of the Schiff base ligand TPMP

The other peaks appeared in the mass spectrum (abundance range 1-100%) is attributed to the fragmentation of Schiff base molecules obtained from the rupture of different bonds inside the molecule. The fragmentation of the heterocycle rings, which includes pyrazole ring, is as a result of small and stable, neutral molecules,

which are analogous to HCN, such as C=NH as well as HC=CH and thus is not discussed herein.

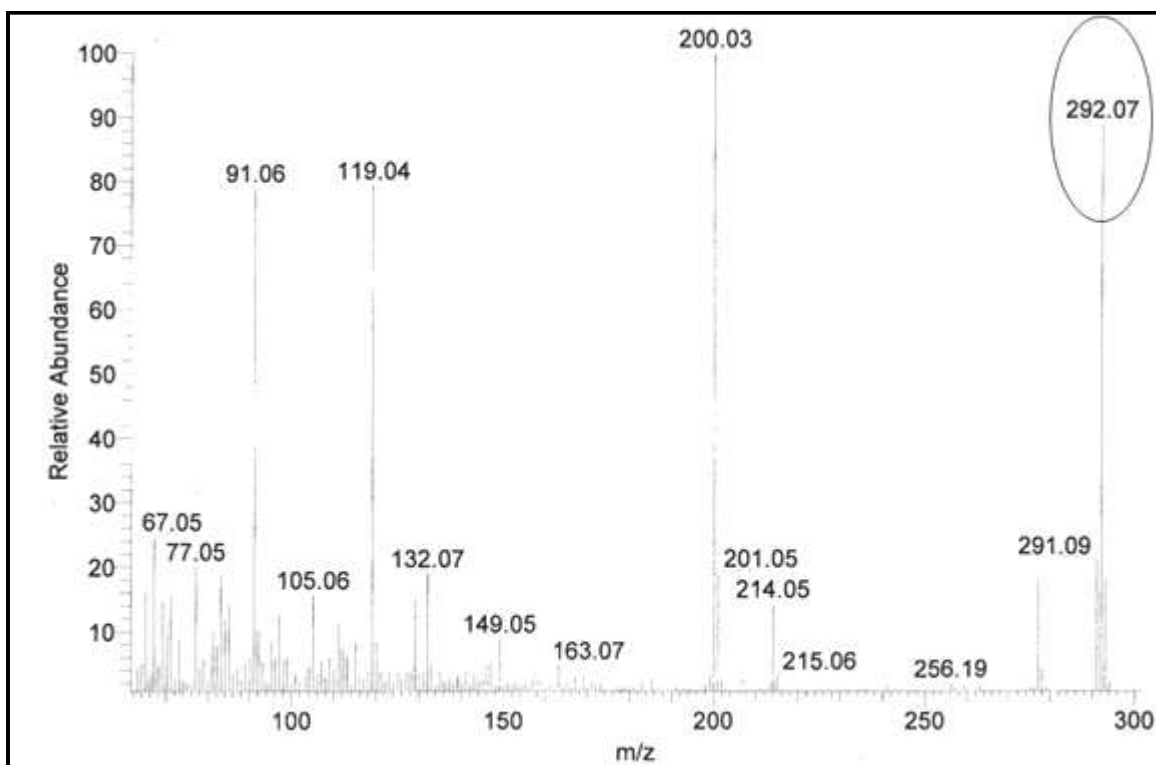


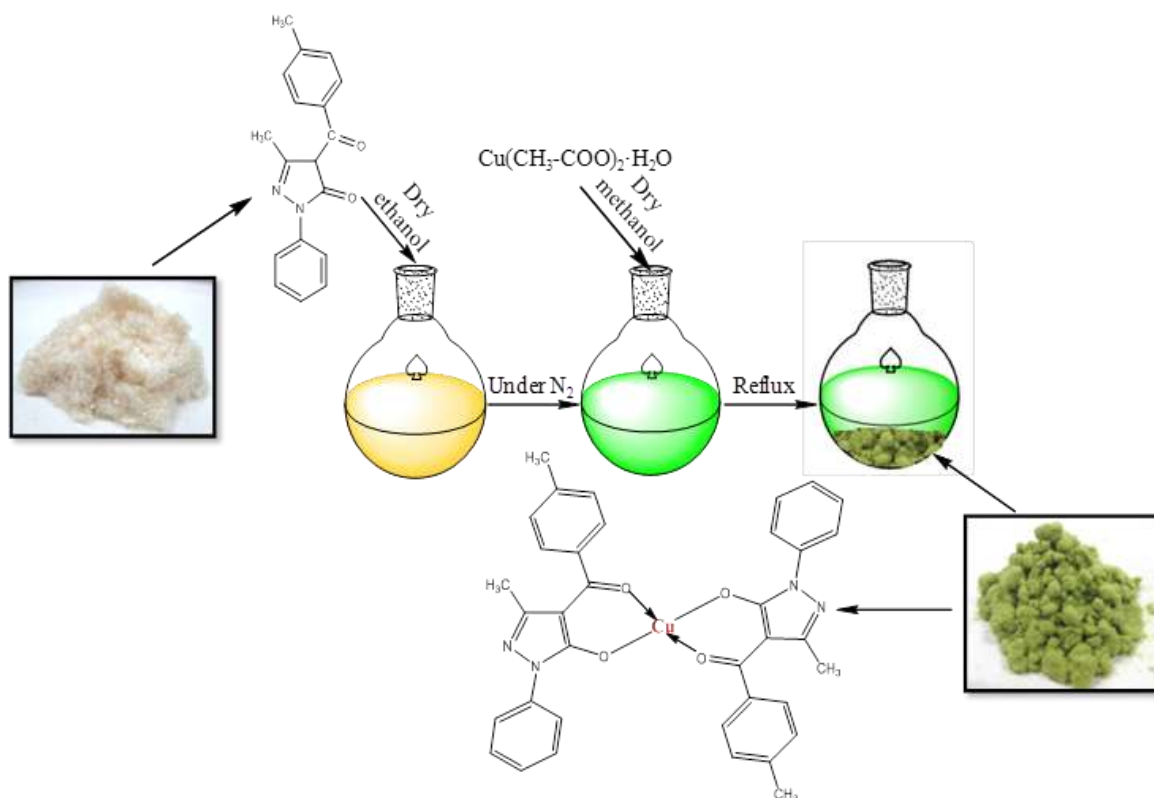
Fig. 1.41. The Mass spectrum of the TPMP

1.5. Syntheses of Cu(II) complexes of 4-acyl pyrazolones

1.5.1. Syntheses of binary complexes of 4-acyl pyrazolones

1.5.1.1. Cu(TPMP)₂ (1):

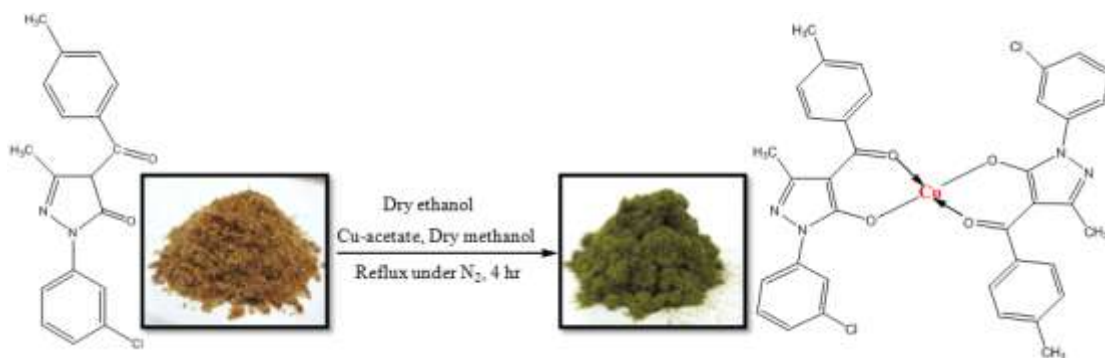
An ethanolic solution (60 cm³) of the ligand TPMP (0.584 gms, 2 mmol) was added to a methanolic solution (10 cm³) of Cu(OAc)₂·H₂O (0.199, 1mmol). A green precipitate was formed immediately. The reaction mixture was set aside overnight and the solid product was filtered off, washed with methanol and recrystallized from acetonitrile. The reaction was carried out under a N₂ stream [109].



Scheme 1.8. Synthesis of $\text{Cu}(\text{TPMP})_2$

1.5.1.2. $\text{Cu}(\text{TMCPMP})_2$ (2):

It was prepared analogously from TMCPMP and $\text{Cu}(\text{OAc})_2 \cdot \text{H}_2\text{O}$. The solid product thus obtained was filtered off, washed with methanol and recrystallized.



Scheme 1.9. Synthesis of $\text{Cu}(\text{TMCPMP})_2$

1.5.1.3. Cu(TPTPMP)₂ (3):



Scheme 1.10. Synthesis of Cu(TPTPMP)₂

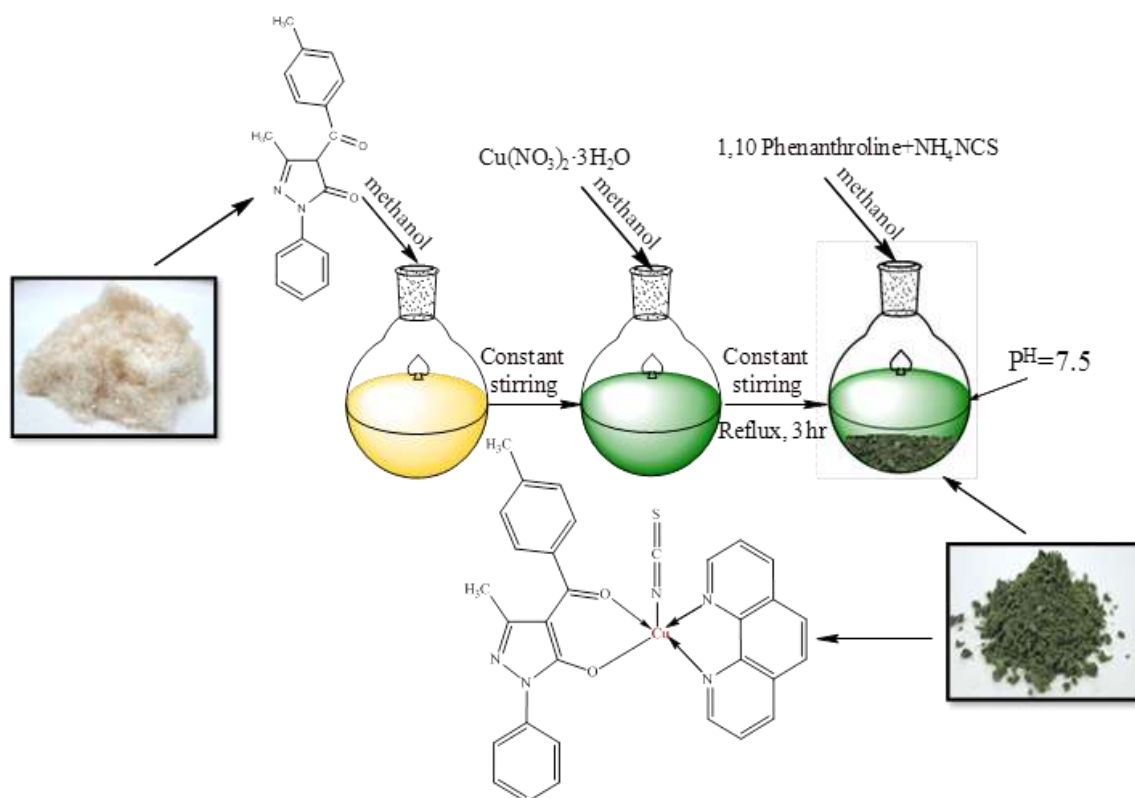
It was prepared analogously from TPTPMP and Cu(OAc)₂·H₂O. The solid product thus obtained was filtered off, washed with methanol and recrystallized.

1.5.2. Syntheses of ternary complexes

1.5.2.1. Syntheses of ternary complexes of 4-propionyl pyrazolones

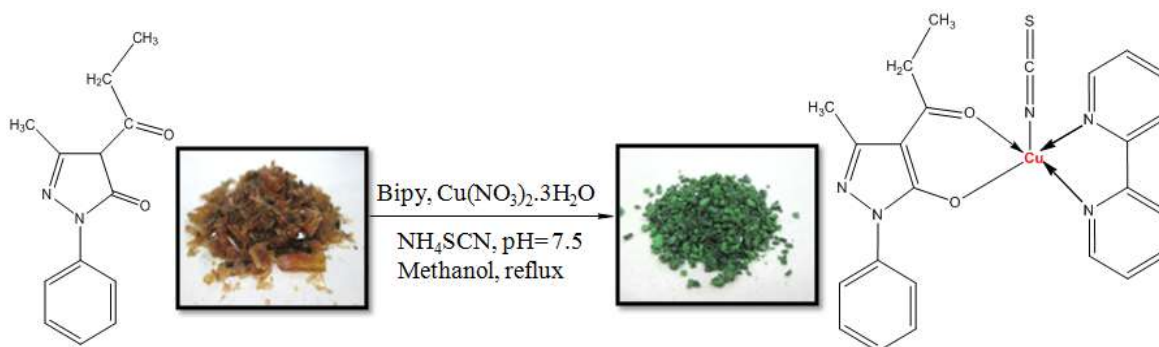
1.5.2.1.1. [Cu(PPMP)(Phen)NCS] (4)

To the solution of Cu(NO₃)₂·3H₂O (1mmol, 0.241 gms) in methanol (5 mL), a solution of PPMP (1 mmol, 0.230 g) in methanol (10 mL) was added while stirring. To this, a solution of 1, 10 phenanthroline (1 mmol, 0.198 g) in methanol (5 mL) was added, followed by a solution of NH₄NCS (2 mmol, 0.152 g) as appropriate in warm methanol (5 mL). The pH of the reaction mixture was maintained around 7.5 by adding a 10% methanolic solution of ammonia. The resultant mixture was refluxed for 3 h. The solid green crystalline product obtained was filtered off, washed with methanol and dried.



Scheme 1.11. Synthesis of $[\text{Cu}(\text{PPMP})(\text{Phen})\text{NCS}]$

1.5.2.1.2. $[\text{Cu}(\text{PPMP})(\text{Bipy})\text{NCS}]$ (5)

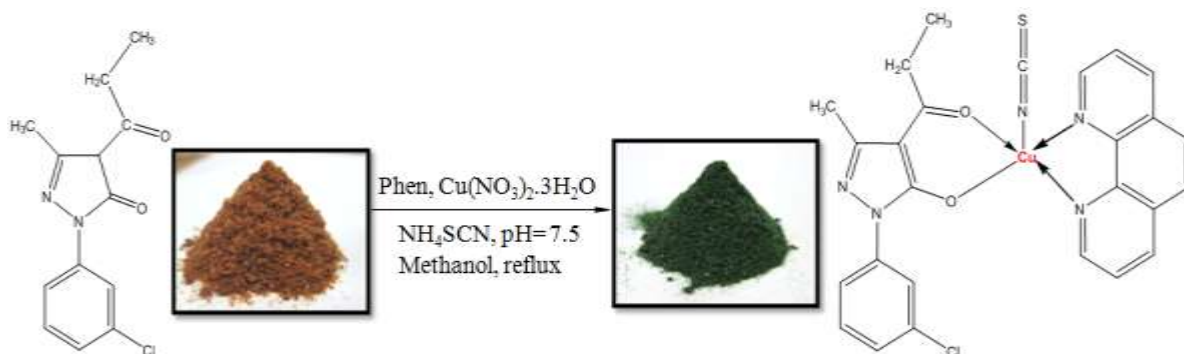


Scheme 1.12. Synthesis of $[\text{Cu}(\text{PPMP})(\text{Bipy})\text{NCS}]$

It was prepared analogously from PPMP, $\text{Cu}(\text{NO}_3)_2 \cdot 3\text{H}_2\text{O}$, 2, 2' bipyridyl and NH_4NCS . The solid green crystalline product obtained was filtered off, washed with methanol and dried.

1.5.2.1.3. [Cu(PMCPMP)(Phen)NCS] (6)

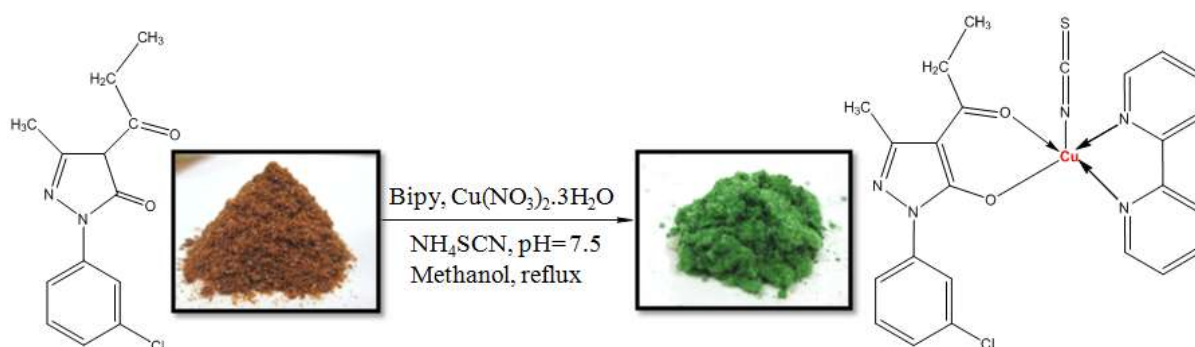
It was prepared analogously from PMCPMP, $\text{Cu}(\text{NO}_3)_2 \cdot 3\text{H}_2\text{O}$, 1, 10 phenanthroline and NH_4NCS . The solid green crystalline product obtained was filtered off, washed with methanol and dried.



Scheme 1.13. Synthesis of [Cu(PMCPMP)(Phen)NCS]

1.5.2.1.4. [Cu(PMCPMP)(Bipy)NCS] (7)

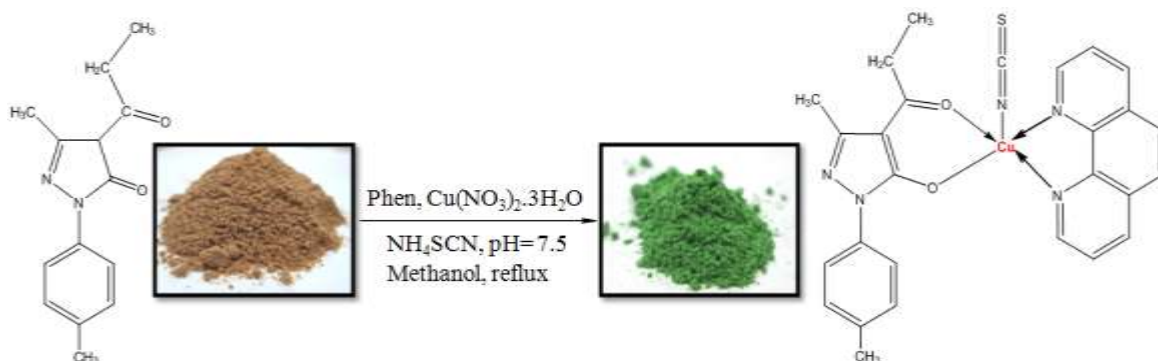
It was prepared analogously from PMCPMP, $\text{Cu}(\text{NO}_3)_2 \cdot 3\text{H}_2\text{O}$, 2, 2' bipyridyl and NH_4NCS . The solid green crystalline product obtained was filtered off, washed with methanol and dried.



Scheme 1.14. Synthesis of [Cu(PMCPMP)(Bipy)NCS]

1.5.2.1.5. [Cu(PPTPMP)(Phen)NCS] (8)

It was prepared analogously from PPTPMP, $\text{Cu}(\text{NO}_3)_2 \cdot 3\text{H}_2\text{O}$, 1, 10 phenanthroline and NH_4NCS . The solid green crystalline product obtained was filtered off, washed with methanol and dried.



Scheme 1.15. Synthesis of [Cu(PPTPMP)(Phen)NCS]

1.5.2.1.6. [Cu(PPTPMP)(Bipy)NCS] (9)

It was prepared analogously from PPTPMP, $\text{Cu}(\text{NO}_3)_2 \cdot 3\text{H}_2\text{O}$, 2, 2' bipyridyl and NH_4NCS . The solid green crystalline product obtained was filtered off, washed with methanol and dried.



Scheme 1.16. Synthesis of [Cu(PPTPMP)(Bipy)NCS]

1.5.2.2. Syntheses of ternary complexes of 4-toluoyl pyrazolones

1.5.2.2.1. [Cu(TPMP)(Phen)NCS] (10)

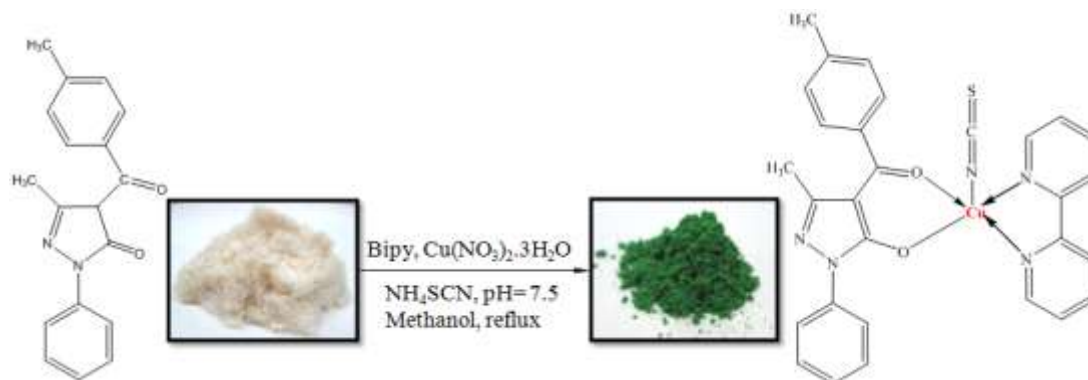
It was prepared analogously from TPMP, $\text{Cu}(\text{NO}_3)_2 \cdot 3\text{H}_2\text{O}$, 1, 10, phenanthroline and NH_4NCS . The solid green crystalline product obtained was filtered off, washed with methanol and dried.



Scheme 1.17. Synthesis of [Cu(TPMP)(Phen)NCS]

1.5.2.2.2. [Cu(TPMP)(Bipy)NCS] (11)

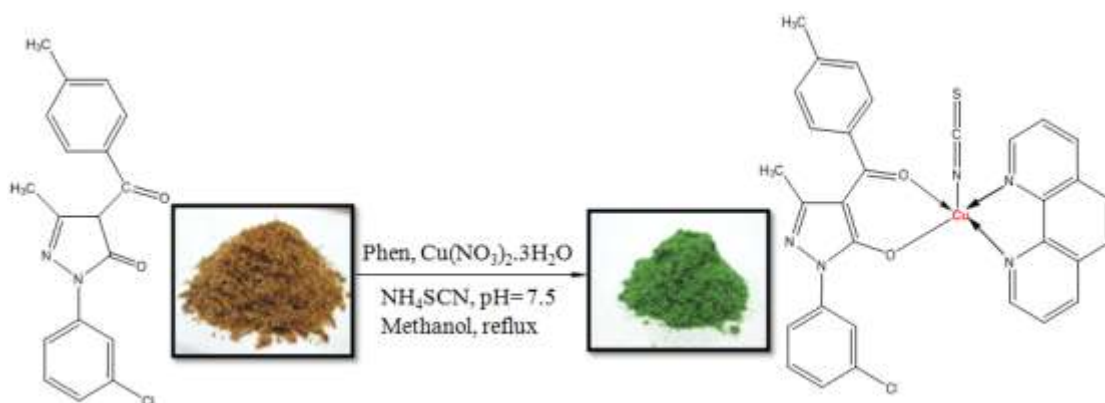
It was prepared analogously from TPMP, $\text{Cu}(\text{NO}_3)_2 \cdot 3\text{H}_2\text{O}$, 2, 2' bipyridyl and NH_4NCS . The solid green crystalline product obtained was filtered off, washed with methanol and dried.



Scheme 1.18. Synthesis of [Cu(TPMP)(Bipy)NCS]

1.5.2.2.3. [Cu(TMCPMP)(Phen)NCS] (12)

It was prepared analogously from TMCPMP, $\text{Cu}(\text{NO}_3)_2 \cdot 3\text{H}_2\text{O}$, 1, 10 phenanthroline and NH_4NCS . The solid green crystalline product obtained was filtered off, washed with methanol and dried.



Scheme 1.19. Synthesis of [Cu(TMCPMP)(Phen)NCS]

1.5.2.2.4. [Cu(TMCPMP)(Bipy)NCS] (13)

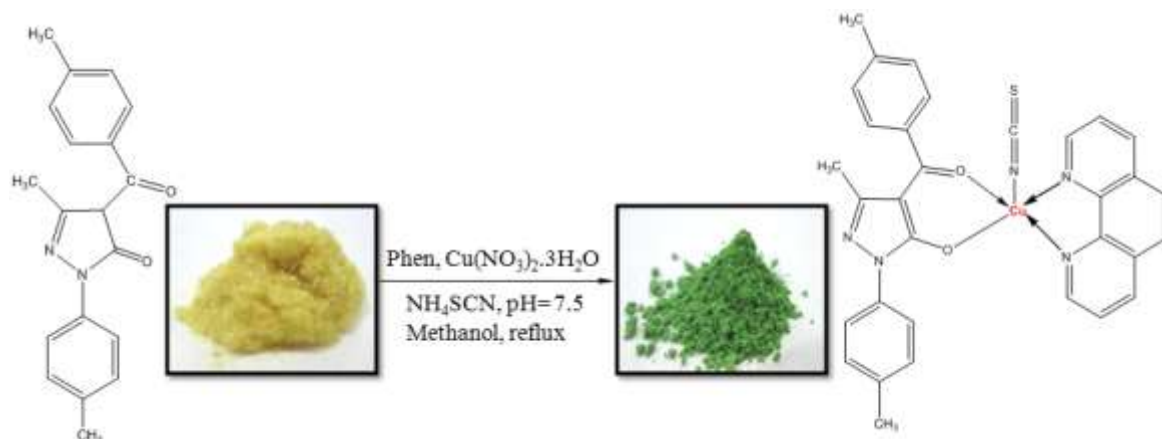
It was prepared analogously from TMCPMP, $\text{Cu}(\text{NO}_3)_2 \cdot 3\text{H}_2\text{O}$, 2, 2' bipyridyl and NH_4NCS . The solid green crystalline product obtained was filtered off, washed with methanol and dried.



Scheme 1.20. Synthesis of [Cu(TMCPMP)(Bipy)NCS]

1.5.2.2.5. [Cu(TPTPMP)(Phen)NCS] (14)

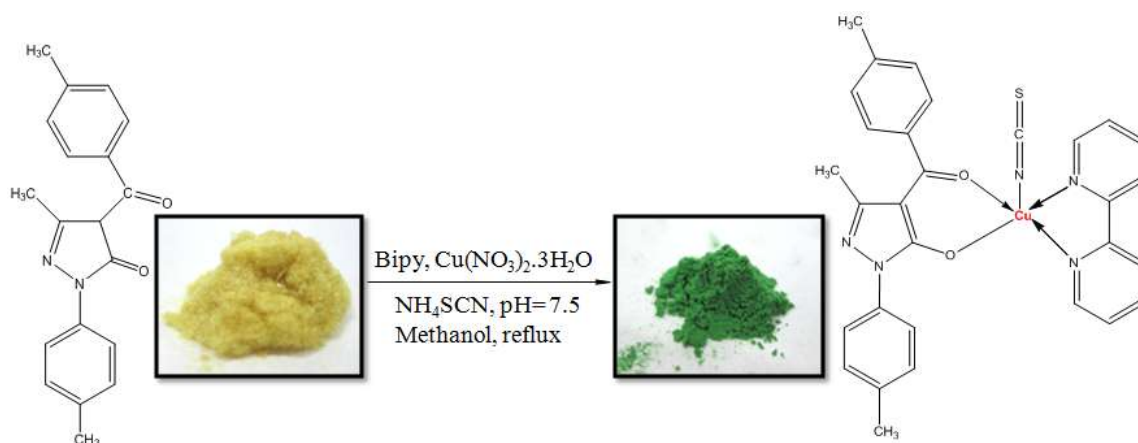
It was prepared analogously from TPTPMP, $\text{Cu}(\text{NO}_3)_2 \cdot 3\text{H}_2\text{O}$, 1, 10 phenanthroline and NH_4NCS . The solid green crystalline product obtained was filtered off, washed with methanol and dried.



Scheme 1.21. Synthesis of [Cu(TPTPMP)(Phen)NCS]

1.5.2.2.6. [Cu(TPTPMP)(Bipy)NCS] (15)

It was prepared analogously from TPTPMP, $\text{Cu}(\text{NO}_3)_2 \cdot 3\text{H}_2\text{O}$, 2, 2' bipyridyl and NH_4NCS . The solid green crystalline product obtained was filtered off, washed with methanol and dried.



Scheme 1.22. Synthesis of [Cu(TPTPMP)(Bipy)NCS]

1.6. Characterization of Cu(II) complexes of 4-acyl pyrazolones

1.6.1. Physicochemical properties of the synthesized complexes

The complexes have been synthesized in a very facile and essentially identical way. The Ligand acts as a bidentate O, O donor towards the metal(II) core. The complexes are obtained from a refluxing mixture of the respective ligand and metal salt precursors, taken in 1:2 (in the case of binary complexes) and (1:1 in case of ternary complexes) molar proportions in purified solvent. All these complexes are intensively colored, air and moisture free crystalline solids. They are insoluble in common organic solvents and only soluble in Acetonitrile, DMF and DMSO. Molar conductance value of the complexes soluble in DMF (10^{-3} M solution at room temperature), indicates that the complexes are electrically non-conducting in nature [110]. The elemental analyses data concur well with the planned formulae for the ligands and also recognized the $[ML_2(EtOH)_2]$ composition of the Ca(II) complex, $[ML_2]$ composition of Cu(II) binary complexes and $[M(L)(Phen/Bipy)NCS]$ for ternary complexes. The physicochemical and analytical data of the complexes are listed in Table 1.1.

Table 1.1. Physicochemical and analytical data of the complexes

Complexes	Formula Weight(g mol ⁻¹)	Colour	Yield (%)	Melting Point(°C)	Analysis (%) Found(calcd)				$\Lambda_M(\Omega^{-1} \text{cm}^2 \text{mol}^{-1})$
					C	H	N	Cu	
1	646.19	Green	44.62	>250	66.82 (66.91)	4.56 (4.68)	8.84 (8.67)	9.77 (9.83)	7
2	715.08	Green	45.73	>250	60.62 (60.47)	3.68 (3.95)	7.97 (7.83)	8.56 (8.89)	11
3	674.25	Green	41.04	>250	67.87 (67.69)	5.16 (5.08)	8.64 (8.31)	9.34 (9.42)	10
4	531.09	Dark green	80.35	>250	58.75 (58.80)	3.69 (3.99)	13.23 (13.19)	11.61 (11.97)	16
5	507.07	Dark green	86.59	>250	56.68 (56.85)	4.05 (4.17)	13.73 (13.81)	12.35 (12.53)	11
6	565.53	Dark green	82.98	>250	55.09 (55.22)	3.43 (3.56)	12.29 (12.38)	11.37 (11.24)	14
7	541.51	Dark green	84.62	>250	53.18 (53.23)	3.59 (3.72)	12.84 (12.93)	11.63 (11.73)	12
8	545.11	Green	87.22	>250	59.39 (59.49)	4.12 (4.25)	12.62 (12.85)	11.53 (11.66)	11
9	520.09	Dark green	84.68	>250	57.43 (57.62)	4.28 (4.45)	13.35 (13.44)	12.35 (12.19)	16
10	593.16	Dark green	89.99	>250	62.66 (62.77)	3.86 (3.91)	11.73 (11.81)	10.27 (10.71)	12
11	569.14	Dark green	86.78	>250	61.09 (61.20)	4.16 (4.07)	12.23 (12.31)	11.43 (11.17)	9
12	627.60	Dark green	88.62	>250	59.26 (59.33)	3.48 (3.53)	11.06 (11.16)	10.27 (10.13)	15
13	603.58	Dark green	85.23	>250	57.60 (57.71)	3.54 (3.67)	11.46 (11.60)	10.89 (10.53)	11
14	607.18	Green	84.33	>250	63.21 (63.30)	4.05 (4.15)	11.46 (11.53)	10.34 (10.47)	14
15	583.16	Green	81.65	>250	61.68 (61.79)	4.20 (4.32)	12.15 (12.01)	10.73 (10.90)	10

1.6.2. Crystal structure description

1.6.2.1. Crystal structure description of binary complexes

1.6.2.1.1. Intermediate $[\text{Ca}(\text{TPMP})_2(\text{EtOH})_2]$

In this chapter, the acyl pyrazolone ligands are used and prepared by method suggested by Jensen [24]. In contrast to conventional Claisen condensations, this method produces acyl derivative of the pyrazolone in good yield and is relatively easy to prepare. In these synthesis, condensations of acid chlorides with pyrazolones in dioxane, catalyzed by suspended calcium hydroxide results Ca(II) intermediate complex and then decomposition in 2M hydrochloric acid to give acyl pyrazolone ligands. The intermediate Ca(II) complex, $[\text{Ca}(\text{TPMP})_2(\text{EtOH})_2]$, was isolated for the first time by us and its crystal structure is also reported by us for the first time. The molecular structure of $[\text{Ca}(\text{TPMP})_2(\text{EtOH})_2]$ together with the atom-numbering scheme is illustrated in Fig. 1.42. The crystal packing of the complex projected down the *a* axis is illustrated in Fig. 1.43. The crystallographic data of the complex is listed in Table 1.2. Important bond lengths and angles for the complex are listed in Table 1.3. The X-ray analysis revealed that the complex is a 6-coordinate mononuclear Ca(II) complex with two oxygen atoms of the ethanol molecules and four oxygen atoms of two bidentate pyrazolonates. Taking into consideration that it usually adopts an octahedral conformation because of the large ligand field stabilization energy, this configuration is quite ideal. The coordination plane around Ca(1) ion is composed of O(1), O(2) and O(3) atoms with normal bond distances of Ca(1)–O(1):2.3215(15), Ca(1)–O(2):2.3301(16) and Ca(1)–O(3):2.3834(17) [91]. In the equatorial plane, the trans angles in O(2)–Ca(1)–O(2) and O(3)–Ca(1)–O(3) are exactly 180°, while 94.94(6)° for the angles of O(3)–Ca(1)–O(2) and O(2)–Ca(1)–O(3) and 85.06(6)° for the angles O(2)–Ca(1)–O(3) and O(3)–Ca(1)–O(2), add up to 360(24)° [91]. Bond angles show that the coordination geometry around the calcium ion in the complex is slightly distorted octahedral [111]. Atoms O(1) and O(2) of both the ligand molecules occupy the equatorial positions of the octahedron and O(3) atom of both the ethanol

molecules occupy two axial positions. Ca(II) is located in the center of the octahedral [111].

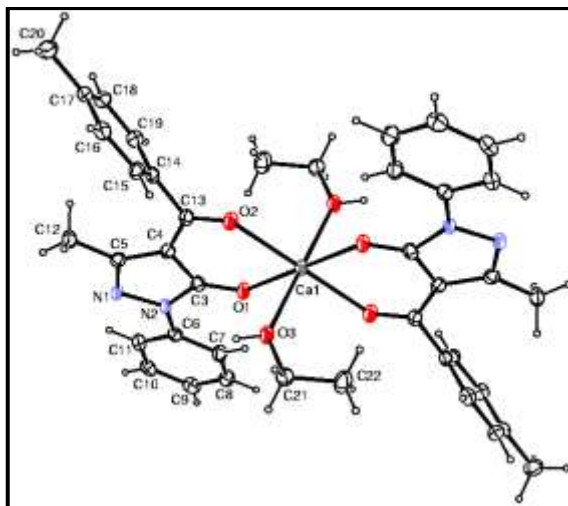


Fig. 1.42. The molecular structure of the $[\text{Ca}(\text{TPMP})_2(\text{EtOH})_2]$ complex, showing the atom numbering scheme. Displacement ellipsoids are drawn at the 50% probability level and H atoms are shown as small spheres of arbitrary radii. The Ca^{II} cation lies on an inversion centre.

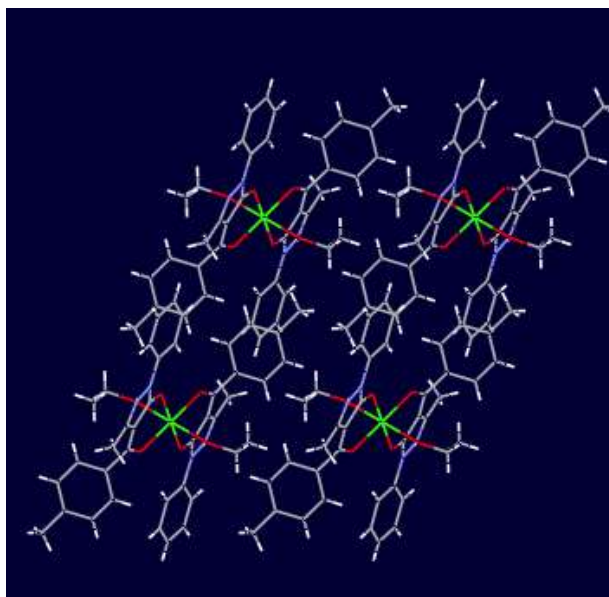


Fig. 1.43. The crystal packing of $[\text{Ca}(\text{TPMP})_2(\text{EtOH})_2]$ complex projected down the a axis

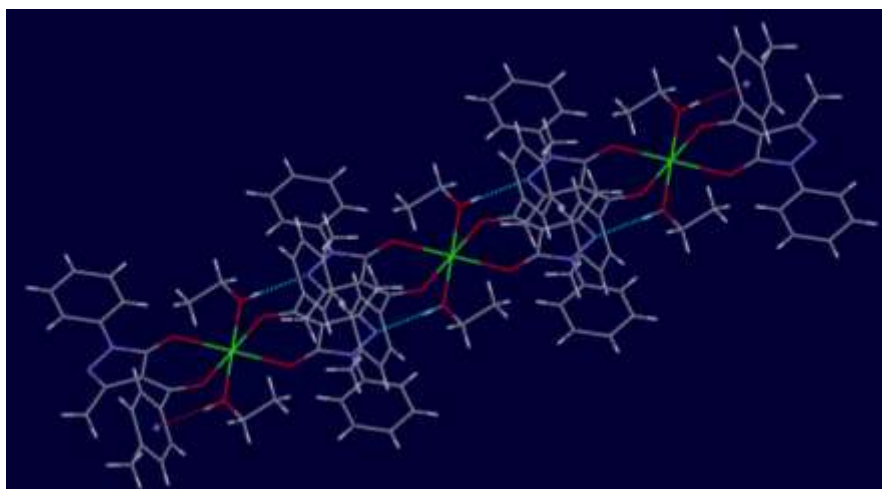


Fig. 1.44. A small portion of the 3D crystal structure of the $[\text{Ca}(\text{TPMP})_2(\text{EtOH})_2]$ complex due to hydrogen bonding interactions (dashed lines)

Table 1.2. Summary of crystallographic data for $[\text{Ca}(\text{TPMP})_2(\text{EtOH})_2]$ and complex 1

Complex	$[\text{Ca}(\text{TPMP})_2(\text{EtOH})_2]$	1
Chemical formula	$\text{C}_{40}\text{H}_{42}\text{CaN}_4\text{O}_6$	$\text{C}_{36}\text{H}_{30}\text{CuN}_4\text{O}_4$
Formula weight	714.86	646.18
Crystal description	Yellow Plate	Dark Green Rectangular
a(Å)	9.2055(18)	6.9189(3)
b(Å)	10.146(2)	9.3336(4)
c(Å)	11.039(2)	12.4621(6)
α (°)	109.522(3)	84.928(2)
β (°)	106.806(3)	83.774(2)
γ (°)	100.840(3)	72.492(3)
Z	1	1
V(Å ³)	882.7(3)	761.65(6)
Reflection collected	4818	12841
Independent Reflections	2661	2244
R(int)	0.0535	0.0324
Number of parameters	236	207
Crystal system	Triclinic	Triclinic
Space group	P-1	P-1
$\rho_{\text{calcd.}}$ (g cm ⁻³)	1.345	1.409
Abs coeff, μ (cm ⁻¹)	0.232	0.764
F(000)	378	335
Temp(°C)	23	23
GOF on F ²	1.014	1.002
R1 /wR2([I]>2 σ (I)])	0.0535 / 0.1321	0.0324 / 0.0877
R1 /wR2(all data)	0.0688 / 0.1422	0.0435 / 0.1017
CCDC	803539	809686

Table 1.3. Important bond lengths and angles for the complexes [Ca(TPMP)₂(EtOH)₂] and complex 1

Bond distances (Å) with es d's in parentheses		Bond angles(Å) with es d's in parentheses	
[Ca(TPMP)₂(EtOH)₂]			
Ca1 O1	2.3215(15)	O1 Ca1 O1	180.0
Ca1 O2	2.3301(16)	O1 Ca1 O2	78.96(5)
Ca1 O3	2.3834(17)	O1 Ca1 O2	101.04(5)
O1 C3	1.255(3)	O2 Ca1 O2	180.0
O2 C13	1.251(3)	O2 Ca1 O3	94.94(6)
O3 C21	1.440(3)	O1 Ca1 O3	93.32(6)
C4 C13	1.433(3)	O3 Ca1 O3	180.00(9)
C5 C12	1.498(3)	O1 Ca1 C3	161.86(5)
C14 C19	1.395(3)	O2 Ca1 C3	118.64(6)
C17 C20	1.512(3)	O1 Ca1 C3	161.86(5)
N1 N2	1.405(2)	C3 O1 Ca1	126.70(14)
N2 C6	1.414(3)	C13 O2 Ca1	133.75(15)
1			
Cu1 O1	1.9013(14)	O1 Cu1 O1	180.00(9)
Cu1 O2	1.9193(15)	O2 Cu1 O2	180.000(1)
C7 O1	1.271(2)	O1 Cu1 O2	93.18(6)
C9 O2	1.261(2)	C7 O1 Cu1	119.46(13)
N1 N2	1.397(2)	C9 O2 Cu1	129.29(14)
C9 C10	1.484(3)	O1 C7 N1	123.09(19)
C7 N1	1.363(3)	O1 C7 C8	130.86(19)
C16 N2	1.303(3)	O2 C9 C8	121.47(19)

In the complex, the bond length of O(1)-C(3) and O(2)-C(13) are 1.255(3) Å and 1.251(3) Å, respectively, which are shorter than 1.43 Å for a C–O single bond and longer than 1.22 Å for a C=O double bond length [111]. Moreover, the C(3)-N(2) bond length is close to the C=N double bond length, confirming that the keto form of the ligand tautomerizes to the enol form [91]. All atoms of the complex and the pyrazolone rings are not in the same plane. As a result, the compound is a non-planar molecule. The complex contains two ethanol molecules, which are bridged together through hydrogen bond and connect one pyrazolone-ring N(1) atom with the neighboring pyrazolone-ring N(1) atom through intermolecular hydrogen bonds [O(3)–H(3)...N(1)]. Thus, the molecules are stringed together as shown in Fig. 1.44, and three-dimensional non-planar molecule structure supramolecule is formed. In above, H-bonding interactions play an important role in forming the supramolecular structure by self-assembly and stabilizing. A small portion of the 3D crystal structure

of the complex due to hydrogen bonding interactions (dashed lines) is shown in Fig. 1.44.

1.6.2.1.2. Complex 1

The molecular structure of **1** together with the atom-numbering scheme is illustrated in Fig. 1.45. The crystal packing of the complex projected down the *a* axis is illustrated in Fig. 1.46. The crystallographic data of the complex is listed in Table 1.2. Important bond lengths and angles for the complex are listed in Table 1.3. The X-ray analysis revealed that the compound was a 4-coordinate mononuclear Cu(II) complex with the four oxygen atoms of two bidentate pyrazolonates [111]. The coordination plane around Cu(1) ion is composed of O(1) and O(2) atoms with normal bond distances of Cu(1)–O(1): 1.9013(14), and Cu(1)–O(2): 1.9193(15) [84]. In the equatorial plane, the trans angles in O(1)–Cu(1)–O(1) and O(2)–Cu(1)–O(2) are exactly 180°, while 93.18(6)° for the angles of O(1)–Cu(1)–O(2) and O(1)–Cu(1)–O(2) and 86.82(6)° for the angles O(1)–Cu(1)–O(2) and O(1)–Cu(1)–O(2), add up to 360(24)° [85, 111]. Bond angles show that the coordination geometry around the copper ion in the complex is slightly square planer. Atoms O(1) and O(2) of both the ligand molecules occupy the equatorial positions of the square plane and Cu(II) is located in the center of the plane [84].

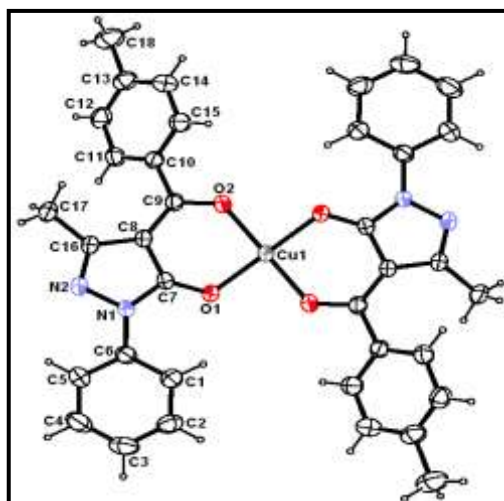


Fig. 1.45. ORTEP view of the complex **1** with displacement ellipsoids drawn at 50%. H atoms are shown as small spheres of arbitrary radii

In the complex, the bond length of O(1)-C(7) and O(2)-C(9) are 1.271(2) Å and 1.261(2) Å, respectively, which are shorter than 1.43 Å for a C–O single bond and longer than 1.22 Å for a C=O double bond length [85, 111]. Moreover, the C(7)-N(1) bond length is close to the C=N double bond length, confirming that the keto form of the ligand isomerizes to the enol form. All atoms of the complex and the pyrazolone rings are in the same plane. As a result, the complex is a planar molecule.

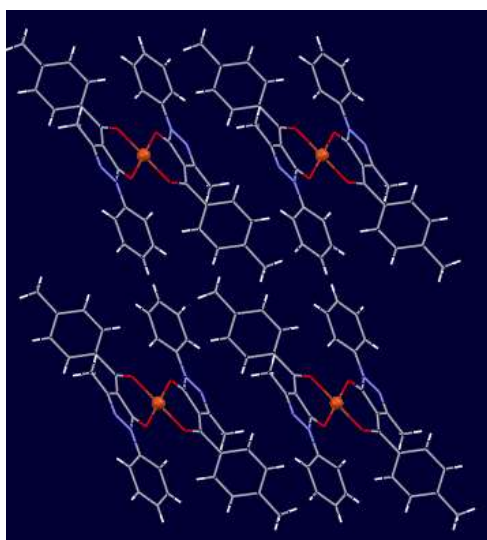


Fig. 1.46. The packing arrangement of complex **1** viewed down the *a*-axis.

1.6.2.2. Crystal structure description of ternary complexes

The five complexes have been characterized by X-ray crystallography. The crystallographic data of these complexes are listed in Table 1.4.

To obtain the quantitative degree of distortion of the copper polyhedron the ratio between the two basal angles, defined as $\tau = [(\theta-\phi)/60]$, that represents the trigonal distortion from square pyramidal geometry [112], was used. For an ideal SP, τ is 0 while for an ideal TBP τ is 1. As these complexes are pentacoordinated, τ values have been calculated for all the complexes. Therefore we can find out the degree of distortion of the polyhedron from SP to TBP.

1.6.2.2.1. Ternary complexes containing 4-propionyl pyrazolones

1.6.2.2.1.1. Complex 5

The molecular structure of **5** together with the atom-numbering scheme is illustrated in Fig. 1.47. The crystal packing of the complex projected down the *c* axis is illustrated in Fig. 1.48. As shown in Fig. 1.47, the crystallographically independent Cu(II) ion is pentacoordinated by three nitrogen atoms (N16-thiocyanate, bipy-N19 and N30) and two oxygen donors (pyrazolone-O1 and O2). The coordination sphere is of the type Cu-N19-N30-O1-O2-N16, exhibiting a geometry close to square pyramidal (SP). The coordination geometry of the complex can best be described as square pyramidal (SP) with O1, O2, N19 and N30 forming the plane, and N16 occupying axial position, with a slight deviation at the axial site. The Cu–O1 bond length is the shortest bond length followed by Cu–O2.

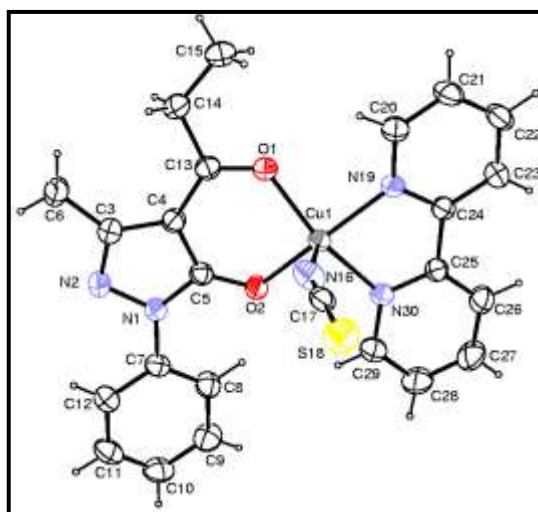


Fig. 1.47. ORTEP view of the complex **5** with displacement ellipsoids drawn at 50%. H atoms are shown as small spheres of arbitrary radii

A distorted SP arrangement can be visualized as N19, N30, O1 and O2 form an approximate square plane and N16 occupies an axial position. Although the expected bond angle formed by the axial N16 atom with any other donor atom is 90° at the copper centre, it is observed to vary in the range 98.99 - 103.37° , suggesting slight distortion from an ideal sp arrangement [87].

Table 1.4. Summary of crystallographic data of the ternary complexes

Complex	5	9	10	11	13
Chemical formula	C ₂₄ H ₂₁ CuN ₅ O ₂ S	C ₂₅ H ₂₃ CuN ₅ O ₂ S	C ₃₁ H ₂₃ CuN ₅ OS, C ₂ H ₃ N	C ₂₉ H ₂₃ CuN ₅ O ₂ S, 0.5 CH ₃ OH	C ₂₉ H ₂₂ ClCuN ₅ O ₂ S
Form. Weight	507.06	521.08	634.20	585.15	603.57
a(Å)	8.1512(2)	8.4591(5)	11.0580(5)	24.894(2)	10.0100(15)
b(Å)	8.5064(2)	10.9739(14)	12.2614(5)	8.8679(6)	10.8736(16)
c(Å)	17.9150(6)	14.3201(19)	12.9478(5)	25.108(2)	13.259(2)
α(°)	103.396(2)	111.090(12)	113.881(4)	90.00	76.147(14)
β(°)	93.458(2)	93.411(7)	109.248(4)	101.798(9)	80.058(13)
γ(°)	107.537(3)	102.790(8)	90.425(3)	90.00	71.423(14)
Z	2	2	2	8	2
V(Å ³)	1140.82(5)	1195.3(2)	1495.20(11)	5425.7(8)	1320.9(4)
Refl. collected	30635	7202	21841	11018	7953
Ind. Refl.	4473	3985	5244	5319	4590
R(int)	0.0350	0.1088	0.0357	0.0343	0.0711
No. of param.	382	309	391	359	352
Crystal system	Triclinic	Triclinic	Triclinic	monoclinic	Triclinic
Space group	P-1	P-1	P-1	C2/c	P-1
ρ _{calcd.} (g cm ⁻³)	1.476	1.448	1.409	1.433	1.518
Abs coeff, μ(cm ⁻¹)	1.081	1.034	0.841	0.921	1.045
F(000)	522	538	654	2416	618
Temp(°C)	23	23	23	23	23
GOF on F ²	1.046	0.937	1.008	1.027	1.033
R1/wR2 ([I>2σ(I)])	0.0311/0.0754	0.0978/0.1949	0.0366/0.0894	0.0522/0.1274	0.0824/0.1088
R1/wR2 (all data)	0.0382/0.0794	0.2036/0.2280	0.0465/0.0946	0.0886/0.1502	0.1628/0.1381
CCDC	869540	865764	842200	865376	868564

The deviation from a perfect TBP as well as SP structure may be due to the difference in the electronegativities of all the different coordinating atoms in the equatorial as well as axial sites, resulting in different bond lengths and bond angles. A comparison of the bond lengths of the central metal-donor atoms shows that the two oxygen donors and two nitrogen donors are almost similar in the nature of coordination. This has a net effect that the five bond lengths are almost similar,

resulting in SP structure. Similarly, the adjacent five and six membered chelate rings might also be responsible for distortion from either of the ideal geometries.

For this complex (see Fig. 1.47 for labelling) the relevant angles, $\theta = 160.46$ and $\phi = 160.10$ (Table 1.5) yields a τ value of 0.006 which is almost near to 0 and it indicates a geometry close to SP.

Table 1.5. Selected bond lengths and angles in the ternary complexes of 4-propionyl pyrazolones

5		9	
Bond distances (Å) with esd's in parentheses			
Cu1 O2	1.9534(14)	Cu1 O2	1.928(6)
Cu1 O1	1.9687(14)	Cu1 O1	1.967(6)
Cu1 N30	1.9991(17)	Cu1 N19	2.000(6)
Cu1 N19	2.0082(16)	Cu1 N30	2.054(7)
Cu1 N16	2.134(2)	Cu1 N17	2.136(11)
O1 C13	1.256(2)	S1 C18	1.606(15)
O2 C5	1.279(2)	O1 C14	1.247(9)
N16 C17	1.154(3)	O2 C5	1.304(9)
C17 S18	1.621(3)	N17 C18	1.177(14)
N19 C20	1.338(3)	N19 C24	1.339(10)
N19 C24	1.341(3)	N19 C20	1.354(11)
C25 N30	1.347(3)	C25 N30	1.329(10)
C29 N30	1.344(3)	C29 N30	1.314(10)
Bond angles (Å) with esd's in parentheses			
O2 Cu1 O1	92.55(6)	O2 Cu1 O1	93.1(3)
O2 Cu1 N30	90.46(6)	C5 O2 Cu1	121.4(6)
O1 Cu1 N30	160.10(7)	O2 Cu1 N19	161.4(3)
O2 Cu1 N19	160.46(7)	O1 Cu1 N19	91.8(3)
O1 Cu1 N19	90.10(6)	O2 Cu1 N30	88.9(3)
N30 Cu1 N19	80.77(7)	O1 Cu1 N30	160.3(3)
O2 Cu1 N16	98.99(7)	N19 Cu1 N30	80.5(3)
O1 Cu1 N16	95.58(8)	O2 Cu1 N17	98.9(3)
N30 Cu1 N16	103.37(8)	O1 Cu1 N17	96.2(3)
N19 Cu1 N16	100.02(7)	N19 Cu1 N17	98.4(3)
C13 O1 Cu1	127.96(13)	N30 Cu1 N17	102.8(4)
C5 O2 Cu1	119.45(12)	C14 O1 Cu1	128.2(6)
C17 N16 Cu1	160.1(2)	O2 C5 N1	121.9(8)
N16 C17 S18	179.5(2)	O2 C5 C4	129.0(7)
C20 N19 Cu1	126.35(16)	O1 C14 C4	121.3(8)
C24 N19 Cu1	114.71(13)	O1 C14 C15	117.3(8)
C29 N30 Cu1	126.72(16)	C29 N30 Cu1	124.7(6)
C25 N30 Cu1	114.97(13)	C25 N30 Cu1	113.7(6)

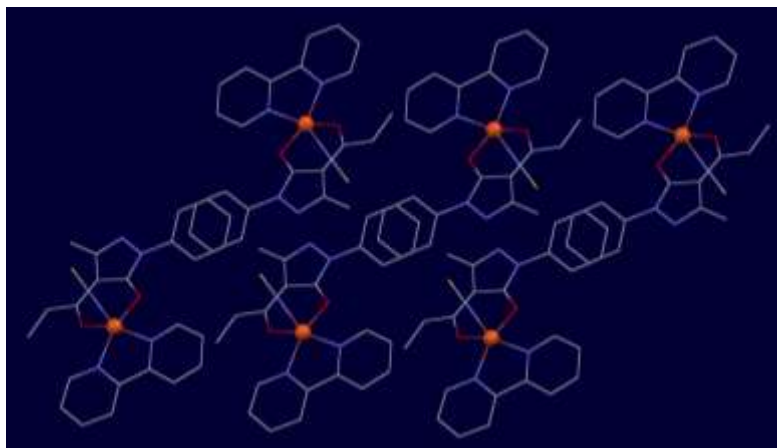


Fig. 1.48. The packing arrangement of complex **5** viewed down the *c*-axis

1.6.2.2.1.2. Complex **9**

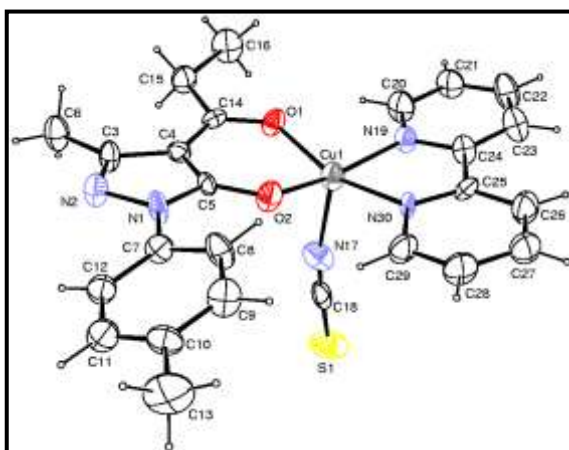


Fig. 1.49. *ORTEP* view of the complex **9** with displacement ellipsoids drawn at 50%. H atoms are shown as small spheres of arbitrary radii

The molecular structure of **9** together with the atom-numbering scheme is illustrated in Fig. 1.49. The crystal packing of the complex projected down the *c* axis is illustrated in Fig. 1.50. In this complex, everything is similar to the complex **5**. The only difference is the thiocyanate-N has been labeled as N17, when it is N16 in the case of **5**. The coordination sphere is of the type Cu-N19-N30-O1-O2-N17, exhibiting a geometry of slightly distorted square pyramidal (SP). The coordination geometry of the complex can best be described with O1, O2, N19 and N30 forming the plane, and

N17 occupying axial position, with a slight deviation at the axial site. The Cu–O1 bond length is the shortest bond length followed by Cu–O2.

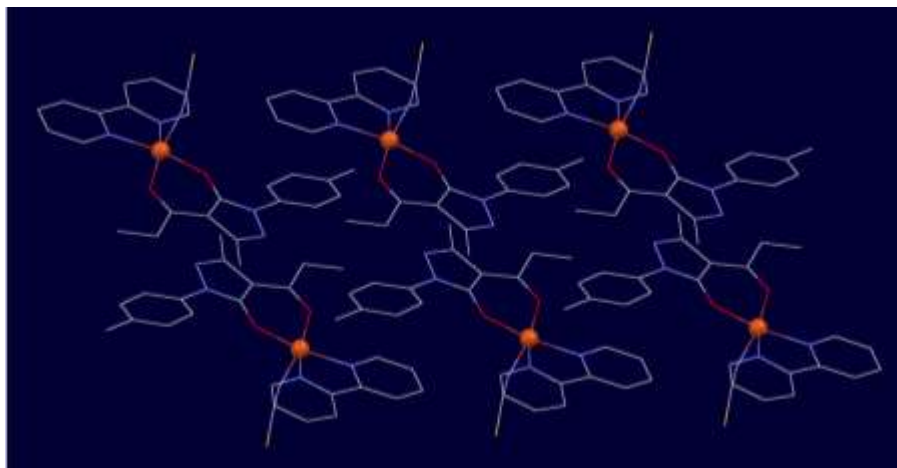


Fig. 1.50. The packing arrangement of complex **9** viewed down the *c*-axis.

For this complex (see Fig. 1.49 for labelling) the relevant angles, $\theta = 161.4$ and $\varphi = 160.3$ (Table 1.5) yields a τ value of 0.018 which is almost near to 0 and it indicates a geometry of slightly distorted SP.

1.6.2.2.2. Ternary complexes containing 4-toluoyl pyrazolones

1.6.2.2.2.1. Complex 10

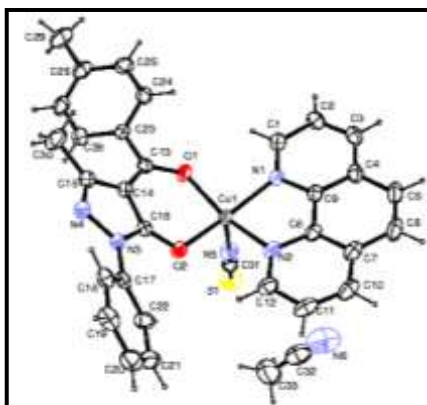


Fig. 1.51. ORTEP view of the complex **10** with displacement ellipsoids drawn at 50%. H atoms are shown as small spheres of arbitrary radii

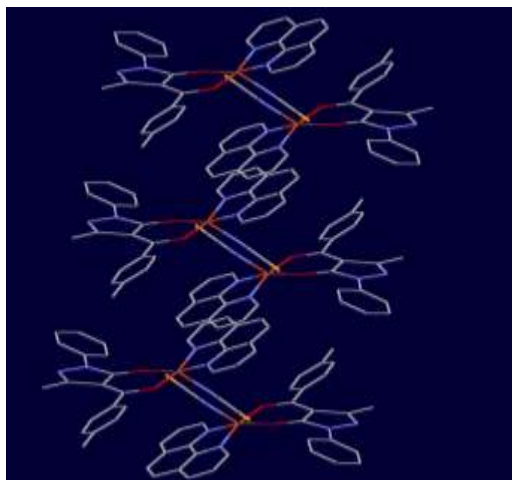


Fig. 1.52. The packing arrangement of **10** viewed down the *c*-axis

The molecular structure of **10** together with the atom-numbering scheme is illustrated in Fig. 1.51. The crystal packing of the complex projected down the *c* axis is illustrated in Fig. 1.52. The structure of the complex consists of two discrete monomeric Cu(II) species in the unit cell of the triclinic crystal system belonging to the space group P1 with the metal in a (4 + 1) square-pyramidal CuN_3O_2 coordination geometry and two lattice acetonitrile molecules. The TPMP and phen ligands are coordinated in a bidentate fashion to the metal ion Cu1 through oxygen (O1 and O2 of pyrazolone) and nitrogen (N1 and N2 of phen) atoms forming the equatorial plane. The NCS^- molecule is coordinated to Cu1 via nitrogen atom ($\text{Cu1}\dots\text{N5}=2.139(2)$ Å) at the axial position, generating neutral distorted square pyramidal complex in the same crystal lattice. Unlike in crystals of the complex, there is no H-bond network, as there are no solvent water molecules or anions in the lattice. The bond angles and bond lengths are in good agreement with the earlier reports for a square pyramidal Cu(II) complexes [87, 113].

For this complex (see Fig. 1.51 for labelling) the relevant angles, $\theta = 162.13$ and $\phi = 160.79$ (Table 1.6) yields a τ value of 0.022 which is almost near to 0 and it indicates a geometry close to SP. The coordination sphere is of the type Cu1-N1-N2-N5-O2-O1, exhibiting a geometry near to square pyramidal (SP).

1.6.2.2.2. Complex 11

The molecular structure of **11** together with the atom-numbering scheme is illustrated in Fig. 1.53. The crystal packing of the complex projected down the *b* axis is illustrated in Fig. 1.54. The structure of the complex consists of two discrete monomeric Cu(II) species in the unit cell of the monoclinic crystal system belonging to the space group *C2/c* with the metal in a (4+1) square-pyramidal CuN_3O_2 coordination geometry. The TPMP and bipy ligands are coordinated in a bidentate fashion to the metal ion Cu1 through oxygen (O1 and O2 of pyrazolone) and nitrogen (N21 and N32 of bipy) atoms forming the equatorial plane. The NCS^- molecule is coordinated to Cu1 *via* nitrogen atom ($\text{Cu1}\dots\text{N3}=2.442(4)$ Å) at the axial position, generating neutral square pyramidal complex in the same crystal lattice. The bond angles and bond lengths are in good agreement with the earlier reports for a square pyramidal Cu(II) complexes [87, 113].

For this complex (see Fig. 1.53 for labelling) the relevant angles, $\theta = 168.88$ and $\phi = 167.04$ (Table 1.6) yields a τ value of 0.018 which is almost near to 0 and it indicates a geometry close to SP. The coordination sphere is of the type Cu1-N21-N32-N3-O1 , exhibiting a geometry near to square pyramidal (SP).

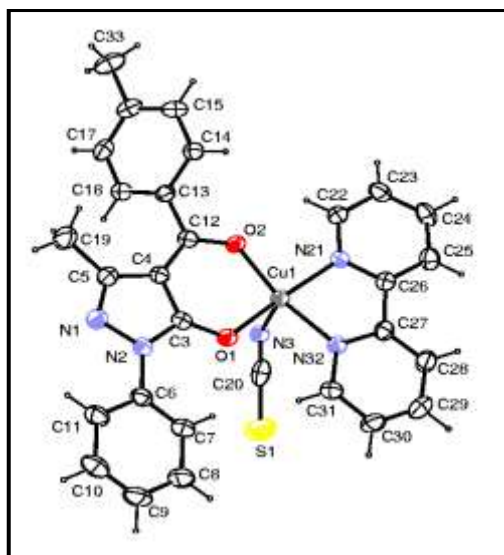


Fig. 1.53. ORTEP view of the complex **11** with displacement ellipsoids drawn at 50%. H atoms are shown as small spheres of arbitrary radii. Solvent molecule has been removed for clarity

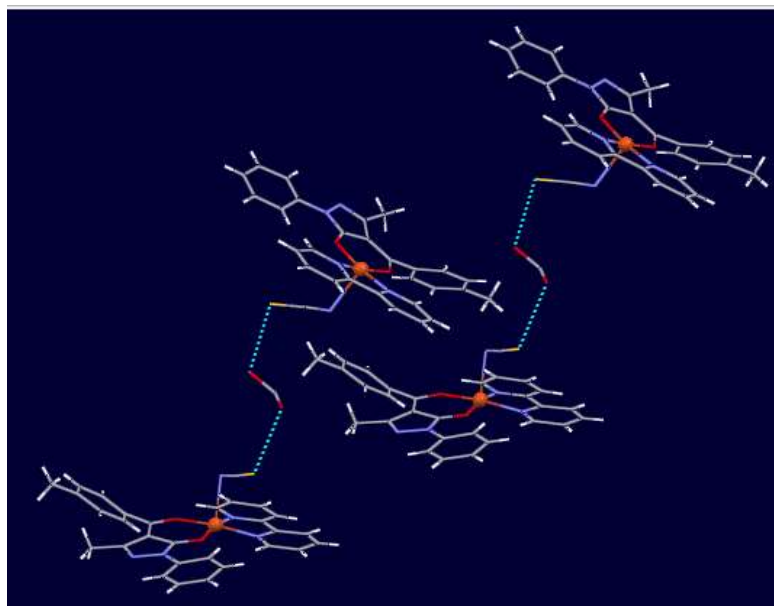


Fig. 1.54. The packing arrangement of **11** viewed down the *b*-axis, along with H-bonding

1.6.2.2.2.3. Complex 13

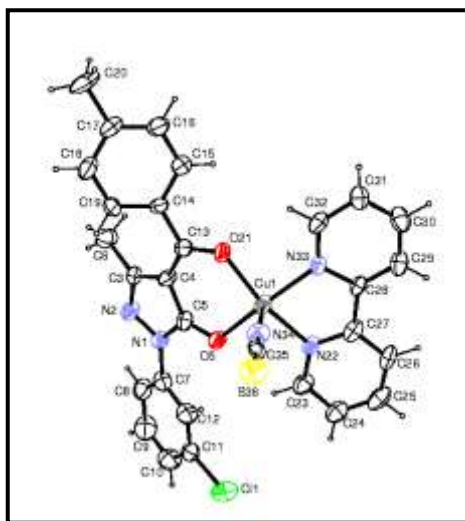


Fig. 1.55. ORTEP view of the complex **13** with displacement ellipsoids drawn at 50%. H atoms are shown as small spheres of arbitrary radii

The molecular structure of **13** together with the atom-numbering scheme is illustrated in Fig. 1.55. The crystal packing of the complex projected down the *b* axis is illustrated in Fig. 1.56. In this complex, everything is similar to the complex **11**.

The only difference is in labeling. The coordination sphere is of the type Cu1-N22-N33-O5-O21-N34, exhibiting a geometry of slightly distorted square pyramidal (SP).

Table 1.6. Selected bond lengths and angles in the ternary complexes of 4-toluoyl pyrazolones

10		11		13	
Bond distances (Å) with esd's in parentheses					
C13 O1	1.279(3)	C3 O1	1.273(4)	Cu1 O5	1.943(4)
C16 O2	1.274(3)	C12 O2	1.278(4)	Cu1 O21	1.958(4)
C16 N3	1.365(3)	C20 N3	1.109(5)	Cu1 N22	2.004(4)
C17 N3	1.416(3)	C20 S1	1.638(5)	Cu1 N33	2.013(5)
C31 N5	1.147(3)	C22 N21	1.348(4)	Cu1 N34	2.129(5)
C31 S1	1.637(3)	C26 N21	1.344(4)	C5 O5	1.273(6)
N1 Cu1	2.0315(19)	C34 O3	1.482(13)	C13 O21	1.282(7)
N2 Cu1	2.020(2)	C34 O3	1.482(13)	N22 C23	1.315(7)
N3 N4	1.395(3)	N3 Cu1	2.442(4)	N22 C27	1.346(8)
N5 Cu1	2.139(2)	N21 Cu1	1.993(3)	C28 N33	1.354(6)
O1 Cu1	1.9726(16)	N32 Cu1	1.998(3)	C32 N33	1.326(6)
O2 Cu1	1.9398(15)	O1 Cu1	1.925(2)	N34 C35	1.150(6)
C13 C14	1.409(3)	O2 Cu1	1.922(2)	C35 S36	1.618(6)
Bond angles(Å)with esd's in parentheses					
O2 Cu1 O1	92.26(7)	O2 C12 C4	121.5(3)	O5 Cu1 O21	92.76(16)
O2 Cu1 N2	89.31(8)	O2 C12 C13	114.5(3)	O5 Cu1 N22	90.68(19)
O1 Cu1 N2	162.13(8)	C26 N21 Cu1	114.9(2)	O21 Cu1 N22	162.30(18)
O2 Cu1 N1	160.79(7)	C20 N3 Cu1	112.1(3)	O5 Cu1 N33	162.87(18)
O1 Cu1 N1	91.65(7)	C22 N21 Cu1	126.2(2)	O21 Cu1 N33	91.39(18)
N2 Cu1 N1	81.37(8)	C31 N32 Cu1	126.2(2)	N22 Cu1 N33	80.6(2)
O2 Cu1 N5	102.25(8)	C27 N32 Cu1	114.7(2)	O5 Cu1 N34	99.15(19)
O1 Cu1 N5	96.86(8)	C3 O1 Cu1	121.1(2)	O21 Cu1 N34	99.52(16)
N2 Cu1 N5	100.20(8)	C12 O2 Cu1	129.6(2)	N22 Cu1 N34	97.06(18)
N1 Cu1 N5	95.93(8)	O2 Cu1 O1	94.18(10)	N33 Cu1 N34	96.53(19)
N1 Cu1 N5	123.2(2)	O2 Cu1 N21	89.92(11)	O5 C5 C4	129.8(6)
C16 O2 Cu1	118.84(14)	O1 Cu1 N21	168.88(11)	C5 O5 Cu1	120.7(4)
C13 O1 Cu1	127.86(14)	O2 Cu1 N32	167.04(11)	C13 O21 Cu1	127.1(4)
N5 C31 S1	178.6(2)	O1 Cu1 N32	93.31(11)	C23 N22 Cu1	125.2(5)
C1 N1 Cu1	129.93(17)	N21 Cu1 N32	80.87(11)	C27 N22 Cu1	114.6(4)
C9 N1 Cu1	112.20(15)	O2 Cu1 N3	96.39(11)	C32 N33 Cu1	125.8(4)
C12 N2 Cu1	128.96(19)	O1 Cu1 N3	90.14(10)	C28 N33 Cu1	114.9(4)
C8 N2 Cu1	112.79(15)	N21 Cu1 N3	99.68(11)	C35 N34 Cu1	177.5(5)
C31 N5 Cu1	171.3(2)	N32 Cu1 N3	94.15(11)	N34 C35 S36	178.5(5)

For this complex (see Fig. 1.55 for labelling) the relevant angles, $\theta = 168.88$ and $\phi = 167.04$ (Table 1.6) yields a τ value of 0.009 which is almost near to 0 and it indicates a SP geometry. The coordination sphere is of the type Cu1-N33-N22-O5-O21-N34, exhibiting a square pyramidal (SP) geometry.

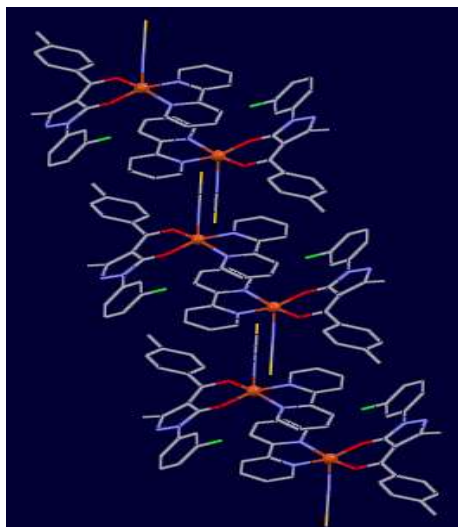


Fig. 1.56. The packing arrangement of **13** viewed down the *b*-axis

1.6.3. IR spectral studies

The characteristic IR bands for all the complexes recorded as KBr discs are listed in Table 1.7.

Table 1.7. Important IR frequencies of the complexes

Complex	$\nu_{C=N}$ (cyclic)	ν_{C-O}	$\nu_{N=CS}$	ν_{N-N}	$\nu_{NC=S}$	ν_{M-O}	ν_{M-N}
1	1571	1484	-	-	-	479	-
2	1570	1472	-	-	-	482	-
3	1571	1480	-	-	-	480	-
4	1599	1491	2060	1144	846	469	428
5	1590/1608	1481	2079	1160	835	476	417
6	1535/1615	1468	2082	1144	842	471	430
7	1608/1585	1471	2047	1153	843	474	418
8	1585	1482	2040	1150	840	482	414
9	1599	1485	2047	1104	822	469	413
10	1581	1469	2083	1157	846	476	430
11	1580	1469	2088	1123	843	479	415
12	1590	1430	2069	1154	845	468	431
13	1602	1470	2085	1159	831	478	415
14	1611/1586	1480	2096	1182	847	491	420
15	1596	1475	2090	1165	838	480	422

1.6.3.1. IR spectral studies of binary complexes

All the complexes show absorption in the region 3000-2900 cm^{-1} , which may be due to $\nu_{\text{C-H}}$. The IR spectrum of the ligands has one prominent band appearing between 1630-1641 cm^{-1} due to $\nu_{\text{C=O}}$ stretching modes. This band disappeared on complexation and a new $\nu_{\text{C-O}}$ band at 1472-1492 cm^{-1} appeared [114]. Furthermore, comparison of the IR spectra of the ligands with those of their metal(II) complexes, indicates that the ligands are coordinated to metal(II) by two sites, that is the ligands are bidentate. The band due to $\nu_{\text{C=O}}$ is completely missing in the spectra of the complexes, suggests enolization of the ligand on complexation. This is supported by the fact that no band for ν_{OH} is observed in the infrared spectra of the ligands and their metal(II) complexes. Instead, a band due to $\nu_{\text{C-O}}$ was observed for all the complexes, which supports the observation of their enolization during coordination. This fact suggests that the ligand remains in the keto form in the solid state, but in solution both the keto and enol forms remain in equilibrium. Deprotonation occurs from the enol form on complexation. In addition, the new band at 429-482 cm^{-1} is assigned to M-O bond [115]. The wave no. of cyclic C=N does not change in all the complexes, indicates no coordination via C=N cyclic. By comparing the IR spectra of ligands and metal complexes, it is easy to predict that the ligand binds to the metal ion *via* O and O i.e. bidentate manner.

1.6.3.2. IR spectral studies of ternary complexes

All the complexes show absorption in the region 3000-2900 cm^{-1} , which may be due to $\nu_{\text{C-H}}$. Bands around 1,518, 1,425 and 721 cm^{-1} in all the complexes, assigned to $\nu(\text{C=N})$, $\nu(\text{C=C})$ and out-of-plane C-H stretching vibrations confirm the presence of phen/bipy ligands in the coordination spheres of these complexes [116].

In metal ion compounds the linear thiocyanate ion can coordinate through either the sulfur or the nitrogen atoms, or both [117]. Examples of complexes containing each type of bonded thiocyanate group are known but in general the compounds with first-row transition metals are known to be N-bonded from X-ray data [118]. Criteria for establishing the mode of bonding in thiocyanate complexes

have been worked out based on the frequency ranges found for the three vibrational modes of the thiocyanate ion, *i.e.*, the C-N and C-S stretching modes $\nu(\text{CN})$ and $\nu(\text{CS})$ and the degenerate bending mode $\delta(\text{NCS})$. For $\nu(\text{CS})$, which is most diagnostic of S or N bonding, the frequency range is from 792 to 850 cm^{-1} for Cu(II) thiocyanate and its complexes. The frequency observed for the complexes clearly indicates N-bonding. The remarkable feature in all the spectra presented is the strong band in the range 2040-2090 cm^{-1} with a shoulder at slightly higher frequencies. This band is attributed to the C=N stretching of the thiocyanate group [119].

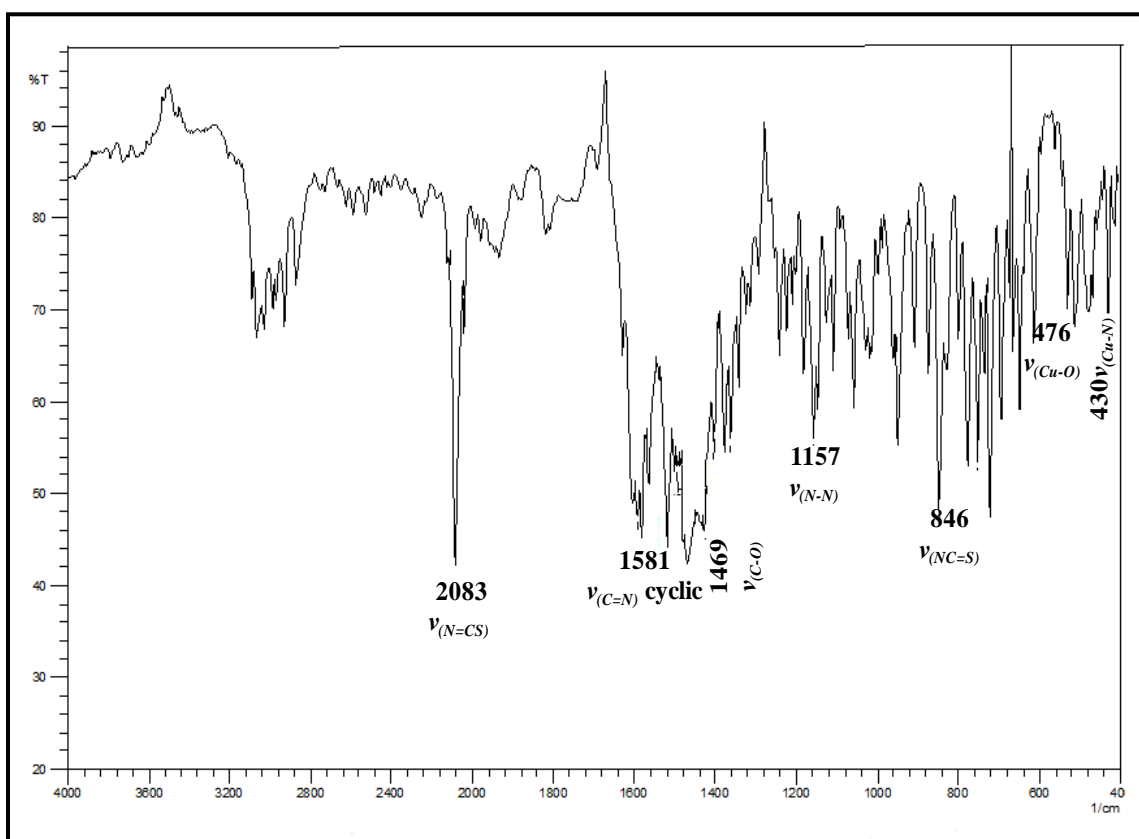


Fig. 1.57. IR spectrum of complex 10

Furthermore, comparison of the IR spectra of the ligands with those of their Cu(II) complexes, indicates that the ligand is coordinated to metal(II) by two sites, that is the ligand is bidentate. That the band due to $\nu_{\text{C=O}}$ is completely missing in the spectra of the complexes, suggests enolization of the ligand on complexation. This is supported by the fact that no band for ν_{OH} is observed in the infrared spectra of the

ligand and its Cu(II) complex. Instead, a band due to ν_{C-O} was observed for the complex, which supports the observation of its enolization during coordination. This fact suggests that the ligand remains in the keto form in the solid state, but in solution both the keto and enol forms remain in equilibrium. Deprotonation occurs from the enol form on complexation. In addition, the new band in the range $460-490\text{ cm}^{-1}$ is assigned to Cu-O bond [120]. The new band in the range $410-440\text{ cm}^{-1}$ is assigned to Cu-N bond. The wave no. of cyclic C=N does not change in all the complexes, indicates no coordination *via* C=N cyclic. By comparing the IR spectra of ligands and metal complexes, it is easy to predict that the ligand binds to the metal ion *via* N and O i.e. bidentate manner. The IR spectrum of the complex **10** is shown in Fig. 1.57.

1.6.4. Mass spectral studies

1.6.4.1. Mass spectral studies of binary complexes

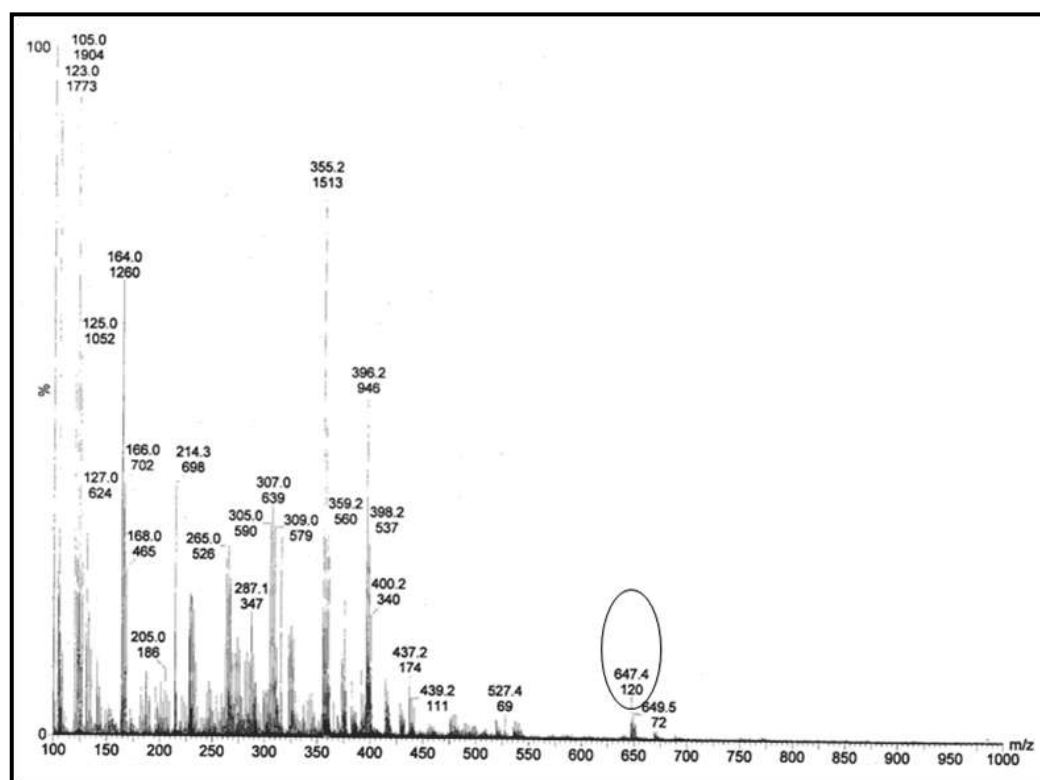


Fig. 1.58. Mass spectrum of the complex 1

The mass spectral study of one of the binary complexes (Complex **1**) has been carried out. The mass spectrum of this complex is shown in Fig. 1.58. The mass spectrum of the complex revealed the molecular ion peak at m/z **647.4** which coincident with the formula weight **646.1** supporting the identity of the proposed structure. Other peaks are due to the further fragmentation of the molecule. The fragmentation pattern of the complex is shown in Scheme 1.23.

1.6.4.2. Mass spectral studies of ternary complexes

The mass spectra of two ternary complexes have been studied. The mass spectra of complexes **9** and **10** are shown in Figs. 1.59 & 1.60, respectively. The mass spectra of the complexes revealed the molecular ion peak at m/z **462.2** (**9**) and **534.2** (**10**), which coincident with the formula weight (462.09) for **9** and (534.16) for **10**. These peaks are due to the removal of thiocyanate molecules, which support the identity of the proposed structures. The fragmentation pattern of **10** is shown in Scheme 1.24.

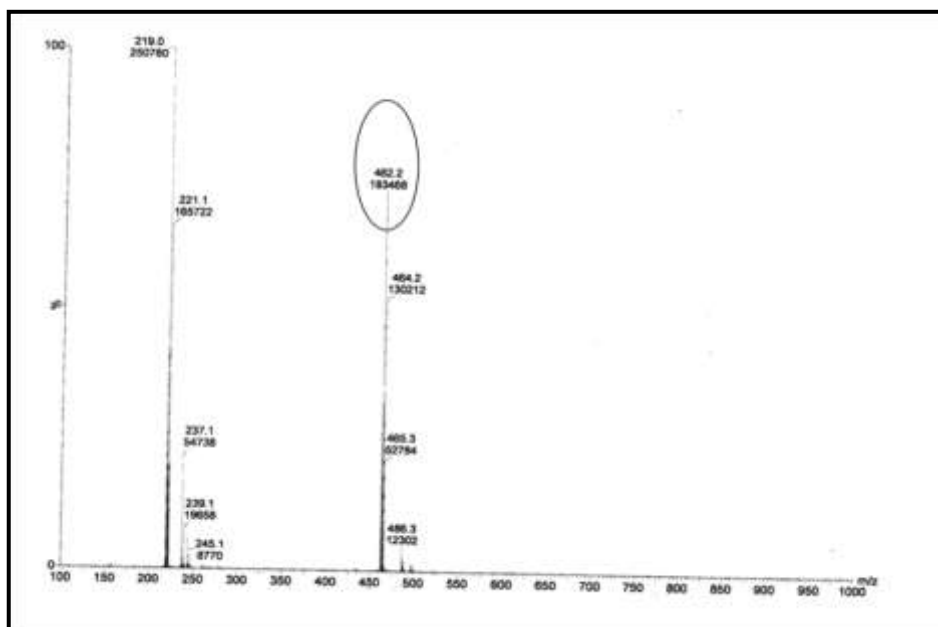
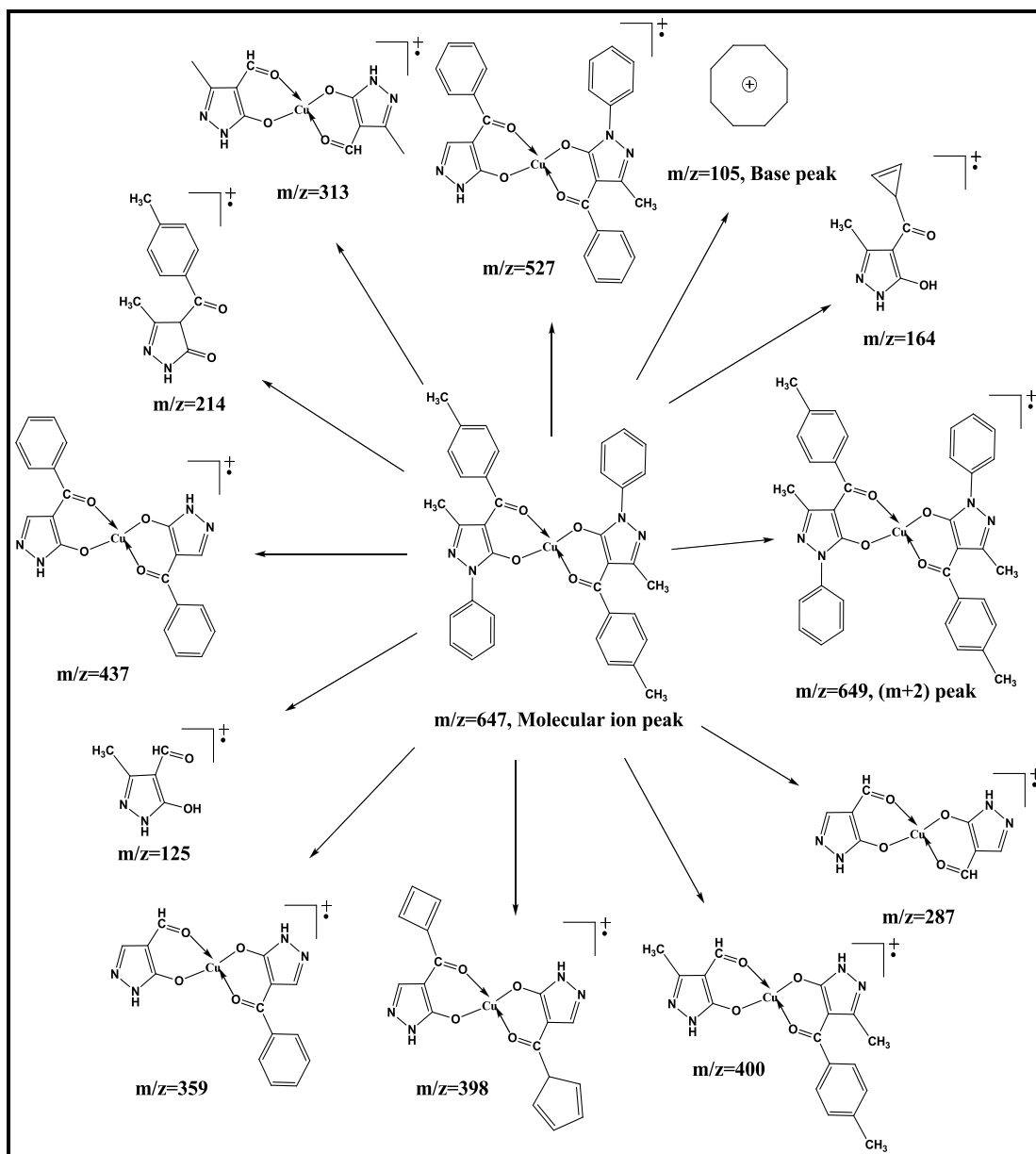
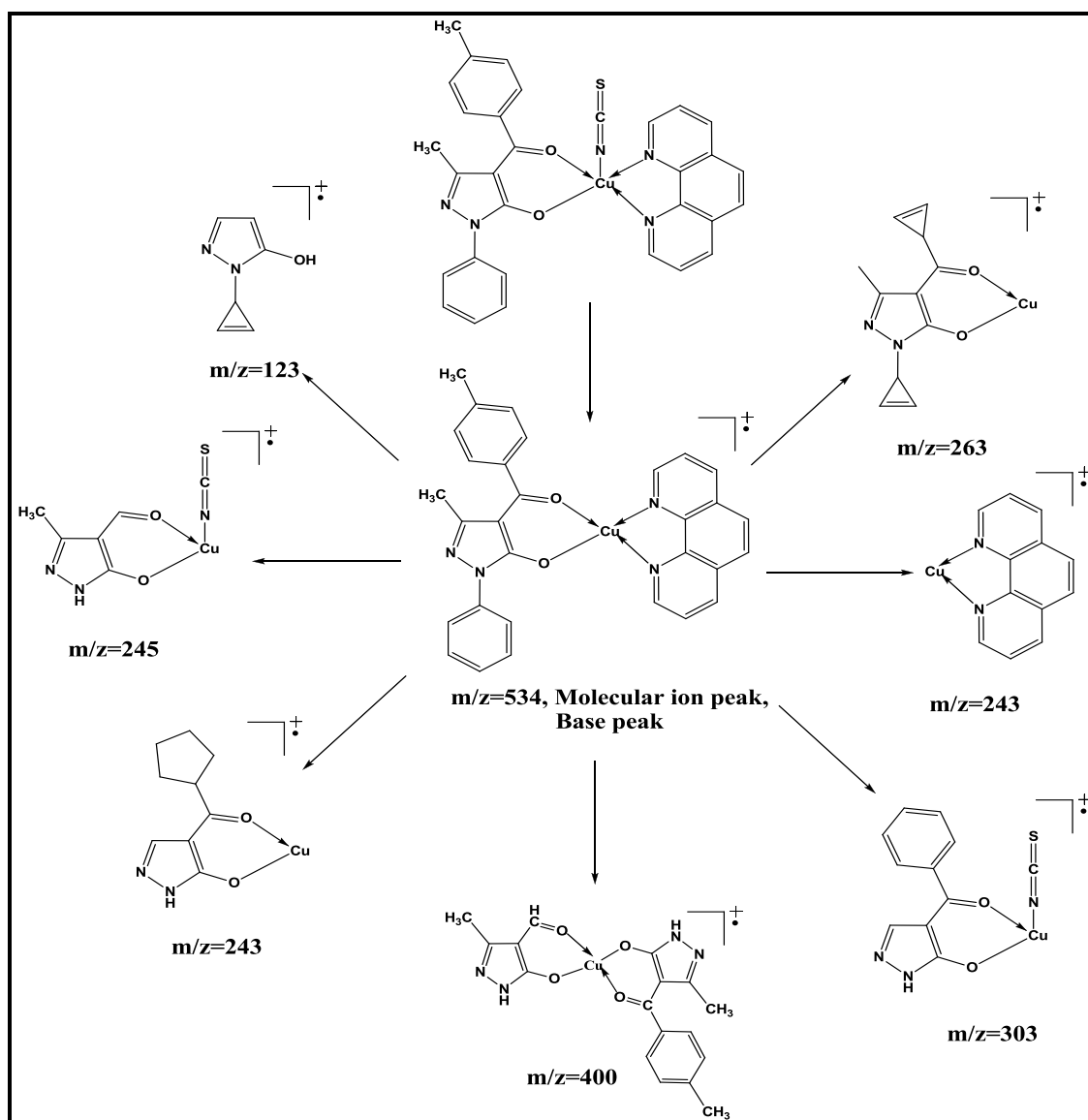


Fig. 1.59. Mass spectrum of complex **9**



Scheme 1.23. Fragmentation pattern of the complex 1



Scheme 1.24. Fragmentation pattern of complex 10

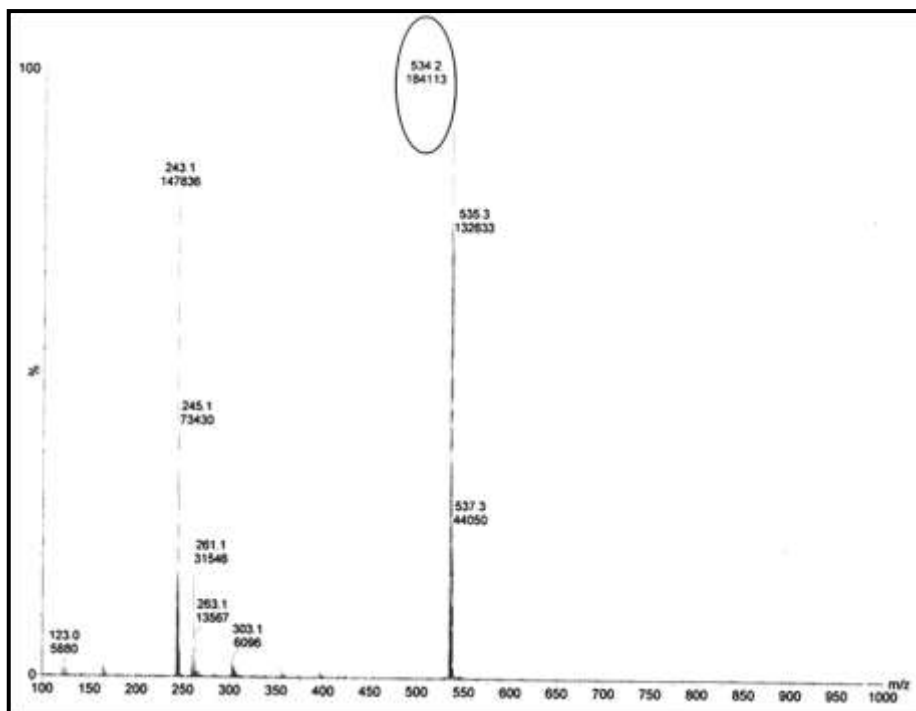


Fig. 1.60. Mass spectrum of the complex **10**

1.6.5. Electronic spectral studies

Electronic spectral data of the complexes are listed in Table 1.8.

1.6.5.1. Electronic spectral studies of binary complexes

These complexes are magnetically normal with magnetic moments of 1.76-1.89 BM. Electronic absorption spectra of the complexes in DMF solution shows a *d-d* transition at around 720 nm, which can be assigned as the ${}^2B_{1g} \rightarrow {}^2A_{1g}$ transition, revealing that the Cu(II) complexes exist in the square-planar geometry [121]. The electronic spectrum of the complex **2** is shown in Fig. 1.61.

1.6.5.2. Electronic spectral studies of ternary complexes

The visible spectra for the complexes under investigation were measured in DMF. In DMF, the complexes displayed absorbance maxima in the 670–720 nm range. For five-coordinate Cu(II) complexes, this spectral feature is typical for SP or distorted SP geometries, which generally exhibit a band in the 550–660 nm range (d_{xz} ,

$d_{yz} \rightarrow d_{x^2-y^2}$); the geometry around each Cu is SP or distorted SP. In contrast, TBP Cu(II) complexes usually show a maximum at $\lambda > 800$ nm ($d_{xz}, d_{x^2-y^2} \rightarrow d_z^2$) with a higher energy shoulder. Thus, in DMF, the geometry about the Cu(II) centre in the complexes is closer to SP. These data are consistent with the reported literature for the square pyramidal Cu(II) complexes [122]. The electronic spectrum of the complex **12** is shown in Fig. 1.62.

Table 1.8. Electronic spectral data of the complexes

Complex	d-d transition	
	$\lambda_{\text{max/nm}}$	ϵ ($\text{dm}^3 \text{mol}^{-1} \text{cm}^{-1}$)
1	725	148
2	723	157
3	720	100
4	686	87
5	661	73
6	657	59
7	656	64
8	667	68
9	652	58
10	713	54
11	673	82
12	668	62
13	672	67
14	673	69
15	662	85

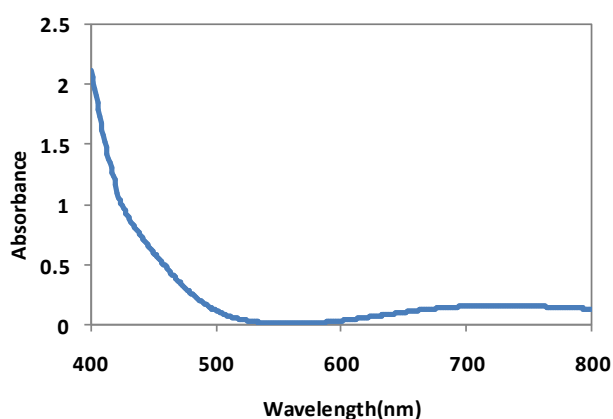


Fig. 1.61. Electronic spectrum of complex 2

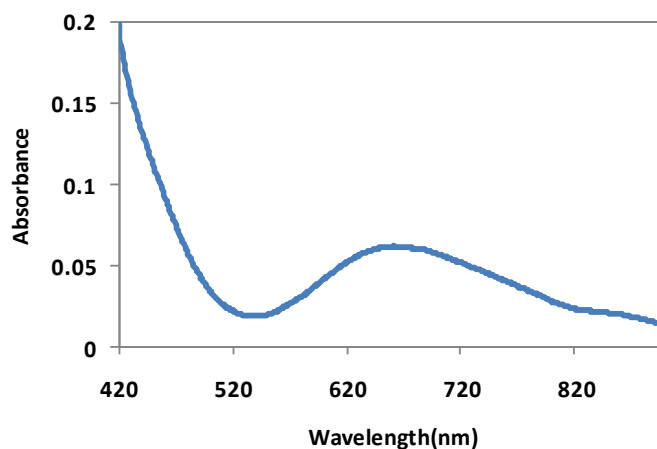


Fig. 1.62. Electronic spectrum of complex **12**

1.6.6. Thermal studies

To investigate the stability of these complexes, thermogravimetric analyses (TG) and differential thermal analyses (DTA) on the crystalline sample were carried out under the nitrogen atmosphere with a heating rate of 10 °C/min.

1.6.6.1. Thermal studies of binary complexes

The aim of thermal analysis is to open up new possibilities for the investigation of metal complexes and to obtain information concerning the thermal stability of the investigated complexes, to decide whether water molecules are inside or outside the coordination sphere. Here, all the synthesized binary Cu(II) complexes are having square planar geometry with two toluoyl pyrazolones coordinated to Cu(II). So, in this case there is no possibilities for the presence of any solvent molecules or else and hence the thermal studies of the binary complexes have not been carried out.

The TG curve of the complex $[\text{Ca}(\text{TPMP})_2(\text{EtOH})_2]$ is shown in Fig. 1.63. The TG curve of the complex $[\text{Ca}(\text{TPMP})_2(\text{EtOH})_2]$ follows the decrease in sample mass with increase in temperature. The decomposition of the complex undergoes in three stages. The degradation of one mole of EtOH molecule takes place in the first stage at

191°C with a mass loss of 6.41% (calcd.: 6.40%). The maximum rate of mass loss is indicated by the DTG peak at 193°C. One endotherm is observed in the DTA trace at 194°C. In second stage, the mass loss occurred at 380°C corresponds to decomposition of two EtOH molecules with 12.82% (calcd.: 12.81%). The DTG peak is observed at 354°C and the DTA peak is observed at 353°C. The third stage shows the mass loss at 470°C corresponding to decomposition of one ligand molecule. The observed mass loss is 40.73%, which is consistent with the theoretical value of 40.66%. In this stage, DTG peak is observed at 436°C.

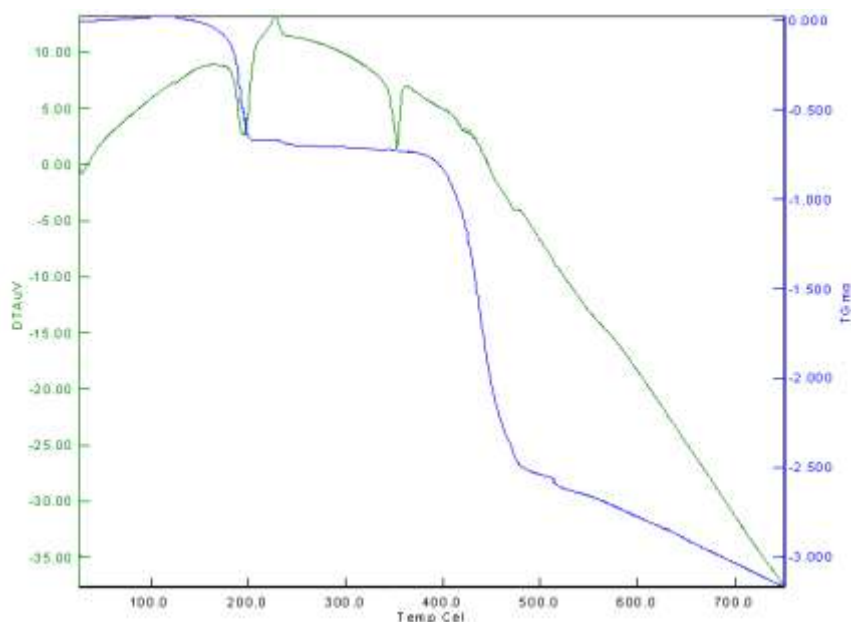


Fig. 1.63. Thermogram of the complex $[\text{Ca}(\text{TPMP})_2(\text{EtOH})_2]$

1.6.6.2. Thermal studies of ternary complexes

There is no mass loss up to 250°C, showing that complex **10** is free from water or other solvent molecules. This desolvated complex was stable up to 250°C and then began to decompose. Based on the percentage of weight loss, the DTA curve and the complexation sustainment, a two-step process of decomposition is proposed for this mixed ligand complex. Degradation of thiocyanate molecule takes place at 268°C [11]. The observed mass loss (9.83%) coincides with the theoretical value (9.79%). The DTA curves of complex have an endothermic peak around 240°C and

the corresponding TG curves both exhibit a weight loss. The experimental values are in agreement with the theoretical ones within the experimental error. The second loss at 333°C corresponds to decomposition of the 1, 10 phenanthroline molecule with a mass loss of 43.23% (Calc. 43.21%). It is also proved by the observed endotherm in DTA curve at 353°C. These results are in accordance with the compositions of the compounds determined by elemental analyses. Meanwhile, they answered for the crystal structure. The results prove that the complexes have the relatively high thermal stability, and that the thiocyanate in the complex is coordinated, which is in agreement with the IR study. The thermogram of the complex **10** is shown in Fig. 1.64.

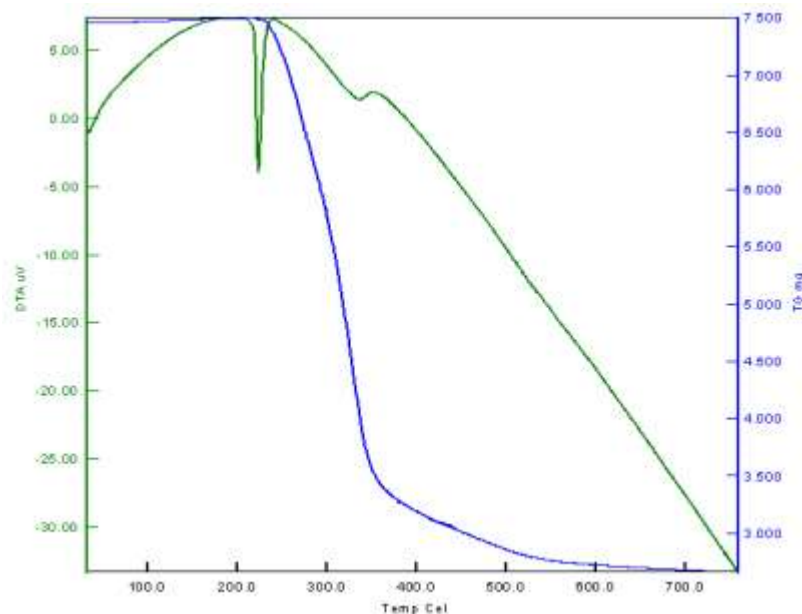


Fig. 1.64. Thermogram of the complex **10**

1.6.7. Magnetic measurement studies

Magnetic moment measurements of all the complexes show μ_{eff} of 1.76-1.89 BM, which corresponds to one unpaired electron and is expected from mononuclear Cu(II) complexes (d^9) with some orbital contribution. The magnetic moment values of the copper complexes correspond to the spin only value of 1.73 B.M. for the Cu(II) complexes [123].

1.6.8. ESR studies

1.6.8.1. ESR studies of binary complexes

The powder as well as the solution ESR spectra of the complex **1** was studied. The spectra are shown in Figs. 1.65 & 1.66, respectively. The spectrum of the complex at 300K shows one intense absorption band in the high field region and is isotropic due to tumbling motion of the molecules. Hamiltonian parameters g_{\parallel} , g_{\perp} , A_{\parallel} and A_{\perp} were also calculated. The magnetic susceptibility value reveals that the copper complex has a magnetic moment, 1.76 B.M., corresponding to the one unpaired electron, indicating that the complex is mononuclear. This fact was also evident from the absence of a half field signal, observed in the spectrum at 1600 G due to the $m_s = \pm 2$ transitions, ruling out any Cu-Cu interaction [124].

The ESR spectrum of the complex at 77 K indicates a poorly resolved nitrogen super hyperfine structure in the perpendicular region due to the interaction of the Cu(II) odd electron. The ESR spectrum of the complex at 77 K indicates a poorly resolved nitrogen super with nitrogen atoms.

Complex shows the $g_{\parallel} = 2.40$ and $g_{\perp} = 2.03$, for Cu(II) g_{\parallel} indicates covalence with $g_{\parallel} < 2.3$ for covalent complexes and $g_{\parallel} \geq 2.3$ for ionic [125]. g_{\parallel} value of the complex of 2.40 indicates covalency for M-L bond. The frozen DMF solution is axial with $g_{\parallel} > g_{\perp} > 2.0023$, indicating a $d_{x^2-y^2}$ ground state which is in agreement with the electronic absorption spectroscopic assignments. A factor potentially contributing to increase of g_{\parallel} is distortion from square planar geometry [126]. From the observed values, it is clear that A_{\parallel} (**150**) $>$ A_{\perp} (**20**); g_{\parallel} (2.4) $>$ g_{\perp} (2.03) $>$ 2.0023 and the ESR parameters of the complex coincide well with related systems which suggest that the complex has square-planar geometry and the system is axially symmetric.

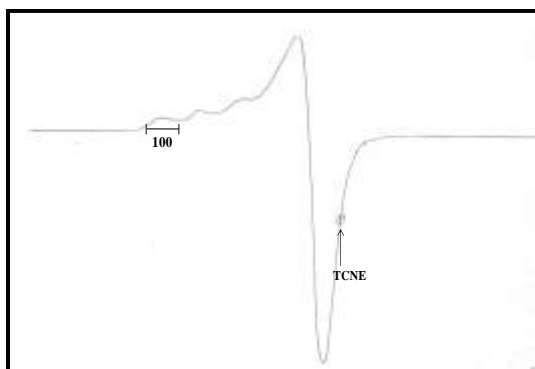


Fig. 1.65. X-band ESR spectrum of complex **1** in solution state at RT

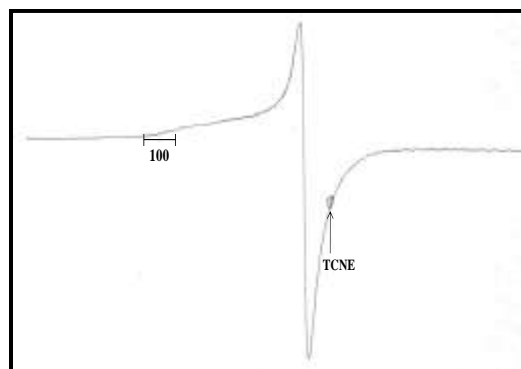


Fig. 1.66. X-band ESR spectrum of complex **1** in polycrystalline state at RT and LNT

1.6.8.2. ESR studies of ternary complexes

The powder as well as the solution ESR spectra of the complex **10** was studied. The spectra are shown in Figs. 1.67 & 1.68, respectively. Hamiltonian parameters $g_{||}$, g_{\perp} and $A_{||}$ were also calculated.

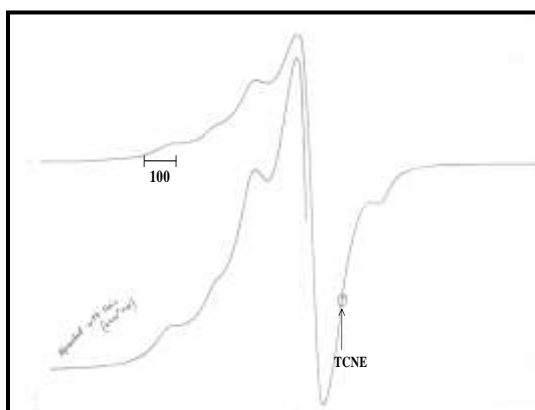


Fig. 1.67. X-band ESR spectrum of complex **10** in solution state at RT

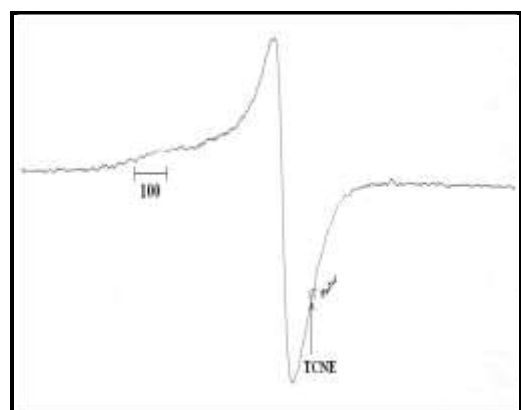


Fig. 1.68. X-band ESR spectrum of complex **10** in polycrystalline state at RT and LNT

Complex shows the $g_{||} = 2.37$ and $g_{\perp} = 2.07$, for Cu(II) $g_{||}$ indicates covalence with $g_{||} < 2.3$ for covalent complexes and $g_{||} \geq 2.3$ for ionic [125]. $g_{||}$ value of the complex of 2.37 indicates covalency for M-L bond. The frozen DMF solution is axial

with $g_{\parallel} > g_{\perp} > 2.0023$, indicating a $d_x^2 - y^2$ ground state which is in agreement with the electronic absorption spectroscopic assignments. A factor potentially contributing to increase of g_{\parallel} is distortion from geometry [126]. ESR parameters of the complex coincide well with related systems which suggest that the complex has square pyramidal geometry.

Conclusions

The 4-acyl pyrazolones have been synthesized using Jensen's method. They have been characterized by elemental analyses, IR, NMR and Mass spectrometry. During this synthesis, the isolation of Ca-complex intermediate has been done here for the first time. The molecular structure of this complex has been determined by X-ray crystallography. This study shows that the Ca(II) center is six-coordinated octahedron with two 4-acyl pyrazolones acting as bidentate O, O donor ligands and two ethanol molecules acting as O, O donor ligands. The crystal structure of Ca(II) complex is stabilized by O-H \cdots N, C-H \cdots π and π - π stacking interactions. Three new binary complexes containing 4-acyl pyrazolone have been synthesized and thoroughly characterized by elemental analyses, metal estimation, molar conductance measurements, IR, Mass, UV-Visible, TGA-DTA, ESR studies. The molecular geometry of one of these complexes has been determined by single crystal X-ray study. The X-ray diffraction analyses of the complexes show that the Cu(II) center is four-coordinated with square planar geometry. Further, a new series of ternary complexes containing 4-acyl pyrazolone and polypyridyls has also been synthesized and characterized by different techniques. The molecular geometries of five complexes have been studied using X-ray crystallography. The study shows that the ternary complexes are five coordinated with 4-acyl pyrazolone acting as bidentate O, O donor ligand, polypyridyl as bidentate N, N donor ligand and fifth position is occupied by thiocyanate molecule *via* N atom. The τ (tau) values have also been calculated for the ternary complexes and it suggests that the complexes possess the geometry close to square pyramidal rather than trigonal bipyramidal, as they have the τ values near to 0 (zero).

Literature cited.

- [1] F. Bellina, S. Cauteruccio, R. Rossi, *Tetrahedron* 63 (2007) 4571.
- [2] S. Park, O. H. Kwon, S. Kim, M. G. Choi, M. Cha, *J. Am. Chem. Soc.*, 127 (2005) 10070.
- [3]. Knorr; *Ger. Pat.*, 26 (1883) 429.
- [4]. Knorr, Blank, *Ber.*, 16 (1887) 2597.
- [5]. Knorr, Blank, *Ber.*, 18 (1885) 311.
- [6] L. Knorr, *Ber.*, 17 (1883) 2032.
- [7] D. Lednicer, L.A. Georg, *The Organic Chemistry of Drug Synthesis*, vol.1, John Wiley & Sons, New York, (1977).
- [8] A. G. Gilman, T. W. Rall, A. S. Nies, P. Taylor, Goodman and Gilman's, *The Pharmacological Basis of Therapeutics*, 8th ed., Pergamon Press, Oxford, (1996).
- [9] H. R. Wiley, P. Wiley, *Pyrazolones, Pyrazolidones and Derivatives*, Interscience Publishers, (1964).
- [10] M. P. Clark, R.G. Bookland, *Expert Opin. Ther. Pat.* 15 (2005) 1617.
- [11] A. Omotowa, M.A. Mesubi, *Appl. Organomet. Chem.* 11 (1997) 1.
- [12] F. Caruso, M. Rossi, J. Tanski, R. Sartori, R. Sariego, S. Moya, S. Diez, E. Navarrete, A. Cingolani, F. Marchetti, C. Pettinari, *J. Med. Chem.* 43 (2000) 3665.
- [13] K. L. Kees, J. J. Fitzgerald Jr., K. E. Steiner, J. F. Mattes, B. Mihan, T. Tosi, D. Mondoro, M. L. McCaleb, *J. Med. Chem.* 39 (1996) 3928.
- [14] R. Bose, D. S. R. Murty, G. Chakrapani, *J. Radioanal. Nucl. Chem.* 265 (2005) 115.
- [15] T. Ito, C. Goto, K. Noguchi, *Anal. Chim. Acta* 443 (2001) 41.
- [16] A. Whitaker, *J. Soc. Dyers Colour* 111 (1995) 66.
- [17] F. Bao, X. Lu, B. Kang, Q. Wu, *Eur. Polym. J.* 42 (2006) 928.
- [18] M. Shi, F. Li, T. Yi, D. Zhang, H. Hu, C. Huang, *Inorg. Chem.* 44 (2005) 8929.
- [19] N. Raman, A. Kulandaisamy, A. Shunmugasundaram, K. Jeyasubramanian, *Transit. Met. Chem.* 26 (2001) 131.
- [20] T. Yoshikuni, *J. Mol. Catal. A: Chem.* 148 (1999) 285.

- [21] B. A. Uzoukwu, P. U. Adiukwu, S. S. Al-Juaid, P. B. Hitchcock, J. D. Smith, *Inorg. Chim. Acta* 250 (1996) 173.
- [22] N. Kalarani, S. Sangeetha, P. Kamalakannan, D. Venkappayya, *Russ. J. Coord. Chem.* 29 (2003) 845.
- [23] F. Stoltz, *J. Prakt. Chem.*, 55 (1897) 145.
- [24] B. S. Jensen, *Acta Chem. Scand.* 13 (1959) 1668.
- [25] N. Adhikari, S. Chaudhuri, R. J. Butcher, N. Saha, *Polyhedron* 18 (1999) 1323.
- [26] C. Pettinari, F. Marchetti, A. Drozdov, *β -Diketones and Related Ligands Comprehensive Coordination Chemistry II*, vol. 1, Elsevier, 2003, p. 97 (chapter 1.6).
- [27] F. Marchetti, C. Pettinari, R. Pettinari, *Coord. Chem. Rev.* 249 (2005) 2909.
- [28] E. C. Okafor, *Spectrochim. Acta A* 37 (1981) 951.
- [29] X. -C. Gao, H. Cao, C. -H. Huang, S. Umetani, G.-O. Chen, P. Jiang, *Synth. Met.* 99 (1999) 127.
- [30] C. Pettinari, F. Marchetti, A. Cingolani, D. Leonesi, E. Mundorff, M. Rossi, F. Caruso, *J. Organomet. Chem.* 557 (1998) 187.
- [31] B. Bovio, A. Cingolani, F. Marchetti, C. Pettinari, *J. Organomet. Chem.* 458 (1993) 39.
- [32] C. Pettinari, F. Marchetti, A. Cingolani, A. Gindulyte, L. Massa, M. Rossi, F. Caruso, *Eur. J. Inorg. Chem.* (2001) 2171.
- [33] A. Cingolani, Effendy, F. Marchetti, C. Pettinari, R. Pettinari, B.W. Skelton, A.H. White, *Inorg. Chem.* 43 (2004) 4387.
- [34] G. Bombieri, A. Polo, J. Wang, J. Wu, G. Xu, *Inorg. Chim. Acta* 132 (1987) 263.
- [35] F. Marchetti, C. Pettinari, A. Cingolani, R. Pettinari, M. Rossi, F. Caruso, *J. Organomet. Chem.* 645 (2002) 134.
- [36] B. Chantegrel, A.I. Nadi, S. Gelin, *Heterocycles* 20 (1983) 1801.
- [37] A. Cingolani, Effendy, F. Marchetti, C. Pettinari, R. Pettinari, B. W. Skelton, A. H. White, *Inorg. Chim. Acta* 329 (2002) 100.
- [38] C. Pettinari, F. Marchetti, R. Pettinari, A. Pizzabiocca, A. Drozdov, S. Troyanov, V. Vertlib, *J. Organomet. Chem.* 688 (2003) 216.
- [39] C. Pettinari, F. Marchetti, A. Gregori, A. Cingolani, J. Tanski, M. Rossi, F. Caruso, *Inorg. Chim. Acta* 257 (1997) 37.

- [40] C. Pettinari, F. Marchetti, A. Cingolani, A. Lorenzotti, E. Mundorff, M. Rossi, F. Caruso, *Inorg. Chim. Acta* 262 (1997) 33.
- [41] S. K. Mohanty, R. Sridhar, S. Y. Padmanavan, S. Rao, A. S. Mitra, *Indian J. Chem.* 15B (1977) 1146.
- [42] S. Gelin, B. Chantegrel, A. I. Nadi, *J. Org. Chem.* 48 (1983) 4078.
- [43] M. J. O'Connell, C. G. Ramsay, P. J. Steel, *Aust. J. Chem.* 38 (1985) 401.
- [44] S. Miyazaki, H. Mukai, S. Umetani, S. Kihara, M. Matsui, *Inorg. Chem.* 28 (1989) 3014.
- [45] C. Pettinari, F. Marchetti, R. Pettinari, D. Martini, A. Drozdov, S. Troyanov, *J. Chem. Soc. Dalton Trans.* (2001) 1790.
- [46] C. Pettinari, F. Marchetti, A. Drozdov, V. Vertlib, S. Troyanov, *Inorg. Chem. Commun.* 4 (2001) 290.
- [47] D. W. Johnson, J. Xu, R. W. Saalfrank, K. N. Raymond, *Angew. Chem. Int. Ed.* 38 (1999) 2882.
- [48] J. Xu, K.N. Raymond, *Angew. Chem. Int. Ed.* 39 (2000) 2745.
- [49] S. Saxena, Y.P. Singh, A.K. Rai, *Synth. React. Inorg. Met. Org. Chem.* 12 (1982) 501.
- [50] S. Saxena, Y. P. Singh, A.K. Rai, *J. Organomet. Chem.* 270 (1984) 301.
- [51] S. Saxena, P. N. Saxena, A. K. Rai, S. C. Saxena, *Toxicology* 35 (1985) 241.
- [52] P. N. Saxena, S. Saxena, S.C. Saxena, *Indian Biologist* 20 (1988) 23.
- [53] E. R. Menzel, D. R. Lorenz, J. R. Wasson, K. R. Radigan, B. J. Mc- Cormik, *J. Inorg. Nucl. Chem.* 38 (1976) 993.
- [54] B. A. Uzoukwu, *Synth. React. Inorg. Met. Org. Chem.* 21 (1991) 881.
- [55] B. A. Uzoukwu, *Synth. React. Inorg. Met. Org. Chem.* 22 (1992) 185.
- [56] R. C. Maurya, S. Rajput, *J. Mol. Struct.* 687 (2004) 35.
- [57] R. C. Maurya, H. Singh, *Synth. React. Inorg. Met. Org. Chem.* 34 (2004) 269.
- [58] R. C. Maurya, S. Rajput, *Synth. React. Inorg. Met. Org. Chem.* 33 (2003) 1877.
- [59] S. Parihar, S. Pathan, R. N. Jadeja, A. Patel, V. K. Gupta, *Inorg. Chem.* 51 (2012) 1152.
- [60] B. A. Uzoukwu, K. Gloe, P.U. Adiukwu, *Synth. React. Inorg. Met. Org. Chem.* 30 (2000) 433.

- [61] M. Y. Mirza, F.I. Nwabue, *J. Inorg. Nucl. Chem.* 43 (1981) 1817.
- [62] P. M. Parikh, J.R. Shah, *Synth. React. Inorg. Met. Org. Chem.* 15 (1985) 769.
- [63] R. C. Maurya, D.D. Mishra, *Synth. React. Inorg. Met. Org. Chem.* 21 (1991) 845.
- [64] R. C. Maurya, D.D. Mishra, *Indian J. Chem.* 29A (1990) 1230.
- [65] Y. Akama, S. Yajima, *J. Thermal Anal.* 44 (1995) 1107.
- [66] Y. Akama, T. Iwadate, A. Tong, Y. Takahashi, S. Tanaka, *J. Chromatogr. A* 789 (1997) 479.
- [67] E. C. Okafor, *Spectrochim. Acta A* 37 (1981) 945.
- [68] E. C. Okafor, *Spectrochim. Acta A* 37 (1981) 939.
- [69] E. C. Okafor, *Talanta* 29 (1982) 275.
- [70] L. Yang, W. Jin, J. Lin, *Polyhedron* 19 (2000) 93.
- [71] B.A. Uzoukwu, K. Gloe, H. Duddeck, *Synth. React. Inorg. Met. Org. Chem.* 28 (1998) 207.
- [72] B.V. Patel, B.T. Thaker, *Synth. React. Inorg. Met. Org. Chem.* 16 (1986) 1319.
- [73] E. C. Okafor, *Z. Naturforsch.* 36b (1981) 213.
- [74] P. Morales, H. Nekimken, C.S. Bartholdi, P. T. Cunningham, *Spectrochim. Acta A* 44 (1988) 165.
- [75] G. E. Buono-Core, G. Leon, *J. Coord. Chem.* 21 (1990) 323.
- [76] E.C. Okafor, P. U. Adiukwu, B.A. Uzoukwu, *Synth. React. Inorg. Met. Org. Chem.* 23 (1993) 97.
- [77] E. C. Okafor, B.A. Uzoukwu, *Synth. React. Inorg. Met. Org. Chem.* 22 (1992) 921.
- [78] A. B. Uzoukwu, S.S. Al-Juaid, P.B. Hitchcock, J.D. Smith, *Polyhedron* 12 (1993) 2719.
- [79] B. A. Uzoukwu, *Synth. React. Inorg. Met. Org. Chem.* 23 (1993) 1087.
- [80] B. A. Uzoukwu, K. Gloe, P.U. Adiukwu, *Synth. React. Inorg. Met. Org. Chem.* 30 (2000) 335.
- [81] A. Louati, A. Kuncaka, M. Gross, C. Hauptmann, M. Bernard, J. J. Andr`e, J. P. Brunette, *J. Organomet. Chem.* 486 (1995) 95.

- [82] F. Caruso, L. Massa, A. Gindulyte, C. Pettinari, F. Marchetti, R. Pettinari, M. Ricciutelli, J. Costamagna, J.C. Canales, J. Tanski, M. Rossi, *Eur. J. Inorg. Chem.* (2003) 3221.
- [83] B. A. Uzoukwu, *Spectrochim. Acta A* 48 (1992) 1021.
- [84] S. K. Deya, B. Baga, D. K. Dey, V. Gramlich, Y. Li, S. Mitra, *Z. Naturforsch. B* 58 (2003) 1009.
- [85] A. Drozdov, V. Vertlib, I. Timokhin, S. Troyanov, C. Pettinari, F. Marchetti, *Russ. J. Coord. Chem.* 28 (2002) 259.
- [86] F. Marchetti, C. Pettinari, A. Cingolani, D. Leonesi, M. Camalli, A. Pifferi, *Polyhedron* 15 (1996) 3835.
- [87] F. Marchetti, C. Pettinari, R. Pettinari, A. Cingolani, M. Camalli, R. Spagna, *Inorg. Chim. Acta* 299 (2000) 65.
- [88] C. Pettinari, F. Marchetti, C. Santini, R. Pettinari, A. Drozdov, S. Troyanov, G. Battiston, R. Gerbasi, *Inorg. Chim. Acta* 315 (2001) 88.
- [89] A. Drozdov, S. Troyanov, O. Fedorchenko, G. Battiston, C. Pettinari, F. Marchetti, A. Cingolani, *J. Phys. IV* 9 (1999) 929.
- [90] Y. Akama, *J. Therm. Anal.* 45 (1995) 1501.
- [91] (a) F. Marchetti, C. Pettinari, A. Cingolani, D. Leonesi, A. Drozdov, S. Troyanov, *J. Chem. Soc. Dalton Trans.* (1998) 3325; (b) E. Uhlemann, U. Schilde, F. Weller, *Zeitsch. Naturforsch. B* 50 (1995) 31.
- [92] R. C. Maurya, S. Pillai, S.K. Thakur, *J. Inst. Chem.* 72 (2000) 9.
- [93] G. J. Goetz-Grandmont, A. Tayeb, D. Matt, J.P. Brunette, *Acta Cryst. C*, 51 (1995) 53.
- [94] B. A. Uzoukwu, *Spectrochim. Acta A* 49 (1993) 281.
- [95] W. Mickler, A. Reich, S. Sawusch, U. Schilde, E. Uhlemann, *Acta Cryst. C*, 54 (1998) 776.
- [96] J. -L. Wang, X. Zhang, M. Yu, F. -M. Miao, *Pol. J. Chem.* 75 (2001) 1367.
- [97] F. Marchetti, C. Pettinari, R. Pettinari, D. Arriva, S. Troyanov, A. Drozdov, *Inorg. Chim. Acta* 307 (2000) 97.
- [98] W. L. F. Armarego, D. D. Perrin, *Purification of Laboratory Chemicals*, 4th edn., The Bath Press, Butterworth-Heinemann Publication, (1997).

- [99] Bruker, SMART (Version 5.631), SAINT (Version 6.45) and SADABS (Version 2.05). Bruker AXS Inc., Madison, Wisconsin, USA, (2003).
- [100] G. M. Sheldrick, SHELXS97 and SHELXL97, Germany, University of Gottingen, (1997).
- [101] C. K. Johnson, ORTEP II; Report ORNL-5138, Oak Ridge National Laboratory, Oak Ridge, TN, (1976).
- [102] A. L. Spek, PLATON for Windows. September 1999 Version. University of Utrecht, Netherlands, 1999.
- [103] M. Nardelli, PARST95- an update to PARST: a system of Fortran routines for calculating molecular structure parameters from the results of crystal structure analyses, *J. Appl. Cryst.* 28 (1995) 659.
- [104] K. Nakamoto, C. Udovich and J. Takemoto, *J. Am. Chem. Soc.*, 92 (1970) 3973 and references therein; B. Hutchinson, D. Eversdyk and S. Olbricht, *Spectrochim. Acta*, 30A (1974); R. C. Mehrotra, T. Bohra, D.P. Gaur, *Metal p-diketonares and allied derivatives*, Academic Press, New York, 1978.
- [105] Y. Akama, A. Tong, *Microanalytical Journal* 53 (1996) 34.
- [106] Z. Y. Yang, R. D. Yang, F. S. Li, K. B. Yu, *Polyhedron* 19 (2000) 2599.
- [107] D. H. Williams, I. Fleming, *Spectroscopic methods in organic chemistry*, 4th ed. (1988).
- [108] R. N. Jadeja, J. R. Shah, E. Suresh, P. Paul, *Polyhedron*, 23 (2004) 2465
- [109] F. Marchetti, C. Pettinari, A. Cingolani, D. Leonesi, *Polyhedron* 15 (1996) 3835.
- [110] W. J. Geary, *Coord. Chem. Rev.*, 7 (1971) 81.
- [111] R.N. Jadeja, K. M. Vyas, V. K. Gupta, R. G. Joshi, C. Ratna Prabha, *Polyhedron* 31 (2012) 767.
- [112] Duggan, M.; Ray, N.; Hathaway, B.; Tomlinson, G.; Brint, P.; Pelin, K. *J. Chem. Soc., Dalton Trans.* **1980**, 1342.
- [113] O. O. E. Onawumi, O. O. P. Faboya, O. A. Odunola, T. K. Prasad, M. V. Rajasekharan, *Polyhedron* 27 (2008) 113.
- [114] P. N. Remya, C.H. Suresh, M.L.P. Reddy, *Polyhedron* 26 (2007) 5016.

-
- [115] K. M. Vyas, R. N. Jadeja, V. K. Gupta, K. R. Surati, *J. Mol. Struct.* 990 (2011) 110.
- [116] S. Sarkar, A. Patra, M. G. B. Drew, E. Zangrando, P. Chattopadhyay, *Polyhedron* 28 (2009) 1.
- [117] S. E. Livingstone, *Quart. Rev. (London)*, 19 (1965) 386.
- [118] B. W. Brown, E. C. Lingafelter, *Acta Cryst.*, 16 (1963) 753.
- [119] R. H. Toeniskoetter, S. Solomon, *Inorg. Chem.*, 7 (1968) 617.
- [120] V. A. Sawant, B. A. Yamgar, S. S. Chavan, *Trans. Met. Chem.*, 35 (2010) 357.
- [121] A. B. P. Lever, *Inorganic Electronic Spectroscopy*, Elsevier, Amsterdam, (1984) pp. 355.
- [122] S. S. Massoud, F. A. Mautner, M. A. M. Abu-Youssef, N. M. Shuaib, *Polyhedron* 18 (1999) 2061.
- [123] S. A. Abdel-Latif, H. B. Hassib, *J. Therm. Anal. Calorimet.*, 68 (2002) 983.
- [124] D.E. Fenton, *Biocoordination Chemistry*, Oxford, (1995).
- [125] A. Syamal, R. L. Dutta, *Elementals of Magneto Chemistry*, East-West Press Pvt. Ltd., New Delhi, (1993).
- [126] A.W. Addison, in: K.D. Karlin, J. Zubieta (Eds.), *Copper Coordination Chemistry: Biochemical and Inorganic Perspectives*, Adenine, Guilderland, NY, (1983).

CHAPTER

2

Synthesis, characterization and crystal structure of metal complexes containing pyrazolone based thiosemicarbazones

2.1. Introduction

Thiosemicarbazones belong to a group of **thiourea** derivatives; have been studied due to their wide range of potential biological uses, wide application in industry and analytical determination of various metal ions. Thiosemicarbazones are obtained by condensation of thiosemicarbazide with suitable aldehydes or ketones. In solution thiosemicarbazones probably exist in an equilibrium mixture of **thiol** and **thione** tautomers (Fig. 2.1).

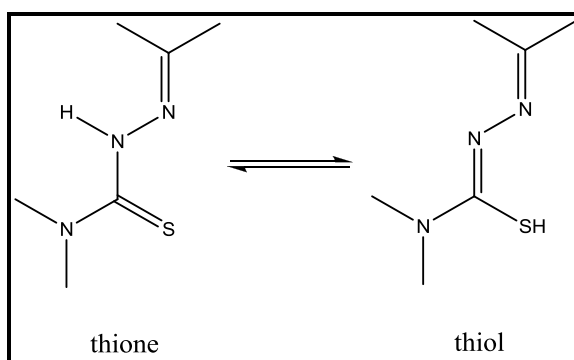


Fig. 2.1. Tautomeric forms of thiosemicarbazone

2.1.1. Thiosemicarbazones of 4-acyl pyrazolones

In the field of thiosemicarbazones, many reports are available which have different substitutions and introduction of thiosemicarbazone moiety on many aliphatic, aromatic and heterocyclic compounds. The introduction of this field is endless and here, it is not of concern also. So, here the introduction part describes the literature on thiosemicarbazones of 4-acyl pyrazolones only.

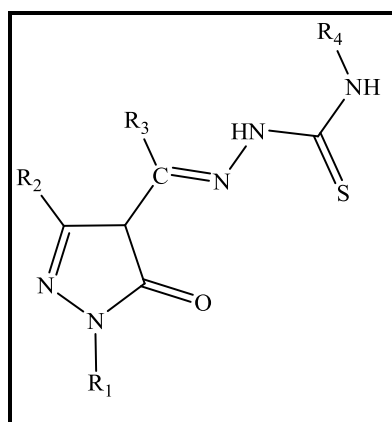


Fig. 2.2. General structure of pyrazolone based thiosemicarbazone

As described in earlier chapters 4-acyl pyrazolone derivatives are an important class of ligands. Among them thiosemicarbazones with 4-acyl pyrazolones have aroused with significant interest in the field of chemistry and biology due to their different applications mainly photochromism and biological activities. A detailed introduction on the biological activities of this class of compounds will be discussed later in Chapter-4. The literature on the thiosemicarbazones of 4-acyl pyrazolones is quite less than other derivatives of pyrazolone. Among them most of the reports describes the photochromism properties of these ligands. **Dianzeng Jia** and co-workers have great contribution in this field. The general structure of the thiosemicarbazones is shown in Fig. 2.2. The pyrazolone based thiosemicarbazones found in the literature are listed in Table 2.1.

Table 2.1. Pyrazolone based thiosemicarbazones

Ligand	R ₁	R ₂	R ₃	R ₄	Ref.
HL ¹	Ph	Me	Ph	H Me Ethyl	[1-6]
HL ²	Ph	Me	<i>p</i> -Br-Ph	Me	[7]
HL ³	Ph	Ph	<i>m</i> -Cl-Ph	Me	[8]
HL ⁴	Ph	Me	<i>p</i> -toluoyl	H	[9]
HL ⁵	Ph	Me	furoyl	Me	[10]
HL ⁶ HL ⁷	Ph H	Me Ph	H	H	[11]
HL ⁸	Ph	Me	<i>p</i> -F-Ph	Me	[12, 13]
HL ⁹	Ph	Me	<i>p</i> -toluoyl	Ethyl	[14]
HL ¹⁰	Ph	Ph	<i>p</i> -F-Ph	Ethyl	[15]
HL ¹¹	Ph	Me	<i>p</i> -Br-Ph	H	[16, 17]
HL ¹²	Ph	Ph	<i>m</i> -Br-Ph	Ph	[18]
HL ¹³	Ph	Ph	<i>p</i> -Br-Ph <i>p</i> -toluoyl	Me	[19]

All these ligands have been synthesized by the direct condensation of 4-acyl pyrazolones with the corresponding thiosemicarbazides in 1:1 molar ratio in methanolic/ethanolic medium. They have been characterized by different techniques like elemental analysis, IR, NMR, Mass and most of them have been characterized by X-ray crystallography.

The photochromic properties and photochemical kinetics of HL¹⁻¹³ have been studied by UV reflectance spectra under irradiation of 365 nm light. The crystal

structure analyses of photocolored product show the photochromism is due to the photoisomerization from enol form to keto form through an intermolecular proton transfer. Theoretical calculations have been made on the structure of some of the ligands. The crystal structures of few ligands have been depicted in Fig. 2.3.

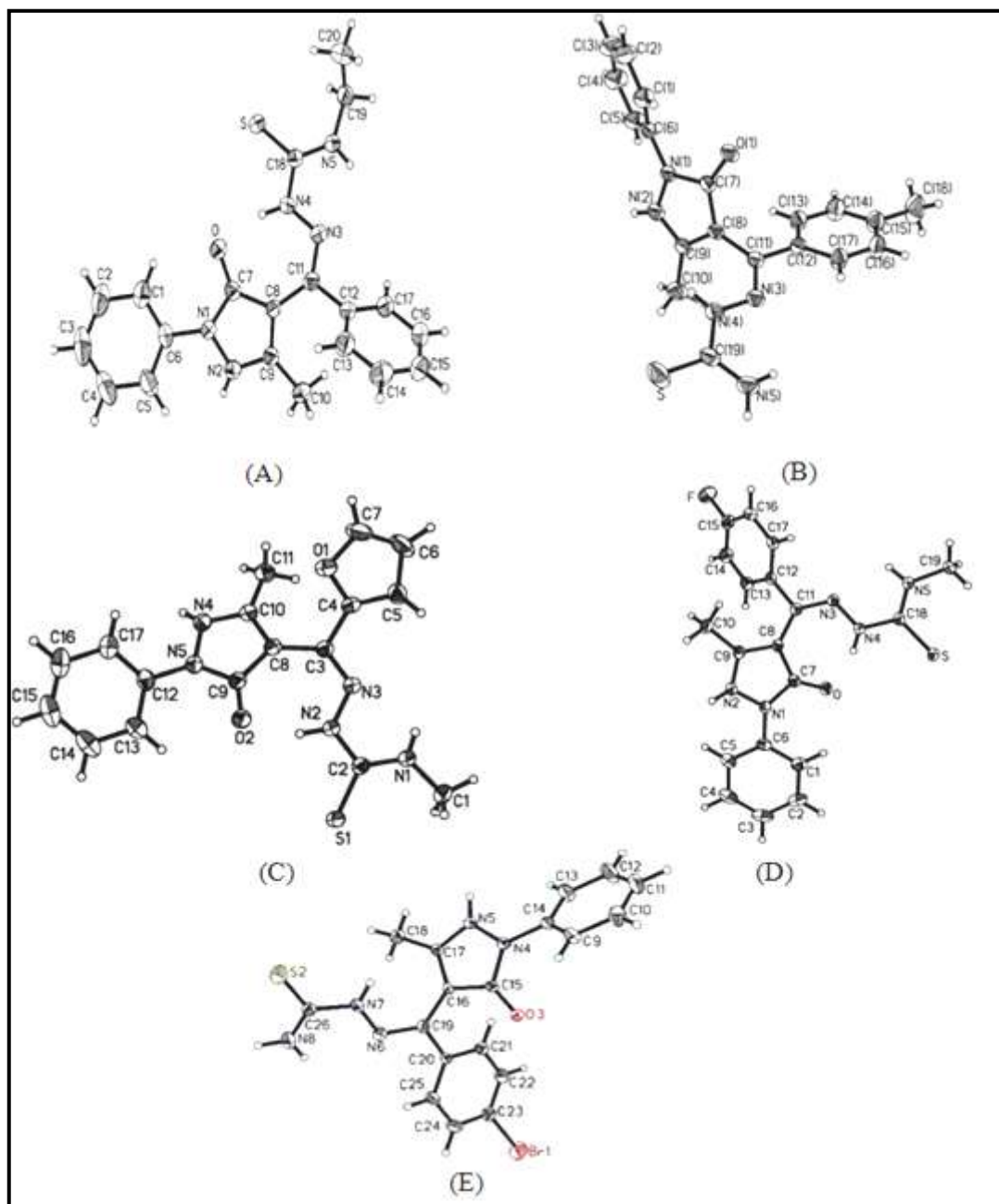


Fig. 2.3. Crystal structures of thiosemicarbazones reported in literature (A) HL¹, (B) HL⁴, (C) HL⁵, (D) HL⁸, and (E) HL¹¹

2.1.2. Metal complexes of thiosemicarbazones

Metal complexes of thiosemicarbazones have been extensively studied and have been the subject of several reviews [20, 21]. The stereochemistries adopted by thiosemicarbazone ligands while interacting with transition metal ions, depend essentially upon the presence of an additional coordination centre in the ligand moiety and the charge on the ligand, which in turn is influenced by the **thione** \rightleftharpoons **thiol** equilibrium. It has been shown [22] that the arrangement of the non-hydrogen atoms in the thiosemicarbazide molecule is nearly planar and the sulphur atom and hydrazinic $-NH_2$ group are *trans* with respect to the C-N bond. When forming complexes in this configuration, bonding occurs *via* the sulphur atoms as a monodentate ligand. Gerbeleu *et al.* [23] have shown that coordination occurs through the hydrazido and imide nitrogens if the sulphur centre is substituted. However in most complexes [24], thiosemicarbazones coordinate as bidentate ligands *via* the azomethine nitrogen and thione/thiol sulphur. When an additional coordinating functionality is present in the proximity of the donating centres (e.g. 2-heterocyclic thiosemicarbazones) the ligands bond in a tridentate manner. This can be accomplished by either the neutral molecule [25] or by the monobasic anion upon loss of a hydrogen from N [26]. There are instances reported, however, where the heterocyclic atom and the azomethine nitrogen are involved in bidentate coordination [27] and the sulphur atom is considered not to be coordinated weakly coordinated to the same metal centre [28].

Besides the dentacity variation, consideration of the charge distribution is complicated in thiosemicarbazones due to the existence of thione and thiol tautomers. Although the thione form predominates in the solid state, solutions of thiosemicarbazone molecules show a mixture of both tautomers. As a result, depending upon the preparative conditions (particularly solvent and pH), the metal complexes can be cationic, neutral or anionic. Furthermore, it is possible to isolate complexes containing two inequivalent ligands--one protonated and one deprotonated--within the same metal complex [29-31].

Thiosemicarbazones can coordinate to metal as neutral molecules or after deprotonation, as anionic ligands and can adopt a variety of different coordination modes. The possibility of their being able to transmit electronic effects between a reduce unit and a metal centre is suggested by the delocalization of the π bonds in the thiosemicarbazone chain [32]. Transition metal complexes with thiosemicarbazone exhibit a wide range of stereochemistry, biomimic activity and have potential application as sensors.

The metal complexes are far more biologically active than uncoordinated thiosemicarbazone and their enhanced biological activity has been an active area of investigation among medicinal researchers [33]. In general, thiosemicarbazones as chelating ligands with transition metal ions by binding through the thioketo sulphur and hydrazine nitrogen atoms and therefore this type of compounds can coordinate *in vivo* to metal ions. Because of such coordination, the thiosemicarbazones moiety undergoes a sterical reorientation that could favour its biological activity.

2.1.3. Metal complexes of pyrazolone based thiosemicarbazones

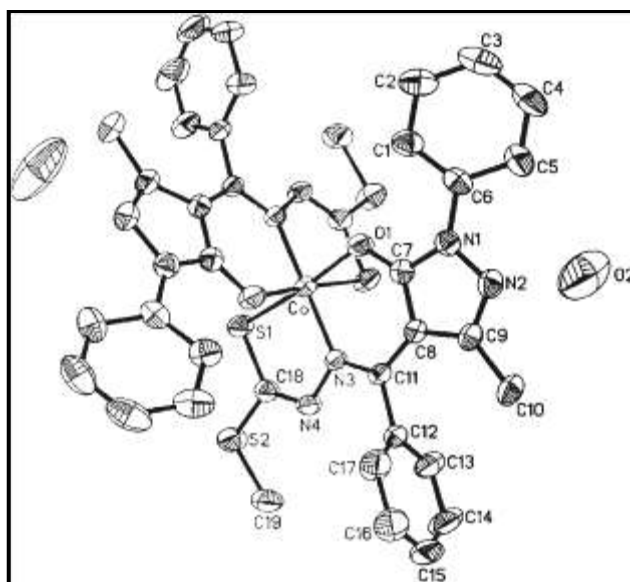


Fig. 2.4. Crystal structure of $[\text{Co}(\text{HL}^1)_2] \cdot 2\text{H}_2\text{O}$

The metal complexes containing this type of ligands have not been much explored. Dianzeng Jia *et al* [5] have synthesized Co(II) complex, $[\text{Co}(\text{HL}^1)_2] \cdot 2\text{H}_2\text{O}$ (Fig. 2.4) by the reaction of an ethanolic solution of ligand with the aqueous solution

of $\text{Co}(\text{OAc})_2 \cdot 4\text{H}_2\text{O}$. It has been characterized by IR spectrum and single crystal X-ray diffraction. The cobalt ion is octahedrally coordinated by two tridentate Schiff base ligands with ONS donor atoms. The molecules are bridged together by two water molecules through H-bond along b axis and one-dimensional indented chain structure is formed.

V.M. Leovac *et al* [11] have synthesized new polymeric Cu(II) complexes (Fig. 2.5) with two tridentate ONS thiosemicarbazone ligands containing substituted pyrazolone moiety by the reaction of $\text{CuCl}_2 \cdot 2\text{H}_2\text{O}$ with HL^6 & HL^7 . Complexes have been characterized by means of spectroscopic, electrochemical and crystallographic techniques. While ligand exist as different tautomers in the solid state and DMSO- d_6 solution, Cu(II) ion coordinates the ligands from the same tautomeric form with square-pyramidal geometry around each Cu atom. In the crystal structures, the Cu(II) complex cation forms polymeric chains $\{[\text{Cu}(\text{L})\text{Cl}]^+\}_n$ with a bridging chlorine atom. One of the complexes was found to have a significantly higher cytotoxic potential in comparison with cisplatin in inhibition of several cell lines (HL60, REH, C6, L929 and B16). The results obtained on the basis of flow cytometry indicated that apoptosis could be possible mechanism of cell death [11].

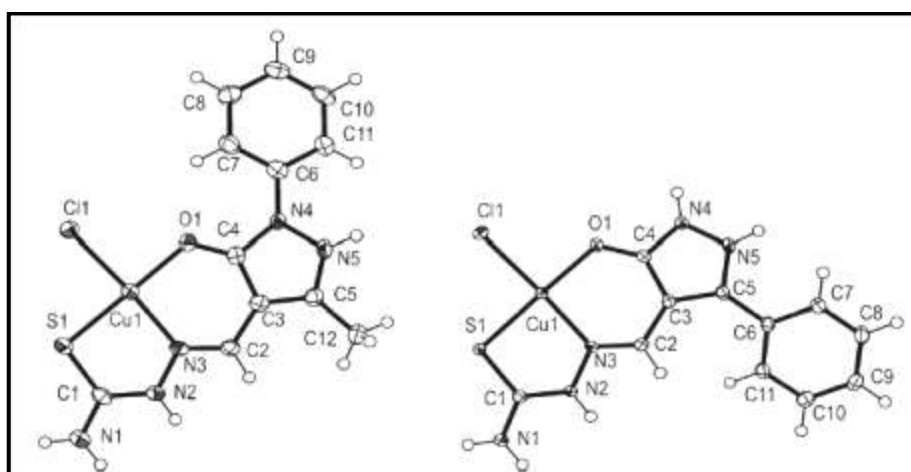


Fig. 2.5. Cu(II) complexes $[\text{Cu}(\text{HL}^6)\text{Cl}]\text{Cl}$ and $[\text{Cu}(\text{HL}^7)\text{Cl}]\text{Cl} \cdot \text{H}_2\text{O}$

P. Yadav *et al* have synthesized Pd complexes [38] by the reaction of three thiosemicarbazones with K_2PdCl_4 to produce complexes, with imine nitrogen and

thiolate sulphur of the anionic thiosemicarbazone moiety acting as coordinating atoms. The thiosemicarbazones and their palladium complexes have been characterized by spectral IR, UV-Vis, ^1H , ^{13}C NMR and electrochemical techniques. The crystal structure of one complex (Fig. 2.6) has been obtained and found to be highly symmetrical with a trans arrangement of the two bidentate ligands.

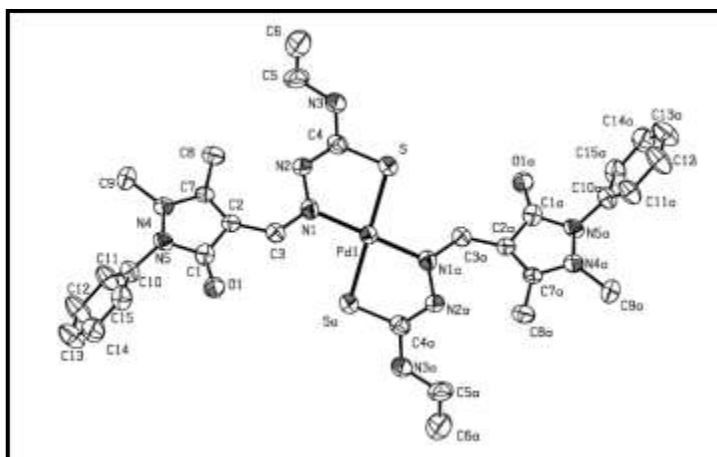


Fig. 2.6. Crystal structure of $[\text{Pd}(\text{HL})_2]$

2.2. Experimental

2.2.1. Materials

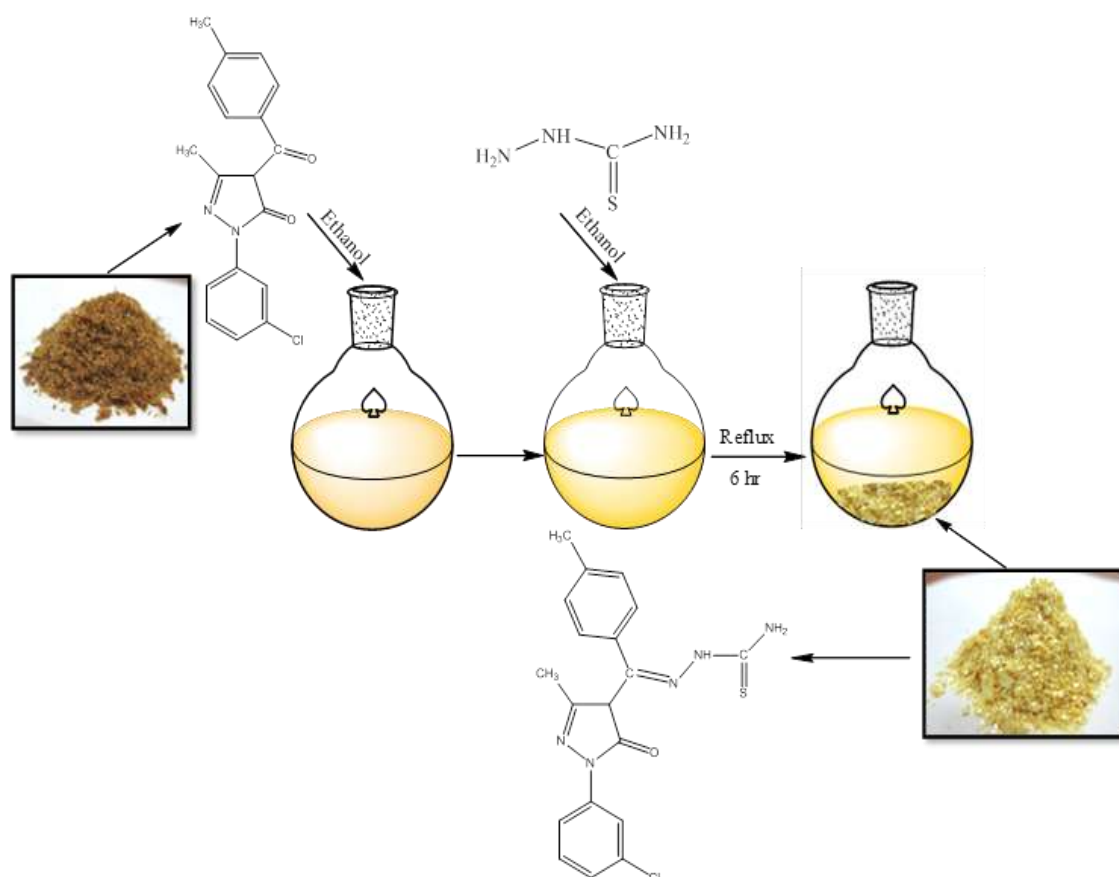
The compounds 5-methyl-4-(4-methyl-benzoyl)-2-phenyl-2,4-dihydro-pyrazol-3-one [TPMP], 2-(3-chloro-phenyl)-5-methyl-4-(4-methyl-benzoyl)-2,4-dihydro-pyrazol-3-one [TMCPMP] and 5-methyl-4-(4-methyl-benzoyl)-2-*p*-tolyl-2,4-dihydro-pyrazol-3-one [TPTMP] were synthesized (**Chapter-1**) and used after recrystallization. Thiosemicarbazide was obtained from Sisco-Chem. Pvt. Ltd., Mumbai. Ethanol was obtained from Baroda Chem. Industries Ltd, Baroda, and was used after distillation. Calcium hydroxide, $\text{Cu}(\text{OAc})_2 \cdot \text{H}_2\text{O}$, $\text{Cu}(\text{NO}_3)_2 \cdot 3\text{H}_2\text{O}$, sodium acetate, 1, 10 phenanthroline and 2, 2' bipyridyl were obtained from LOBA Chem. Pvt. Ltd., Mumbai and used as supplied. Methanol was obtained from Spectrochem., Mumbai, India. All the chemicals used were of AR grade. Solvents used in this study were purified and dried following the standard procedures wherever required [39]. The compound TPMP-TS was synthesized following the standard procedure reported in literature [9].

2.2.2. Single crystal X-ray structure determination

The detail of this section has been given in Chapter 1 (section 1.2.2).

2.3. Syntheses of thiosemicarbazone ligands

2.3.1. (Z)-2-((1-(3-chlorophenyl)-3-methyl-5-oxo-4,5-dihydro-1H-pyrazol-4-yl)(p-tolyl)methylene)hydrazinecarbothioamide [TMCPMP-TS]:



Scheme 2.1. Synthesis of TMCPMP-TS

Equimolar (150 ml) ethanolic solution of 2-(3-chlorophenyl)-5-methyl-4-(4-methylbenzoyl)-2,4-dihydro-pyrazol-3-one (0.326, 1mmol) and thiosemicarbazide (0.091, 1mmol) was refluxed for 6 h in round bottom flask. During the reflux a microcrystalline light yellow compound was separated, which was isolated by filtration and dried in air and finally crystallized in appropriate solvent.

TMCPMP-TS is light yellow crystals. Yield 85.33 % m.p. 198°C Anal. calc. for $C_{19}H_{18}ClN_5OS$ M.W.: 399.90, C(57.07%), H(4.54%), N(17.51%), S(8.02%), found: C(57.01%), H(4.43%), N(17.44 %), S(7.95%); 1H NMR (DMSO- d_6) δ ppm: 1.79(s, 3H, PZ C-CH₃), 2.34(s, 3H, N-TL C-CH₃), 7.68(s, 2H, NH₂), 10.19(s, 1H, OH), 7.20–7.36(m, 4H, Ph), 7.43–7.55(m, 4H, TL), 8.34(s, 1H, N-CH), 9.83(s, 1H, NH-tsc); IR (KBr) ν (cm⁻¹): 3274(b) (-NH₂), 3163(b) (-NH-tsc), 839(m) (C=S), 1625(m) (C=N, cyclic), 1230 (C=N, azomethane), 1270(m) (PZ-C-CH₃), 935(s) (N-N), 1476(m) (Ph-C-C), 2965(b) (Ph-C-H); ^{13}C NMR (DMSO- d_6) δ ppm: 15.97-21.40 [methyl groups], 117.68-133.78 [substituted benzene ring]; MS: m/z = 398.76 [$C_{19}H_{18}ClN_5OS$, MIP]⁺, 364 [$C_{19}H_{18}N_5OS$]⁺, 334 [$C_{17}H_{12}N_5OS$]⁺, 289 [$C_{13}H_{14}N_5OS$]⁺, 261 [$C_{11}H_{11}N_5OS$]⁺, 186 [$C_5H_9N_5OS$]⁺, 156 [$C_9H_5N_2O$]⁺, 214 [$C_{12}H_{12}N_3O$]⁺, 187 [$C_{10}H_9N_3O$]⁺, 91 [C_7H_7 , Base peak]⁺.

2.3.2. (Z)-2-((3-methyl-5-oxo-1-p-tolyl-4,5-dihydro-1H-pyrazol-4-yl)(p-tolyl)methylene)hydrazinecarbothioamide [TTPMP-TS]:



Scheme 2.2. Synthesis of TTPMP-TS

It was prepared analogously from 3-methyl-4-(4-methylbenzoyl)-1-p-tolyl-1H-pyrazol-5(4H)-one (0.306, 1 mmol) and thiosemicarbazide (0.091, 1 mmol). The colored crystals (TMCPMP-TS) thus obtained were separated by filtration and recrystallized.

TPTPMP-TS is light yellow crystals. Yield 82.78 % m.p. 215°C Anal. calc. for $C_{20}H_{21}N_5OS$ M.W.: 379.48, C(63.30%), H(5.58%), N(18.46%), found: C(63.22%), H(5.46%), N(18.33%); 1H NMR (DMSO- d_6) δ ppm: 1.78(s, 3H, PZ-C-CH₃), 2.40(s, 3H, N-TL, C-CH₃), 2.50(s, 3H, TL-C-CH₃) 7.82(s, 2H, NH₂), 10.37(s, 1H, OH), 7.20–7.33(m, 4H, Ph), 7.36–7.67(m, 4H, TL), 8.33(s, 1H, N-CH), 9.74(s, 1H, NH-tsc); IR (KBr) ν (cm^{-1}): 3274(s) (-NH₂), 3167(b) (-NH-tsc), 836(m) (C=S), 1618(m) (C=N), 1282(s) (PZ-C-CH₃), 933(s) (N-N), 1470(m) (Ph-C-C), 2923(b) (Ph-C-H); ^{13}C NMR (DMSO- d_6) δ ppm: 19.03–21.38 [methyl groups], 121.04–129.92 [substituted benzene ring]; MS: m/z = 364.32 [$C_{19}H_{19}N_5OS$]⁺, 288.24 [$C_{13}H_{15}N_5OS$]⁺, 187.57 [$C_5H_7N_5OS$]⁺, 90.85 [C_7H_7]⁺.

2.4. Characterization of thiosemicarbazones

2.4.1. Physicochemical properties

Analytical data of the ligands are presented in section 2.3. The ligands have been synthesized in a very facile and essentially identical way. They are coloured, air and moisture free crystalline solids. They are less soluble in common organic solvents. The structure of the ligands can be confirmed from these data along with spectroscopic and crystallographic evidence discussed in section 2.4.5. The elemental analysis matches well with the empirical formulae of the ligands.

2.4.2. IR spectral studies

In the current studies, thiosemicarbazones related compounds are capable of exhibiting keto-enol tautomerism and react with metal cations to form metal complexes. The assignments of IR spectra of the ligands beside with their assignments are reported in section 2.3. The band that appears in the range of 3163-3167 cm^{-1} is assigned to the stretching vibration of (N-H) of thiosemicarbazone. A new prominent band at 1592-1625 cm^{-1} , due to azomethane $\nu(C=N)$ association appeared in both the ligands, indicates that condensation between ketone moiety of pyrazolone and that of amino group of thiosemicarbazone has taken place ensuing

into the creation of the desired ligands. A broad band at 3274 cm^{-1} is assigned to the stretching vibration of N-H of $-\text{NH}_2$ group. Band due to C-H stretching appears in the range of $2920\text{--}2970\text{ cm}^{-1}$. A band corresponding to C-C stretching appears at $\sim 1470\text{ cm}^{-1}$. The medium band in the range of $1610\text{--}1630\text{ cm}^{-1}$ is assigned to the $\nu(\text{C}=\text{N}$ cyclic). A band due to C=S stretching vibrations appears at $\sim 839\text{ cm}^{-1}$.

2.4.3. NMR spectral studies

2.4.3.1. ^1H NMR spectral studies

The ^1H NMR spectra of both the ligands were recorded in DMSO-d_6 at room temperature and the data are presented in section 2.3. The ^1H NMR spectrum of the ligand TPTPMP-TS is shown in Fig. 2.7.

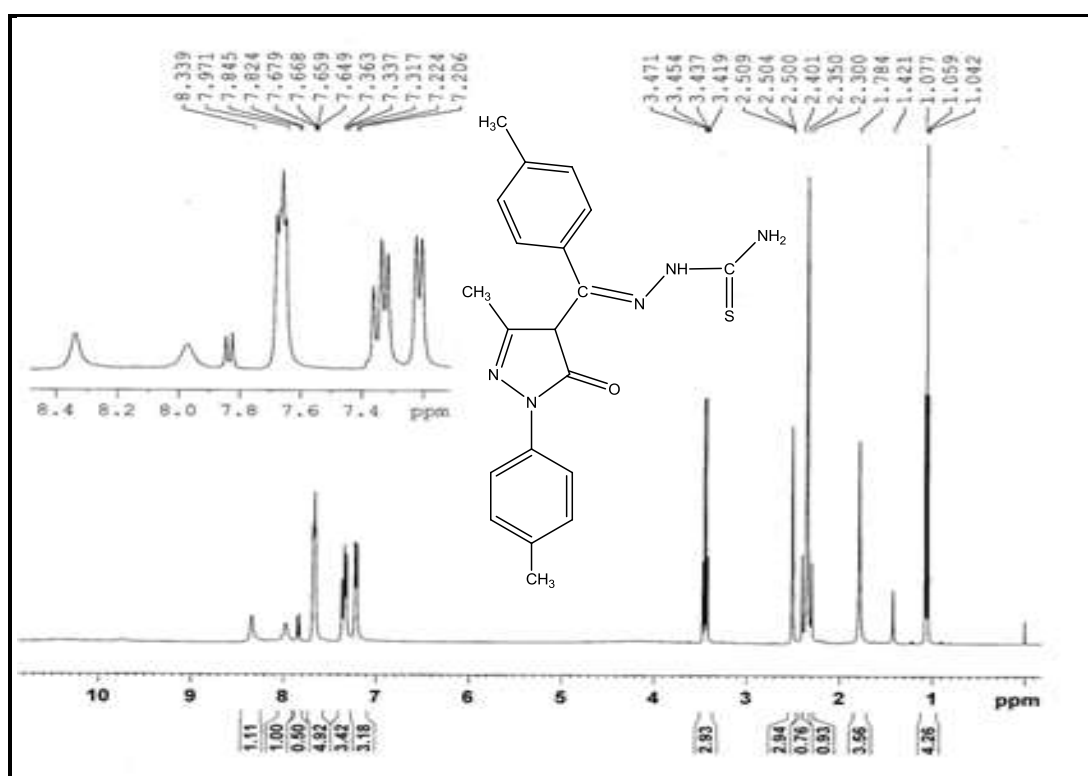


Fig. 2.7. ^1H NMR spectrum of the ligand TPTPMP-TS

In the aliphatic region, singlet corresponding to methyl protons of pyrazolone ring is observed in the range of δ 1.78-1.79 ppm. The methyl protons of toluoyl rings

appear as a singlet in the range of δ 2.34-2.50 ppm in the spectra of both the ligands. In the aromatic region, the aryl protons of two benzene rings resonate in the range of δ 7.20-7.67 ppm as multiplets. The singlet corresponding to $-\text{NH}_2$ protons, appeared in the range of 7.68-7.82 ppm in the NMR spectra of both the ligands. The C-H proton of the pyrazolone ring appeared as singlet in the range of 8.33-8.34 ppm. The singlet due to the N-H proton of thiosemicarbazone appeared in the range of 9.74-9.83 ppm.

2.4.3.2. ^{13}C NMR spectral studies

^{13}C NMR spectral data of the ligands are presented in section 2.3. The ^{13}C NMR spectrum of ligand TMCPMP-TS is shown in Fig. 2.8.

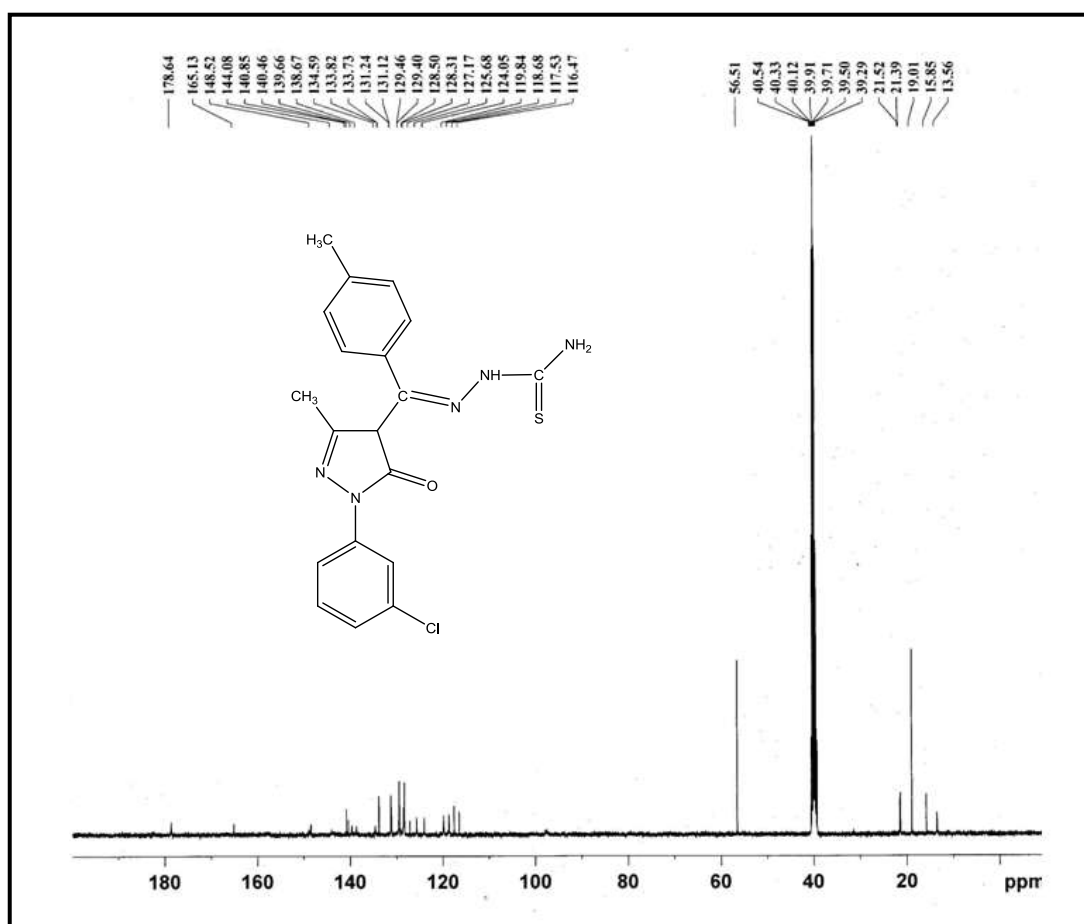


Fig. 2.8. ^{13}C NMR spectrum of ligand TMCPMP-TS

2.4.4. Mass spectral studies

Melting point of each ligand is high, as a result of this, the mass spectra were carried out by EI. The mass spectral assignments for the ligands are shown in section 2.3. The fragmentation pattern of the ligand TMCPMP-TS is shown in Scheme 2.3.

The mass spectra of the ligands are in good agreement with proposed structures. The mass spectrum of the ligand TMCPMP-TS is shown in Fig. 2.9. It shows a molecular ion peak at m/z 398 with a less relative intensity, which is equivalent to its molecular weight.

The mass spectra of the ligands revealed the molecular ion peak at m/z 398.76 (TMCPMP-TS), which coincident with the formula weight (399) for TMCPMP-TS, supporting the identity of the proposed structures.

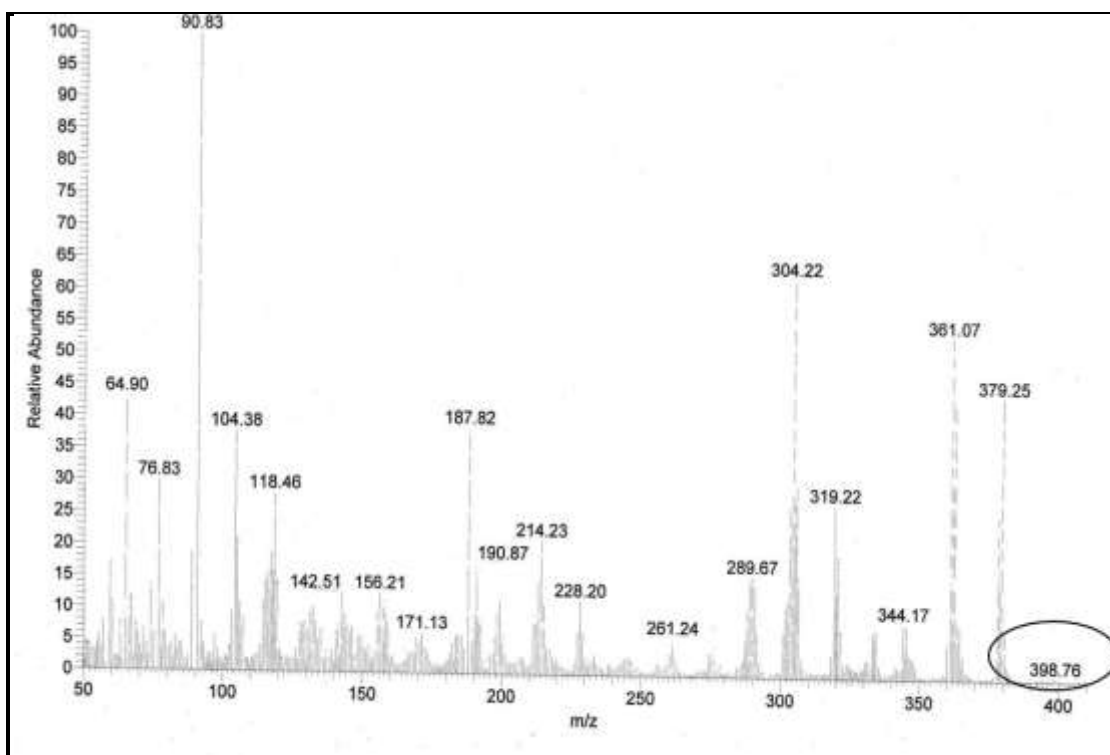
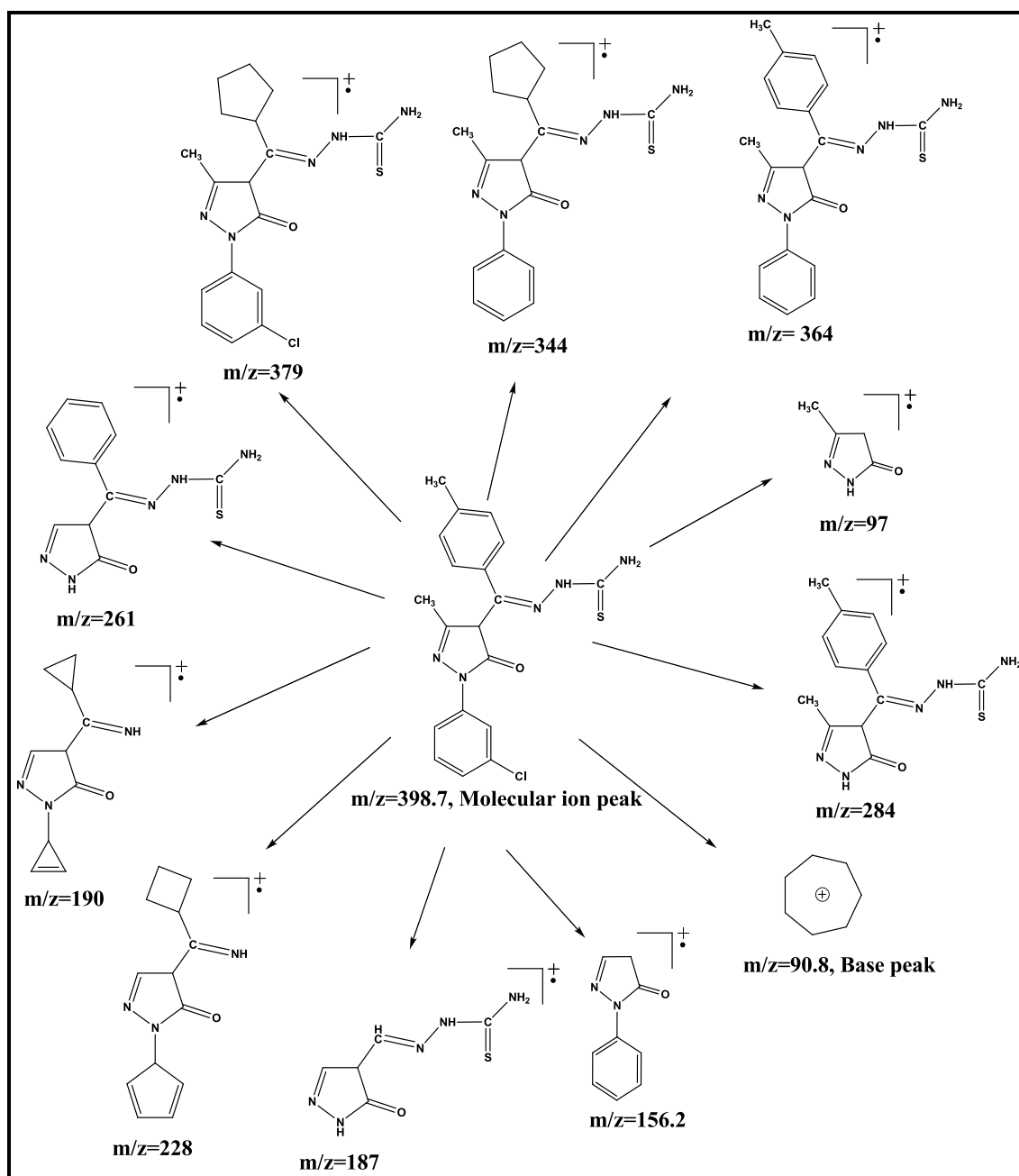


Fig. 2.9. Mass spectrum of ligand TMCPMP-TS



Scheme 2.3. Fragmentation pattern of ligand TMCPMP-TS

A peak corresponding to substituted tropolinium ion can be observed at m/z (90.8) in the mass spectra of both the ligands, which itself is a base peak with 100% relative abundance in case of TMCPMP-TS, whereas in case of TPTPMP-TS, peak at m/z 362 is the base peak. Besides this, many peaks were observed in the spectra of

both the ligands which were attributed to the further fragmentation of the ligand molecules.

2.4.5. Molecular structure of ligand TMCPMP-TS

The molecular structure of the ligand together with the atom-numbering scheme is illustrated in Fig. 2.10. The crystal packing of the ligand projected down the *a* axis is illustrated in Fig. 2.11. Crystallographic data of the ligand is listed in Table 2.3. Important bond lengths and angles for the ligand are listed in Table 2.4.

By slowly evaporating the solution of ethanol without avoiding the sunlight at room temperature, we obtained the yellowish, transparent single crystal of TMCPMP-TS. X-ray structure determination reveals that the keto tautomer is favoured over the enol form for the Schiff base. This is evident from the observed bond distances. C=O bond distance of 1.253 Å, which is consistent with the C=O double bond indicating more characteristic of ketone than C-OH bond. The high configuration effect existing in the pyrazolone-ring induces a narrow range of bond distances. Similarly, the C13–N21 distance of 1.286 Å is also in agreement with a C=N double bond, and C5–N1 with a distance of 1.338 Å is apparently single bond. The bond distances shown in Table 2 indicate that the C23–S25 bond length of 1.682 Å is intermediate between that of C–S single bond distance of 1.82 Å and that of C=S double bond length 1.56 Å. The bond distances around C23, which is 1.363, 1.307 and 1.682 Å for N22, N24 and S25, respectively. These values are indicative of partial double-bond character. Thus, elongation of the C=S bond and shrinkage of the C23–N24 bond are observed, such a configuration would be expected to increase the strength of the intermolecular hydrogen bond, which stabilizes in the keto form in the crystal state. Similarly, the shorter bond length of N21–N22 (1.366 Å) indicates conjugation in the thiosemicarbazone part (Shortening of the N–N bond is observed in thiosemicarbazone, which has an extensively delocalized group on N21). This confirms that the compound is delocalized conjugation system. The bond length of C4–C13 (1.481 Å) suggests a more large conjugate system is formed between the pyrazolone-ring and the side

chain group $C=NNHC(S)NH_2$, showing that the incorporation of the thiosemicarbazone group greatly improves the systematic conjugacy, which could be advantageous to divert energy to form new hydrogen bond. In the compound, there are intermolecular hydrogen bonds $N1-H \cdots O$, $N22-H \cdots O$, $N24-H \cdots O$, but there was no intramolecular hydrogen bond in the crystal (Fig. 2.8. Dashed line).

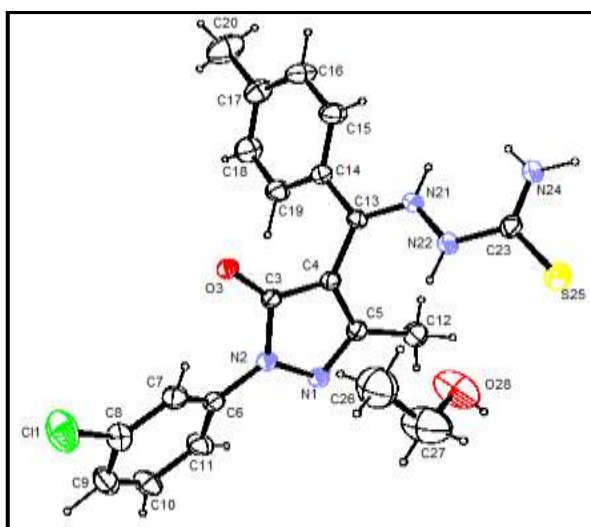


Fig. 2.10. ORTEP view of the TMCPMP-TS with displacement ellipsoids drawn at 50%. H atoms are shown as small spheres of arbitrary radii

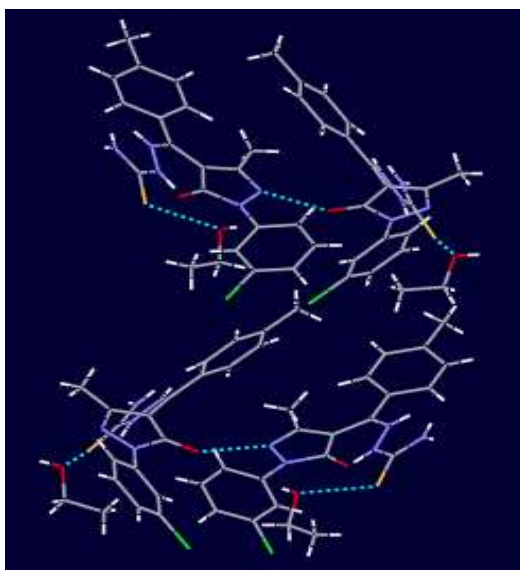


Fig. 2.11. Packing diagram of TMCPMP-TS down the a -axis

Table 2.3. Crystallographic data for the ligand TMCPMP-TS

Compound	TMCPMP-TS
Chemical formula	C ₂₁ H ₂₄ ClN ₅ O ₂ S
Formula Weight	445.96
a(Å)	18.4253(6)
b(Å)	12.0095(4)
c(Å)	20.5326(10)
α(°)	90.00
β(°)	90.00
γ(°)	90.00
Z	8
V(Å ³)	4543.4(3)
Reflections collected	13568
Independent Reflections	2965
R(int)	0.0505
No. of param.	327
Crystal system	Orthorhombic
Space group	Pbca
ρ _{calcd.} (g cm ⁻³)	1.304
Abs coeff, μ(cm ⁻¹)	0.287
F(000)	1872
Temp(°C)	23
GOF on F ²	1.005
R1/wR2 ([I]>2σ(I)]	0.0505/0.1344
R1/wR2 (all data)	0.0712/0.1483
CCDC	815002

Table 2.4. Selected bond lengths and angles in the ligand TMCPMP-TS

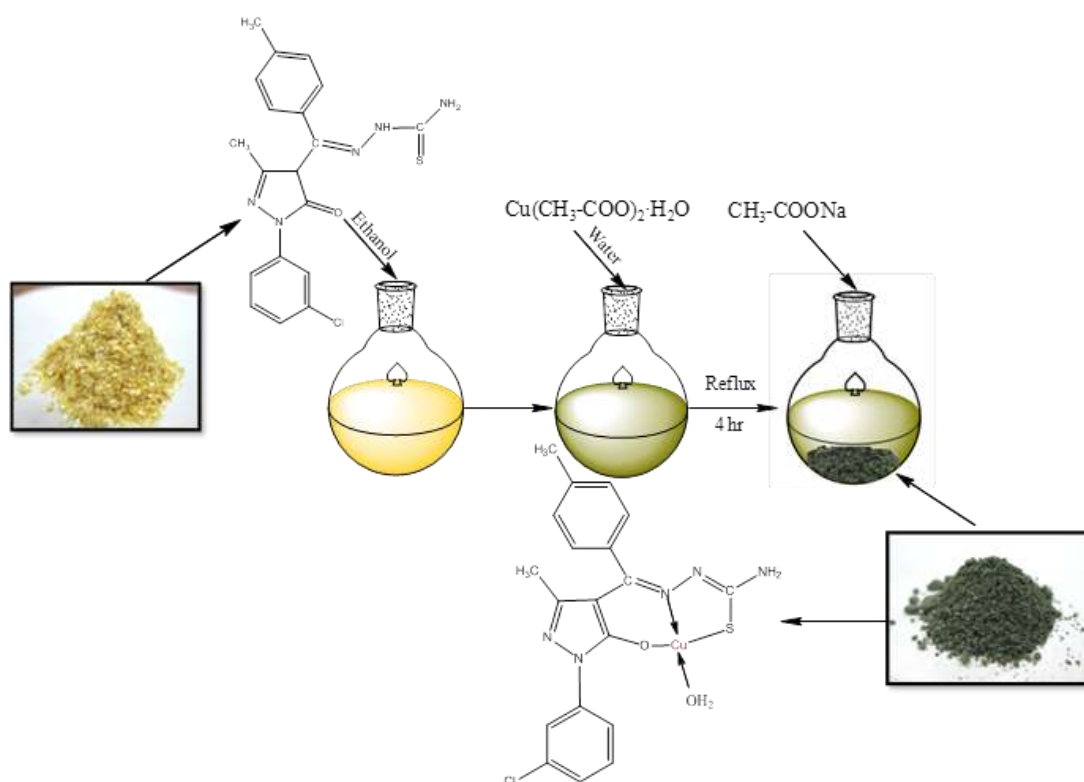
Bond distances (Å) with esd's in parentheses		Bond angles(Å) with esd's in parentheses	
Cl1 C8	1.741(3)	C5 N1 N2	108.74(16)
N1 C5	1.338(3)	N1 N2 C3	108.87(17)
N1 N2	1.385(2)	N1 N2 C6	121.01(16)
N2 C3	1.399(3)	O3 C3 N2	123.2(2)
N2 C6	1.412(3)	O3 C3 C4	131.95(19)
O3 C3	1.253(2)	N2 C3 C4	104.89(17)
N21 N22	1.366(3)	N1 C5 C4	109.31(19)
N22 C23	1.363(3)	N1 C5 C12	121.9(2)
C23 N24	1.307(3)	C9 C8 C11	119.0(2)
C23 S25	1.682(3)	N24 C23 S25	122.92(19)
C13 N21	1.286(3)	N22 C23 S25	120.04(19)
C5 C12	1.480(3)	C13 N21 N22	118.6(2)

So, the compound of yellow crystal is keto form. Unfortunately, though we made numerous attempts to obtain its colourless crystal, the conformation of the compound of white powder is uncertain so far because it has become yellow after the X-ray diffraction. So, a photoisomerization reaction must take place during the irradiation process. It is inferred that the energy barrier for the isomerization of the chromophore is considerably lower in the excited state. Furthermore, there is a strong π -electron conjugation in the thiosemicarbazone part.

2.5. Syntheses of Cu(II) complexes

2.5.1. Syntheses of simple complexes

2.5.1.1. [Cu(TMCPMP-TS)(H₂O)] (16):



Scheme 2.4. Synthesis of [Cu(TMCPMP-TS)(H₂O)]

The metal salt, Cu(OAc)₂·H₂O (0.199, 1mmol) was dissolved in water and

the solution was added to a hot ethanolic solution of TMCPPMP-TS (0.399, 1 mmol). After the complete addition little amount of sodium acetate was added and the mixture was refluxed for 4 h. A crystalline solid was obtained, which was isolated by filtration, washed with hot water and then with ethanol and dried in air.

2.5.1.2. [Cu(TPTPMP-TS)(H₂O)] (17) :



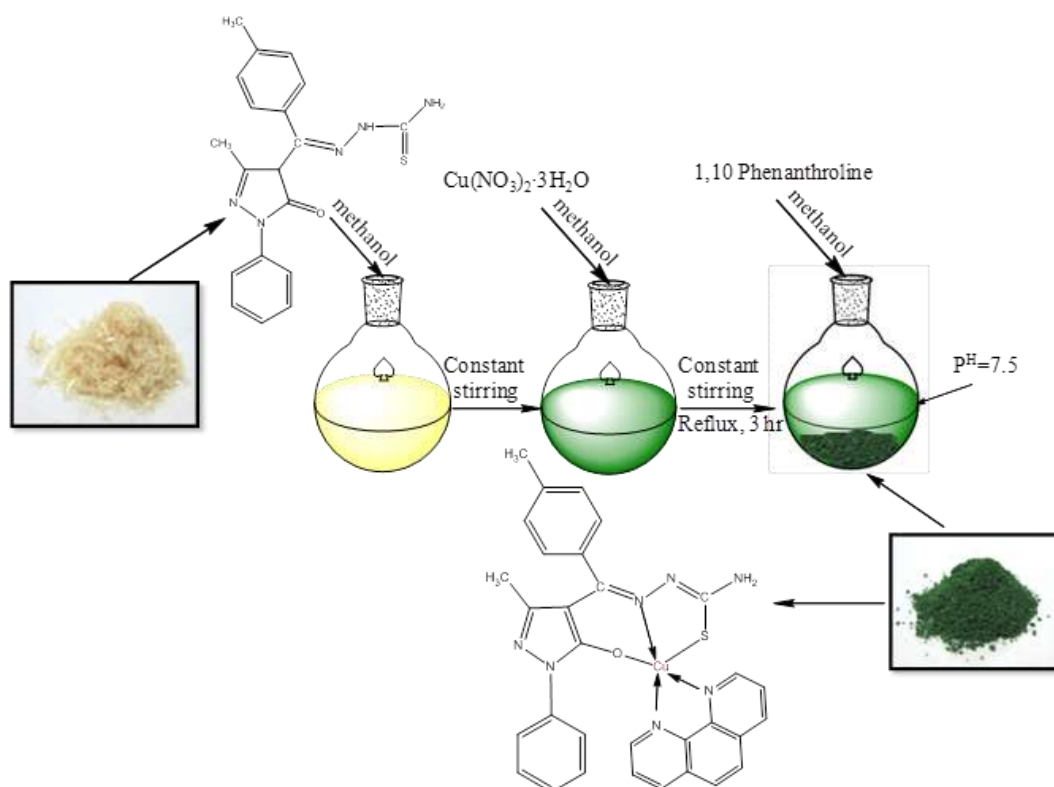
Scheme 2.5. Synthesis of [Cu(TPTPMP-TS)(H₂O)]

It was prepared analogously from TPTPMP-TS and Cu(OAc)₂·H₂O. A crystalline solid thus obtained was isolated by filtration, washed with hot water and then with ethanol and dried in air.

2.5.2. Syntheses of ternary complexes

2.5.2.1. [Cu(TPMP-TS)(Phen)] (18):

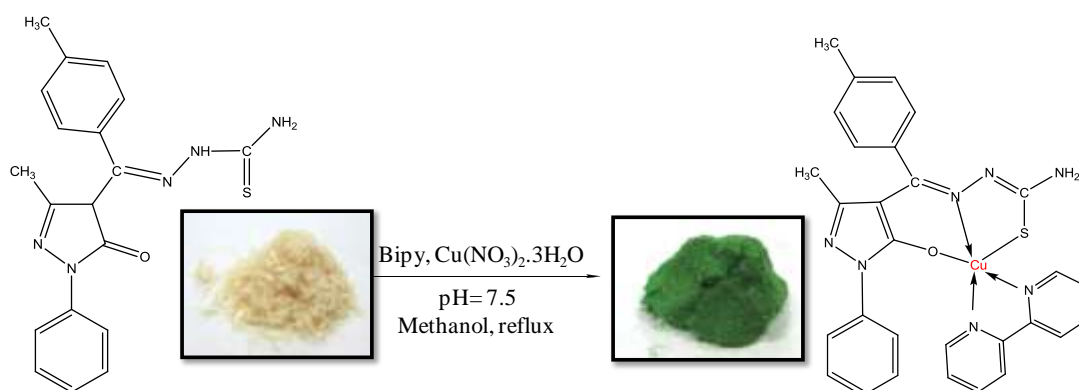
To the solution of Cu(NO₃)₂·3H₂O (0.241 gms, 1 mmol) in methanol (5 mL), a solution of TPMP-TS (0.365 g, 1 mmol) in methanol (10 mL) was added while stirring. To this, a solution of 1, 10 phenanthroline (0.198 g, 1 mmol) in methanol (5 mL) was added as appropriate in warm methanol (5 mL). The p^H of the reaction mixture was maintained around 7.5 by adding a 10% methanolic solution of ammonia. The resultant mixture was refluxed for 3 h. The solid green crystalline product obtained was filtered off, washed with methanol and dried under *vacuum*.



Scheme 2.6. Synthesis of [Cu(TPMP-TS)(Phen)]

2.5.2.2. [Cu(TPMP-TS)(Bipy)] (19):

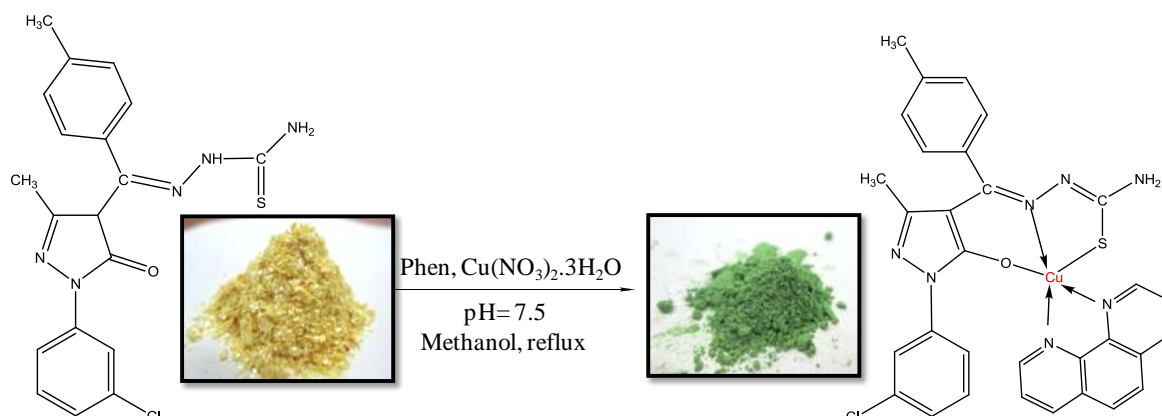
It was prepared analogously from TPMP-TS, Cu(NO₃)₂·3H₂O and 2, 2' bipyridyl. The solid green crystalline product obtained was filtered off, washed with methanol and dried under *vacuum*.



Scheme 2.7. Synthesis of [Cu(TPMP-TS)(Bipy)]

2.5.2.3. [Cu(TMCPMP-TS)(Phen)] (20):

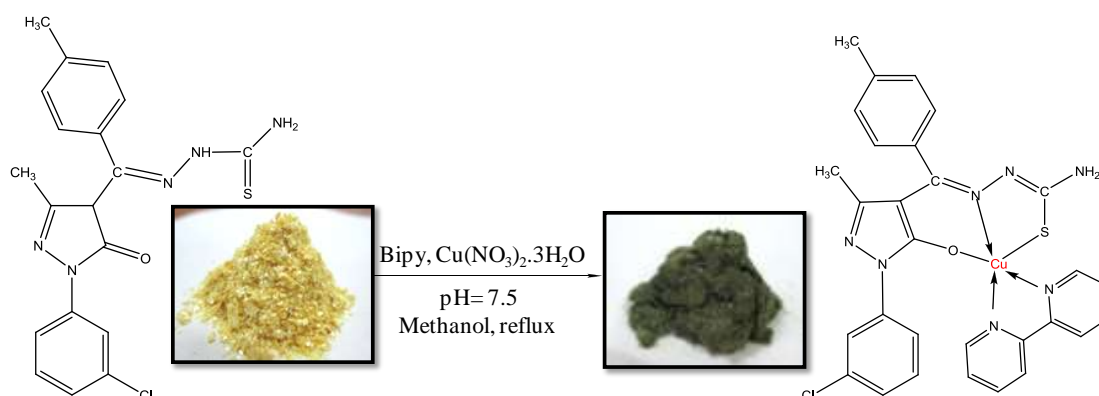
It was prepared analogously from TMCPMP-TS, $\text{Cu}(\text{NO}_3)_2 \cdot 3\text{H}_2\text{O}$ and 1, 10, phenanthroline. The solid green crystalline product obtained was filtered off, washed with methanol and dried under *vacuum*.



Scheme 2.8. Synthesis of [Cu(TMCPMP-TS)(Phen)]

2.5.2.4. [Cu(TMCPMP-TS)(Bipy)] (21):

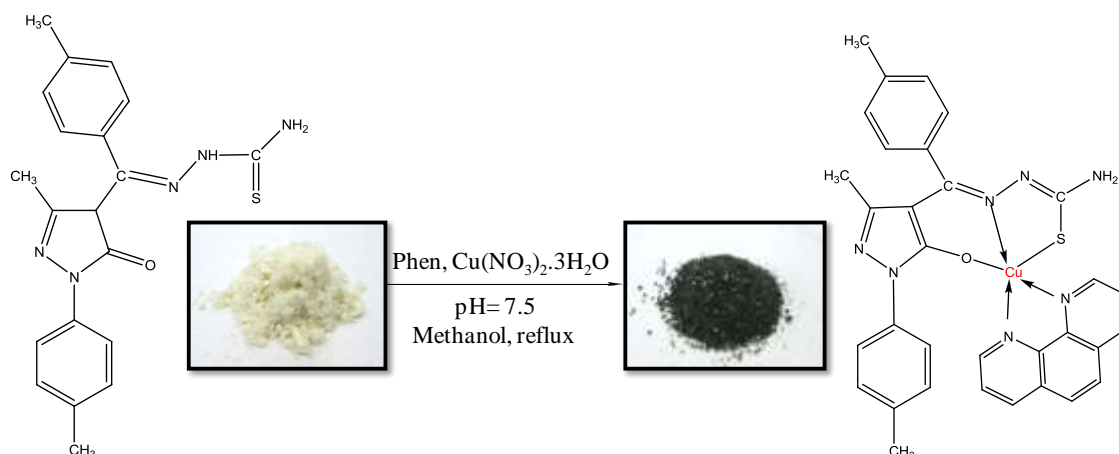
It was prepared analogously from TMCPMP-TS, $\text{Cu}(\text{NO}_3)_2 \cdot 3\text{H}_2\text{O}$ and 2, 2' bipyridyl. The solid green crystalline product obtained was filtered off, washed with methanol and dried under *vacuum*.



Scheme 2.9. Synthesis of [Cu(TMCPMP-TS)(Bipy)]

2.5.2.5. [Cu(TPTPMP-TS)(Phen)] (22):

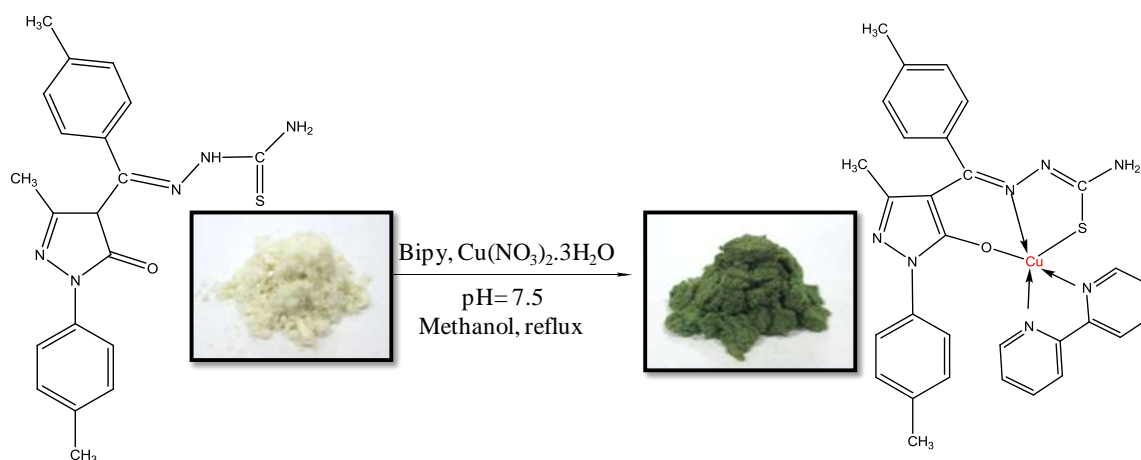
It was prepared analogously from TPTPMP-TS, $\text{Cu}(\text{NO}_3)_2 \cdot 3\text{H}_2\text{O}$ and 1, 10, phenanthroline. The solid green crystalline product obtained was filtered off, washed with methanol and dried under *vacuum*.



Scheme 2.10. Synthesis of [Cu(TPTPMP-TS)(Phen)]

2.5.2.6. [Cu(TPTPMP-TS)(Bipy)] (23):

It was prepared analogously from TPTPMP-TS, $\text{Cu}(\text{NO}_3)_2 \cdot 3\text{H}_2\text{O}$ and 2, 2' bipyridyl. The solid green crystalline product obtained was filtered off, washed with methanol and dried under *vacuum*.



Scheme 2.11. Synthesis of [Cu(TPTPMP-TS)(Bipy)]

2.6. Characterization of Cu(II) complexes

2.6.1. Physicochemical properties of the synthesized complexes

The physicochemical data of all the complexes are listed in Table 2.5. The complexes have been synthesized in a very facile and essentially identical way. The Ligand acts as a tridentate N, S, O donor towards the Cu(II) core. The complexes are obtained from a refluxing mixture of the respective ligand and metal salt precursors, taken in 1:1 molar proportions in purified solvent. All these complexes are intensively colored, air and moisture free crystalline solids. They are insoluble in common organic solvents and only soluble in Acetonitrile, DMF and DMSO. Molar conductance value of the complexes soluble in DMF (10^{-3} M solution at room temperature), indicates that the complexes have molar ratio of metal: ligand as 1:1. The lesser molar conductance values indicate that the complexes are electrically non-conducting in nature [40]. The elemental analyses data concur well with the planned formulae for the ligands and also recognized the [Cu(L)(H₂O)] composition for the simple complexes and [Cu(L)(Phen/Bipy)] composition for ternary complexes.

Table 2.5. Physicochemical and analytical data of the complexes

Complex	Formula Weight(g mol ⁻¹)	Colour	Yield (%)	Melting Point(°C)	Analysis (%) Found(calcd)				$\Lambda_M(\Omega^{-1} \text{cm}^2 \text{mol}^{-1})$
					C	H	N	Cu	
16	480.44	Green	66.76	240	47.38 (47.60)	3.62 (3.78)	14.45 (14.61)	13.10 (13.25)	7
17	460.02	Brown	65.89	255	52.19 (52.33)	4.45 (4.61)	15.13 (15.26)	13.71 (13.84)	12
18	607.19	Dark green	75.38	>250	61.20 (61.32)	4.19 (4.15)	16.22 (16.15)	10.50 (10.47)	13
19	583.17	Dark green	77.56	>250	59.78 (59.73)	4.39 (4.32)	16.76 (16.81)	10.80 (10.90)	11
20	641.63	Dark green	70.58	>250	58.10 (58.03)	3.76 (3.77)	15.15 (15.28)	9.78 (9.90)	6
21	617.61	Dark green	74.62	>250	56.54 (56.40)	3.97 (3.92)	15.80 (15.88)	10.21 (10.29)	9
22	621.21	Green	67.29	>250	61.80 (61.87)	4.40 (4.38)	15.70 (15.78)	10.20 (10.23)	6
23	597.19	Dark green	64.62	>250	60.30 (60.34)	4.51 (4.56)	16.48 (16.42)	10.69 (10.64)	8

2.6.2. Crystal structure description of ternary complex

2.6.2.1. Complex 20

The molecular structure and the atom labeling scheme is shown in Fig. 2.12. The crystallographic data of the complex are listed in Table 2.6. The main bond distances and angles are listed in Table 2.7. The packing diagram of the complex is shown in Fig. 2.13.

As shown in Fig. 2.6, the Cu(II) ion is pentacoordinated by three nitrogen atoms (azomethane N21 and pyridine N26, N37), one oxygen donor (enol O1) and one sulphur donor (thiol S25). The Cu-Nphen distances observed [Cu1-N26, 2.033(3) Å; Cu1-N37, 2.261(4) Å] fall within the range for Cu-Nimine distances observed for other diimine complexes already reported [41]. The three donors of the thiosemicarbazone molecule occupy the basal sites of the pyramidal structure, whereas the phenanthroline ligand binds the copper at the apical site also.

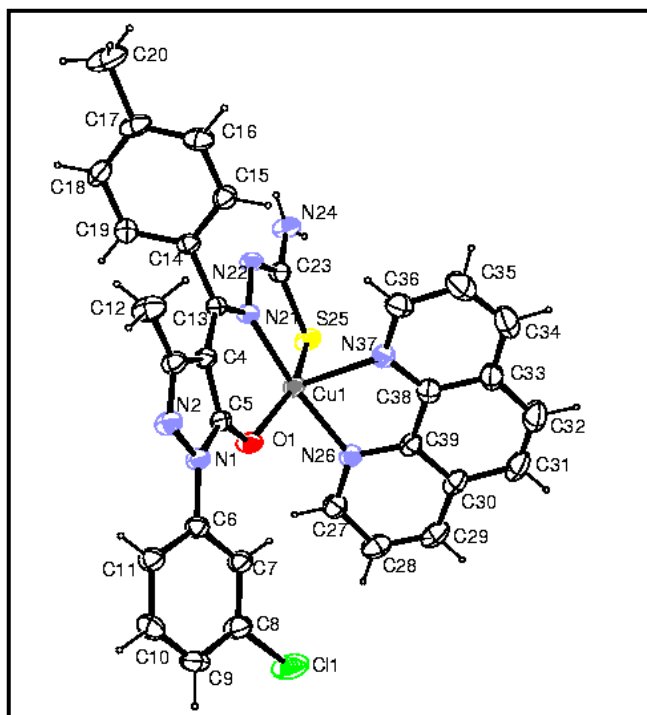
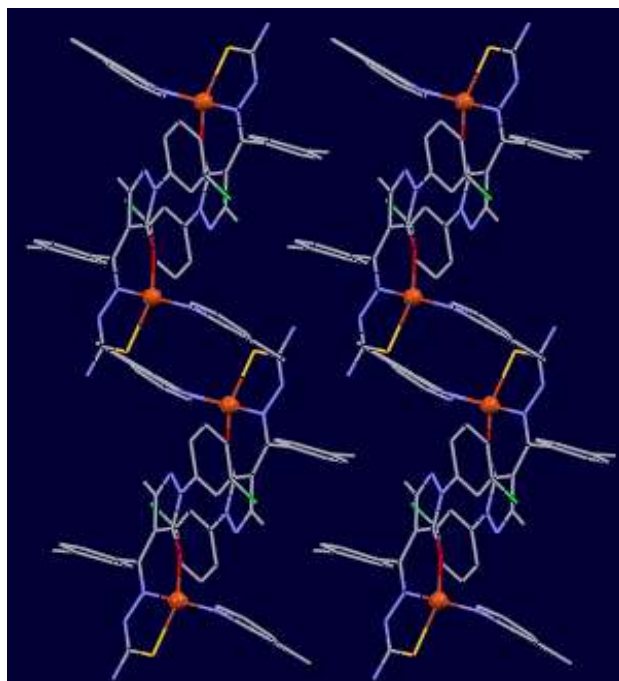
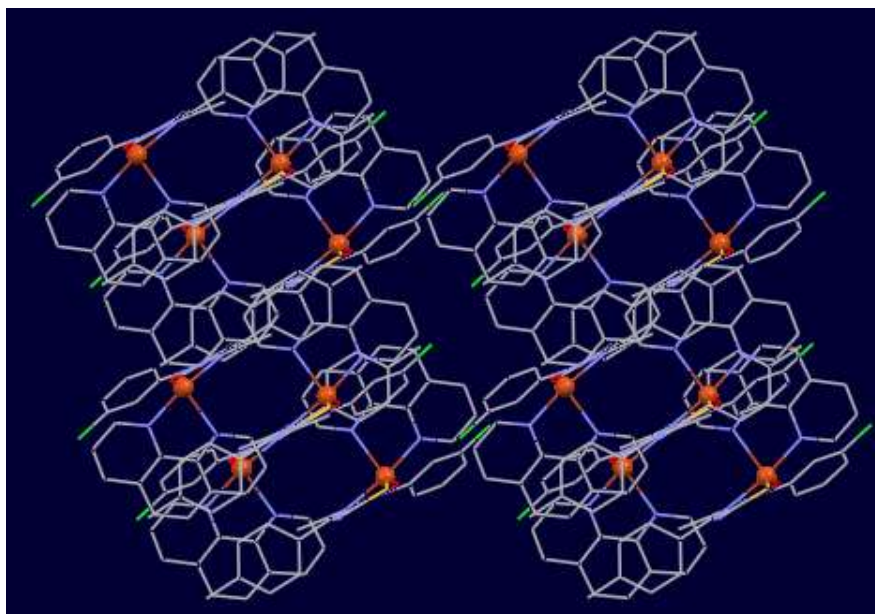


Fig. 2.12. ORTEP view of complex 20 with displacement ellipsoids drawn at 50%. H atoms are shown as small spheres of arbitrary radii. Solvent molecule has been removed for clarity.



(a)



(b)

Fig. 2.13. The packing diagrams of complex **20**

In the complex, the copper atom occupies a distorted square pyramidal environment (SP), formed by three atoms (N, S, O) supplied by one thiosemicarbazone and one atom supplied by the phen ligand. The another arm of the phen ligand completes the fifth coordination site. The four donors (N21, S25, O1, N26) of the thiosemicarbazone and phen molecules occupy the basal sites of the pyramidal structure, whereas another N37 of the phen ligand binds the copper at the apical site. The Cu–N/O/S distances of the basal plan are Cu(1)–O(1)=1.932(3), Cu(1)–N(21)=1.972(3), Cu(1)–S(25)=2.2624(11) and Cu(1)–N(26)=2.033(3) Å, and the Cu(1)–N(37) distance is 2.261(4) Å. The longest distance does not correspond to the terminal Cu–N(37), but instead to one of the basal Cu–S25 distance of the thiosemicarbazone molecule.

Table 2.6. Crystallographic data for the complex 20

Complex	20
Chemical formula	C ₃₁ H ₂₄ ClCuN ₇ OS, C ₂ H ₆ OS
Formula weight	719.54
Crystal description	Dark green block
a(Å)	9.5066(4)
b(Å)	11.8229(5)
c(Å)	14.9547(5)
α(°)	78.535(3)
β(°)	79.135(3)
γ(°)	83.427(3)
Z	2
V(Å ³)	1612.59(11)
Reflection collected/unique	95559/6331
R(int)	0.1094
Number of parameters	449
Crystal system, Space group	Triclinic, P-1
Limiting indices	-13 ≤ h ≤ 13, -14 ≤ k ≤ 14, -15 ≤ l ≤ 15
Crystal size	0.3 x 0.2 x 0.2 mm
ρ _{calcd.} (g cm ⁻³)	1.482
Abs coeff, μ(cm ⁻¹)	0.933
F(000)	742
Temp(°C)	23
GOF on F ²	1.065
R1 /wR2([I > 2σ(I)])	0.0588/0.1238
R1 /wR2(all data)	0.0905/0.1388
CCDC	885025

To obtain the quantitative degree of distortion of the copper polyhedron the ratio between the two basal angles, defined as $\tau = [(\theta - \phi) / 60] \times 100$, that represents the percentage of trigonal distortion from square pyramidal geometry [42], was used. For an ideal SP, τ is 0 while for an ideal TBP τ is 100. Thus, for title complex (see Fig. 2.12 for labelling) the relevant angles, $\theta = 172.21$ and $\phi = 152.38$ (Table 2.7) yields a τ value of 33% which indicates a geometry close to SP. The coordination sphere is of the type Cu1-N26-N37-S25-N21-O1, exhibiting a geometry in between trigonal bipyramidal (TBP) and square pyramidal (SP).

Table 2.7. Important bond lengths and bond angles of complex 20

Bond distances (Å) with esd's in parentheses		Bond angles(Å) with esd's in parentheses	
Cu1 O1	1.932(3)	O1 Cu1 N21	94.86(12)
Cu1 N21	1.972(3)	O1 Cu1 N26	88.35(12)
Cu1 N26	2.033(3)	N21 Cu1 N26	172.21(14)
Cu1 N37	2.261(4)	O1 Cu1 N37	110.79(13)
Cu1 S25	2.2624(11)	N21 Cu1 N37	94.42(13)
S25 C23	1.739(4)	N26 Cu1 N37	77.80(13)
O1 C5	1.279(4)	O1 Cu1 S25	152.38(10)
N21 C13	1.320(5)	N21 Cu1 S25	86.04(9)
N21 N22	1.408(4)	N26 Cu1 S25	94.40(10)
N22 C23	1.309(5)	N37 Cu1 S25	96.61(9)
N24 C23	1.350(5)	C23 S25 Cu1	93.63(13)
N26 C27	1.311(5)	C5 O1 Cu1	118.4(2)
N26 C39	1.362(5)	C13 N21 Cu1	125.0(3)
N37 C36	1.323(5)	N22 N21 Cu1	119.2(2)
N37 C38	1.353(5)	C27 N26 Cu1	126.5(3)
N1 C5	1.378(5)	C39 N26 Cu1	115.4(3)
N1 N2	1.389(4)	C36 N37 Cu1	131.6(3)
N1 C6	1.417(5)	C38 N37 Cu1	108.3(3)

2.6.2.1.1. Changes in the bond distances in ligand on complexation

Complex formation can also be proven by comparing the X-ray data of the ligand and the title complex. It is clearly seen that there are some changes in the bond distances in ligand on complexation. The changes are listed in Table 2.8.

Table 2.8. Changes observed in the bond distances on complexation

Bond distance	Ligand	Complex	Effect
N21-N22	1.366(3)	1.408(4)	Increase
C3-O3	1.253(2)	1.279(4)	Increase
N22-C23	1.363(3)	1.309(5)	Decrease
S25-C23	1.682(3)	1.739(4)	Increase
C4-C13	1.481(3)	1.422(5)	Decrease
C13-N21	1.286(3)	1.320(5)	Increase
C23-N24	1.307(3)	1.350(5)	Increase

2.6.3. IR spectral studies

The characteristic IR bands for all the complexes recorded as KBr discs are listed in Table 2.9. The IR spectra of the complexes **16** and **20** are shown in Figs. 2.14 & 2.15.

On comparison of the IR spectra of the ligands with Cu(II) complexes, IR spectra of the complexes showed a major shift to lower wave numbers by 20-30 cm^{-1} in azomethane $\nu(\text{C}=\text{N})$ suggesting involvement of the azomethane-N with Cu(II) ion in the complexation. The band corresponding to the stretching vibration of the C=S group appears at 839 cm^{-1} in the ligand. The absence of this band in the IR spectra of the complexes can be explained by the tautomerism of the C=S group with one of the imino groups to form the C-SH and the coordination of sulphur after deprotonation. The band due to $\nu_{\text{C}=\text{O}}$ is completely missing in the spectrum of the complex, suggests enolization of the ligand on complexation. A new band that appears in the range 1420-1490 cm^{-1} is thus assigned to the $\nu(\text{C}-\text{O})$ in the IR spectra of the complexes, which supports the observation of its enolization during coordination. This fact suggests that the ligand remains in the keto form in the solid state, but in solution both the keto and enol forms remain in equilibrium. Deprotonation occurs from the enol form on complexation. These overall data suggest that the azomethane-N and enol-O and thiol-S groups are involved in coordination with the Cu(II) ion during complexation [43]. In the low-frequency region, spectrum of the complex exhibits new bands which are not present in the spectra of the ligands. These bands appeared in the range 490-600 cm^{-1} , 460-520 cm^{-1} and 410-500 cm^{-1} recognized to $\nu(\text{Cu}-\text{N})$,

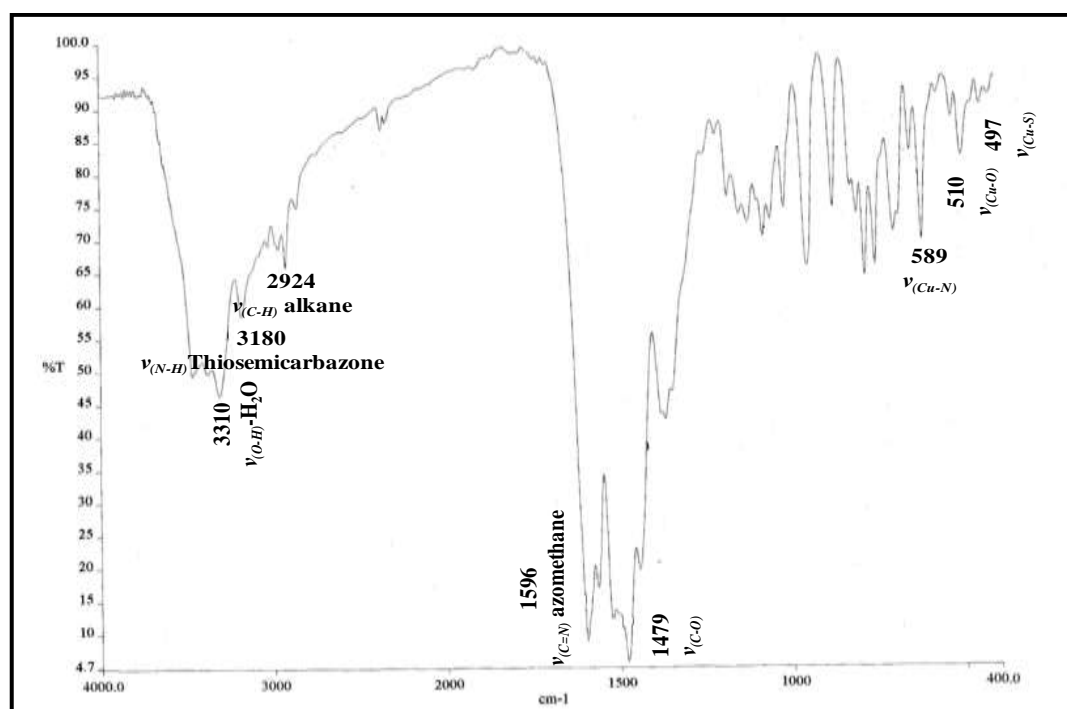


Fig. 2.14. IR spectrum of complex 16

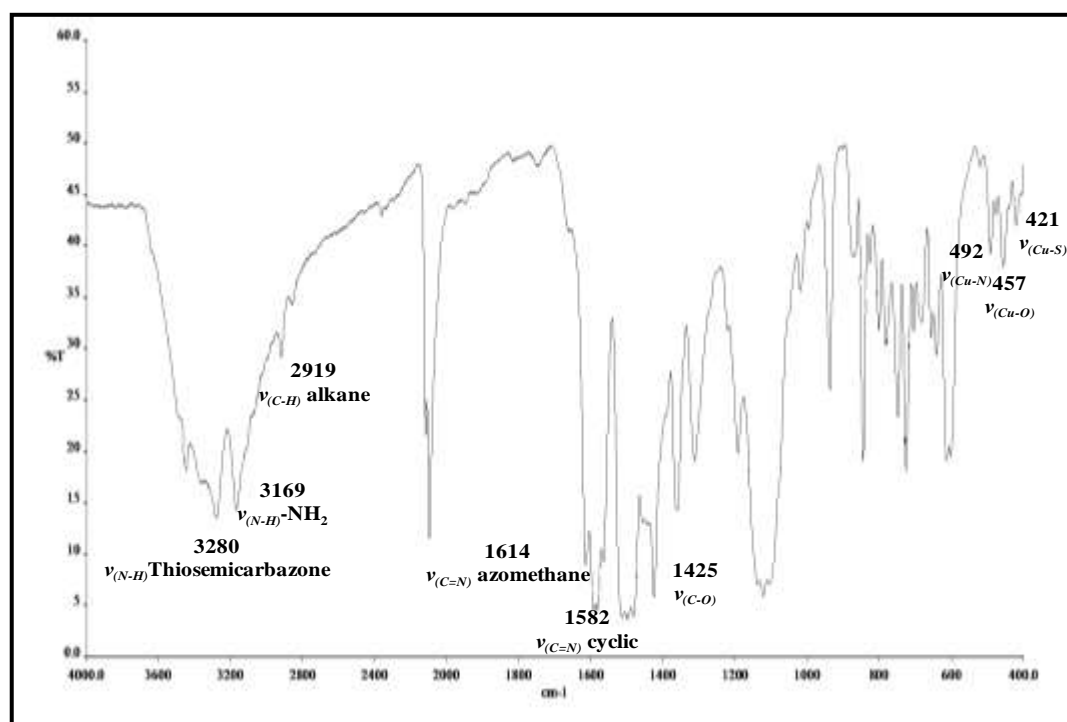


Fig. 2.15. IR spectrum of complex 20

$\nu(\text{Cu-O})$ and $\nu(\text{Cu-S})$, respectively. Bands at around 1,518, 1,425 and 721 cm^{-1} in the ternary complexes, assigned to $\nu(\text{C=N})$, $\nu(\text{C=C})$ and out-of-plane -CH stretching vibrations of 1, 10-phenanthroline, confirm the presence of polypyridyl ligands in the coordination sphere of the ternary complexes [44].

Table 2.9. IR spectral assignments of the complexes

Complex	$\nu_{(\text{OH})\text{coordinated H}_2\text{O}}$	$\nu_{\text{N-H}} (-\text{N-H-tsc})$	$\nu_{\text{N-H}} (-\text{NH}_2)$	$\nu_{\text{C=N}} (\text{cycl.})$	$\nu_{\text{C=N}} (\text{azo-methane})$	$\nu_{\text{C-O}}$	$\nu_{\text{Cu-O}}$	$\nu_{\text{Cu-N}}$	$\nu_{\text{Cu-S}}$	$\nu_{\text{C=N}} (\text{phen})$
16	3310	-	3180	1550	1596	1479	510	589	497	-
17	3307	-	3185	1563	1596	1485	512	598	419	-
18	-		3192	1568	1590	1480	487	498	426	1510
19	-		3178	1572	1599	1474	473	502	430	1508
20	-	3280	3169	1582	1614	1425	457	492	421	1499
21	-	3276	3169	1581	1614	1439	460	492	421	1525
22	-	3286	3178	1586	1611	1480	491	594	435	1511
23	-	3282	3170	1584	1613	1459	493	591	430	1519

2.6.4. Mass spectral studies

The mass spectral assignments for simple complexes are shown in section 2.3.

2.6.4.1. Mass spectral studies of simple complexes

The mass spectrum of the complex **16** is shown in Fig. 2.16. The complexes gave a molecular ion peak at m/z **480.80** (MIP, 480.44) and m/z **481.80** (M+1, 481.44) with a relative intensity 18% and 98%, respectively. The intensities of these peaks gave the idea of the stability and abundance of the fragments. This is in good agreement with the micro analytical data. The fragmentation pattern of the complex **16** is shown in Scheme 2.12.

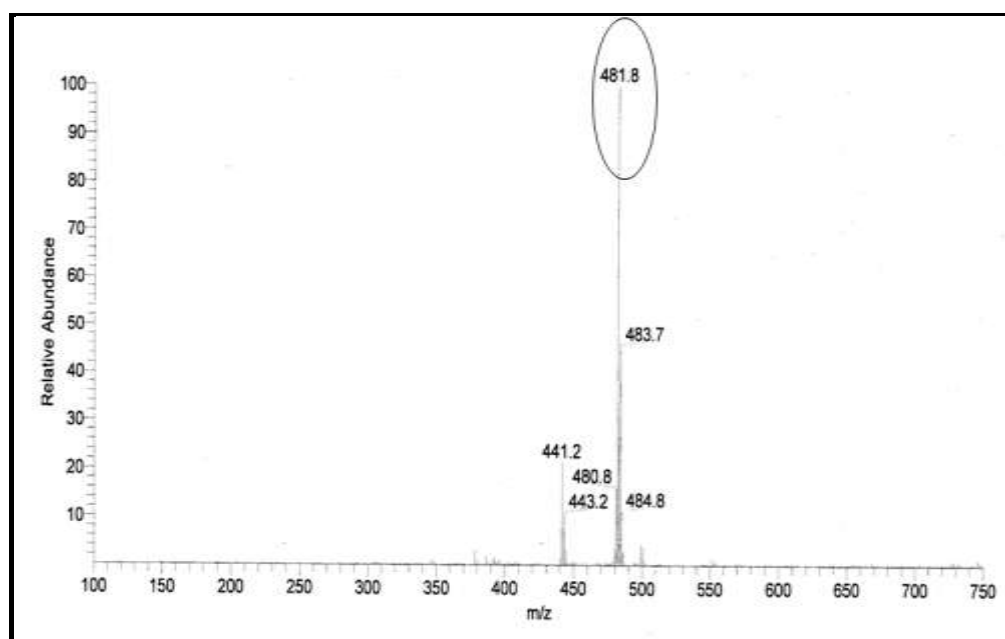
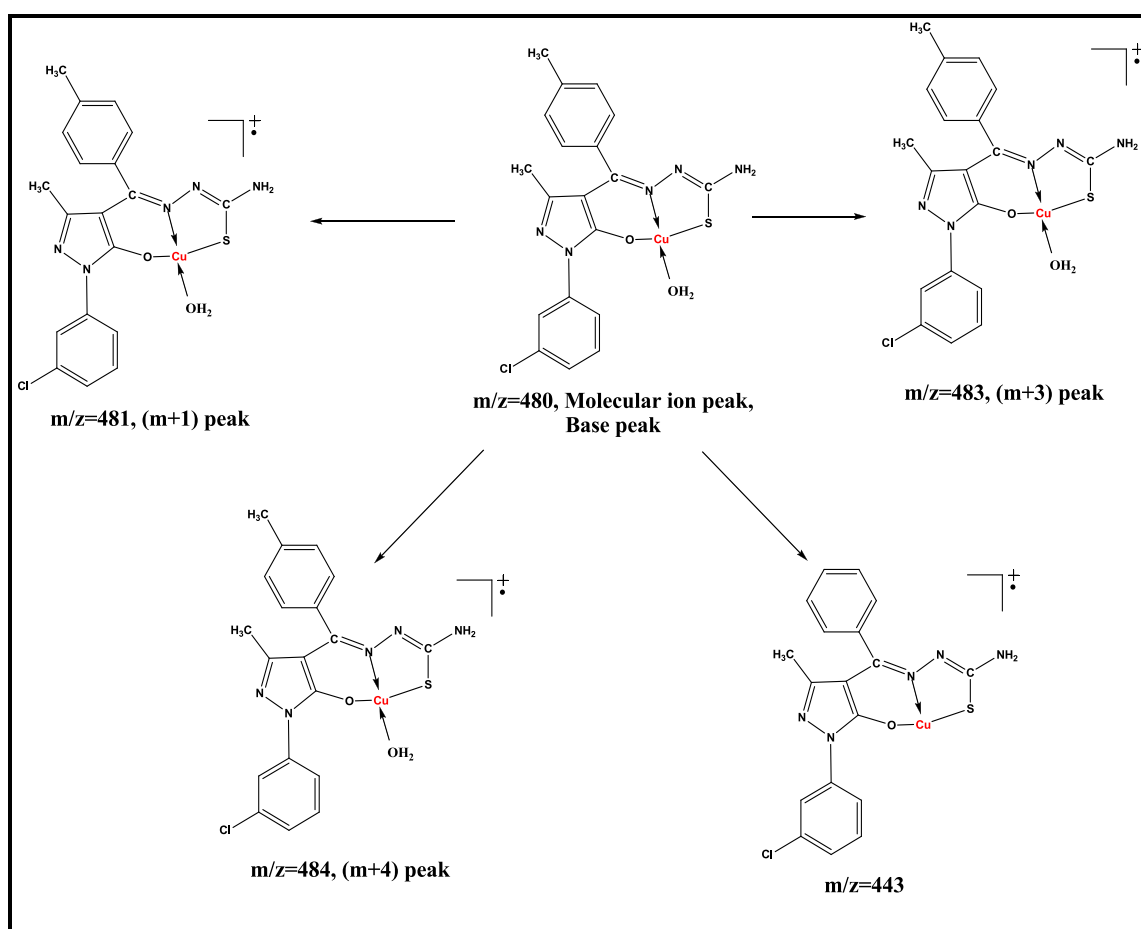


Fig. 2.16. Mass spectrum of the complex 16



Scheme 2.12. Fragmentation pattern of the complex 16

2.6.4.2. Mass spectral studies of ternary complexes

The electronic impact mass spectrum of complex **22** is shown in Fig. 2.17. It shows a molecular ion peak at m/z **621.4** with a relative intensity near to 20%, which coincident with the formula weight 621.2. It also gives (M+2) peak at m/z **623**. The peak appeared at m/z **303** is a base peak and it is due to the substituted pyrazolone moiety.

The other peaks appeared in the mass spectrum (abundance range 1-100%) are attributed to the fragmentation of molecule obtained from the rupture of different bonds inside the molecule. The fragmentation of the heterocyclic rings, which includes pyrazole ring, is result of small and stable, neutral molecules, which are analogous to HCN, such as C=NH as well as HC=CH and thus is not discussed herein. The fragmentation pattern of the complex **22** is shown in Scheme 2.13.

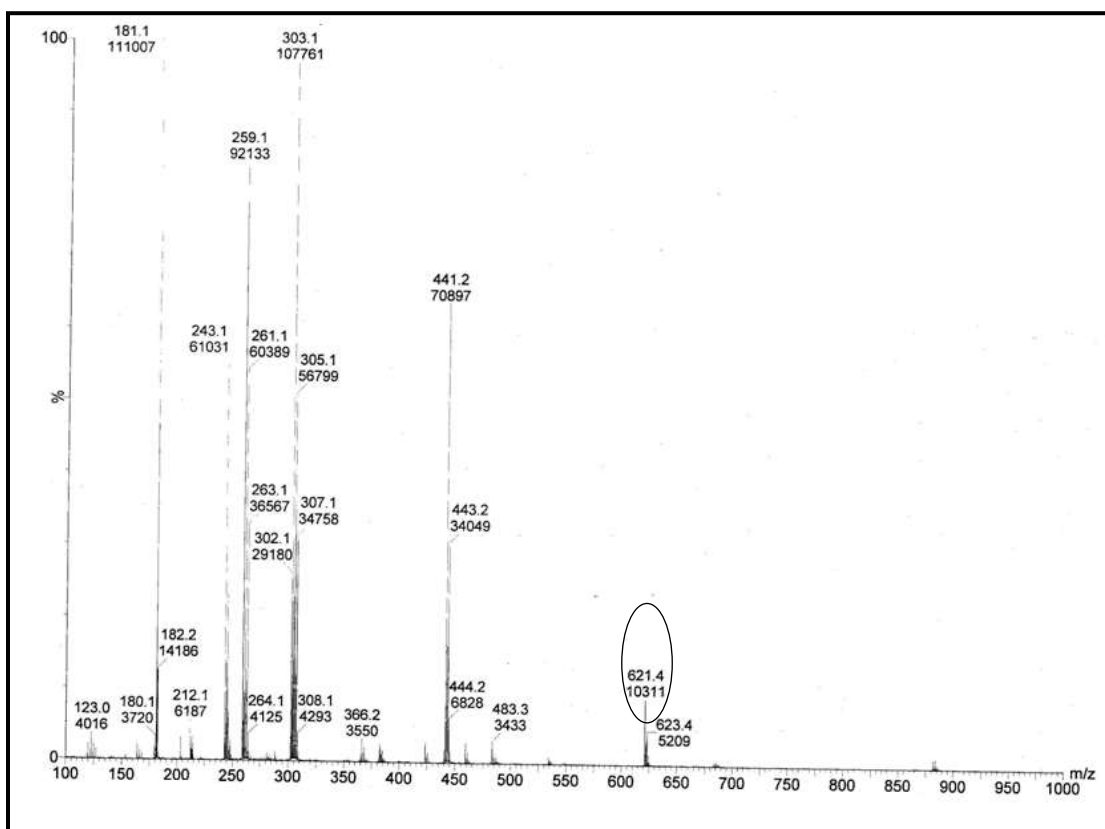
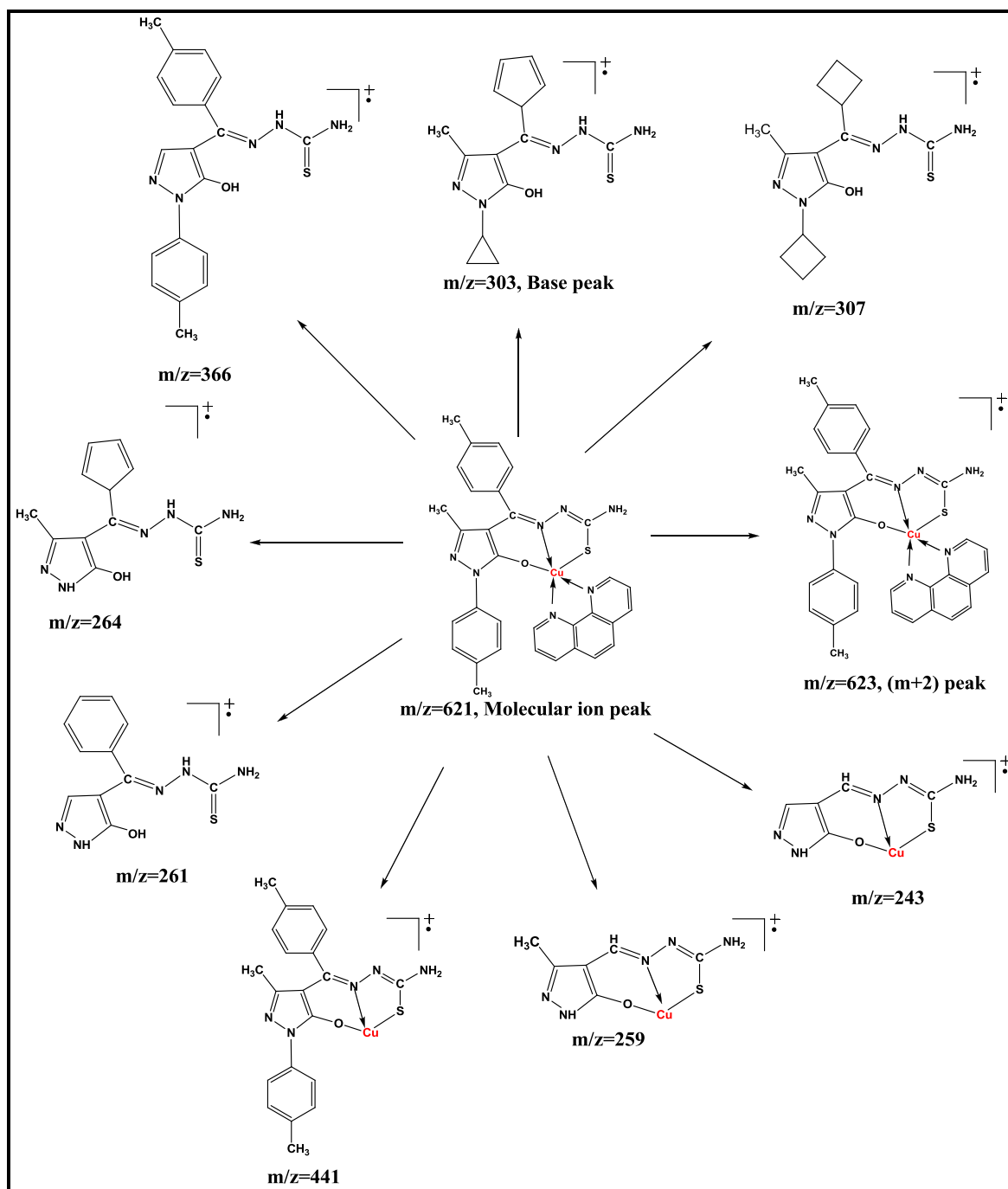


Fig. 2.17. Mass spectrum of the complex **22**



Scheme 2.13. Fragmentation pattern of the complex 22

2.6.5. Electronic spectral studies

Electronic spectral studies serve as a tool to distinguish between the different geometries of the complexes. The electronic spectral data of the complexes are shown

in Table 2.10. The electronic spectra of the complexes **17** & **18** are shown in Figs. 2.18 & 2.19.

Table 2.10. Electronic spectral data of the complexes

Complex	d-d transition	
	$\lambda_{\text{max/nm}}$	ϵ ($\text{dm}^3 \text{mol}^{-1} \text{cm}^{-1}$)
16	566	201
17	570	226
18	714	58.5
19	686	77.5
20	651	127.7
21	612	105.5
22	647	89.8
23	653	86.3

2.6.5.1. Electronic spectral studies of simple complexes

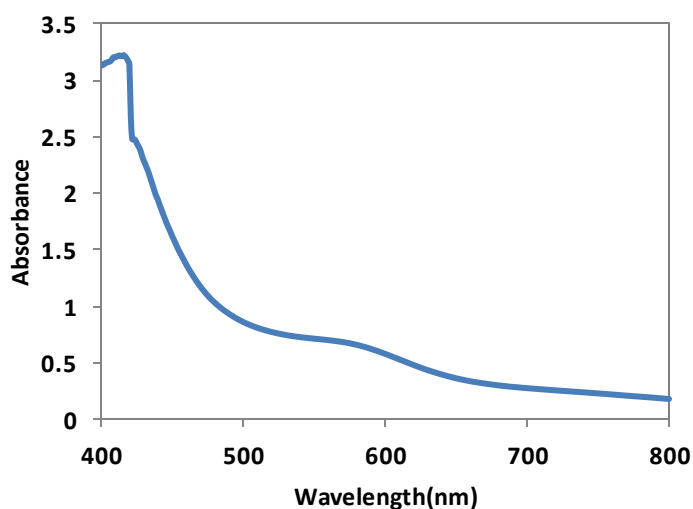


Fig. 2.18. Electronic spectrum of **17**

These complexes are magnetically normal with magnetic moments of 1.83 and 1.78 BM, respectively. Electronic absorption spectra of the complexes in DMF solution shows a d-d transition at about 566 and 570 nm, respectively which can be assigned as the ${}^2B_{1g} \rightarrow {}^2A_{1g}$ transition, revealing that the Cu(II) complexes exist in the square-planar geometry [45].

2.6.5.2. Electronic spectral studies of ternary complexes

The visible spectra for the complexes under investigation were measured in DMF. In DMF, the complexes displayed absorbance maxima in the 670–720 nm range with a shoulder around 900 nm. For five-coordinate Cu(II) complexes, this spectral feature is typical for SP or distorted SP geometries, which generally exhibit a band in the 550–660 nm range ($d_{xz}, d_{yz} \rightarrow d_{x^2-y^2}$); the geometry around each Cu is SP or distorted SP. In contrast, TBP Cu(II) complexes usually show a maximum at $\lambda > 800$ nm ($d_{xz}, d_{x^2-y^2} \rightarrow d_z^2$) with a higher energy shoulder. Thus, in DMF, the geometry about the Cu(II) centre in the complexes is closer to SP. These data are consistent with the reported literature for the distorted square pyramidal Cu(II) complexes [46].

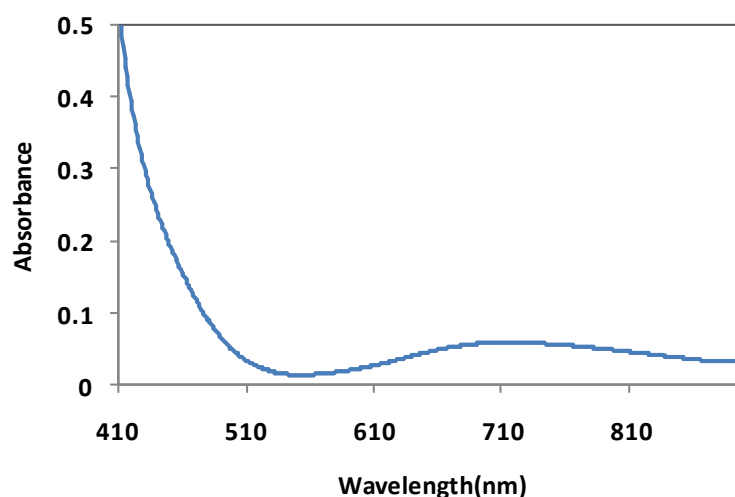


Fig. 2.19. Electronic spectrum of complex 18.

2.6.6. Thermal studies

The aim of thermal analysis is to open up new possibilities for the investigation of metal complexes and to obtain information concerning the thermal stability of the investigated complexes, to decide whether water molecules or solvent molecules are inside or outside the coordination sphere. In our case, there are two types of complexes. In the case of simple complexes, we have proposed and proved that water molecule is there in the complex composition, whereas, in the case of

ternary complexes, there is no water/solvent molecule in the complex composition. Therefore, we have carried out the thermal analysis in the case of only simple complexes.

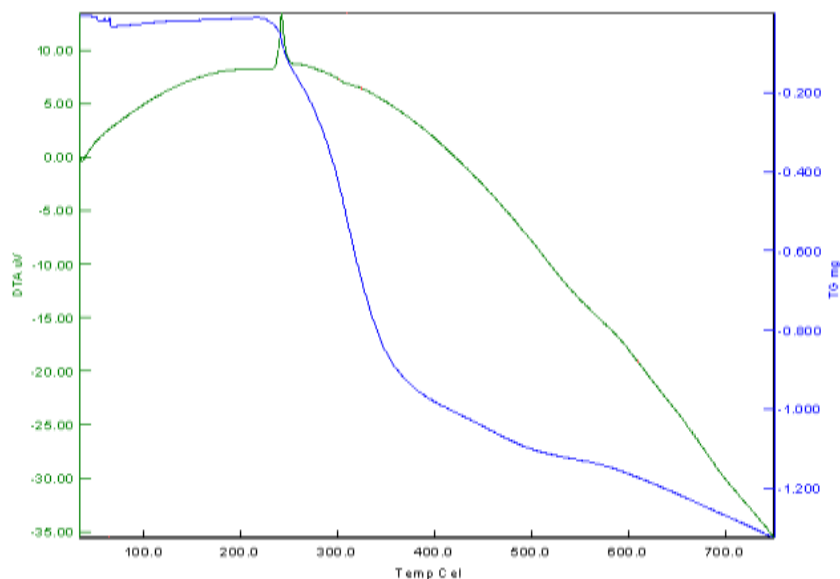


Fig. 2.20. Thermogram of the complex 16.

Thermal stability and thermal behaviors of both the simple complexes were studied by thermogravimetric analysis (TGA-DTA) at the atmosphere of nitrogen in the temperature range 25-700°C. The correlations between the different decomposition steps of the complexes with the corresponding weight losses are discussed in terms of the proposed formulae of the complexes. The thermal behavior studies of both the complexes are almost same. Hence, the representative complexes have been discussed in general. The TGA profiles over the temperature range 30-250°C are usually due to loss of moisture, water of hydration and water of coordination. The complexes have first decomposition stage in the range 200-250°C. This dehydration process probably is due to the loss of coordinated water, which may be bound to hydroxyl group of the ligand by hydrogen bonds. Above 250°C, complexes decompose in a gradual manner, which may be due to fragmentation and thermal degradation of the organic moiety. The continuous loss of weights is observed up to 700°C respectively. This process is accompanied by exothermic process at around 250°C in DTA and DTG curves of both complexes. The thermogram of the

complex **16** is shown in Fig. 2.20. The thermoanalytical data of both the complexes are presented in Table 2.11.

From the above thermogravimetric analyses, the overall weight losses for the complexes agree well with the proposed formulae obtained by elemental analyses, IR, Mass and magnetic susceptibility measurements.

Table 2.11. Thermoanalytical data of the simple complexes

Complexes	TG range (°C)	DTA max(°C)	Mass loss(%) obs.(calcd.)	Assignments
16	30-250	242	3.74(3.75)	Loss of one coordinate water molecule
17	30-250	245	3.90(3.92)	Loss of one coordinate water molecule

2.6.7. Magnetic measurement studies

Magnetic moment measurements of all the complexes show μ_{eff} of 1.78-1.83 B.M., which corresponds to one unpaired electron and is expected from mononuclear Cu(II) complexes (d^9) with some orbital contribution. The magnetic moment values of the copper complexes correspond to the spin only value of 1.73 B.M. for the Cu(II) complexes [47].

2.6.8. ESR studies

2.6.8.1. ESR studies of simple complexes

As we could not get well-shaped single crystals, the X-band ESR spectra were recorded only for solution and powder samples for the complex **16** at RT and LNT to obtain further information about the stereochemistry and the site of the metal-ligand bonding and to determine the magnetic environment in the metal complexes. The spectra are shown in Figs. 2.21 & 2.22, respectively. The powder sample was recorded in quartz tube to avoid Mn(II) or Fe(II) impurities and solution spectra was recorded in DMF solution in capillary tube. The solution spectrum was recorded to confirm that the complex does not undergo structural change in solution.

The powder as well as the solution ESR spectra of the complex **16** was studied. The spectrum of the complex at 300K shows one intense absorption band in the high field region and is isotropic due to tumbling motion of the molecules. Hamiltonian parameters g_{\parallel} , g_{\perp} , A_{\parallel} and A_{\perp} were also calculated. The magnetic susceptibility value reveals that the copper complex has a magnetic moment, 1.82 B.M., corresponding to the one unpaired electron, indicating that the complex is mononuclear. This fact was also evident from the absence of a half field signal, observed in the spectrum at 1600 G due to the $m_s = \pm 2$ transitions, ruling out any Cu-Cu interaction [48].

The ESR spectrum of the complex at 77 K indicates a poorly resolved nitrogen super hyperfine structure in the perpendicular region due to the interaction of the Cu(II) odd electron. The ESR spectrum of the complex at 77 K indicates a poorly resolved nitrogen super with nitrogen atoms. The RT solution ESR consists of four asymmetrical but equally spaced hyperfine lines characteristic of the Cu(II) nuclear hyperfine interaction ($Cu=I=3/2$ for ^{63}Cu and ^{65}Cu). Complex shows the $g_{\parallel} = 2.316$ and $g_{\perp} = 2.136$, for Cu(II) g_{\parallel} indicates covalence with $g_{\parallel} < 2.3$ for covalent complexes and $g_{\parallel} \geq 2.3$ for ionic [49]. g_{\parallel} value of the complex of 2.316 indicates covalency for M-L bond. The frozen DMF solution is axial with $g_{\parallel} > g_{\perp} > 2.0023$, indicating a $d_{x^2-y^2}$ ground state which is in agreement with the electronic absorption spectroscopic assignments. The most remarkable feature is that the g_{\parallel} value (2.31) is substantially higher than the majority of known Cu(II) complexes. A factor potentially contributing to increase of g_{\parallel} is distortion from square-planar geometry [50]. From the observed values, it is clear that A_{\parallel} (**190**) $>$ A_{\perp} (**17**); g_{\parallel} (2.316) $>$ g_{\perp} (2.136) $>$ 2.0023 and the ESR parameters of the complex coincide well with related systems which suggest that the complex has square-planar geometry and the system is axially symmetric.

In the axial spectra the g-values are related with exchange interaction coupling constant (G). The nature of ligand is also evaluated from G value by the expression,

$$G = \frac{g_{\parallel} - 2}{g_{\perp} - 2} \cong 4.0$$

According to Hathaway [50], if the G value is larger than four, the exchange interaction is negligible because the local tetragonal axes are aligned parallel or are slightly misaligned. If the G value is less than four, the exchange interaction is considerable and the local tetragonal axes are misaligned. The observed value for the exchange interaction parameter for the Cu(II) complex ($G = 2.350$) suggests that the ligand forming complex is regarded as a strong field, and the local tetragonal axes are misaligned, and the unpaired electron is present in the $d_{x^2-y^2}$ orbital and the exchange coupling effects are not operative in the present Cu(II) complex.

For $G < 4.0$, the ligand forming the Cu(II) complex is regarded as a strong field ligand. For this complex $G = 2.350$, indicating that the ligands are strong field ligands and the metal-ligand bonding in these complexes is covalent. It also indicates that the stereochemistry of complex [50].

The degree of geometrical distortion was ascertained by a parameter $g_{\parallel}/A_{\parallel}$ (A_{\parallel} in cm^{-1}) with the values less than 140 cm associated with the square-planar structure, whereas higher values indicate distortion towards tetrahedron. For a square planar Cu(II) complexes, this ratio usually falls in the range 90-140 cm. For the present Cu(II) complex, the ratio is **121 cm**, which is in agreement with significant deviation from planarity and which is further confirmed by the bonding parameter α^2 whose value is less than unity [50].

Electron paramagnetic resonance and optical spectra have been used to determine the covalent bonding parameters for the Cu(II) ion in various environments. Since there has been wide interest in the nature of bonding parameters in the system, we adopted the simplified molecular orbital theory to calculate the molecular orbital co-efficients such as α^2 (covalent in-plane σ -bonding) and β^2 (covalent in-plane π -bonding) were calculated by using the following equations [48].

$$\alpha^2 = -(A_{\parallel}/0.036) + (g_{\parallel} - 2.0023) + \frac{3}{7}(g_{\perp} - 2.0023) + 0.04$$

$$\beta^2 = (g_{\parallel} - 2.0023)E/(-8\lambda\alpha^2)$$

If the α^2 value is 0.5, it indicates a complete covalent bonding, while the value of $\alpha^2 = 1.0$ suggests a complete ionic bonding. The observed value of α^2 (**0.931**) indicates that the complex has covalent character and $\beta^2 = 1.02$ suggest that in plane π -bonding is also present in complex. The observed values indicate that there is

interaction in the out-plane π -bonding, whereas in- plane σ -bonding is completely ionic. This is also confirmed by orbital reduction factors (K_{\parallel} and K_{\perp}) which are calculated from the following equations:

$$K_{\parallel}^2 = (g_{\parallel} - 2.0023)(E/8\lambda)$$

$$K_{\perp}^2 = (g_{\perp} - 2.0023)(E/8\lambda)$$

where, $\lambda = -828\text{cm}^{-1}$ for the free metal ion and E is $20,166\text{ cm}^{-1}$. In the case of pure σ - bonding $K_{\parallel} = K_{\perp}$, whereas $K_{\parallel} < K_{\perp}$ implies considerable in-plane π -bonding while for out-plane π -bonding $K_{\parallel} > K_{\perp}$. For the present complex, the observed order is K_{\parallel} (**0.95**) $>$ K_{\perp} (**0.40**) implying a greater contribution from out-plane π -bonding than from in-plane π -bonding in metal ligand π -bonding.

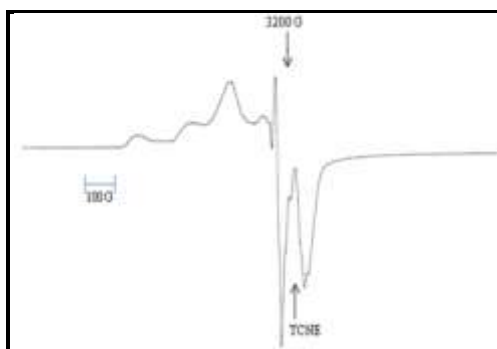


Fig. 2.21. X-band ESR spectrum of complex **16** in solution state at RT

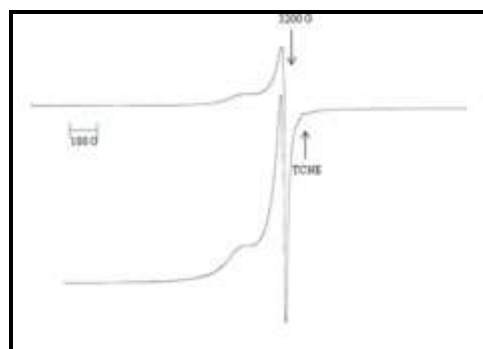


Fig. 2.22. X-band ESR spectrum of complex **16** in polycrystalline state at RT and LNT

2.6.8.2. ESR studies of ternary complexes

The ESR spectra of the complex **22** in solution and polycrystalline state are shown in Figs. 2.23 & 2.24, respectively. The ESR spectrum of the complex **22** shows four well resolved copper hyperfine lines, characteristic of a mononuclear Cu(II) complex, and it exhibits two distinct features at **2.25** and **2.05**, corresponding to a distorted *tbp/sp* structure, which is in good agreement with the reported literature for distorted *tbp/sp* Cu(II) complexes [51].

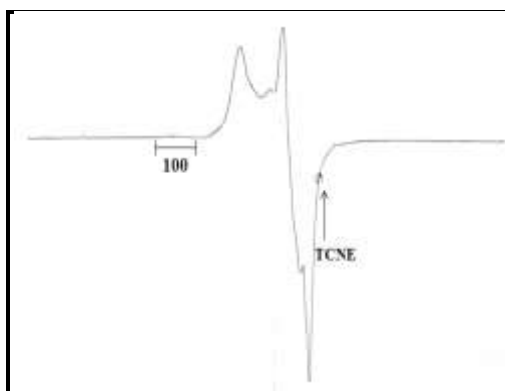


Fig. 23. X-band ESR spectrum of complex **22** in solution state at RT

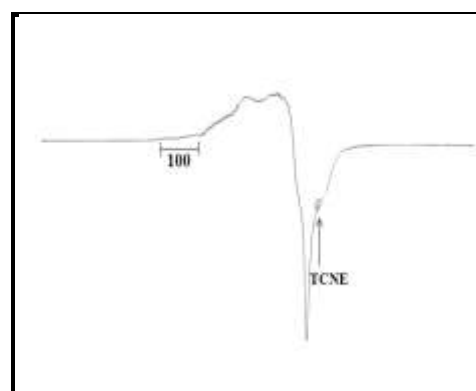


Fig. 24. X-band ESR spectrum of complex **22** in polycrystalline state at RT and LNT

Conclusions

The thiosemicarbazones containing pyrazolone moiety have been synthesized and characterized. Based on the above observations of the elemental analysis, IR, NMR and X-ray crystallographic data, it is possible to determine the type of coordination of the ligands in their metal complexes. The spectral data show that both the ligands exist as tridentate ligands by bonding to the metal ion through the deprotonated enol-O, thiol-S groups and azomethine nitrogen. The analytical data show the presence of one metal ion per one ligand molecule and suggest a mononuclear structure for the complexes. The correlation of the experimental data allows assigning a square planar stereochemistry for the simple complexes. Further, six ternary complexes have also been synthesized and characterized by different techniques. The molecular geometry of one of the ternary complexes has been determined by X-ray crystallography. The structure of the complex, based on the trigonality index τ (tau), suggests an intermediate geometry between square pyramidal (SP) and trigonal bipyramidal (TBP) as it has a value of 0.33. The Cu(II) ion in the complex exhibited distorted square pyramidal geometry with the pyrazolone-thiosemicarbazone acting as a tridentate chelating agent coordinating a Cu(II) ion *via* one N, one O and one S atoms and the phenanthroline acting as a bidentate ligand coordinating *via* two N atoms.

Literature cited.

- [1] J. Wang, L. Liu · G-f Liu, L. Zhang, D-z. Jia, *Struct Chem* 18 (2007) 59.
- [2] B-h. Peng, G-f. Liu, L. Liu, D-z, Jia, K-b. Yu, *J. Mol. Struct.* 692 (2004) 217.
- [3] D-L. Wu, L. Liu, G-F. Liu, D-Z. Jia, *J. Mol. Struct.: THEOCHEM* 806 (2007) 197.
- [4] L. Liu, D-Z. Jia, Y-L. Ji, K-B. Yu, *J. Photochem. Photobio. A: Chemistry* 154 (2003) 117.
- [5] Y. Ji, L. Liu, D-z. Jia, Y-M. Qiao, K-b. Yu, *J. Chem. Crystallog.* 32 (2002) 505.
- [6] D. Wu, D-Z. Jia, L. Liu, A. Liu, *Internation. J. Quant. Chem.*, 109 (2009) 1341.
- [7] G-F. Liu, L. Liu, D-Z. Jia, L. Zhang, *Chinese J. Chem.* 24 (2006) 569.
- [8] J. Guo, L. Liu, G-f. Liu, D-z. Jia, X. Xie, *Org. Lett.* 9 (2007) 3989.
- [9] B-H. Peng, G-F. Liu, L. Liu, D-Z. Jia, K-B. Yu, *J. Photochem. Photobio. A: Chemistry* 171 (2005) 243.
- [10] T. Zhang, G-f. Liu, L. Liu, D-z. Jia, L. Zhang, *Chem. Physic. Lett.* 427 (2006) 443.
- [11] V. M. Leovac, G. A. Bogdanović, L. S. Jovanović, L. Joksović, V. Marković, M. D. Joksović, S. M. Denčić, A. Isaković, I. Marković, F. W. Heinemann, S. Trifunović, I. Đalović, *J. Inorg. Biochem.* 105 (2011) 1413.
- [12] L. Liu, D-z. Jia, Y-l. Ji, K-b. Yu, *J. Mol. Struct.* 655 (2003) 221.
- [13] Y. Zhong, L. Liu, G-f Liu, D. Wu, J. Guo, D-z. Jia, *J. Mol. Struct.* 889 (2008) 259.
- [14] B-h. Peng, G-f. Liu, L. Liu, D-z. Jia, *Tetrahedron* 61 (2005) 5926.
- [15] H. Chai, G-f. Liu, L. Liu, D-z. Jia, *Spectrochim. Acta Part A* 61 (2005) 2590.
- [16] Y. Guo, G-f. Liu, L. Liu, D-z. Jia, *J. Mol. Struct.: THEOCHEM* 712 (2004) 223.
- [17] G-f. Liu, L. Liu, D-z. Jia, K-b. Yu, *Struct. Chem.* 16 (2005) 135.
- [18] L. Liu, X. Xie, D-z. Jia, J. Guo, X. Xie, *J. Org. Chem.* 75 (2010) 4742.
- [19] J-H. Wang, L. Liu, G-f. Liu, J. Guo, D-Z. Jia, *Sci China Ser B-Chem.* 51 (2008) 661.
- [20] S. Padhye, G. B. Kauffinan, *Coord Chem. Rev.* 63 (1985) 127.
- [21] D. X. West, S. B. Padhye, P. B. Sonawane, *Structure and Bonding*, 76 (1991) 1.

- [22] P. Domiano, G.G. Fava, M. Nardelli, P. Sgarabotto, *Acta Crystallogr.* 258 (1969) 343; G. D. Andreto, P. Dorniano, G.G. Fava, M. Nardelli, P.Sgarabotto, *Acta Crystallogr.* 26 (1970) 1005.
- [23] N. V. Gerbeleu, N. D. Revenko, V.M. Leovac, *Russ. J. Inorg. Chem.* 22 (1977) 1009.
- [24] F. Tui, K.I. Turta, N. V. Gerbeleu, *Russ. J. Inorg. Chem.* 22 (1977) 1497.
- [25] D. X. West, D. L. Huffinan, *Transition Met. Chem.*, 14 (1989) 190.
- [26] D. X. West, P. M. Ahrweiler, G. Ertem, I. P. Scovill, D. L. Klayman, I. L. Flippen-Anderson, R. Gilaradi, C. George, L. K. Pannell, *Transition Met. Chem.* 10 (1985) 264.
- [27] H. K. Parwana, G. Singh, *Indian J. Chem.* 26A (1987) 591.
- [28] M. D. Timken, S. R. Wilson, D. N. Hendrickson, *Inorg. Chem.*, 24 (1985) 3450.
- [29] D. X. West, R. M. Makeever, I.P. Scovill, D. L. Klayman, *Polyhedron* 3 (1984) 947.
- [30] P. Sonawane, R. Chikate, A. Kumbhar, S. Padhye, R. J. Doedens, *Polyhedron* 13 (1994) 395.
- [31] R. Bindu, Spectroscopic, electrochemical and biological studies of transition metal complexes of NSO donor ligands, Ph. D. Thesis submitted to the Cochin university, Kerala, India, (1997).
- [32] S. K. Jain, B. S. Garg, Y. K. Bhoon, *Transition Met. Chem.* 11 (1986) 89.
- [33] S. P. Mittal, S. K. Shanna, R. V. Singh, J. P. Tandon, *Curr. Sci.* 50 (1981) 483 and the references therein.
- [34] T. Klimova, E. I. Klimova, M. Mertinez Garcia, J. M. Mendez Stivalet, L. R. Ramirez, *J. Organomet. Chem.* 633 (2001) 137.
- [35] M. M. B. Pessoa, G. F. S. Andrade, V. R. P. Monteiro, M. L. A. Temperini, *Polyhedron* 20 (2001) 3133.
- [36] A. E. Liberta, D. X. West, *Biometals* 5 (1992) 121.
- [37] N. Raman, R. Jeyamurugan, B. Raj Kapoor, V. Mehesh, *Appl. Organometal. Chem.* 23 (2009) 283.
- [38] P. N. Yadav, M. A. Demertzis, D. Kovala-Demertzi, S. Skoulika, D. X. West, *Inorg. Chim. Acta* 349 (2003) 30.

-
- [39] W. L. F. Armarego, D. D. Perrin, *Purification of Laboratory Chemicals*, 4th edn., The Bath Press, Butterworth-Heinemann Publication, (1997).
- [40] W. J. Geary, *Coord. Chem. Rev.*, 7 (1971) 81.
- [41] L. Li, K. D. Karlin, S. E. Rokita, *J. Am. Chem. Soc.*, 127 (2) (2005) 520.
- [42] M. Duggan, N. Ray, B. Hathaway, G. Tomlinson, P. Brint, K. Pelin, *J. Chem. Soc., Dalton Trans.*, (1980) 1342.
- [43] R. J. Yadav, K. M. Vyas, R. N. Jadeja, *J. Coord. Chem.*, 63 (2010) 1820.
- [44] V. A. Sawant, B. A. Yamgar, S. S. Chavan, *Trans. Met. Chem.*, 35 (2010) 357.
- [45] A. B. P. Lever, *Inorganic Electronic Spectroscopy*, Elsevier, Amsterdam, (1984) pp. 355
- [46] S. S. Massoud, F. A. Mautner, M. A. M. Abu-Youssef, N. M. Shuaib, *Polyhedron* 18 (1999) 2061.
- [47] S. A. Abdel-Latif, H. B. Hassib, *J. Therm. Anal. Calorimet.*, 68 (2002) 983.
- [48] D.E. Fenton, *Biocoordination Chemistry*, Oxford, (1995).
- [49] A. Syamal, R. L. Dutta, *Elementals of Magneto Chemistry*, East–West Press Pvt. Ltd., New Delhi, (1993).
- [50] A.W. Addison, in: K.D. Karlin, J. Zubieta (Eds.), *Copper Coordination Chemistry: Biochemical and Inorganic Perspectives*, Adenine, Guilderland, NY, (1983).
- [51] R. S. Sancheti, R. S. Bendre, A. A. Kumbhar, *Polyhedron* 31 (2012) 12.

CHAPTER

3

Synthesis, characterization and crystal structures of some bidentate heterocyclic Schiff base ligands of 4-acyl pyrazolones with aromatic amines and their mononuclear metal complexes

3.1. Introduction

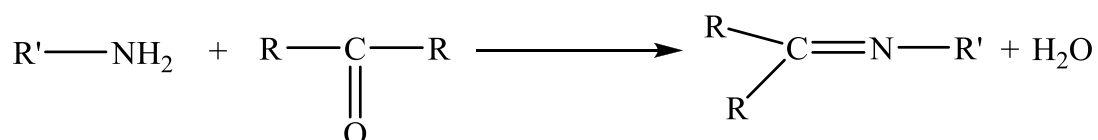
Over the past thirty years, extensive chemistry has surrounded the use of Schiff base ligands in inorganic chemistry. Schiff bases of pyrazolone have been playing an important part in the development of coordination chemistry. Schiff base metal complexes have been studied extensively because of their attractive chemical and physical properties and their wide range of applications in numerous scientific areas. These types of complexes have been vigorously explored in recent years and such studies have been the subject of many papers and reviews. **It is difficult to cover in this chapter the literature on Schiff base metal complexes, which embraces very wide and diversified subjects comprising vast areas of coordination compounds and various aspects of bioinorganic chemistry.** Therefore, the introduction part is limited to a brief discussion on the Schiff bases of pyrazolone, their metal complexes and general applications of Schiff base complexes with an emphasis on applications. Many of them are centred on the biological activity of Schiff base complexes, which will be discussed in **Chapter-4**.

3.1.1. Schiff base ligands

Schiff base was first reported by a German chemist **Hugo Schiff** in **1864** [1]. Schiff bases can be prepared by condensing carbonyl compounds and amines in different conditions and in different solvents with the elimination of water molecules. The common structural feature of these compounds is the **azomethine** group with a general formula **RHC=N-R'**, where R and R' are alkyl, aryl, cyclo alkyl or heterocyclic groups which may be differently substituted. Presence of a **lone pair** of electrons in a **sp²** hybridised orbital of nitrogen atom of the azomethine group is of considerable chemical importance and impart excellent chelating ability especially when used in combination with one or more donor atoms close to the azomethane group. This **chelating ability** of the Schiff bases combined with the ease of preparation and flexibility in varying the chemical environment about the C=N group makes it an **interesting ligand in coordination chemistry**.

3.1.1.1. Formation of Schiff bases

A Schiff base is nitrogen analogue of an aldehyde or ketone in which the C=O group is replaced by a C=N-R group. It is usually formed by condensation of an aldehyde or ketone with a primary amine according to the following scheme:



Scheme 3.1. Formation of Schiff base by condensation reaction

where, R and R' may be an alkyl or aryl group. Schiff bases those contain aryl substituents are substantially more stable and more readily synthesized, while those which contain alkyl substituents are relatively unstable. Schiff bases of aliphatic ketones are relatively unstable and readily polymerizable, while those of aromatic ketones having **effective conjugation** are more stable [2]. The Schiff base formation is a sequence of two types of reactions, i.e. **addition followed by elimination**.

3.1.2. Chemistry of Pyrazolone compounds and their structural analogues

The chemistry of 4-acyl pyrazolones (which are known as “**β-diketones**”) and its derivatives attracts continuous attention because of their wide applicability in various areas. A discussion on the synthesis of 4-acyl pyrazolones and their metal complexes are discussed in **Chapters 1 & 2** and the synthesis of their Schiff bases and metal complexes are included in this chapter.

3.1.2.1. 4-alkyl (or aryl)aminomethylidene-5-pyrazolones with (–C4–C–N(H)–C–) unit

The Schiff bases containing this type of pyrazolones (Figs. 3.1 & 3.2) are listed in Table 3.1. When free, they can exist in three tautomeric forms; imine-one, imine-ol and amine-ol, with the later usually found in the solid state. In their complexes, these pyrazolones usually adopt the imine-ol form and chelate the metal through the O1 and N3 atoms. Less common is monocoordination through N2 and

and three-coordination through O1, N3 and O2 (with O2 being an additional donor atom on R4). This type of ligands has been synthesized by the reaction of 4-acyl-5-pyrazolones with the corresponding primary amines [4-27].

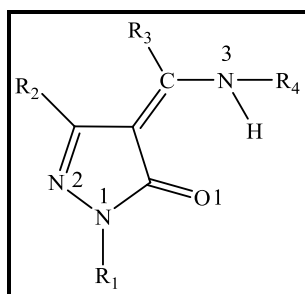


Fig. 3.1. Structure of the Schiff bases

L^1 - L^3 , L^5 - L^{23}

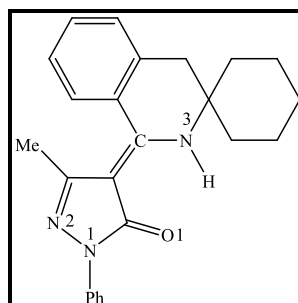


Fig. 3.2. Structure of Schiff base L^4

3.1.2.2. 4-Hydrazone-5-pyrazolones (-C4-C=N-N-C- unit)

3.1.2.2.1. Schiff bases containing salicylidenehydrazones

The Schiff bases identified with this type of pyrazolones are listed in Table 3.2. The common structure of the Schiff bases is shown in Fig. 3.3. This type of ligands has been prepared by reaction of 4-acyl-5-pyrazolones and salicylidene hydrazone in anhydrous ethanol, using a few drops of glacial acetic acid as a catalyst. In these compounds the occurrence of keto-enol tautomerism is possible, although an X-ray study of L^{25} indicates that it mainly exists in the keto form in the solid state [29].

Table 3.1. 4-alkyl(or aryl)aminomethylidene-5-pyrazolones and their metal complexes

Liga-nd	Complex	R1	R2	R3	R4	Donor atoms	Ref.
L ¹	[Zn(L ¹) ₂].MeOH	Ph	¹ Pr	H	cyclohexyl	O1, N3	[4]
L ²	[Ru(L ²) ₂ (H ₂ O) ₂]	Ph	Me	Ph	<i>p</i> -methoxyphenyl <i>m</i> -ethoxyphenyl <i>m</i> -tolyl	O1, N3	[5]
L ³	[Co(L ³) ₂]	Ph	Me	Ph	<i>p</i> -tolyl	O1, N3	[6]
L ⁴	[Cu(L ⁴) ₂].2HL ⁴	Ph	Me	H	-	N2	[7]
L ⁵	[Cu(L ⁵) ₂ (H ₂ O)]	Ph	Me	Ph	<i>p</i> -acetylphenyl	O1, N3	[8]
L ⁶	[Ag(L ⁶) ₂]PF ₆	Ph	Me	Ph	naphthyl	N2	[9]
L ⁷	[Co(L ⁷) ₂ (MeOH) ₂](NO ₃) [Cu(L ⁷) ₂ (DMF) ₂] [Cu(L ⁷) ₂ (DMF) ₂]	Ph	Me	Ph	-OH	O1,N3	[10]
L ⁸	[Co(L ⁸) ₂]	Ph	Me	Ph	<i>o</i> -chlorophenyl	O1, N3	[11]
L ⁹	[Co(L ⁹) ₂ (DMF) ₂]	Ph	Me	Ph	nitrophenyl	O1, N3	[12]
L ¹⁰	[Cu ₂ (L ¹⁰) ₂ (DMF) ₂]	Ph	Me	H	<i>o</i> - hydrxy(O2)benzoy l	O1, N3,O2	[13]
L ¹¹	[CuL ¹¹ (H ₂ O) ₂]	<i>p</i> -tolyl	Me	Me	benzoyl/ <i>o</i> / <i>m</i> / <i>p</i> - tolyl/ <i>o</i> / <i>m</i> / <i>p</i> - chlorophenyl	O1, N3	[14]
L ¹²	-	Ph	Me	Ph	Ph	O1, N3	[15]
L ¹³	[Ni(L ¹³) ₂ (CH ₃ CH ₂ OH) ₂] [Co(L ¹³) ₂ (CH ₃ CH ₂ OH) ₂]	Ph	Me	Ph	<i>p</i> -fluorophenyl	O1, N3	[16]
L ¹⁴	[Cu(L ¹⁴) ₂]	<i>n</i> - hexyl	Me	Et	Ph	O1, N3	[17]
L ¹⁵	[Zn(L ¹⁵) ₂]	Ph	Me	H	<i>p</i> - ¹ Buphenyl	O1, N3	[18]
L ¹⁶	-	<i>p</i> -tolyl	Me	Me	<i>p</i> -chlorophenyl	O1, N3	[19]
L ¹⁷	[Cu(L ¹⁷) ₂]	Ph	Me	Ph	benzyl	O1, N3	[20]
L ¹⁸	[Cu ₂ (L ¹⁸) ₂]	Ph	Me	H	<i>o</i> - hydrxy(O2)phenyl	O1, N3,O2	[21]
L ¹⁹	[Cu(L ¹⁹) ₂] [Ni(L ¹⁹) ₂ (CH ₃ CH ₂ OH) ₂]	Ph	Me	Ph	<i>o</i> -tolyl	O1, N3	[22,23]
L ²⁰	[OV(L ²⁰) ₂ (H ₂ O)]	<i>p</i> -tolyl	Me	Ph	benzoyl/ <i>o</i> -tolyl/ <i>p</i> - tolyl/ <i>m</i> - tolyl/ <i>o</i> / <i>m</i> / <i>p</i> - chlorophenyl	O1, N3	[24]
L ²¹	[VO(L ²¹) ₂ .H ₂ O] [Mn(L ²¹) ₂] ClO ₄ .H ₂ O	Ph/ <i>p</i> - tolyl/ <i>p</i> - BSA	Me	H	hydroxyethyl	O1, N3	[25]
L ²²	[VO(L ²²) ₂ H ₂ O]	<i>o</i> / <i>m</i> / <i>p</i> - chloro sulpho amido	Me	H	hydroxyethyl/prop yl	O1, N3	[26]
L ²³	[UO ₂ (L ²³) ₂ (H ₂ O) ₂]	Ph	Me	<i>n</i> - prop yl	<i>p</i> -methoxyphenyl <i>m</i> -ethoxyphenyl <i>p</i> -tolyl	O1, N3	[27]

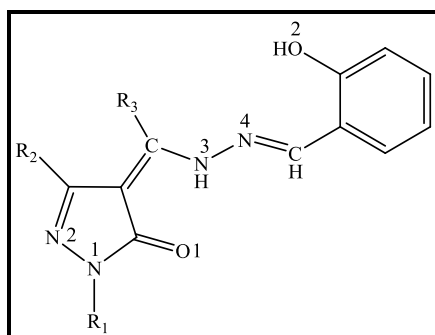


Fig. 3.3. Common structure of the Schiff bases L^{24} - L^{30}

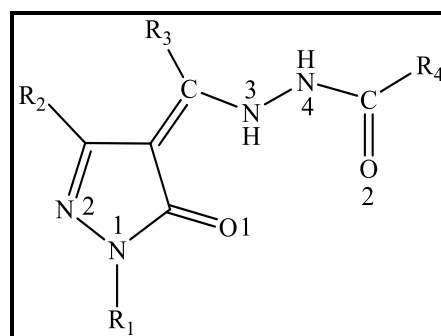


Fig. 3.4. Common structure of the Schiff bases L^{31} - L^{35}

Table. 3.2 Salicylidenehydrazones and their metal complexes

Ligand	Complex	R1	R2	R3	Donor atoms	Ref.
L^{24}	-	Ph	Me	Ph	O1, N3, N4, O2	[28]
L^{25}	$[\text{Cu}_2(\text{L}^{25})_2] \cdot 0.5\text{H}_2\text{O}$ $[\text{Zn}_4(\text{L}^{25})_4]$	Ph	Ph	$-\text{CH}_2\text{Ph}$	O1, N3, N4, O2	[29]
L^{26}	$[\text{Ni}(\text{L}^{26})_2(\text{EtOH})_2]$	Ph	Ph	Ph	O1, N3	[30]
L^{27}	$\text{Ln}(\text{L}^{27})_2(\text{CH}_3\text{OH})_2$	Ph	Me	propyl	O1, N3, N4, O2	[31]
L^{28}	$[\text{Cu}_4(\text{L}^{28})_4\text{H}_2\text{O}]_n$	Ph	Me	Me	O1, N3, N4, O2	[32]
L^{29}	$[\text{Ln}(\text{L}^{29})_3 \cdot 2\text{H}_2\text{O} \cdot \text{C}_2\text{H}_5\text{OH}]$	Ph	Me	Et	O1, N3, N4, O2	[33]
L^{30}	$[\text{Zn}(\text{L}^{30})_2]$ $[\text{Zn}(\text{L}^{30})_2 \cdot 3\text{CH}_3\text{OH}]$ $[\text{Zn}(\text{L}^{30})_2 \cdot 2\text{CH}_3\text{OH}]$ $[\text{Zn}_4(\text{L}^{30})_4]$	Ph	Ph	Et/Me/Ph/benzyl	O1, N3, N4, O2	[34]

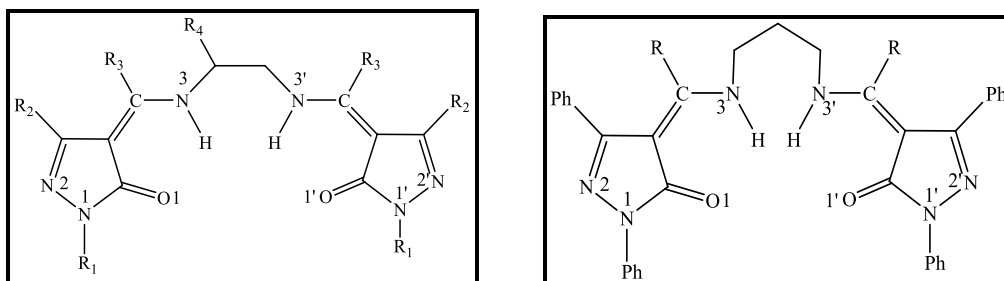
3.1.2.2.2. Schiff bases containing acylhydrazones

Table 3.3. Acylhydrazones and their metal complexes

Ligand	Complex	R1	R2	R3	R4	Donor atoms	Ref.
L^{31} HL^{31}	$[\text{ReO}(\text{L}^{31})(\text{HL}^{31})] \cdot \text{CH}_2\text{Cl}_2$	Ph	Me	Ph	Ph	O1, N3, O2 N2, O2	[35]
L^{32}	$[\text{Eu}(\text{L}^{32})_3] \cdot 3.5\text{H}_2\text{O} \cdot 0.5\text{MeOH}$	Ph	Me	Ph	4-pyridyl	O1, N3, O2	[36]
L^{33}	$[\text{Ni}(\text{L}^{33})(\text{py})]$	Ph	Me	Ph	2-hydroxyphenyl	O1, N3, O2	[37]
L^{34}	$[\text{Ni}(\text{L}^{34})(\text{py})_3]$ $[\text{Cu}(\text{L}^{34})(\text{py})]$	Ph	Me	Ph	4-nitrophenyl	O1, N3, O2	[38, 39]
L^{35}	$[\text{Ni}(\text{L}^{35})(\text{bipy})(\text{CH}_3\text{OH})]$ $[\text{Zn}(\text{L}^{35})(\text{bipy})(\text{CH}_3\text{OH})]$ $[\text{Cu}(\text{L}^{35})(\text{bipy})] \cdot 2\text{CH}_2\text{Cl}_2$	Ph	Ph	Me	2-hydroxyphenyl	O1, N3, O2	[40]

The 4-acylhydrazone-5-pyrazolones studied so far in the present context are shown in Fig. 3.4 and their complexes are listed in Table 3.3. These ligands can be synthesized by condensation of equimolar quantities of 4-acyl-5-pyrazolones and acylhydrazides in methanol or ethanol under reflux. A few drops of acetic acid are normally used as a catalyst. The X-ray studies on L^{32} and L^{35} .

3.1.2.3. Bis-5-pyrazolones

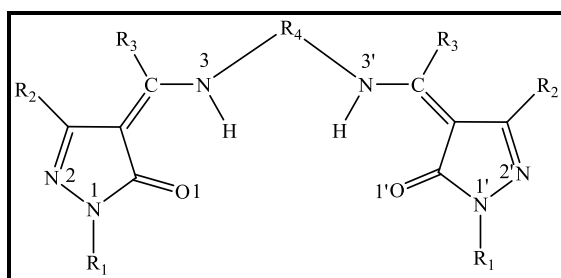


L^{36} , R_1 =Hexyl, R_2 =Me, R_3 =Et, R_4 =H [41]

L^{37} , R_1 =Ph, R_2 =Me, R_3 =H, R_4 =Me [42]

L^{38} , R =Ph [43]

L^{39} , R =*p*-tolyl [43]



L^{40} , R_1 =Ph, R_2 =Me, R_3 =Ph, R_4 =*o*-phenylene/*m*-phenylene/*p*-phenylene/*p*-benzidine [44]

L^{41} , R_1 =Ph, R_2 =Me, R_3 =Ph, R_4 =Ethyl/*n*-hexyl [45]

L^{42} , R_1 =Ph, R_2 =Ph, R_3 =Pr, R_4 =>C=O [46]

L^{43} , R_1 =Ph, R_2 =Me, R_3 =Ph, R_4 = diethenetriamine [47]

L^{44} , R_1 =Ph/*p*-tolyl, R_2 =Me, R_3 =H, R_4 =*o*-phenylene/*p*-phenylene [48]

L^{45} , R_1 =Ph, R_2 =Me, R_3 =Pr, R_4 =*o*-phenylene/*m*-phenylene/*p*-phenylene/*p*-benzidine [27]

Fig. 3.5. Common structures of the Schiff bases L^{36} - L^{45}

The bis-pyrazolones reported in literature and their common structures are given in Fig. 3.5. The ligands have been prepared by condensation of 4-acyl pyrazolones and the corresponding diamines.

- All these Schiff bases found in literature have been synthesized and characterized by different techniques like Elemental analyses, IR, NMR and Mass spectroscopy. Many of them have been characterized using X-ray crystallography. Their single crystal structures have been found to be in good agreement with their proposed structures. These ligands have been used further for the complexation with many metal ions in order to know their coordination behaviour.

3.1.3. Tautomerism in pyrazolone containing Schiff base ligands

Tautomerism in Schiff bases, with –OH group in ortho position to the amino group both in solution and in solid state have been investigated by spectroscopic and X-ray crystallographic techniques [49]. Schiff bases with –OH group in ortho position to the imino group are of interest mainly due to the existence of either O-H---N or O--H-N bonds and due to tautomerism between the enol- imine and keto-amine form [50]. In these compounds hydrogen bond forms between the –OH group in the ortho position to the imino group and imine nitrogen is due to the stereochemistry. In some instances the hydrogen from the –OH group is completely transferred to the imine nitrogen. In other words enol amine keto amine equilibrium shifts predominates [51].

The molecular structures of this type of ligands are such that they can exist in three tautomeric forms as shown in Fig. 3.7. Detailed solution and solid-state studies of these ligands were carried out to establish their geometry [14].

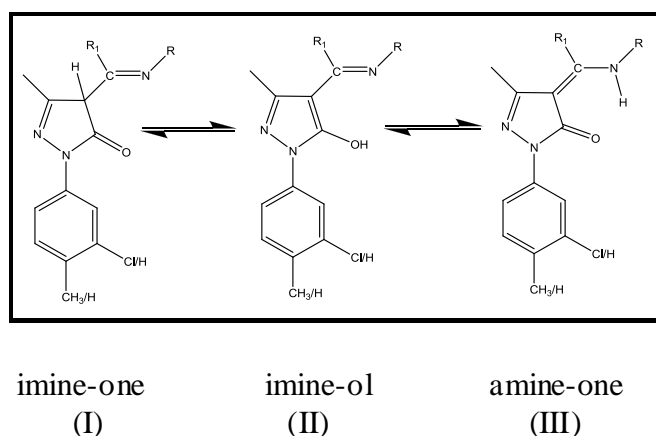


Fig. 3.7. The existence of different tautomeric forms in the Schiff bases

3.1.4. Metal complexes of pyrazolone Schiff bases

Metal-Schiff base complexes have been known since the **mid nineteenth century** [52] and even before the general preparation of Schiff base ligands themselves [1]. Metal-complexes of Schiff bases have occupied a central place in the development of coordination chemistry after the work of **Jorgensen and Werner** [53].

A comprehensive review by J. S. Casas [3] covers much of the Schiff base chemistry known upto 2006 and it has been followed by others. Structure and mechanism of the formation of such complexes and stereochemistry of chelate compounds from pyrazolone Schiff bases and their analogues have been discussed in with 132 references.

➤ *Schiff base metal complexes can be classified in a number of ways, as:*

3.1.4.1. Metal complexes containing 4-alkyl (or aryl)aminomethylidene-5-pyrazolones

Metal complexes of this type are presented in Table 3.1. Some of their structures have also been shown to understand the coordination.

Most of these compounds are Cu(II) complexes obtained by reaction of the corresponding pyrazolone with a metal salt (chloride, nitrate, acetate) in the presence of a deprotonating agent, in some cases [6, 20]. In these complexes the Cu atom is coordinated to two pyrazolonates and in some of them, one or two solvent molecules increase the coordination number of the metal to 5 or 6 [8, 10, 14].

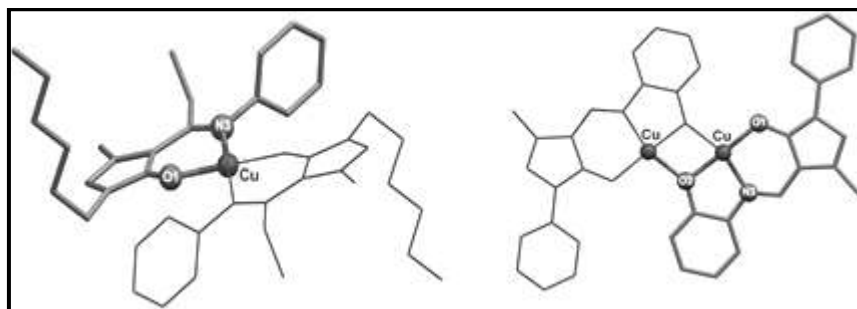


Fig. 3.8. Coordination mode of the ligand in [Cu(L¹⁴)₂] & [Cu₂(L¹⁸)₂]

The dinuclear copper complexes $[\text{Cu}_2(\text{L}^{10})_2(\text{DMF})_2]$ [13] and $[\text{Cu}_2(\text{L}^{18})_2]$ [21] (Fig. 3.8) are formed with two ligands that possess an additional hydroxyl group on R4. These ligands lose two protons and coordinate through the atoms O1, N3 and O2. The oxygen atom O2, which belongs to the deprotonated hydroxyl group, bridges between the two metal centres.

In all the mononuclear copper complexes, the pyrazolone ligand coordinates the metal through the O1, N3 donor atoms (see Fig. 3.8 for $[\text{Cu}(\text{L}^{14})_2]$ [17]). But one exceptions is $[\text{Cu}(\text{L}^4)_2] \cdot 2\text{HL}^4$ [7], in which the coordination occurs through N2 (Fig. 3.9).

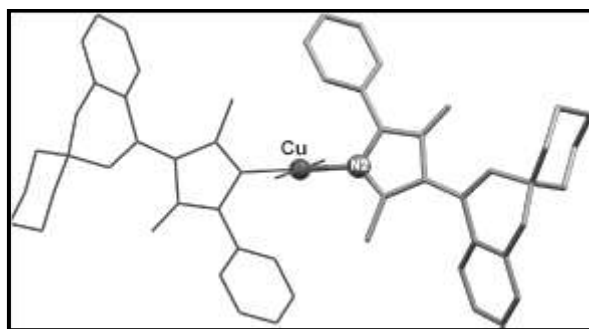


Fig. 3.9. Coordination mode of the ligand in $[\text{Cu}(\text{L}^4)_2] \cdot 2\text{HL}^4$

The complexes of Co(II), Ni(II) and Zn(II) with this type of pyrazolones were prepared in a similar way to the Cu(II) complexes and they are all mononuclear with $[\text{M}(\text{L}^n)_2]$ or $[\text{M}(\text{L}^n)_2(\text{solvent})_2]$ stoichiometries [6, 10-12, 16, 18, 23, 25], as occurs in $[\text{Co}(\text{L}^8)_2]$ [11] (Fig. 3.10), $[\text{Co}(\text{L}^3)_2]$ [6] and $[\text{Zn}(\text{L}^1)_2] \cdot \text{MeOH}$ (Fig. 3.10). In the compounds $[\text{M}(\text{L}^n)_2(\text{solvent})_2]$, the presence of two additional coordinated molecules of solvent increases the coordination number to six and leads to octahedral geometries (see Fig. 3.11 for $[\text{Ni}(\text{L}^7)_2(\text{DMF})_2]$ [10]).

Similarly, the OV(IV) and $\text{UO}_2(\text{II})$ complexes of this type of ligands were synthesized by the reaction of corresponding pyrazolones with vanadyl sulfate pentahydrate and uranyl acetate dehydrate, respectively. They are six coordinated and eight coordinated complexes, respectively [24-27].

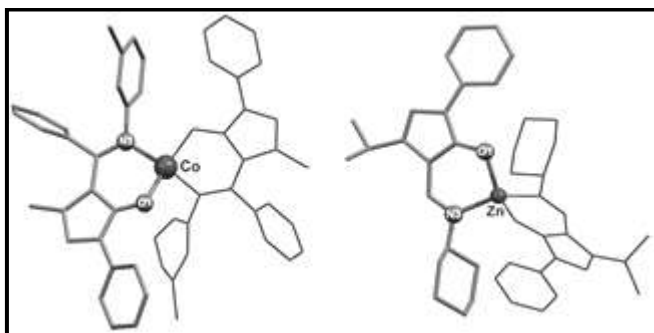


Fig. 3.10. Coordination mode of the ligand in $[\text{Co}(\text{L}^8)_2]$ & $[\text{Zn}(\text{L}^1)_2] \cdot \text{MeOH}$

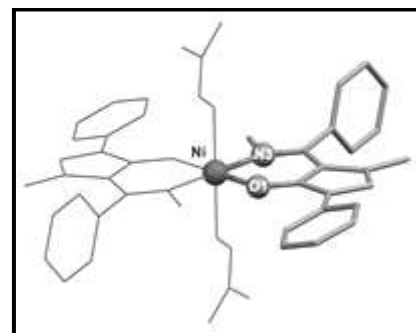


Fig. 3.11. Coordination mode of the ligand in $[\text{Ni}(\text{L}^7)_2(\text{DMF})_2]$

Whereas, in the Ag(I) complex $[\text{Ag}(\text{L}^6)_2]\text{PF}_6$ [9], obtained by reaction of L^6 and silver hexafluorophosphate, two neutral pyrazolone ligands coordinate the metal through the N2 atoms to give a linear geometry same as $[\text{Cu}(\text{L}^4)_2] \cdot 2\text{HL}^4$ (Fig. 3.9).

3.1.4.2. Metal complexes containing salicylidenehydrazones

These ligands, due to their multidentate nature and the location of the donor atoms, can easily bridge between two or more metal ions to give polynuclear complexes (Table 3.2). In fact, of the complexes reviewed here, only $[\text{Ni}(\text{L}^{26})_2(\text{EtOH})_2]$ – obtained by reaction of L^{26} and $\text{Ni}(\text{OAc})_2$ – is mononuclear [30] (Fig. 3.12).

The hydrazone–pyrazolone is singly charged (after losing the proton from the N3–H group) and coordinates to the metal through the O1, N3 atoms. The dinuclear Cu(II) complex $[\text{Cu}_2(\text{L}^{25})_2] \cdot 0.5\text{H}_2\text{O}$ [29] (Fig. 3.12) was obtained by reacting a solution of $\text{Cu}(\text{OAc})_2 \cdot \text{H}_2\text{O}$ in ethanol with a methanolic solution of the ligand (prepared after the addition of aqueous NaOH). The tetradentate ligand is bideprotonated to form two chelating moieties: the first involves the oxygen atom at the 5-position of the pyrazolone (O1) and one of the hydrazone nitrogen atoms (N3) and the other comprises the oxygen of the hydroxyl group (O2) and the other hydrazone nitrogen (N4). Each moiety chelates to a different copper atom, meaning that each copper is coordinated to O1, N3, N4 and O2 atoms in a distorted square planar geometry.

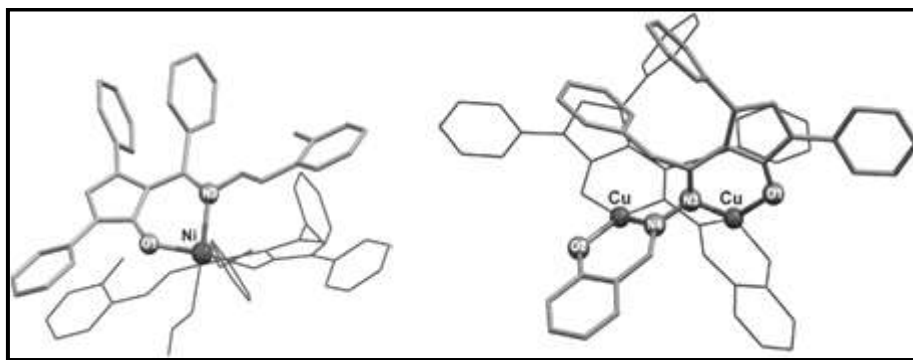


Fig. 3.12. Coordination mode of the ligand in $[\text{Ni}(\text{L}^{26})_2(\text{EtOH})_2]$ & $[\text{Cu}_2(\text{L}^{25})_2] \cdot 0.5\text{H}_2\text{O}$

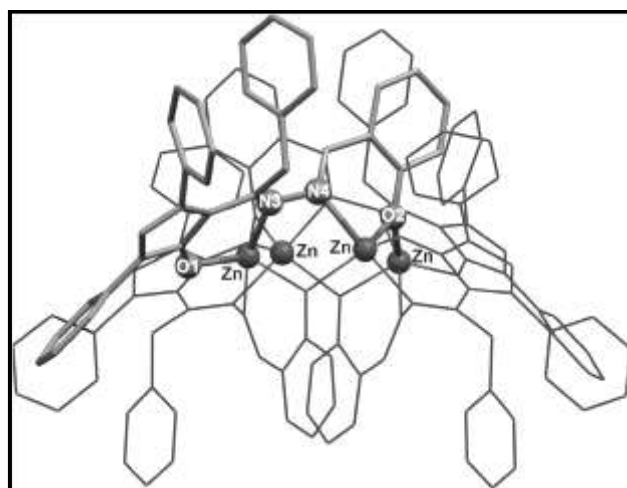


Fig. 3.13. Coordination mode of the ligand in $[\text{Zn}_4(\text{L}^{25})_4]$

The tetranuclear Zn(II) complexes $[\text{Zn}_4(\text{L}^{30})_4]$ [34] and $[\text{Zn}_4(\text{L}^{25})_4]$ [29] (Fig. 3.13) are very similar. Both are obtained by a similar procedure to that previously described for the Cu(II) complex using $\text{Zn}(\text{OAc})_2 \cdot 2\text{H}_2\text{O}$ instead of $\text{Cu}(\text{OAc})_2 \cdot \text{H}_2\text{O}$. The bridging bideprotonated pyrazolonates are coordinated to four Zn(II) cations, two through the O1, N3 donor atoms, another through the N4, O2 atoms and the fourth through O2. In this way, the hydroxyl O2 atom bridges between two metal centres. Each of these centres is pentacoordinated and has a trigonal bipyramidal coordination sphere formed by O1, N3 (from one ligand), N4, O2 (from another) and O2 (from a fourth ligand). The tetranuclear core of these complexes is practically square planar with a Zn---Zn distance of 3.411 Å.

3.1.4.3. Metal complexes containing Acylhydrazones

These complexes are listed in Table 3.3. $[\text{ReO}(\text{L}^{31})(\text{HL}^{31})]\cdot\text{CH}_2\text{Cl}_2$ [35] (Fig. 3.14) was prepared by reacting L^{31} and triethylamine in ethanol with a solution of $\text{ReOCl}_3(\text{PPh}_3)$ in boiling chloroform. In the complex, two acylhydrazone pyrazolone ligands, one monodeprotonated and the other bideprotonated, coordinate the metal. The monodeprotonated ligand is bidentate and binds the rhenium through the N3 and O2 atoms (Fig. 3.14), whereas the bideprotonated ligand is tridentate and binds through the O1, N3 and O2 atoms.

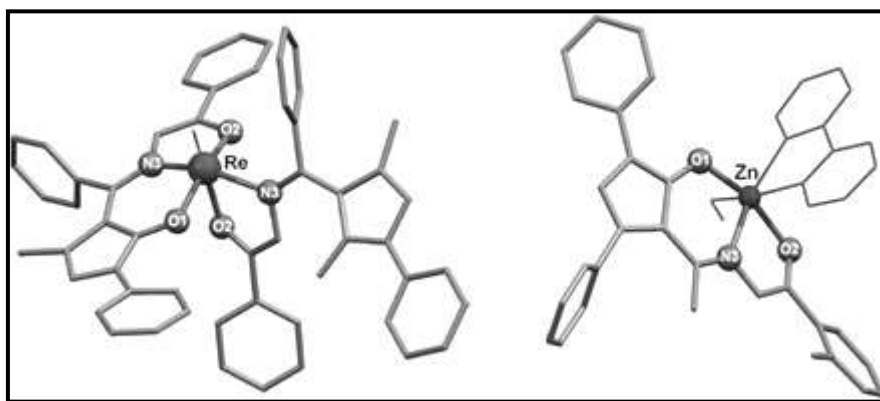


Fig. 3.14. Coordination mode of the ligand in $[\text{ReO}(\text{L}^{31})(\text{HL}^{31})]\cdot\text{CH}_2\text{Cl}_2$ & $[\text{Zn}(\text{L}^{35})(\text{bipy})(\text{CH}_3\text{OH})]$

$[\text{M}(\text{L}^{35})(\text{bipy})(\text{CH}_3\text{OH})]$ ($\text{M} = \text{Ni}, \text{Zn}$) and $[\text{Cu}(\text{L}^{35})(\text{bipy})]\cdot 2\text{CH}_2\text{Cl}_2$ [40] were prepared by reacting the corresponding $\text{M}(\text{OAc})_2\cdot n\text{H}_2\text{O}$ with the ligand L^{35} and 2,2' bipyridine in MeOH at 70°C . In all of these complexes the bideprotonated pyrazolone (only the phenolic proton on R4 remains) coordinates the metal through the O1, N3 and O2 atoms (Fig. 3.14). The same coordination mode occurs in $[\text{Ni}(\text{L}^{33})(\text{py})]$ [37], which was prepared by a similar procedure.

The complexes of L^{34} , i.e. $[\text{Ni}(\text{L}^{34})(\text{py})_3]$ [38] and $[\text{Cu}(\text{L}^{34})(\text{py})]$ [39], were both obtained as follows. Equimolar mixtures of L^{34} and $\text{M}(\text{OAc})_2\cdot\text{H}_2\text{O}$ were ground and dissolved in MeOH. The clear solution was then placed in a Teflon bomb and 1 mL of CH_3CN and 1 mL of pyridine were added to the mixture, which was heated to 120°C for 2 days. Slow cooling to room temperature afforded crystals in both cases.

In these complexes the ligand loses two protons from its enol form and behaves in a tridentate manner through the N3, O1 and O2 atoms (see Fig. 3.15 for $[\text{Cu}(\text{L}^{34})(\text{py})]$ [39]). Three pyridine molecules in the Ni(II) complex and one in the Cu(II) complex completed an octahedral and a square planar coordination sphere, respectively.

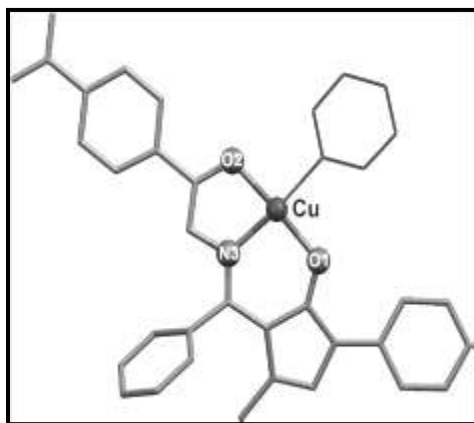


Fig. 3.15. Coordination mode of the ligand in $[\text{Cu}(\text{L}^{34})(\text{py})]$

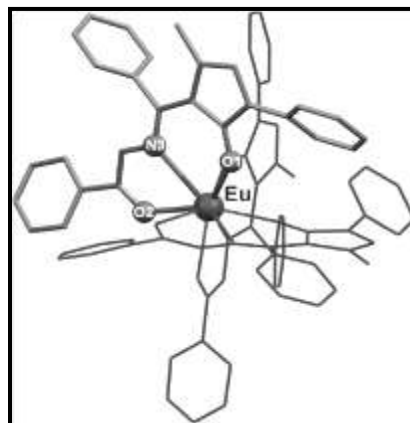


Fig. 3.16. Coordination mode of the ligand in $[\text{Eu}(\text{L}^{32})_3] \cdot 3.5\text{H}_2\text{O} \cdot 0.5\text{MeOH}$

$[\text{Eu}(\text{L}^{32})_3] \cdot 3.5\text{H}_2\text{O} \cdot 0.5\text{MeOH}$ [36] (Fig. 3.16), prepared by reaction of an aqueous solution of L^{32} at pH 7 with an aqueous solution of $\text{EuCl}_3 \cdot 6\text{H}_2\text{O}$, was studied by X-ray diffraction after recrystallization from MeOH/EtOH (1:2). The coordination polyhedron is a tricapped trigonal prism defined by three N atoms (N3) and six O atoms (three O1 and three O2) from three monodeprotonated tridentate pyrazolonates.

3.1.4.4. Metal complexes containing bis-pyrazolones

These types of complexes are listed in Table 3.4.

Reaction of L^{36} with $\text{Mn}(\text{OAc})_3 \cdot 2\text{H}_2\text{O}$ and LiCl gives the complex $[\text{Mn}(\text{Cl})(\text{L}^{36})]$. The reaction of this chloromanganese(III) derivative with aqueous ammonia in a $\text{CH}_2\text{Cl}_2/\text{CH}_3\text{OH}$ mixture and subsequent oxidation with NaOCl enabled the isolation of the nitridomanganese(V) complex $[\text{Mn}(\text{N})(\text{L}^{36})]$ from the organic phase [41]. Crystals suitable for an X-ray study were obtained by slow evaporation of a methylene chloride/hexane solution of the crude product. In this complex (Fig. 3.17) the bideprotonated bis-pyrazolone embraces the cation with its four coordinating

atoms (O1, O1', N3, N3') defining the square-base of an almost perfect square pyramidal environment. The fifth position is occupied by the nitrido ligand. The ability of this complex to transfer nitrogen to styrene in stoichiometric reactions has been tested.

Table 3.4. Metal complexes containing bis-pyrazolones

Complex	Donor atoms	Ref.
[Mn(N)(L ³⁶)]	O1, O1', N3, N3'	[41]
[Ni(L ³⁷)]	O1, O1', N3, N3'	[42]
[Ni(L ³⁸)]·0.5CHCl ₃ [Ni(L ³⁸)(DMSO) ₂]	O1, O1', N3, N3'	[43]
[Ni(L ³⁹)(DMSO) ₂]	O1, O1', N3, N3'	[43]
[MoO ₂ (L ⁴⁰) ₂]	O1, O1', N3, N3'	[44]
[Co(L ⁴¹)]	O1, O1', N3, N3'	[45]
[VO(L ⁴²)(H ₂ O)] [Cr(L ⁴²)(H ₂ O) ₂][NO ₃] [Fe(L ⁴²)(H ₂ O) ₂][NO ₃] [Fe(L ⁴²)(H ₂ O) ₂] [Ni(L ⁴²)(H ₂ O) ₂] [Cu(L ⁴²)(H ₂ O) ₂] [Zn(L ⁴²)(H ₂ O) ₂] [UO ₂ (L ⁴²)]H ₂ O	O1, O1', N3, N3'	[46]
[Zn(L ⁴³)0.5H ₂ O] [Ni(L ⁴³)(C ₂ H ₅ OH)]H ₂ O	O1, O1', N3, N3'	[47]
[Mn(L ⁴⁴)(bipy)(OAc)]ClO ₄ [Mn ₂ (L ⁴⁴) ₂ (o/p-Phd)(bipy)2(OAc) ₂](ClO ₄) ₂	O1, O1', N3, N3'	[48]
[UO ₂ (L ⁴⁵)(H ₂ O) ₂]	O1, O1', N3, N3'	[27]

The Ni(II) complexes with the ligands Lⁿ ($n = 37, 38, 39$) [42, 43] were prepared by reacting the pyrazolones and anhydrous Ni(OAc)₂ in 2-methoxyethanol under reflux [43]. Crystals of these complexes were isolated by recrystallization from CHCl₃, DMSO or mixtures of these two solvents. In all of these Ni(II) derivatives the bis-pyrazolones, which are bideprotonated and tetradentate, show the same coordination behaviour and bind the same metal through four donor atoms (O1, O1', N3 and N3'). These four atoms are almost in a plane in [Ni(L³⁷)] [42] (Fig. 3.17), giving rise to a planar coordination geometry around the metal, and in [Ni(Lⁿ)(DMSO)₂] ($n = 38, 39$) [43] (see Fig. 3.18 for [Ni(L³⁹)(DMSO)₂]), where the metal reaches a pseudo-octahedral environment with the DMSO molecules axial. However, in [Ni(L³⁸)]·0.5CHCl₃ [43] the four donor atoms of the bis-pyrazolone are not in a strictly planar environment (the angle between planes N3–Ni–O1 and N3'–

Ni–O1' is 12.7°), leading to a coordination sphere that is described by the authors as pseudo-tetrahedral.

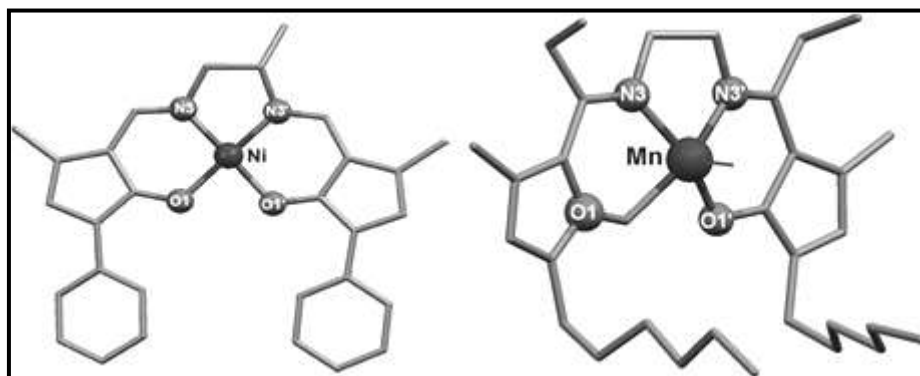


Fig. 3.17. Coordination mode of the ligand in $[\text{Ni}(\text{L}^{37})]$ & $[\text{Mn}(\text{N})(\text{L}^{36})]$

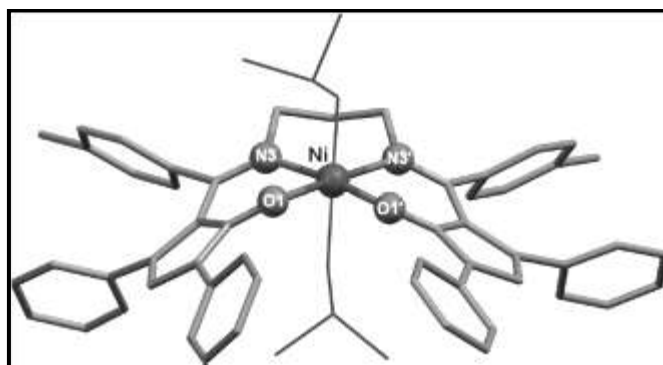


Fig. 3.18. Coordination mode of the ligand in $[\text{Ni}(\text{L}^{39})(\text{DMSO})_2]$

3.2. Experimental

3.2.1. Materials

The compounds 5-methyl-4-(4-methyl-benzoyl)-2-phenyl-2,4-dihydro-pyrazol-3-one [TPMP], 2-(3-chloro-phenyl)-5-methyl-4-(4-methyl-benzoyl)-2,4-dihydro-pyrazol-3-one [TMCPMP] and 5-methyl-4-(4-methyl-benzoyl)-2-*p*-tolyl-2,4-dihydro-pyrazol-3-one [TPTPMP] were synthesized (Chapter-1) and used after recrystallization. The compounds 3-methyl-4-propionyl-1-*p*-tolyl-1H-pyrazol-5(4H)-one [PPTPMP] and 1-(3-chlorophenyl)-3-methyl-4-propionyl-1H-pyrazol-5(4H)-one [PMCPMP] were synthesized (Chapter-2) and used after recrystallization. *p*-toluidine and *p*-bromo aniline were obtained from Sisco-Chem. Pvt. Ltd., Mumbai and used after purification following a standard procedure [54]. Absolute alcohol was obtained from Baroda Chem. Industries Ltd, Baroda, and was used after distillation. Calcium hydroxide and copper acetate were obtained from LOBA Chem. Pvt. Ltd., Mumbai.

3.2.2. Single crystal X-ray structure determination

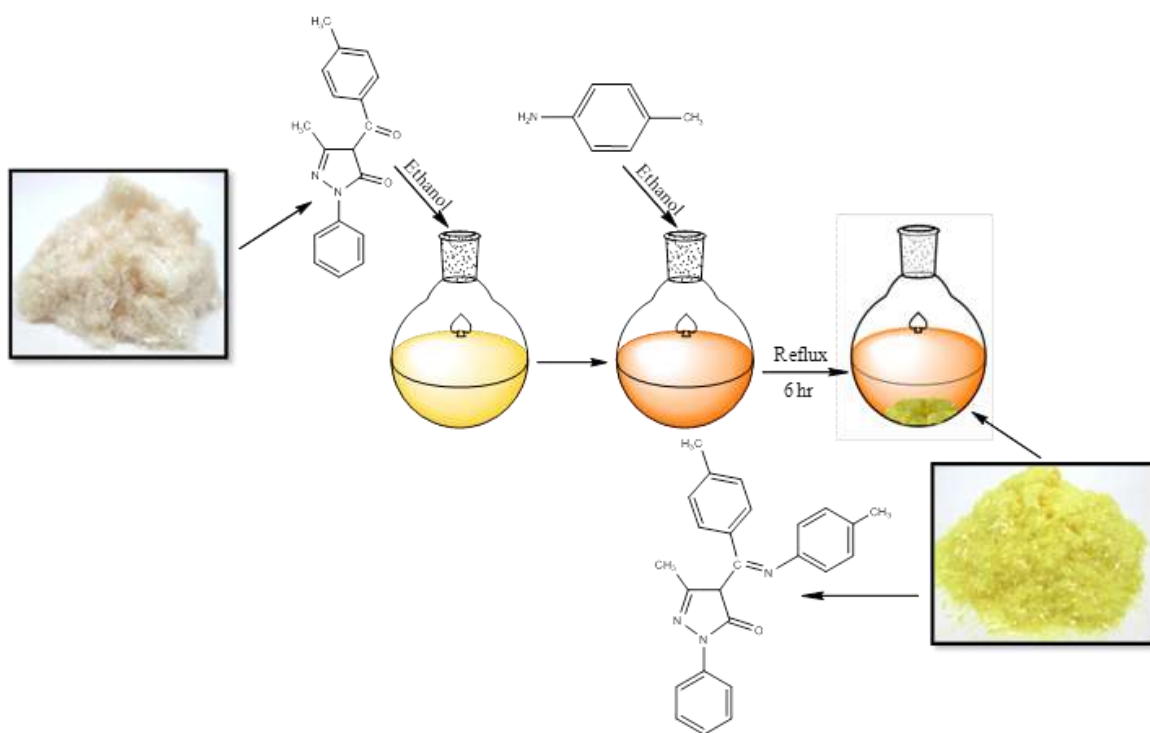
The detail of this section has been given in Chapter 1 (section 1.2.2).

3.3. Syntheses of Schiff base ligands

3.3.1. Syntheses of Schiff base ligands of 4-toluoyl pyrazolones

3.3.1.1. 5-methyl-2-phenyl-4-(*p*-tolyl-*p*-tolylimino-methyl)-2,4-dihydro-pyrazol-3-one [TPMP-T]:

Equimolar ethanolic solution (50 mL) of 5-methyl-4-(4-methyl-benzoyl)-2-phenyl-2,4-dihydro-pyrazol-3-one (0.292 gms, 1 mmol) and *p*-toluidine (0.107 gms, 1 mmol) was refluxed for 6 hours in a round bottom flask. During the reflux a microcrystalline yellow compound was separated, which was isolated by filtration, washed with ethanol, dried under *a vacuum* and finally purified by crystallization in ethanol.



Scheme 3.2. Synthesis of TPMP-T

3.3.1.2. 4-[(4-bromo-phenylimino)-p-tolyl-methyl]-5-methyl-2-phenyl-2,4-dihydro-pyrazol-3-one [TPMP-BA]:

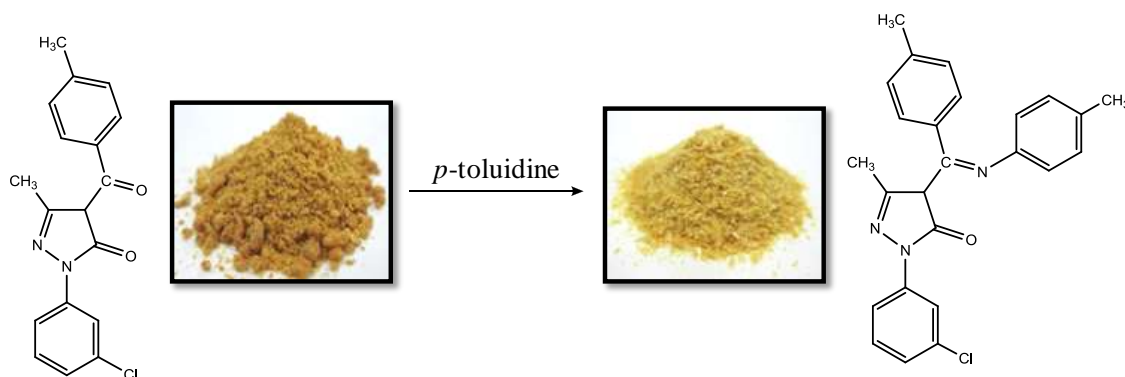
It was prepared analogously from 5-methyl-4-(4-methyl-benzoyl)-2-phenyl-2,4-dihydro-pyrazol-3-one and *p*-bromoaniline, obtained yellow crystals were filtered and dried.



Scheme 3.3. Synthesis of TPMP-BA

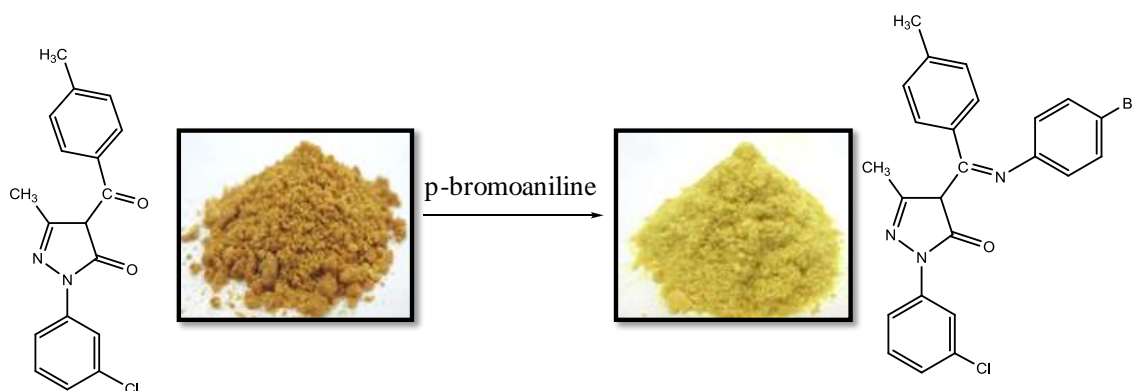
3.3.1.3. 2-(3-chloro-phenyl)-5-methyl-4-(*p*-tolyl-*p*-tolylimino-methyl)-2,4-dihydro-pyrazol-3-one [TMCPMP-T]:

It was prepared analogously from 2-(3-chloro-phenyl)-5-methyl-4-(4-methyl-benzoyl)-2,4-dihydro-pyrazol-3-one and *p*-toluidine, obtained yellow crystals were filtered and dried.



Scheme 3.4. Synthesis of TMCPMP-T

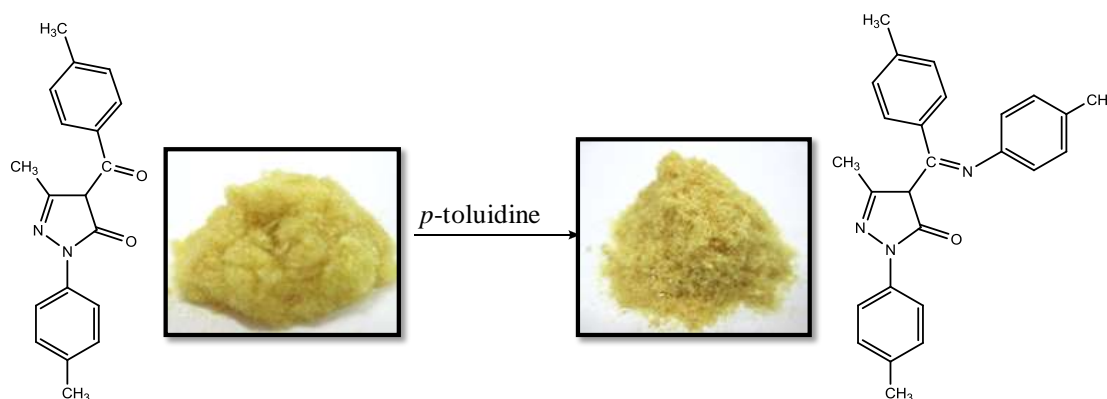
3.3.1.4. 4-[(4-bromo-phenylimino)-*p*-tolyl-methyl]-2-(3-chloro-phenyl)-5-methyl-2-phenyl-2,4-dihydro-pyrazol-3-one [TMCPMP-BA]:



Scheme 3.5. Synthesis of TMCPMP-BA

It was prepared analogously from 2-(3-chloro-phenyl)-5-methyl-4-(4-methyl-benzoyl)-2,4-dihydro-pyrazol-3-one and *p*-bromoaniline, obtained yellow crystals were filtered and dried.

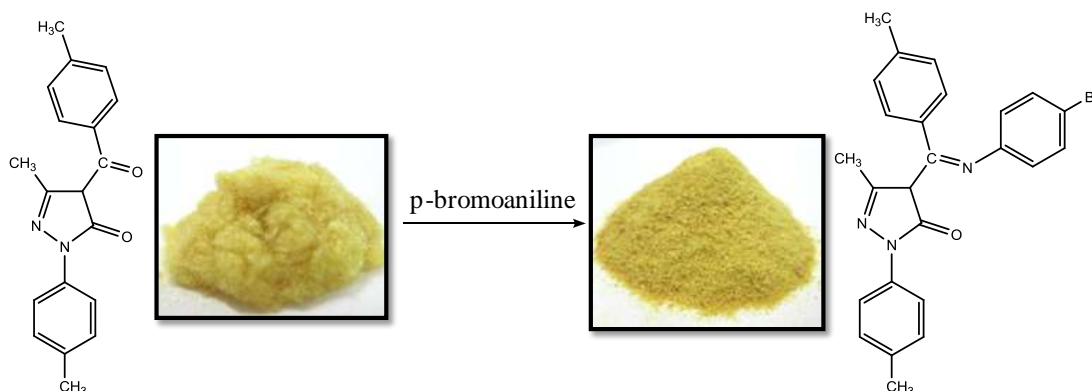
3.3.1.5. 5-methyl-2-*p*-tolyl-4-(*p*-tolyl-*p*-tolylimino-methyl)-2,4-dihydro-pyrazol-3-one [TPTPMP-T]:



Scheme 3.6. Synthesis of TPTPMP-T

It was prepared analogously from 5-methyl-4-(4-methylbenzoyl)-2-*p*-tolyl-2,4-dihydro-pyrazol-3-one and obtained yellow crystals were filtered and dried.

3.3.1.6. 4-[(4-bromo-phenylimino)-*p*-tolyl-methyl]-5-methyl-2-*p*-tolyl-2,4-dihydro-pyrazol-3-one [TPTPMP-BA]:



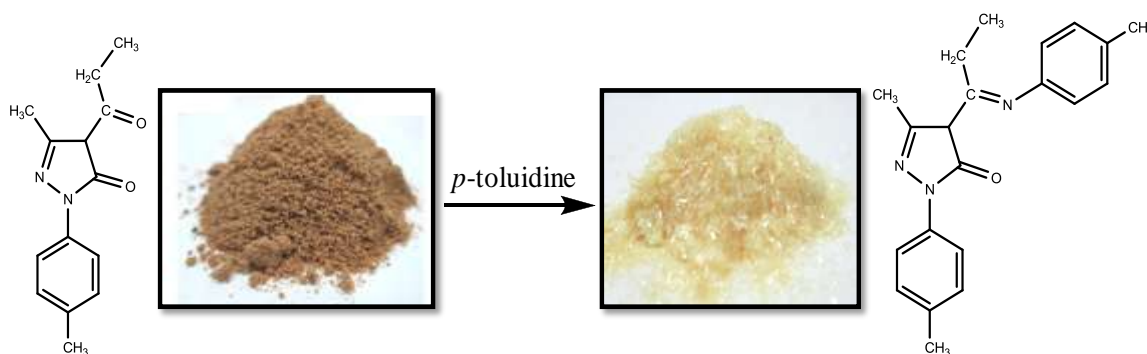
Scheme 3.7. Synthesis of TPTPMP-BA

It was prepared analogously from 5-methyl-4-(4-methylbenzoyl)-2-*p*-tolyl-2,4-dihydro-pyrazol-3-one and *p*-bromoaniline, obtained yellow crystals were filtered and dried.

3.3.2. Syntheses of Schiff base ligands of 4-propionyl pyrazolones

3.3.2.1. 5-methyl-2-*p*-tolyl-4-(1-*p*-tolylimino-propyl)-2H-pyrazol-3-one

[PPTPMP-T]:

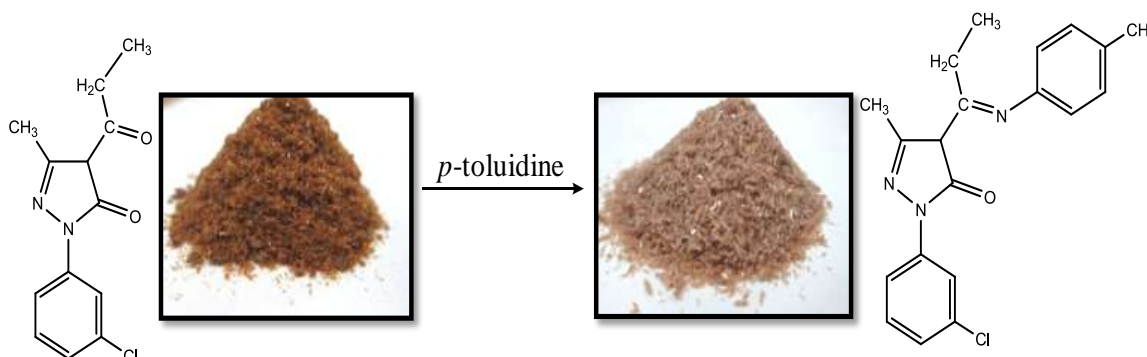


Scheme 3.8. Synthesis of PPTPMP-T

It was prepared analogously from 1-(5-hydroxy-3-methyl-1-*p*-tolyl-1H-pyrazol-4-yl)-propan-1-one and *p*-toluidine, obtained crystals were filtered and dried.

3.3.2.2. 2-(3-chloro-phenyl)-5-methyl-4-(1-*p*-tolylimino-propyl)-2H-pyrazol-3-one

[PMCPMP-T]:



Scheme 3.9. Synthesis of PMCPMP-T

It was prepared analogously from 1-(3-chlorophenyl)-3-methyl-4-propionyl-1H-pyrazol-5(4H)-one and *p*-toluidine, obtained crystals were filtered and dried.

3.4. Characterization of Schiff base ligands

3.4.1. Physicochemical properties of the Schiff base ligands

Analytical data of the Schiff base ligands are presented in Table 3.5. The ligands have been synthesized in a very facile and essentially identical way. All these compounds are intensively coloured, air and moisture free crystalline solids. They are highly soluble in common organic solvents. The structure of the ligands can be confirmed from these data along with spectroscopic and crystallographic evidence discussed in section 3.4.5. The elemental analysis matches well with the empirical formulae of the ligands.

Table 3.5. Analytical data of the Schiff base ligands

Ligands	Formula Weight(g mol ⁻¹)	Colour	Yield (%)	Melting Point(°C)	Elemental Analysis (%) Found(calcd.)		
					C	H	N
TPMP-T	381.47	Yellow	74.42	188	78.68 (78.74)	6.01 (6.03)	12.51 (12.59)
TPMP-BA	446.35	Yellow	71.59	194	64.50 (64.57)	4.42 (4.48)	10.71 (10.76)
TMCPMP-T	415.92	Yellow	51.93	120	72.00 (72.02)	5.25 (5.29)	11.53 (11.55)
TMCPMP-BA	480.78	Yellow	61.29	190	60.02 (60.00)	3.91 (3.95)	10.03 (10.00)
TPTPMP-T	395.50	Yellow	53.18	152	78.94 (78.98)	6.34 (6.32)	12.12 (12.15)
TPTPMP-BA	460.37	Yellow	54.27	212	65.19 (65.21)	4.75 (4.78)	10.61 (10.63)
PPTPMP-T	333.43	Light yellow	75.18	162	74.13 (73.78)	7.09 (6.61)	14.08 (13.63)
PMCPMP-T	353.85	Brown	76.70	135	68.22 (68.08)	5.93 (5.39)	15.21 (14.91)

3.4.2. IR spectral studies

The characteristic IR bands for all the Schiff base ligands recorded as KBr discs are listed in Table 3.6.

IR spectral analysis confirms the presence of characteristic groups present in the ligands. Each of the Schiff base under discussion exhibits two characteristic bands in the ranges 3100-3200 cm⁻¹ and 1600-1640 cm⁻¹, which can either be assigned to

$\nu_{\text{O-H}}$ and $\nu_{\text{C=N}}$ respectively for the tautomeric imine-ol (Fig 3.7, II) form or $\nu_{\text{N-H}}$ and $\nu_{\text{C=O}}$, respectively for the amine-one form (Fig 3.7, III) of the ligands [14]. We assigned this band to $\nu_{\text{N-H}}$ and $\nu_{\text{C=O}}$ for the later form based on the information obtained from crystallographic studies. The strong band at 1570-1595 cm^{-1} is observed in all ligands, is assigned to $\nu_{\text{C=N}}$ of the pyrazolone ring, which also suggests that ligands exist as the keto form in solid state, consisting with the crystal structure. All the ligands display a band in the region 1216-1239 cm^{-1} ascribed to ν_{CO} of the pyrazolone ring.

Table 3.6. Infrared spectral assignments of Schiff bases

Ligands	IR frequencies(cm^{-1})			
	$\nu_{\text{C=N}}$ (cyclic)	$\nu_{\text{C=N}}$ (azomethane)	ν_{CO} (pyrazolone ring)	$\nu_{\text{N-H}}/\nu_{\text{O-H}}$
TPMP-T	1570	1621	1230	3130
TPMP-BA	1570	1618	1229	3125
TMCPMP-T	1587	1620	1227	3210
TMCPMP-BA	1586	1638	1226	3175
TPTPMP-T	1594	1622	1235	3210
TPTPMP-BA	1570	1608	1216	3135
PPTPMP-T	1585	1627	1238	3241
PMCPMP-T	1584	1637	1239	3243
Reference	55	56	55	57

3.4.3. NMR spectral studies

3.4.3.1. ^1H NMR spectral studies

The ^1H NMR spectra of all the ligands were recorded in CDCl_3 at room temperature and the data are presented in Table 3.7.

3.4.3.1.1. ^1H NMR spectral studies of 4-toluoyl pyrazolone based Schiff bases

The signals due to methyl protons (two in the case of TPMP-BA, TMCPMP-BA; three in the case of TPMP-T, TMCPMP-T, TPTPMP-BA and four in the case of TPTPMP-T) appeared as singlet in the range δ 1.20 – 3.73 ppm. In some cases signals of $-\text{CH}_3$ groups are overlapped and all of these signals are so closely spaced that it is

Table 3.7. ^1H NMR spectral data of the Schiff base ligands

Ligand	$-\text{CH}_2-$ protons (δ ppm)	Methyl protons (δ ppm)	Aryl protons (δ ppm)	$-\text{NH}^*$ (δ ppm)
TPMP-T	-	-----[1.60, 2.18, 2.43]----- Singlet 9H	-----[6.70 – 8.04]----- Multiplet 13H	12.84 Singlet 1H
TPMP-BA	-	-----[1.61, 2.44]----- Singlet 6H	-----[6.66 – 8.04]----- Multiplet 13H	12.89 Singlet 1H
TMCPMP-T	-	-----[1.60, 2.25, 2.43]----- Singlet 9H	-----[6.71 – 8.14]----- Multiplet 12H	12.79 Singlet 1H
TMCPMP-BA	-	-----[1.58, 2.43]----- Singlet 6H	-----[6.64 – 8.09]----- Multiplet 12H	12.68 Singlet 1H
TPTPMP-T	-	-[1.20, 2.18, 2.42, 3.71]- Singlet 12H	-----[6.68 – 7.88]----- Multiplet 12H	12.80 Singlet 1H
TPTPMP-BA	-	-----[1.21, 2.43, 3.73]----- Singlet 9H	-----[6.64 – 7.88]----- Multiplet 13H	12.81 Singlet 1H
PPTPMP-T	2.74 Quartet 2H	-[1.21, 2.36, 2.41, 2.47]- Singlet 12H	-----[7.13 – 7.91]----- Multiplet 8 H	13.00 Singlet 1H
PMCPMP-T	2.70 Quartet 2H	-----[1.20, 2.40, 2.44]----- Singlet 9H	-----[7.10 – 8.15]----- Multiplet 8 H	12.86 Singlet 1H

*Not observed when spectra taken in $\text{CDCl}_3 + \text{D}_2\text{O}$

difficult to assign each signal to a particular methyl group unambiguously [24]. Moreover, such assignment will not contribute to establish the geometry of the ligands; therefore, no attempt has been made for such assignment. In the aromatic region, a few doublets and in few cases some overlapping doublets/multiplets are observed in the range δ 6.56 – 8.14 ppm. These doublets/multiplets are due to aryl protons of three benzene rings. Another singlet corresponding to one proton for all compounds is observed in the range δ 12.80-12.84 ppm. This signal disappeared or weakened when a D_2O exchange experiment was carried out. It can be bonding with the other atom (N/O). It may be noted that the integration of this signal perfectly matches with one proton and there is no other fragment(s) of this signal, which suggests that only one tautomeric form of the ligands exist in solution under the experimental conditions. We have not done any temperature dependent experiments. Comparing with the solid state study, we prefer to assign this signal to $-\text{NH}$, however,

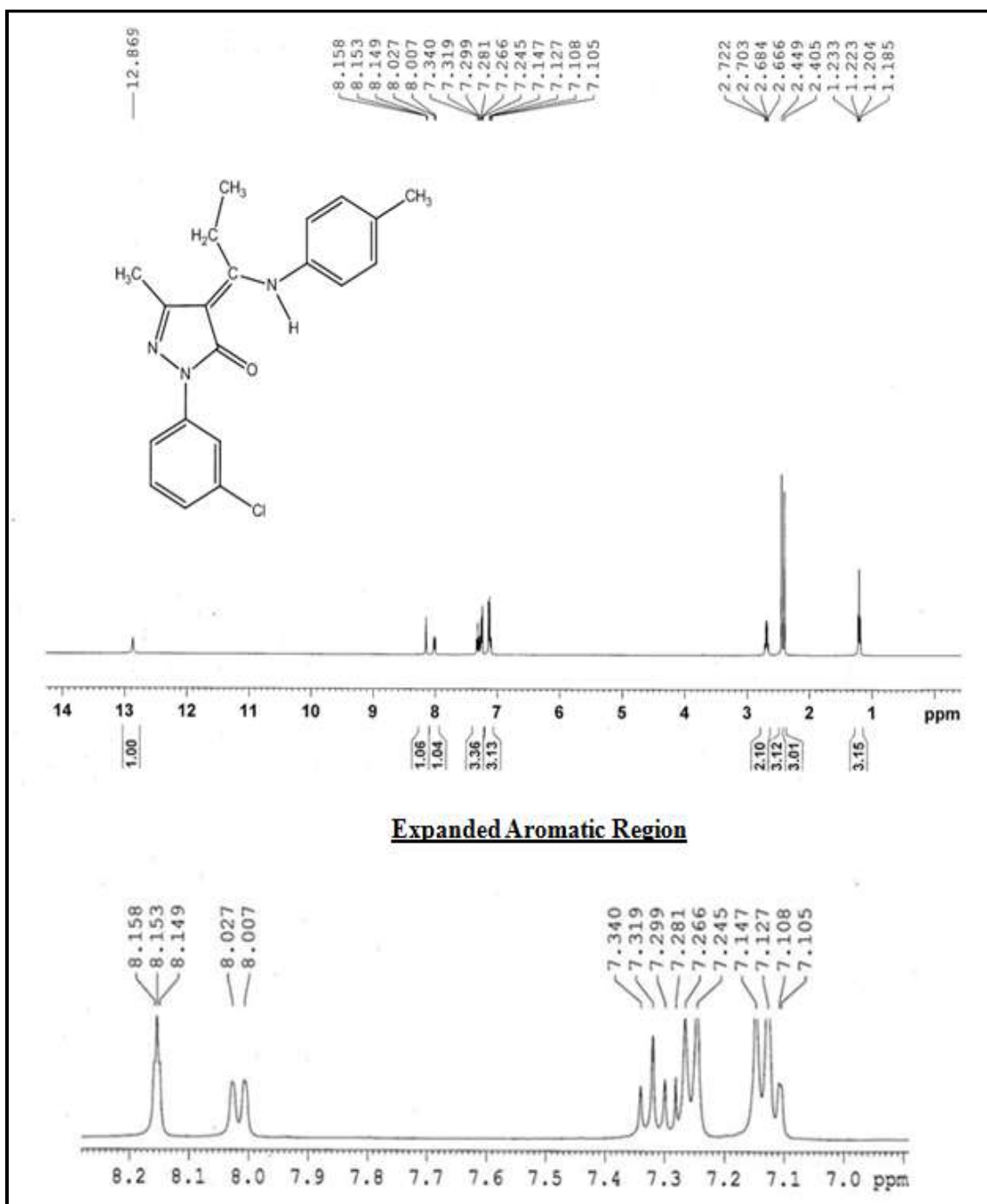


Fig. 3.19. ^1H NMR spectrum of the ligand PMCPMP-T

assignment of this peak to -OH cannot be ruled out provided solid state structural evidence is not considered [24].

3.4.3.1.2. ^1H NMR spectral studies of 4-propionyl pyrazolone based Schiff bases

The proton NMR spectrum of one of the ligand (PMCPMP-T) is shown in Fig. 3.19. In both the spectra, the integral intensities of each signal were found to agree with the number of different types of protons present. The much downfield signal observed at $\sim \delta$ 12.9 ppm is characteristic of intramolecular H-bonded –OH/-NH proton [58].

In the aliphatic region, triplets corresponding to methyl protons of 4-propionyl group are observed in the range of δ 1.19 - 1.25 ppm. The methylene protons appear as a quartet in the range of δ 2.70 - 2.79 ppm in the spectra of both the ligands. 5-methyl protons of pyrazolone ring resonate at $\sim \delta$ 2.45 ppm [59]. The signal due to *p*-substituted methyl group of Schiff base ligands appears at $\sim \delta$ 2.39 ppm as a singlet.

In the aromatic region, the aryl protons of two benzene rings resonate in the range of δ 7.12 - 8.13 ppm. From the proton NMR data it is clear that the ligands exist in amine-one form (III) in the solid as well in solution state.

3.4.3.2. ^{13}C NMR spectral studies

^{13}C NMR spectral data of the Schiff base ligands are presented in Table 3.8. The ^{13}C NMR spectrum of ligand PMCPMP-T is shown in Fig. 3.20.

3.4.3.2.1. ^{13}C NMR spectral studies of 4-toluoyl pyrazolone based Schiff bases

In the ^{13}C NMR spectra, the carbon atoms of the methyl groups appear in the range δ 16.1-21.5 ppm. The carbon atoms of the three benzene rings exhibit signals in the range δ 117.0-136.5 ppm and the number of signals varies from seven to fourteen. Nine signals were observed for ligand TPTPMP-BA, as expected for all *p*-substituted benzene rings because of symmetry [14]. However, nine signals (for ligand TPMP-T), eleven signals (for ligand TPMP-BA) and seven signals (for ligand TPTPMP-T) were observed in the ^{13}C NMR spectra of different ligands. Some of the signals might be overlapped as indicated by the intensity of a few signals. The other two ligands TMCPMP-T and TMCPMP-BA, where one of the benzene rings is *m*-substituted,

show twelve and fourteen signals, respectively, as expected because of the loss of symmetry [14, 60].

3.4.3.2.2. ^{13}C NMR spectral studies of 4-propionyl pyrazolone based Schiff bases

In the ^{13}C NMR spectra the carbon atoms of the methyl groups appear in the range δ 13.59–21.12 ppm (Table 3.8). The carbon atoms of the two benzene rings exhibit signals in the range δ 116.74–147.25 ppm and the number of signals varies from nine to eleven. Nine signals were observed for PPTPMP-T, as expected for the *p*-substituted benzene rings because of symmetry. However, PMCPMP-T shows eleven signals, so some of the signals might be overlapped as indicated by the intensity of a few signals. In the low field region, three signals were observed around δ 147, 166 and 169 ppm, which are associated with the carbon atoms of the heterocyclic ring. The most deshielded signal ($\delta \sim 169$ ppm) can be assigned to $>\text{C}=\text{O}$ and the next signal ($\delta \sim 166$ ppm) could be due to $>\text{C}=\text{N}$ of the heterocyclic ring. The singlet appearing for both compounds in the range $\delta \sim 101$ ppm is assigned to the carbon atom of the $>\text{C}-\text{N}-$ moiety, the significant upfield shift is due to the electron-donating methyl group attached to it.

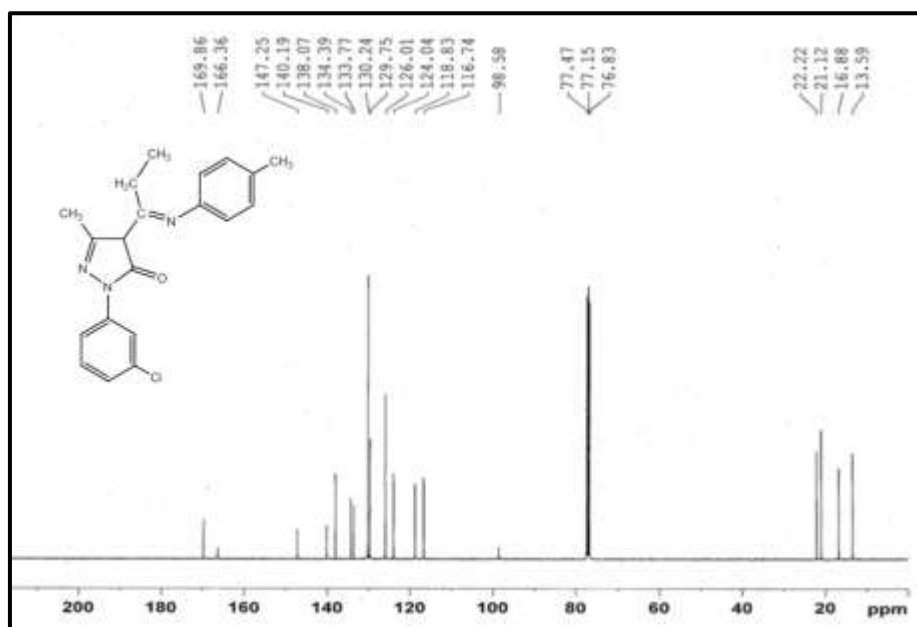


Fig. 3.20. ^{13}C NMR spectrum of ligand PMCPMP-T

Table 3.8. ^{13}C NMR spectral data of the Schiff base ligands

Ligands	-CH ₃ (δ ppm)	-CH ₂ - (δ ppm)	>C-N-	Aromatic (δ ppm)	>C=N	>C=O
TPMP-T	16.14, 20.88, 21.56	-	101.10	119.46, 123.73, 124.49, 128.42, 128.75, 129.49, 129.53, 140.67, 148.28	-	-
TPMP-BA	16.19, 21.58	-	-	119.34, 125.12, 128.38, 128.80, 129.74, 132.07	-	-
TMCPMP-T	-	-	-	123.75, 129.59	-	-
TMCPMP-BA	16.15, 21.58	-	101.64	117.04, 119.10, 119.43, 124.46, 125.31, 127.91, 128.37, 129.75, 129.83, 132.06, 134.48, 136.53, 139.79, 141.24, 148.78	-	-
TPTPMP-T	16.12	-	-	119.46, 123.68, 128.42, 128.62, 129.30, 129.48, 129.52	-	-
TPTPMP-BA	-	-	-	119.48, 125.18, 128.40, 129.34, 129.71, 132.00	-	-
PPTPMP-T	13.60, 16.87, 20.99, 21.11	22.18	98.69	119.31, 126.01, 129.27, 130.18, 133.91, 134.01, 136.59, 137.86, 146.47	165.92	169.52
PMCPMP-T	13.59, 16.88, 21.12	22.22	98.58	116.74, 118.83, 124.04, 126.01, 129.75, 130.24, 133.77, 134.39, 138.07, 140.19, 147.25	166.36	169.86

3.4.4. Mass spectral studies

Melting point of each ligand is high, as a result of this; the mass spectra were carried out by EI. The electron-impact mass spectra of pyrazolone derivatives, such as hydrazones [28-33], usually show an intense molecular ion peak. The mass spectral assignments for all the ligands are shown in Table 3.9.

3.4.4.1. Mass spectral studies of 4-toluoyl pyrazolone based Schiff base ligands

Fragmentation patterns of the ligands were obtained by mass spectrometry which is coupled with GC component as mentioned above. Normally the mass spectral fragmentation of the compound is found to give a characteristic pattern. Each kind of fragment has a particular ratio of mass to charge, or m/z value. For most ions, the charge is 1, so that m/z is simply the mass of the fragment. Thus, for ligand **TPMP-T** it exhibited a systematic fragmentation pattern (Scheme 3.10). The electronic impact mass spectrum of TPMP-T Schiff base is shown in (Fig. 3.21). It gave a molecular ion peak of $m/z = 381$, which is itself a corresponding base peak (the

most intense peak signifying a stable fragment). The mass spectra of the Schiff base ligands revealed the molecular ion peak at m/z **381** of the TPMP-T, m/z **446** for the TPMP-BA, m/z **415** for the TMCPMP-T, m/z **480** for the TMCPMP-BA, m/z **395** for the TPTPMP-T and m/z **460** for the TPTPMP-BA, which coincident with the formula weight (381) for the TPMP-T, (446) for the TPMP-BA, (415) for the TMCPMP-T, (480) for the TMCPMP-BA, (395) for the TPTPMP-T and (460) for the TPTPMP-BA support the identity of the proposed structures.

Table 3.9. Mass spectral data of Schiff base ligands

Ligand	m/z (observed)	Assignments
TPMP-T	381,305,290,276, 212,197,91,80	$C_{25}H_{23}N_3O^+$, $C_{18}H_{16}N_3O^+$, $C_{18}H_{16}N_3O^+$, $C_{17}H_{13}N_3O^+$, $C_{12}H_{10}N_3O^+$, $C_{11}H_7N_3O^+$, $C_7H_7^+$, $C_3N_2O^+$
TPMP-BA	446,366,340,275, 260,197,91,80	$C_{24}H_{20}N_3O^+$, $C_{24}H_{20}N_3O^+$, $C_{16}H_{10}N_3OBr^+$, $C_{17}H_{12}N_3O^+$ $C_{16}H_{10}N_3O^+$, $C_{11}H_7N_3O^+$, $C_7H_7^+$, $C_3N_2O^+$
TMCPMP-T	415,380.5,324,304, 274,197,91,80	$C_{25}H_{22}N_3OCl^+$, $C_{25}H_{22}N_3O^+$, $C_{18}H_{15}N_3OCl^+$, $C_{19}H_{18}N_3O^+$, $C_{17}H_{12}N_3O^+$, $C_{11}H_7N_3O^+$, $C_7H_7^+$, $C_3N_2O^+$
TMCPMP-BA	480,445.5,365.5,274.5 259,197,91,80	$C_{24}H_{19}N_3OBrCl^+$, $C_{24}H_{19}N_3OBr^+$, $C_{24}H_{19}N_3O^+$, $C_{17}H_{12}N_3O^+$, $C_{16}H_{11}N_3O^+$, $C_{11}H_7N_3O^+$, $C_7H_7^+$, $C_3N_2O^+$
TPTPMP-T	395,350,304,289, 213,197,91,80	$C_{26}H_{25}N_3O^+$, $C_{23}H_{16}N_3O^+$, $C_{19}H_{18}N_3O^+$, $C_{18}H_{15}N_3O^+$, $C_{19}H_{18}N_3O^+$, $C_{11}H_7N_3O^+$, $C_7H_7^+$, $C_3N_2O^+$
TPTPMP-BA	460,380,378,369, 289,197,91,80	$C_{25}H_{22}N_3OBr^+$, $C_{25}H_{22}N_3O^+$, $C_{11}H_8N_3OBr^+$, $C_{18}H_{15}N_3OBr^+$, $C_{18}H_{15}N_3O^+$, $C_{11}H_7N_3O^+$, $C_7H_7^+$, $C_3N_2O^+$
PPTPMP-T	332.7, 303.79, 228.13, 213.20, 91.14	$C_{21}H_{23}N_3O^+$, $C_{19}H_{17}N_3O^+$, $C_{13}H_{15}N_3O^+$, $C_{12}H_{13}N_3O^+$, $C_7H_7^+$
PMCPMP-T	352.2, 320.2, 323.6, 287.7, 211.1,110.7,90.6	$C_{20}H_{20}ClN_3O^+$, $C_{20}H_{20}N_3O^+$, $C_{18}H_{14}ClN_3O^+$, $C_{18}H_{14}N_3O^+$, $C_{12}H_{10}N_3O^+$, $C_{12}H_{10}ClN_3O^+$, $C_4H_5N_3O^+$, $C_7H_7^+$

A peak corresponding to the 5 member pyrazolone ring only can be observed at m/z (**80**) in the mass spectra of all ligands. A peak corresponding to the substituted pyrazolone ring can also be observed at m/z (**197**) in the mass spectra of all ligands. The other peaks appeared in the mass spectrum (abundance range 1-100%) are attributed to the fragmentation of Schiff base molecules obtained from the rupture of different bonds inside the molecule.

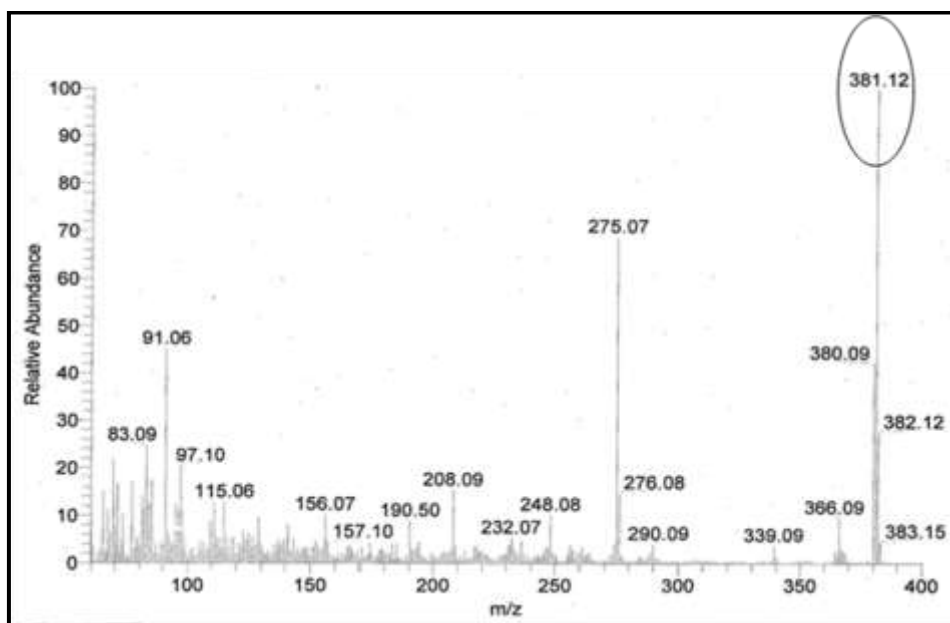


Fig. 3.21. The Mass spectrum of the ligand TPMP-T

3.4.4.2. Mass spectral studies of 4-propionyl pyrazolone based Schiff base ligands

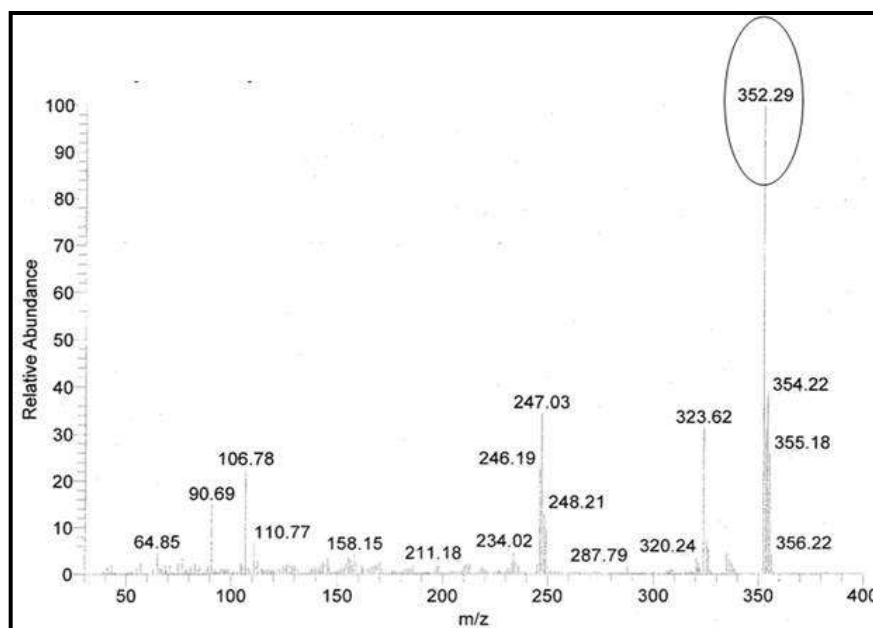
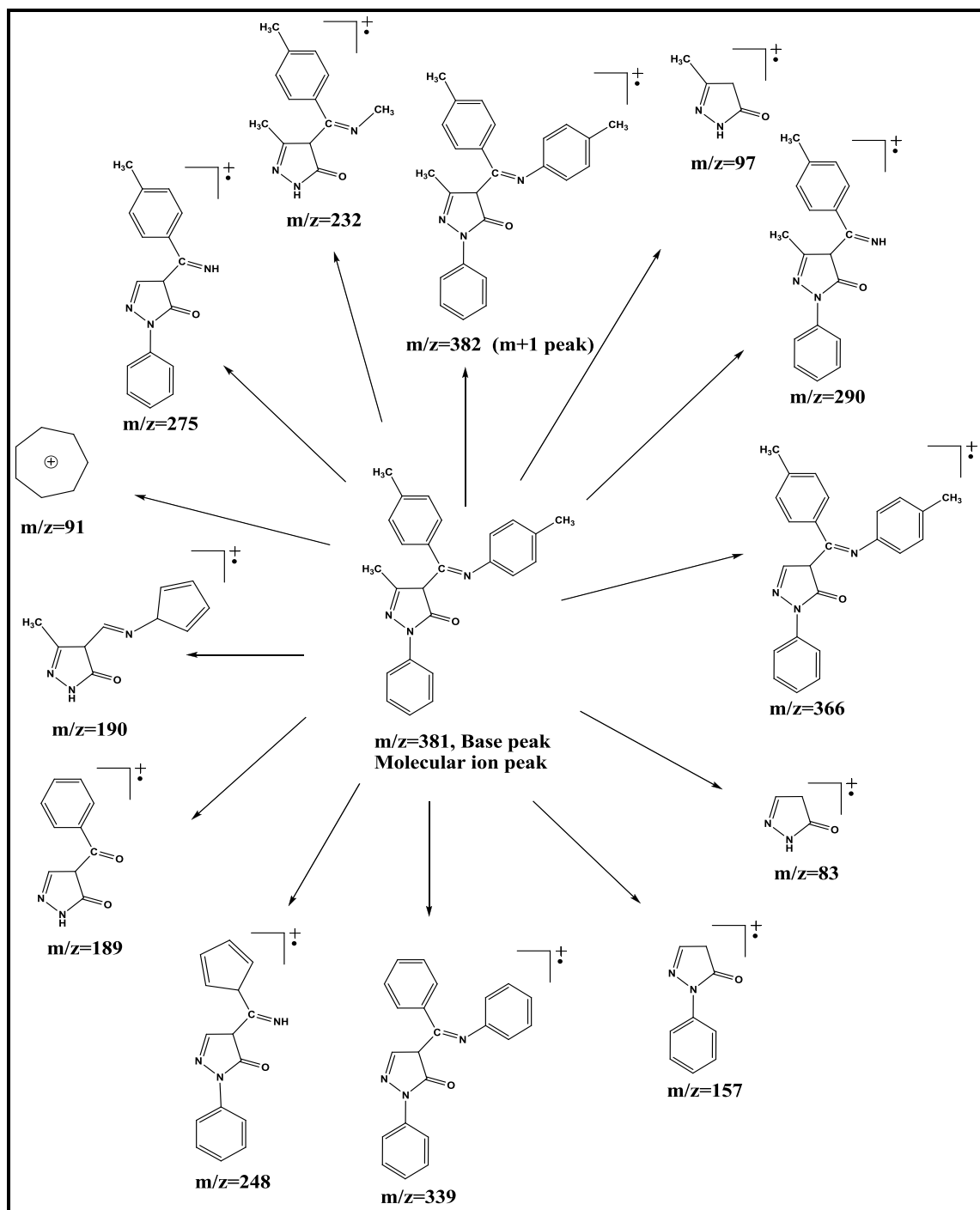


Fig. 3.22. The Mass spectrum of the ligand PMCPMP-T

The mass spectra of both the Schiff base ligands are in good agreement with proposed structures. The electronic impact mass spectrum of PMCPMP-T Schiff base

is shown in (Fig. 3.22). It shows a molecular ion peak at m/z 352.29 with a relative intensity near to 100%, which is equivalent to its molecular weight and this peak itself is a base peak.



The mass spectra of the Schiff base ligands revealed the molecular ion peak at m/z 332.7 of the PPTPMP-T and m/z 352.29 for the PMCPMP-T, which coincident with the formula weight (333) for the PPTPMP-T and (353) for the PMCPMP-T, supporting the identity of the proposed structures. The other peaks appeared in the mass spectrum (abundance range 1-100%) are attributed to the fragmentation of Schiff base molecules obtained from the rupture of different bonds inside the molecule.

A peak corresponding to the tropylium ion can be observed at m/z (91) in the mass spectra of all eight Schiff base ligands. The fragmentation of the heterocycle rings, which includes pyrazole ring, is as a result of small and stable, neutral molecules, which are analogous to HCN, such as C=NH as well as HCCH and thus is not discussed herein.

3.4.5. Molecular structure of ligands

The molecular structures of four ligands (TPMP-BA, TMCPMP-T, TMCPMP-BA and PMCPMP-T) were determined from single crystal X-ray studies. ORTEP diagrams of these ligands with the atom numbering schemes are shown in Fig. 3.23. Crystallographic data of the ligands are listed in Table 3.10. Important bond lengths and angles for the compounds (TPMP-BA, TMCPMP-T and TMCPMP-BA) and for PMCPMP-T are listed in Table 3.11. Existence of acyl pyrazolone derivatives in different tautomeric forms (Fig. 3.7) in solid state is well known phenomenon and thus many studies have been made to establish the geometry of these derivatives including ours [14, 19, 24, 25]. The Schiff base derivatives prepared from 4-acetyl-5-methyl-2-phenyl-2,4-dihydro-pyrazol-3-one and alkyl amines are shown to remain exclusively in the amine-one tautomeric form in chloroform solutions at room temperature has been also proved recently using a combination of ^1H , ^{13}C , APT, COSY, HMQC, and HMBC NMR spectroscopic methods [61].

These compounds exist as a monomeric compound. The single crystal X-ray diffraction study on this compound clearly indicates that the present compound exists in amine-one form without any ambiguity. Infact, the solid state structures support the

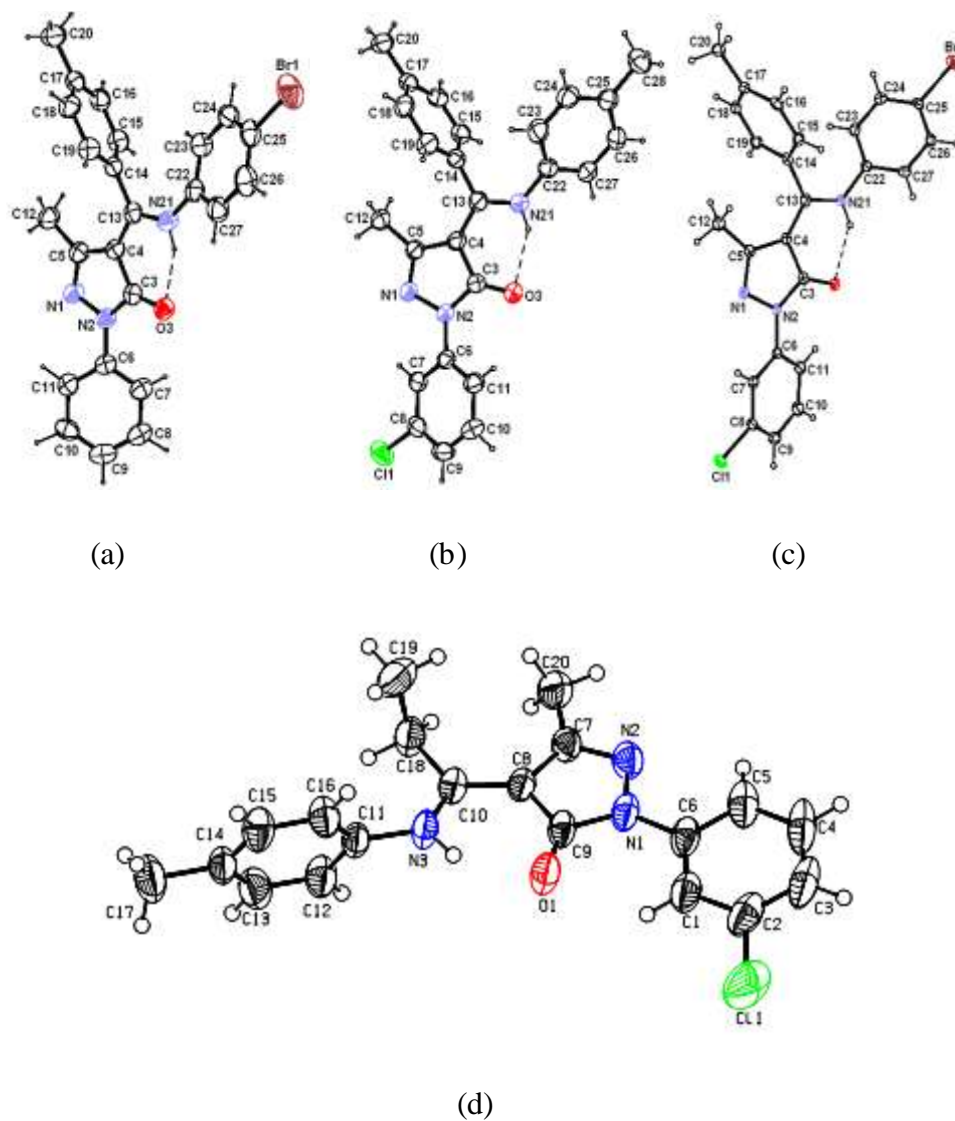


Fig. 3.23. Molecular structures of (a) TPMP-BA (b) TMCPMP-T (c) TMCPMP-BA (d) PMCPMP-T, showing the intramolecular hydrogen bonds and atom labelling scheme. Displacement ellipsoids are drawn at the 50% probability level and H atoms are shown as small spheres of arbitrary radii.

fact that strong hydrogen bonding between amine hydrogen and the pyrazolone C3 carbonyl oxygen helps to stabilize the amine-one tautomer. The N-H unit on the exocyclic C=C double bond in the compounds, which are on the same side of the double bond as the C=O unit of the pyrazolone ring, interacts with the carbonyl group through an intramolecular N—H...O hydrogen bond. The Hydrogen bonding geometry parameters of three ligands are also shown in Table 3.12. The O atom of the pyrazolone unit and the N atom of the amine group are available for coordination with metals. The pyrazolone ring is planar and atoms O1, C3, C4, C13 and N21 (for TPMP-BA, TMCMPMP-T and TMCMPMP-BA) and O1, C8, C9, C10 and N3 (for PMCPMP-T) are coplanar. The bond lengths within this part of the molecule (Table 3.6) lie between classical single- and double-bond lengths, indicating extensive conjugation. The packing arrangement of one of the ligand TPMP-BA molecules viewed down the *b*-axis is shown in Fig. 3.24.

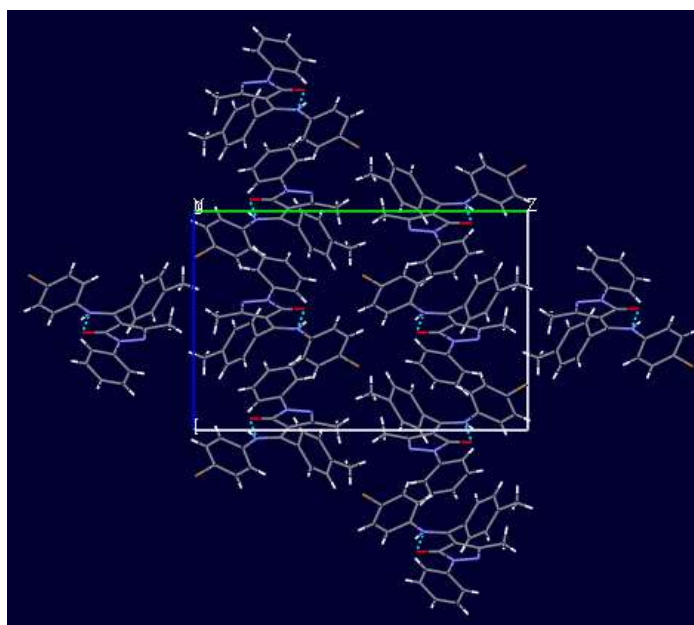


Fig. 3.24. The packing arrangement of TPMP-BA molecules viewed down the *b*-axis.

Table 3.10. Summary of crystallographic data of the ligands and complex

Compound	TPMP-BA	TMCPMP-T	TMCPMP-BA	PMCPMP-T	32
Chemical formula	C ₂₄ H ₂₀ BrN ₃ O	C ₂₅ H ₂₂ ClN ₃ O	C ₂₄ H ₁₉ BrClN ₃ O	C ₂₀ H ₂₀ ClN ₃ O	C ₄₈ H ₃₈ Br ₂ CuN ₆ O ₂
Formula weight	446.34	415.91	480.78	353.84	954.20
a(Å)	9.281(4)	7.3549(3)	7.1797(14)	8.1092(11)	14.2362(10)
b(Å)	18.444(9)	10.7278(5)	10.419(2)	18.034(2)	22.5728(14)
c(Å)	12.598(6)	13.7950(6)	14.336(3)	12.6225(16)	14.3589(12)
α(°)	90.000	78.158(4)	107.185(3)	90.00	90.00
β(°)	104.761(8)	85.465(3)	92.247(3)	96.030(2)	108.347(8)
γ(°)	90.000	84.840(4)	94.151(3)	90.00	90.00
Z	4	2	2	4	4
V(Å ³)	2085(3)	1058.92(8)	1019.8(3)	1835.7(4)	4379.7(5)
Reflection collected	9835	7881	6507	-	16510
Independent Reflections	2288	4752	4654	-	7690
R(int)	0.0603	0.0244	0.0259	-	0.0619
Number of parameters	342	359	271	233	542
Crystal system	Monoclinic	Triclinic	Triclinic	Monoclinic	Monoclinic
Space group	P21/n	P-1	P-1	P 21/n	P 21/c
ρ _{calcd.} (g cm ⁻³)	1.422	1.304	1.566	1.280	1.447
Abs coeff, μ(cm ⁻¹)	1.991	0.202	2.168	0.22	2.369
F(000)	912	436	488	744	1932
Temp(°C)	23	23	23	23	23
GOF on F ²	0.944	1.000	1.001	1.081	1.030
R1 /wR2([I]>2σ(I))	0.0585 / 0.1351	0.0525 / 0.1172	0.0516 / 0.1188	-	0.0636 / 0.0997
R1 /wR2(all data)	0.1251 / 0.1654	0.0974 / 0.1415	0.0695 / 0.1352	-	0.1592 / 0.1373
CCDC	795607	795608	795609	782562	868303

Table 3.11. Selected bond lengths and angles in the Schiff base ligands

Compound	TPMP-BA	TMCPMP-T	TMCPMP-BA	PMCPMP-T	
Bond distances (Å) with esd's in parentheses					
N1-C5	1.311(5)	1.305(3)	1.309(4)	N1 C9	1.380(4)
N1-N2	1.397(4)	1.405(2)	1.404(4)	N1 N2	1.393(3)
N2-C3	1.374(4)	1.380(3)	1.382(4)	N1 C6	1.417(4)
N2-C6	1.415(4)	1.411(3)	1.415(4)	N2 C7	1.312(4)
C3-O3	1.238(4)	1.246(2)	1.245(4)	O1 C9	1.247(3)
C3-C4	1.450(5)	1.438(3)	1.391(5)	N3 C10	1.321(4)
C5-C12	1.496(5)	1.496(3)	1.481(5)	N3 C11	1.437(4)
C13-N21	1.333(5)	1.343(3)	1.345(4)	C10 C8	1.400(4)
C17-C20	1.506(6)	1.495(3)	1.520(5)	C1 C6	1.375(4)
C18-C19	1.371(5)	1.365(3)	1.380(5)	C10 C18	1.498(4)
C7-C8	1.394(6)	1.373(3)	1.393(5)	C18 C19	1.525(5)
C17-C18	1.391(6)	1.387(3)	1.391(5)	C14 C17	1.513(4)
Bond angles (°) with esd's in parentheses					
C5 N1 N2	106.4(3)	106.51(16)	106.9(3)	C9 N1 N2	112.4(2)
C3 N2 N1	112.6(3)	111.87(17)	112.2(3)	C9 N1 C6	129.0(3)
C3 N2 C6	128.5(3)	129.35(18)	129.2(3)	N2 N1 C6	118.5(2)
N1 N2 C6	118.4(3)	118.68(17)	118.6(3)	C7 N2 N1	106.1(2)
O3 C3 N2	126.6(3)	125.7(2)	126.2(3)	C10 N3 C11	127.0(3)
O3 C3 C4	129.5(3)	129.6(2)	129.4(3)	O1 C9 N1	126.2(3)
N2 C3 C4	103.9(3)	104.67(17)	104.3(3)	O1 C9 C8	129.7(3)
N1 C5 C12	118.4(4)	117.8(2)	118.8(3)	N1 C9 C8	104.2(3)
C11 C6 N2	118.9(3)	120.8(2)	120.7(3)	C16 C11 C12	119.6(3)
N21 C13 C4	117.6(3)	118.4(2)	118.1(3)	C16 C11 N3	120.5(3)
N21 C13 C14	121.3(3)	121.3(2)	121.0(3)	C12 C11 N3	119.8(3)

Table 3.12. Hydrogen-bonding geometry (e.s.d.'s in parentheses). Cg1 denotes the centroid of the C6-C11 ring (for TMCPMP-T, TPMP-BA) and C14-C19 ring (for TMCPMP-BA)

Ligand	D-H...A	D-H(Å)	H...A(Å)	D...A(Å)	D-H...A(°)
TMCPMP-BA	N21-H21...O3	0.86	1.96	2.692(4)	142
	C20-H20C...Cg1 ¹	0.96	2.93	3.306(4)	128
TMCPMP-T	N21-H21...O3	0.83(3)	1.99(3)	2.711(3)	145(3)
	C26H26...Cg1	0.96(2)	2.72(2)	3.620(3)	158(2)
TPMP-BA	N21-H21...O3	0.85(3)	1.98(4)	2.695(4)	142(3)
	C15H15...Cg1	0.86(3)	2.69(3)	3.485(5)	153(3)

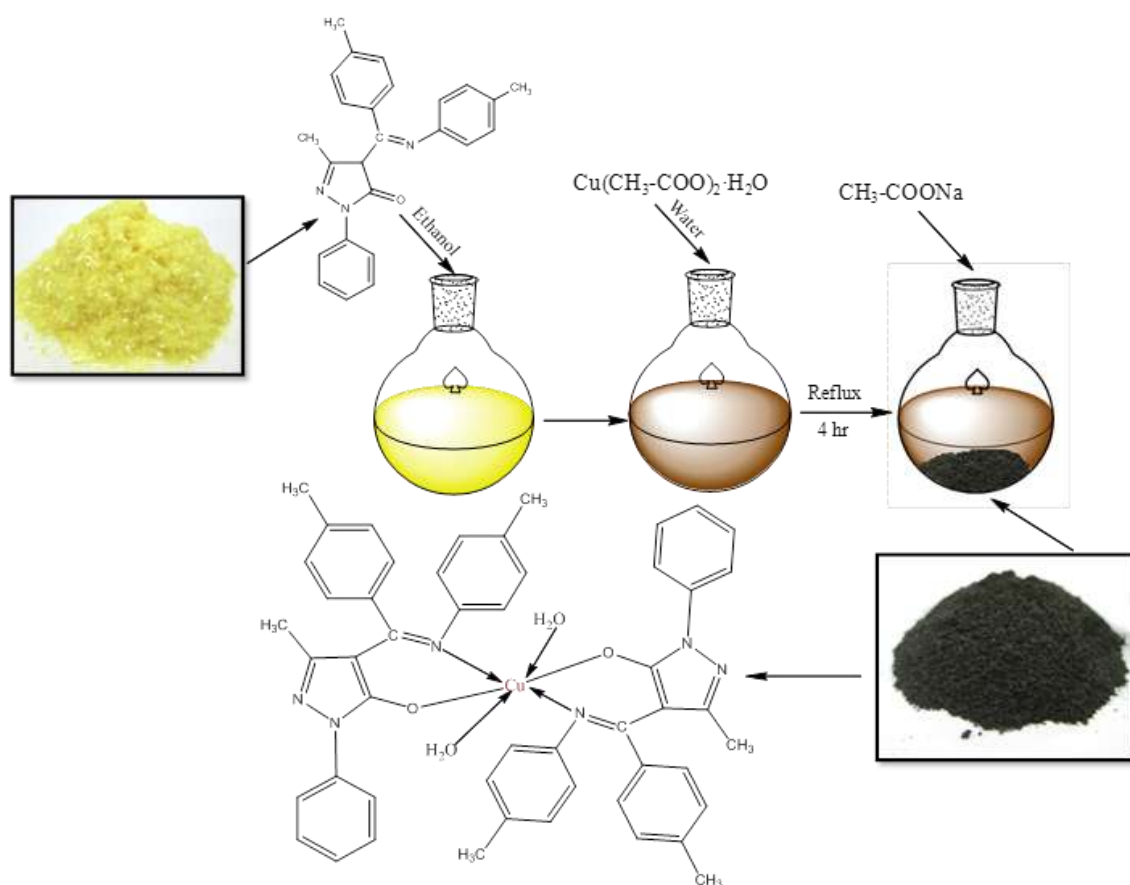
Symmetry code : (i) 1+ x, y, z (ii) 1+ x, y, z for MCPMP-T & PMP-BA

(i) 1- x, 2- y, 1- z for MCPMP-BA

3.5. Syntheses of Cu(II) complexes

3.5.1. [Cu(TPMP-T)₂(H₂O)₂] (24):

The metal salt Cu(OAc)₂·H₂O (0.199 gms, 1 mmol) was dissolved in hot water and the solution was added to a hot ethanolic solution of the TPMP-T (0.762 gms, 2 mmol). After the complete addition little amount of sodium acetate was added and the mixture was refluxed for 4 hours. A brown crystalline solid was obtained, which was isolated by filtration, washed with hot water and finally with ethanol and dried under *a vacuum*.



Scheme 3.11. Synthesis of [Cu(TPMP-T)₂(H₂O)₂]

3.5.2. [Cu(TPMP-BA)₂(H₂O)₂] (25):

It was prepared analogously from TPMP-BA and Cu(OAc)₂·H₂O. A brown crystalline solid was obtained, which was isolated by filtration and dried under *a vacuum*.



Scheme 3.12. Synthesis of [Cu(TPMP-BA)₂(H₂O)₂]

3.5.3. [Cu(TMCPMP-T)₂(H₂O)₂] (26):

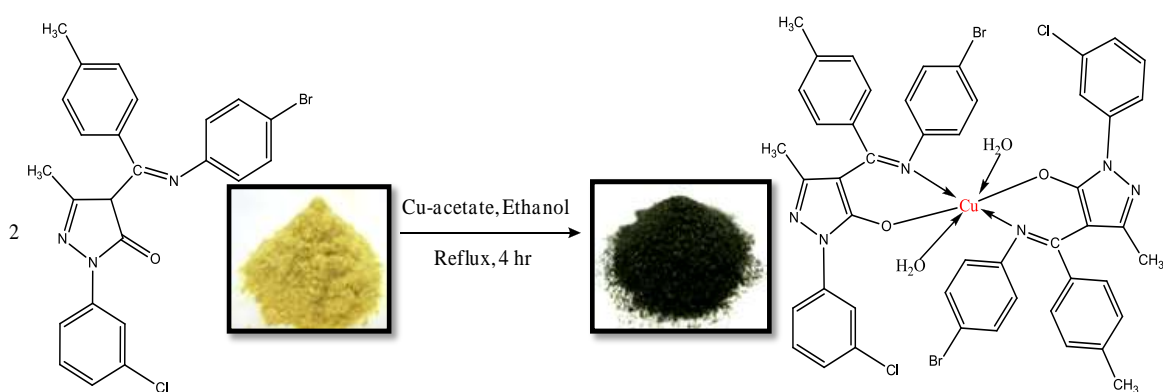


Scheme 3.13. Synthesis of [Cu(TMCPMP-T)₂(H₂O)₂]

It was prepared analogously from TMCPMP-T and Cu(OAc)₂·H₂O. A brown crystalline solid was obtained, which was isolated by filtration and dried under *a vacuum*.

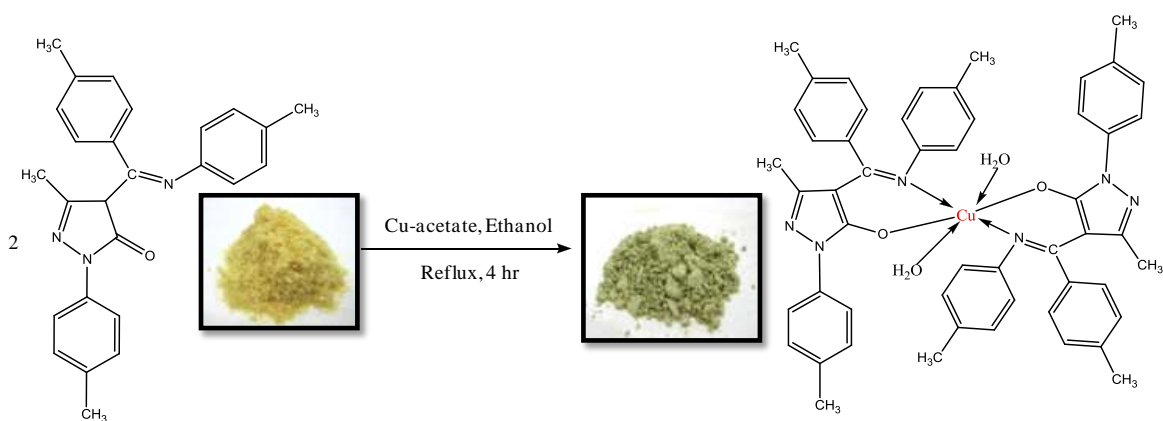
3.5.4. [Cu(TMCPMP-BA)₂(H₂O)₂] (27):

It was prepared analogously from TMCPMP-BA and Cu(OAc)₂·H₂O. A brown crystalline solid was obtained, which was isolated by filtration and dried under *a vacuum*.



Scheme 3.14. Synthesis of $[\text{Cu}(\text{TMCPMP-BA})_2(\text{H}_2\text{O})_2]$

3.5.5. $[\text{Cu}(\text{TPTPMP-T})_2(\text{H}_2\text{O})_2]$ (28):

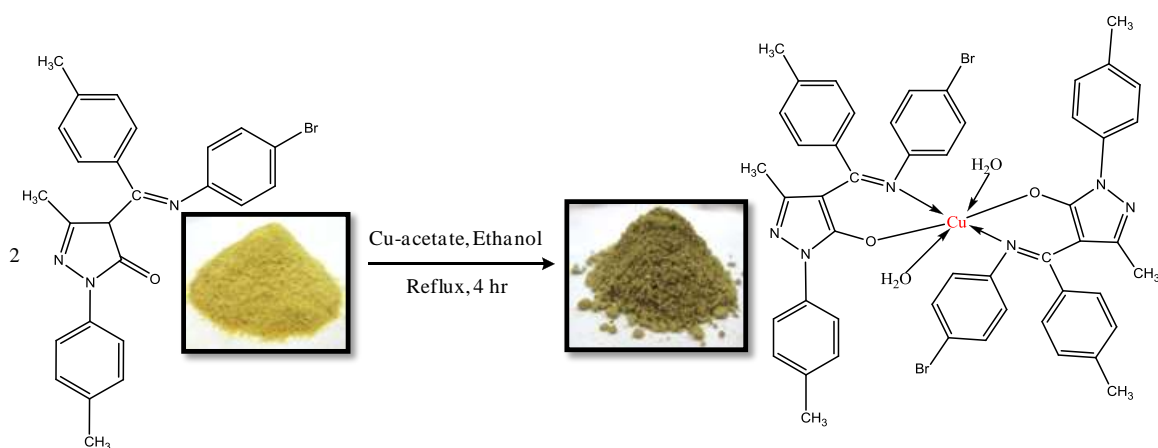


Scheme 3.15. Synthesis of $[\text{Cu}(\text{TPTPMP-T})_2(\text{H}_2\text{O})_2]$

It was prepared analogously from TPTPMP-T and $\text{Cu}(\text{OAc})_2 \cdot \text{H}_2\text{O}$. A green crystalline solid was obtained, which was isolated by filtration and dried under *a vacuum*.

3.5.6. $[\text{Cu}(\text{TPTPMP-BA})_2(\text{H}_2\text{O})_2]$ (29):

It was prepared analogously from TPTPMP-BA and $\text{Cu}(\text{OAc})_2 \cdot \text{H}_2\text{O}$. A green crystalline solid was obtained, which was isolated by filtration and dried under *a vacuum*.



Scheme 3.16. Synthesis of $[\text{Cu}(\text{TPMP-BA})_2(\text{H}_2\text{O})_2]$

3.6. Syntheses of Ni(II) complexes

3.6.1. $[\text{Ni}(\text{PPTPMP-T})_2(\text{H}_2\text{O})_2]$ (30):

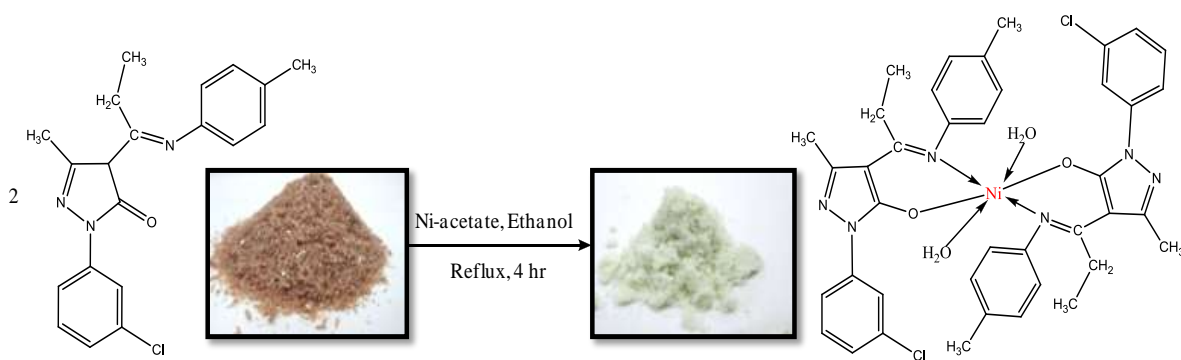


Scheme 3.17. Synthesis of $[\text{Ni}(\text{PPTPMP-T})_2(\text{H}_2\text{O})_2]$

It was prepared analogously from PPTPMP-T and $\text{Ni}(\text{OAc})_2 \cdot 4\text{H}_2\text{O}$. A light green solid was obtained, which was isolated by filtration and dried under *a vacuum*.

3.6.2. $[\text{Ni}(\text{PMCPMP-T})_2(\text{H}_2\text{O})_2]$ (31):

It was prepared analogously from PMCPMP-T and $\text{Ni}(\text{OAc})_2 \cdot 4\text{H}_2\text{O}$. A green crystalline solid was obtained, which was isolated by filtration and dried under *a vacuum*.



Scheme 3.18. Synthesis of $[\text{Ni}(\text{PMCPMP-T})_2(\text{H}_2\text{O})_2]$

3.7. Characterization of metal(II) complexes

3.7.1. Physicochemical properties of the synthesized complexes

The complexes have been synthesized in a very facile and essentially identical way. The Ligand acts as a bidentate O, N donor towards the metal(II) core. The complexes are obtained from a refluxing mixture of the respective ligand and metal salt precursors, taken in 1:1 molar proportions in purified solvent. All these complexes are intensively colored, air and moisture free crystalline solids. They are insoluble in common organic solvents and only soluble in Acetonitrile, DMF and DMSO. Molar conductance value of the complexes soluble in DMF (10^{-3}M solution at room temperature), indicates that the complexes have molar ratio of metal: ligand as 1:1. The lesser molar conductance values ($4\text{-}16 \Omega^{-1} \text{cm}^2 \text{mol}^{-1}$) indicate that the complexes are electrically non-conducting in nature [62]. The elemental analyses data concur well with the planned formulae for the ligand and also recognized the $[\text{ML}_2(\text{H}_2\text{O})_2]$ composition of the metal(II) complexes. The analytical and physical data of the complexes are shown in Table 3.13.

Table 3.13. Physicochemical and analytical data of the complexes

Complex	Formula Weight(g mol ⁻¹)	Colour	Yield (%)	Melting Point(°C)	Analysis (%) Found(calcd)				$\Lambda_M(\Omega^{-1} \text{cm}^2 \text{mol}^{-1})$	$\mu_{\text{eff}}(\text{B.M.})$
					C	H	N	M		
24	860.47	Brown	43.39	>270	69.65 (69.68)	5.54 (5.57)	9.74 (9.75)	7.46 (7.37)	6.00	1.78
25	990.20	Green	30.86	>266	58.11 (58.12)	4.22 (4.23)	8.45 (8.47)	6.55 (6.40)	4.00	1.79
26	929.36	Brown	50.10	>250	64.50 (64.51)	4.93 (4.94)	9.02 (9.03)	7.50 (7.37)	6.00	1.81
27	1058.92	Green	39.90	290	54.31 (54.33)	3.75 (3.77)	7.90 (7.92)	6.10 (5.99)	5.00	1.80
28	888.52	Green	35.19	>290	70.18 (70.19)	5.83 (5.84)	9.43 (9.44)	7.21 (7.14)	10.00	1.76
29	1018.26	Green	38.94	>280	58.86 (58.88)	4.50 (4.51)	8.23 (8.24)	6.46 (6.23)	16.00	1.79
30	759.56	Light green	32.89	190	72.26 (66.41)	6.90 (6.37)	14.83 (11.06)	7.16 (7.73)	9.00	3.03
31	800.40	Light green	40.04	145	62.94 (60.02)	5.57 (5.29)	13.04 (10.50)	6.29 (7.33)	11.00	3.54

3.7.2. IR spectral studies

The characteristic IR bands for all the complexes recorded as KBr discs are listed in Table 3.14. The IR spectrum of one complex **30** is shown in Fig. 3.25.

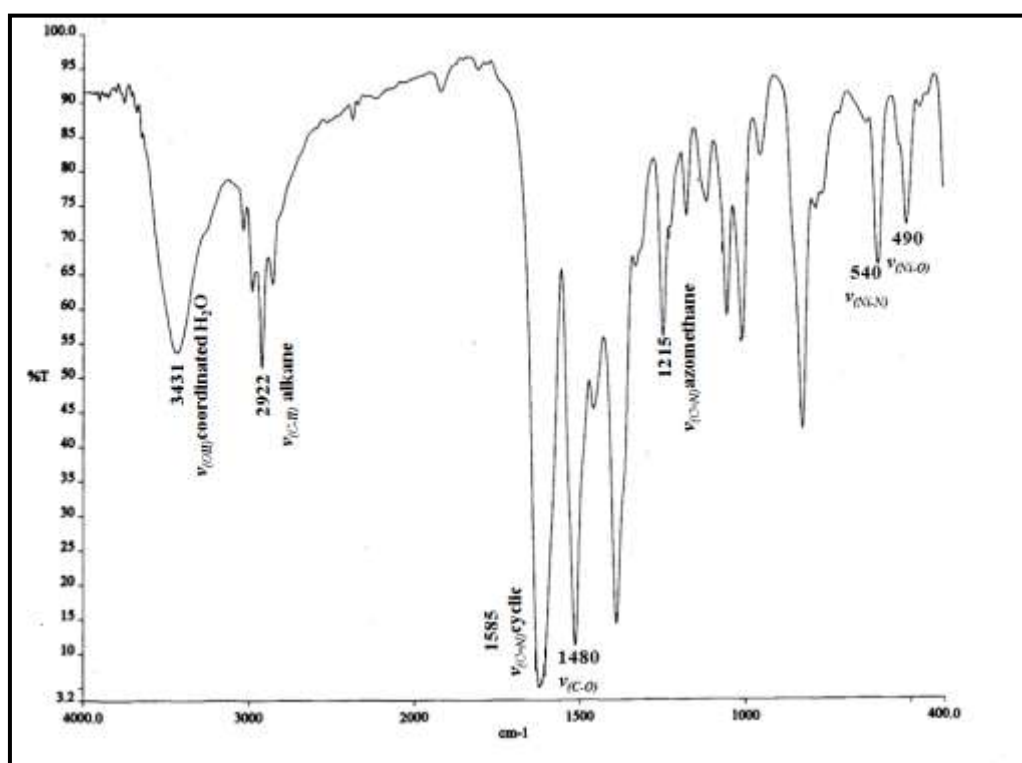


Fig. 3.25. IR spectrum of complex **30**

All the complexes show absorption in the region 3000-2900 cm⁻¹, which may be due to ν_{C-H}. In the IR spectra of the complexes, it can be obviously observed that the N-H stretching vibrations disappear; indicating de-protonation of N-H group in metal complexes and a new band attributed to ν_{C=O} appears at 1470-1485 cm⁻¹. In addition, the new bands at about 480-490cm⁻¹ and 530-550 cm⁻¹ are assigned to M-N and M-O vibrations, respectively. There are other changes like the absorption bands of C=O and C=N slightly shift to the lower wave number, suggesting the coordination through the oxygen atom of pyrazolone ring and azomethane nitrogen to the central metal atom. All complexes show band in the region 3400-3435 cm⁻¹, which may be due to the presence of coordinated water molecules. As shown by TGA of all the

complexes, this band may be assigned to the two coordinated water molecules. The wave no. of cyclic C=N does not change in all the complexes, indicates no coordination via C=N cyclic. By comparing the IR spectra of ligands and metal complexes, it is easy to predict that the ligand binds to the metal ion via N and O i.e. bidentate manner.

In the investigated complexes, the bands observed in the region 3400–3450, 1295–1300, 860–870 and 715–717 cm^{-1} are attributed to OH stretching, bending, rocking and wagging vibrations, respectively due to the presence of water molecules [63]. The presence of rocking band indicates the coordination nature of the water molecule [63].

Table 3.14. Infrared spectral assignments of the complexes

Complex	$\nu_{(OH)}$ coordinated H ₂ O	$\nu_{C=N}$ (cyclic)	$\nu_{C=N}$ (azomethane)	ν_{C-O}	ν_{M-O}	ν_{M-N}
24	3431	1564	1214	1478	483	550
25	3431	1563	1214	1476	483	534
26	3432	1584	1214	1475	485	545
27	3425	1584	1212	1474	485	534
28	3428	1570	1212	1482	489	536
29	3409	1568	1213	1481	482	532
30	3431	1585	1215	-	490	540
31	3429	1585	1214	1480	486	546
Reference	63	63	64	64	56	63

3.7.3. Mass spectral studies

The mass spectral assignments for the complexes are shown in Table 3.15. The FAB–Mass spectra of all the complexes were recorded in m-nitro benzyl alcohol as a matrix. All the complexes gave a parent ion peak corresponding to their molecular weight. These are formed by the complex when two water molecules are removed. So, the parent ion peak is $[\text{Cu}(\text{L})_2-2(\text{H}_2\text{O})]$. A peak corresponding to ligand appears corresponding to its molecular weight in all the complexes. The fragmentation pattern for the complex **24** is presented in Scheme 3.19 and the mass spectra of two complexes **24** and **30** are shown in Figs. 3.26 & 3.27, respectively.

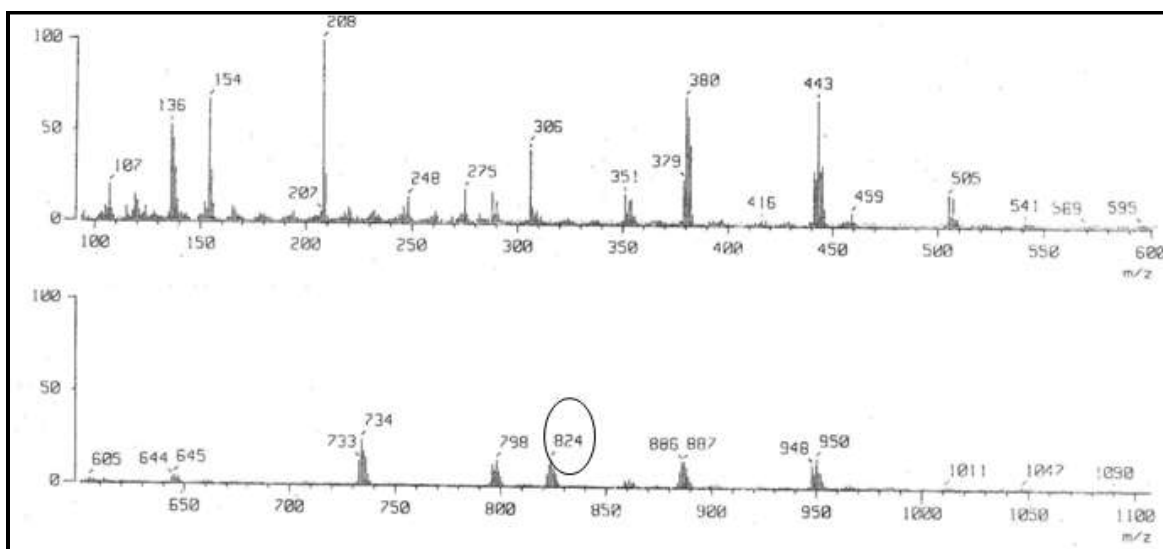


Fig. 3.26. The Mass spectrum of the complex 24

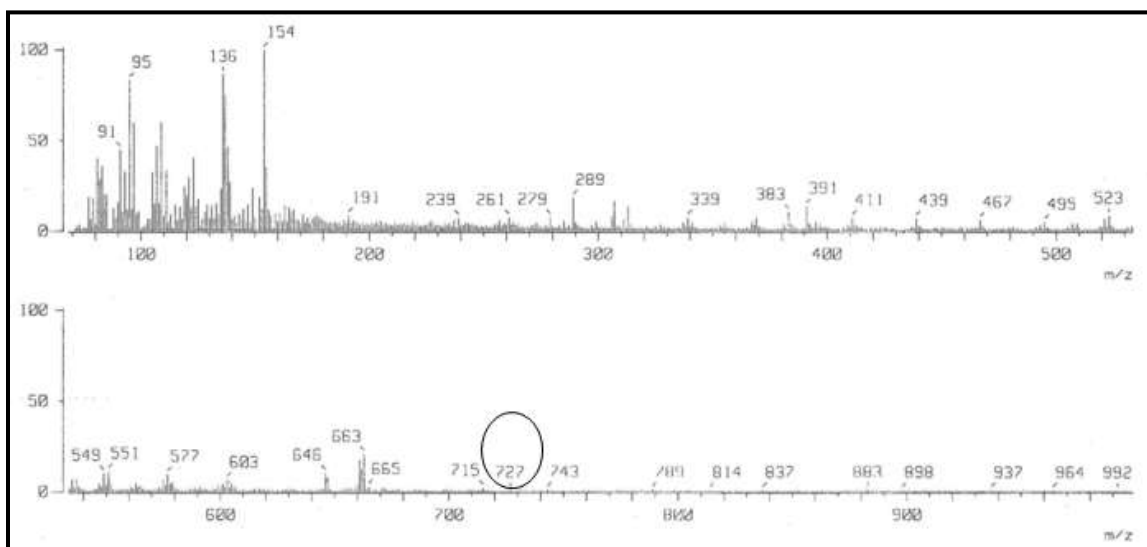
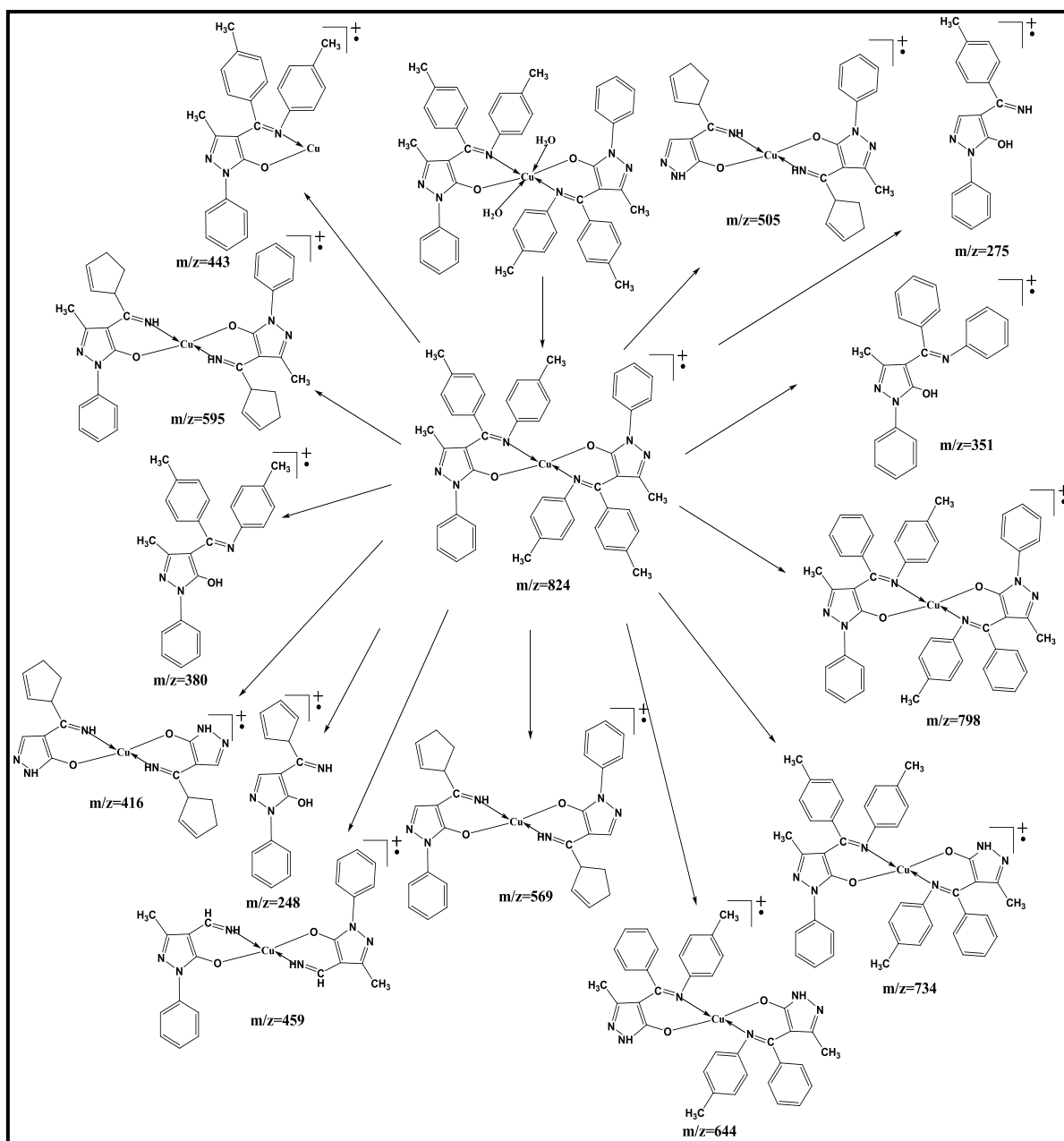


Fig. 3.27. The Mass spectrum of the complex 30



Scheme 3.19. Fragmentation pattern of the complex 24

Table 3.15. Mass spectral data of the complexes

Complex	m/z (observed)	Assignments
24	824,809,670,640, 580,380,275,169	$[\text{Cu}(\text{C}_{25}\text{H}_{22}\text{N}_3\text{O})_2]^+$, $[\text{Cu}(\text{C}_{19}\text{H}_{17}\text{N}_3\text{O})_2]^+$, $[\text{Cu}(\text{C}_{49}\text{H}_{41}\text{N}_6\text{O})]^+$, $[\text{Cu}(\text{C}_{25}\text{H}_{22}\text{N}_3\text{O})_2]^+$, $[\text{Cu}(\text{C}_{16}\text{H}_8\text{N}_3\text{O})_2]^+$, $(\text{C}_{25}\text{H}_{22}\text{N}_3\text{O})^+$, $[\text{Cu}(\text{C}_8\text{N}_6\text{O})]^+$, $[\text{Cu}(\text{C}_4\text{N}_3\text{O})]^+$
25	954,794,611,582, 445,422,275,169	$[\text{Cu}(\text{C}_{24}\text{H}_{19}\text{N}_3\text{OBr})_2]^+$, $[\text{Cu}(\text{C}_{24}\text{H}_{19}\text{N}_3\text{O})_2]^+$, $[\text{Cu}(\text{C}_{17}\text{H}_{11}\text{N}_3\text{O})_2]^+$, $[\text{Cu}(\text{C}_{16}\text{H}_9\text{N}_3\text{OBr})_2]^+$, $(\text{C}_{24}\text{H}_{19}\text{N}_3\text{OBr})^+$, $[\text{Cu}(\text{C}_{16}\text{H}_9\text{N}_3\text{O})_2]^+$, $[\text{Cu}(\text{C}_8\text{N}_6\text{O})]^+$, $[\text{Cu}(\text{C}_4\text{N}_3\text{O})]^+$
26	893,823,641,611, 499,414,275,169	$[\text{Cu}(\text{C}_{25}\text{H}_{21}\text{N}_3\text{OCl})_2]^+$, $[\text{Cu}(\text{C}_{25}\text{H}_{21}\text{N}_3\text{O})_2]^+$, $[\text{Cu}(\text{C}_{18}\text{H}_{14}\text{N}_3\text{O})_2]^+$, $[\text{Cu}(\text{C}_{17}\text{H}_{11}\text{N}_3\text{O})_2]^+$, $[\text{Cu}(\text{C}_{10}\text{H}_4\text{N}_3\text{OCl})_2]^+$, $(\text{C}_{25}\text{H}_{21}\text{N}_3\text{O})^+$, $[\text{Cu}(\text{C}_8\text{N}_6\text{O})]^+$, $[\text{Cu}(\text{C}_4\text{N}_3\text{O})]^+$
27	1022,951,862,791, 579,479,275,169	$[\text{Cu}(\text{C}_{24}\text{H}_{18}\text{N}_3\text{OClBr})_2]^+$, $[\text{Cu}(\text{C}_{24}\text{H}_{18}\text{N}_3\text{O})_2]^+$, $[\text{Cu}(\text{C}_{24}\text{H}_{18}\text{N}_3\text{OCl})_2]^+$, $[\text{Cu}(\text{C}_{24}\text{H}_{18}\text{N}_3\text{OBr})_2]^+$, $[\text{Cu}(\text{C}_{16}\text{H}_8\text{N}_3\text{O})_2]^+$, $(\text{C}_{24}\text{H}_{18}\text{N}_3\text{OClBr})^+$, $[\text{Cu}(\text{C}_8\text{N}_6\text{O})]^+$, $[\text{Cu}(\text{C}_4\text{N}_3\text{O})]^+$
28	852,762,640,488, 394,306,275,169	$[\text{Cu}(\text{C}_{26}\text{H}_{24}\text{N}_3\text{O})_2]^+$, $[\text{Cu}(\text{C}_{23}\text{H}_{15}\text{N}_3\text{O})_2]^+$, $[\text{Cu}(\text{C}_{18}\text{H}_{14}\text{N}_3\text{O})_2]^+$, $[\text{Cu}(\text{C}_{12}\text{H}_{10}\text{N}_3\text{O})_2]^+$, $[\text{Cu}(\text{C}_5\text{H}_3\text{N}_3\text{O})_2]^+$, $(\text{C}_{26}\text{H}_{24}\text{N}_3\text{O})^+$, $[\text{Cu}(\text{C}_8\text{N}_6\text{O})]^+$, $[\text{Cu}(\text{C}_4\text{N}_3\text{O})]^+$
29	982,822,742,488, 459,275,169	$[\text{Cu}(\text{C}_{25}\text{H}_{21}\text{N}_3\text{OBr})_2]^+$, $[\text{Cu}(\text{C}_{25}\text{H}_{21}\text{N}_3\text{O})_2]^+$, $[\text{Cu}(\text{C}_{12}\text{H}_{10}\text{N}_3\text{O})_2]^+$, $[\text{Cu}(\text{C}_{23}\text{H}_{15}\text{N}_3\text{O})_2]^+$, $(\text{C}_{25}\text{H}_{21}\text{N}_3\text{OBr})^+$, $[\text{Cu}(\text{C}_8\text{N}_6\text{O})]^+$, $[\text{Cu}(\text{C}_4\text{N}_3\text{O})]^+$
30	727,663,603,576, 424,333,244,95	$[\text{Ni}(\text{C}_{21}\text{H}_{23}\text{N}_3\text{O})_2]^+$, $[\text{Ni}(\text{C}_{19}\text{H}_{17}\text{N}_3\text{O})_2]^+$, $[\text{Ni}(\text{C}_{17}\text{H}_{12}\text{N}_3\text{O})_2]^+$, $[\text{Ni}(\text{C}_{16}\text{H}_9\text{N}_3\text{O})_2]^+$, $[\text{Ni}(\text{C}_{10}\text{H}_5\text{N}_3\text{O})_2]^+$, $(\text{C}_{21}\text{H}_{23}\text{N}_3\text{O})^+$, $(\text{C}_{14}\text{H}_{16}\text{N}_3\text{O})^+$, $(\text{C}_4\text{H}_4\text{N}_2\text{O})^+$

3.7.4. Electronic spectral studies

Electronic spectral data of the complexes with their tentative assignments are listed in Table 3.16. Electronic spectra serve as a tool to distinguish the geometry of the complexes. In order to shed some light on the geometrical structure of the complexes, the spectra of all the complexes were recorded in DMF in liquid phase at room temperature. The absorption spectra of all the Cu(II) complexes show two bands within the range 400-900 nm assignable to Jahn-Teller distortion. The band between 400-500 nm is due to the intraligand transition ($\pi \rightarrow \pi^*$ transition) and the other band around 715 nm is due to the $d-d$ transition in the metal complexes [65].

In an octahedral geometry, the ^2D state of the free Cu(II) ion (d^9) splits into a lower energy doublet $^2\text{E}_g$ state and a higher energy triplet $^2\text{T}_{2g}$ state, from which a $^2\text{T}_{2g} \rightarrow ^2\text{E}_g$ $d-d$ transition in the visible region is expected. However, a complex with the d^9 configuration of the metal ion is expected to experience Jahn-Teller distortion, which leads to further splitting of the $^2\text{E}_g$ and $^2\text{T}_{2g}$ levels into $^2\text{B}_{1g}$, $^2\text{A}_{1g}$ and $^2\text{B}_{2g}$, $^2\text{E}_g$

levels, respectively. With this splitting three possible transitions are ${}^2A_{1g} \rightarrow {}^2B_{1g}$ (ν_1), ${}^2B_{2g} \rightarrow {}^2B_{1g}$ (ν_2) and ${}^2E_g \rightarrow {}^2B_{1g}$ (ν_3). The energy difference between these levels depends on the extent of the Jahn–Teller distortion. If the energy difference is not large, then all these three transitions are expected to be close in energy and in this situation these bands may not resolve and may appear as a broad band. Therefore, the broad band in the region 700-720 nm could be due to the combination of these three transitions. The electronic spectrum of the complex **27** is shown in Fig. 3.28.

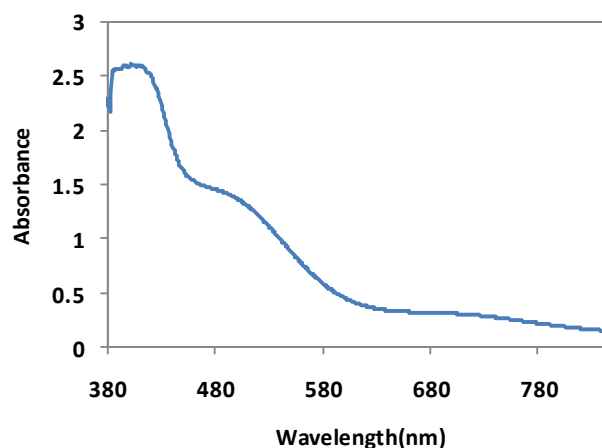


Fig. 3.28. The electronic spectrum of the complex **27**

Table 3.16. Electronic spectral data of the complexes

Complex	d-d transition	
	λ_{\max}/nm	ϵ
24	715	300
25	714	148
26	712	118
27	712	100
28	712	42
29	715	88
30	652	59
31	651	50

The diffuse reflectance spectra of the Ni(II) complexes studied in the present work are typical octahedral Ni(II) spectra consisting of bands within range 400-900nm assignable to ${}^3A_{2g}(F) \rightarrow {}^3T_{1g}(P)$ and ${}^3A_{2g}(F) \rightarrow {}^3T_{1g}(F)$. The electronic spectra of these compounds in DMF solutions were also recorded in the range 300-900 nm,

display absorption bands at ~440-460 assignable to ${}^3A_{2g}(F) \rightarrow {}^3T_{1g}(P)$. The electronic spectral studies in solid and solution state suggests octahedral geometry around Ni(II) ion in the studied complexes [66].

3.7.5. Thermal studies

The aim of thermal analysis is to open up new possibilities for the investigation of metal complexes and to obtain information concerning the thermal stability of the investigated complexes, to decide whether water molecules are inside or outside the coordination sphere. The thermoanalytical data of all the complexes are presented in Table 3.17.

3.7.5.1. Thermal studies of Cu(II) complexes

Thermal analyses of all the Cu(II) complexes were carried out by the TG, DTA and DSC techniques. The experimental results revealed that the degradation occurred in multiple stages, following a complex mechanism. For each stage the kinetic parameters and the thermo gravimetric characteristics have been estimated. Thermal behaviour of all complexes is explained as follows.

The TG curve follows the decrease in sample mass with increase in temperature. In the present investigation heating rates were suitably controlled at $10^\circ\text{C min}^{-1}$ and mass loss followed upto $30\text{-}800^\circ\text{C}$. The complexes slowly started decomposition between $150\text{-}280^\circ\text{C}$. The first mass loss upto 300°C is attributed to the removal of two coordinated water molecules. This process is accompanied by exothermic process at around $200\text{-}350^\circ\text{C}$ in DTA curves of all complexes. The mass loss occurring at temperature $350\text{-}600^\circ\text{C}$ corresponds to the pyrolysis of the one organic ligand molecule. The subsequent temperature range $600\text{-}800^\circ\text{C}$ the mass loss is due to the pyrolysis of another organic ligand molecule. The final product of the thermal decomposition CuO was determined by elemental analysis.

General scheme of degradation of Cu (II) complexes from TG



From the above results it is confirmed that Cu(II) complexes contain two coordinated water molecules. Also degradation of ligand molecules with two stage, respectively. The TG-DTA curve of the complex **24** is shown in Fig 3.29.

Thermal stability measured by TG order of stability is as follows.

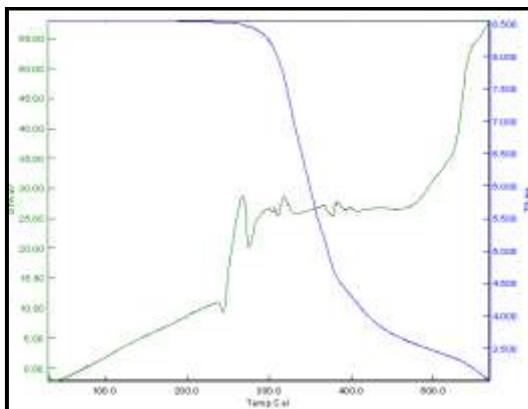


Fig. 3.29. TG-DTA curve of the complex **24**

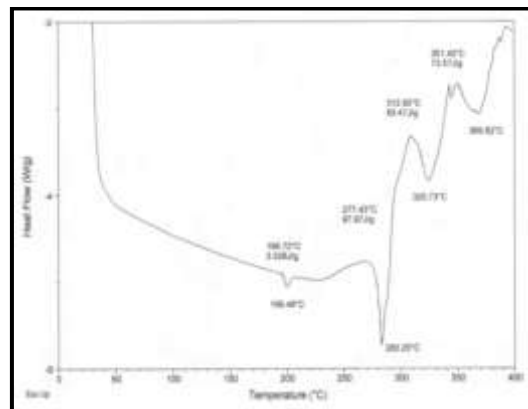


Fig. 3.30. DSC curve of the complex **25**

Differential scanning calorimetry (DSC) is the most widely used thermo analytical technique for studying and characterizing a wide variety of materials. Fig. 3.30 shows the DSC curve of one of the representative complexes. The area of the exothermic and endothermic peak corresponding to the heat of fusion and the peak temperature corresponds to the phase change. The melting (T_p), transition temperature (T_1 , T_2), heat of reaction (ΔH), and entropy (ΔS) of the complexes calculated from DSC results are given in Table 3.17.

Table 3.17. Thermoanalytical data of the complexes

Complex	TG range (°C)	DTA max(°C)	T_s (°C)	T_1 (°C)	T_2 (°C)	T_p (°C)	ΔE^* (kJ mol^{-1})	ΔH^* (kJ mol^{-1})	ΔS^* ($\text{JK}^{-1} \text{mol}^{-1}$)	Mass loss(%) obs.(calcd.)	Assignments
24	50-350	325	272	246	272	249	0.784	25.0	0.10	4.19 (4.18)	Loss of two coordinate water
	350-600	352	-	271	308	285	0.821	59.03	0.20	44.33 (44.33)	Loss of one TPMP-T
	600-800	-	-	-	-	-	-	-	-	8.81 (8.82)	Remaining CuO residue
25	50-350	335	158	196	205	199	0.879	3.52	0.01	3.62 (3.63)	Loss of two coordinated water
	350-600	351	-	277	312	283	0.807	97.97	0.34	45.09 (45.07)	Loss of one TPMP-BA
	600-800	-	-	-	-	-	-	-	-	7.66 (7.65)	Remaining CuO residue
26	50-350	332	279	167	255	222	0.908	145.1	0.65	3.87 (3.87)	Loss of two coordinated water
	350-600	389	-	293	321	293	0.938	150.0	0.51	44.67 (44.75)	Loss of one TMCMPMP-T
	600-800	-	-	-	-	-	-	-	-	8.16 (8.17)	Remaining CuO residue
27	50-350	321	157	150	177	164	0.926	28.73	0.17	3.41 (3.40)	Loss of two coordinated water
	350-600	360	-	287	317	306	0.896	98.06	0.31	45.30 (45.40)	Loss of one TMCMPMP-BA
	600-800	-	-	-	-	-	-	-	-	7.16 (7.17)	Remaining CuO residue
28	50-350	315	240	249	289	269	0.913	137.1	0.50	4.03 (4.05)	Loss of two coordinated water
	350-600	406	-	269	304	289	0.892	150.4	0.51	44.54 (44.51)	Loss of one TPTPMP-T
	600-800	-	-	-	-	-	-	-	-	8.53 (8.55)	Remaining CuO residue
29	50-350	304	-	-	-	-	-	-	-	3.59(3.53)	Loss of two coordinated water
	350-600	443	-	-	-	-	-	-	-	45.21(45.18)	Loss of one TPTPMP-BA
	600-800	-	-	-	-	-	-	-	-	-	Remaining CuO residue
30	50-200	160	-	-	-	-	-	-	-	6.1(6.2)	Loss of two coordinated water
	200-350	349	-	-	-	-	-	-	-	27.74(21.66)	Loss of 2CH ₂ , 6CH ₃
	350-600	537	-	-	-	-	-	-	-	20.98(20.62)	Loss of 2CO,2O
31	50-200	177	-	-	-	-	-	-	-	5.82(5.77)	Loss of two coordinated water
	200-350	374	-	-	-	-	-	-	-	23.52(27.05)	Loss of 2CH ₂ , 6CH ₃
	350-600	518	-	-	-	-	-	-	-	19.14(20.53)	Loss of 2CO,2O

3.7.5.2. Thermal studies of Ni(II) complexes

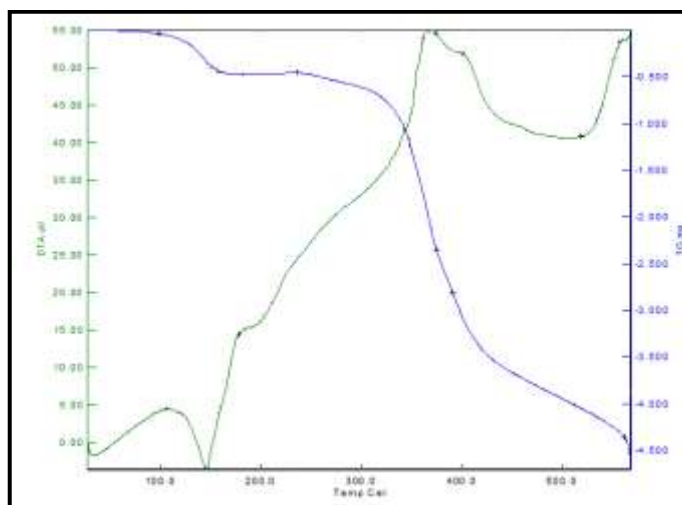


Fig. 3.31. TG-DTA curve of the complex **31**

The TG curve follows the decrease in sample mass with increase in temperature. In the present investigation, heating rates were suitably controlled at $10^{\circ}\text{Cmin}^{-1}$ and mass loss followed up to 100-550 $^{\circ}\text{C}$. From the TG curves (Fig. 3.31) obtained the mass loss for each complex was calculated within the temperature range at which water molecules were expelled [67]. Inspection of TG curve of Ni complex with the investigated ligand reveals an initial mass loss occurring at temperature more than 150 $^{\circ}\text{C}$ and this is attributed to loss of water of coordination. For complex **30**, a mass loss occurred within the temperature range 161-172 $^{\circ}\text{C}$ corresponding to the loss of 6.1% (calctd. 6.2%) for two water molecules. For complex **31**, a mass loss occurred within the temperature range 170-180 $^{\circ}\text{C}$ corresponding to the loss of 5.82% (calctd. 5.77%) for two water molecules. Thus, from the above data it can be said that there are two coordinated water molecules in both complexes.

3.7.6. Magnetic measurement studies

The magnetic data provide great deal of information complementary to that available from the electronic spectra. An unpaired electron in a compound has both spin angular momentum and orbital angular momentum. These reinforce with the applied field to get the resultant magnetic susceptibility of the sample. It is necessary

to subtract diamagnetic contribution to get the pure paramagnetic susceptibility. Deviation occurs due to the quenching of orbital angular momentum, spin-orbit coupling, TIP etc.

3.7.6.1. Magnetic measurement studies of Cu(II) complexes

The magnetic moment values of the complexes are measured at room temperature (at $28 \pm 2^\circ\text{C}$) and the values are presented in Table 3.13. The maximum spin-only magnetic moment for a mononuclear system is given by $\mu_{\text{eff}}^2 = n(n+2)$, where n is the number of unpaired electrons in the complex. Hence for Cu(II), $n = 1$ per copper atom, thus for a one copper system $\mu_{\text{eff}}^2 = 1(1+2) = 3$. μ_{eff} per Cu atom is equal to 3 and hence magnetic moment was expected to be 1.73 B.M. In view of this, the magnetic moment values of the complexes in the range of 1.76-1.81 B.M. suggest that these complexes contain one copper atom. The magnetic moment values of the copper complexes correspond to the spin only value of 1.73 B.M. for the high spin octahedral complex [68].

The values are found to be very close to the spin only value, which indicate the presence of one unpaired electron. All the complexes are ESR active due to the presence of unpaired electron.

3.7.6.1. Magnetic measurement studies of Ni(II) complexes

The spin only magnetic moment value calculated for nickel complex is 2.94 BM. Ni(II) having a coordination number of six in accordance with the data. Usually due to inherent orbital angular moment, regular tetrahedral complex should have high magnetic moment than spin only value. But for distorted complexes, the moments are in same range as in the six-coordinated complexes.

Nickel(II) should exhibit a magnetic moment higher than expected for two unpaired electrons in octahedral, 2.8-3.2 B.M., This increase in magnetic moment value from that of the spin-only value is due to some "mixing in" of upper states via spin-orbit coupling. The paramagnetism observed for the present complexes ranges from 3.0-3.6 consistent with octahedral stereochemistry (Table 3.13) [69].

3.7.7. ESR studies

As we could not get well-shaped single crystals, the ESR spectra were recorded only for powder and solution samples for the complex **24** at RT and LNT. The powder sample was recorded in quartz tube to avoid Mn(II) or Fe(II) impurities and solution spectra was recorded in DMF solution in capillary tube. The solution spectrum was recorded to confirm that the complex does not undergo structural change in solution.

The powder as well as the solution ESR spectra of the complex **24** was studied. The solution and powder ESR spectra of the complex are shown in Figs. 3.32 & 3.33. Hamiltonian parameters g_{\parallel} , g_{\perp} , A_{\parallel} , A_{\perp} and A_{iso} were also calculated. Complex **24** shows the $g_{\parallel} = 2.18$ and $g_{\perp} = 2.11$, for Cu(II) g_{\parallel} indicates covalence with $g_{\parallel} < 2.3$ for covalent complexes and $g_{\parallel} \geq 2.3$ for ionic [70] g_{\parallel} value of the complex of 2.18 indicates covalency for M-L bond. The nature of ligand is evaluated from G value,

For $G < 4.0$, the ligand forming the complex is regarded as a strong field ligand. For complex **24**, $G = 3.5$ it indicates octahedral stereochemistry of complex [71].

The RT solution ESR consists of four asymmetrical but equally spaced hyperfine lines characteristic of the Cu(II) nuclear hyperfine interaction ($Cu=I=3/2$ for ^{63}Cu and ^{65}Cu). From these solution ESR spectra, we have calculated values of $g_{\parallel} = 2.18$, $g_{\perp} = 2.11$, $A_{\parallel} = 205.33 \times 10^{-4}$, $A_{\perp} = 185.26 \times 10^{-4}$. The ratio of $g_{\parallel}/A_{\parallel}$ is used to find the structure of a complex. In present Cu(II) complexes, the ratio obtained is in the range $g_{\parallel}/A_{\parallel} = 104.70 \text{ cm}^{-1}$, which is due octahedral Cu(II) complexes [70, 71].

The frozen solution spectrum of the complex is axial with $g_{\parallel} > g_{\perp} > 2.0$, suggesting the presence of a $d_{x^2-y^2}$ ground state [70].

Molecular orbital co-efficient, α^2 (covalent in-plane σ -bonding) and β^2 (covalent in-plane π -bonding) were calculated by using the following equations [70]. The $\alpha^2 = 0.80$ its state that Cu(II) complex have covalent bonding and $\beta^2 = 0.67$ suggest that in plane π -bonding is also present in complex.

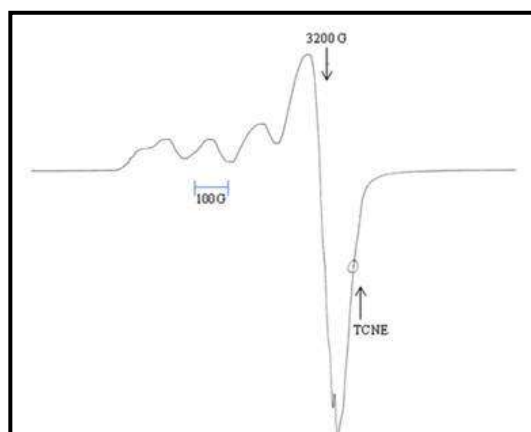


Fig. 3.32. The solution ESR spectrum of **24**

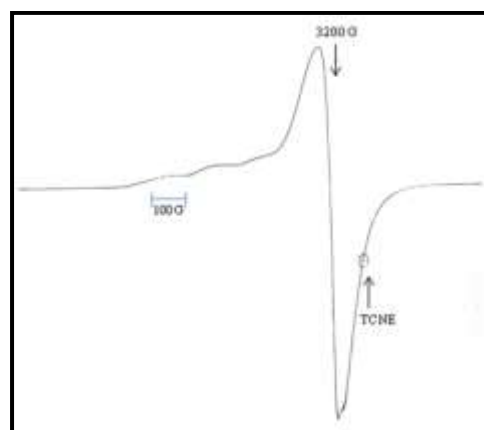
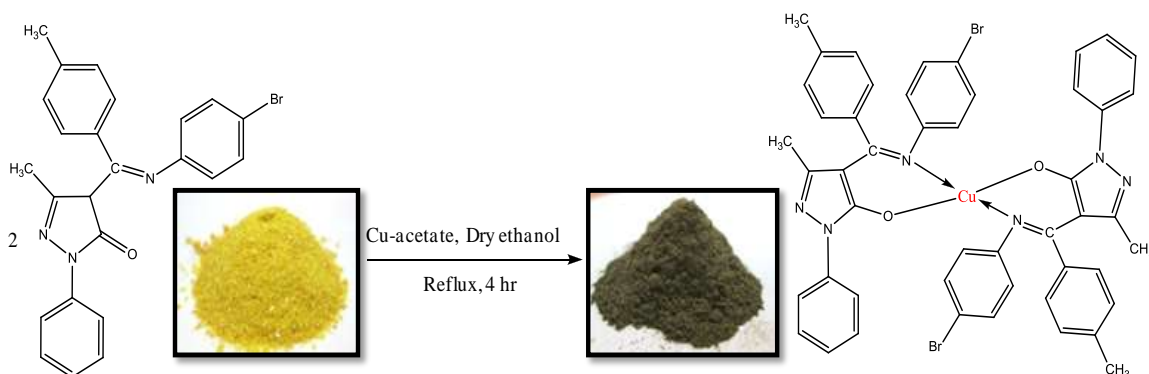


Fig. 3.33. The powder ESR spectrum of **24**

3.8. Modified synthesis in comparison with previous synthesis of Cu(II) complex [Cu(TPMP-BA)₂] (32):

As described in the synthesis of metal complexes, single crystals were grown in different solvents like Acetonitrile, DMF and DMSO. But attempts proved futile. Therefore, in order to get the single crystal, we have modified our synthesis procedure.

Known amount of TPMP-BA (0.446 gms, 1 mmol) was dissolved in hot dry ethanol. Equimolar amount of Cu(OAc)₂·H₂O (0.199 gms, 1 mmol) was dissolved in dry ethanol and then added to the dissolved ligand. After the complete addition, the reaction mixture was refluxed for 4 hours. A dark greenish microcrystalline solid was separated, which was isolated by filtration, washed with hot water and finally with ethanol and dried under *a vacuum*. The solid product was dissolved in hot MeCN and allowed to crystallize at room temperature. Green crystals of single-crystal XRD quality were obtained in 2-4 days. The obtained material was designated as [Cu(TPMP-BA)₂].



Scheme 3.20. Synthesis of $[\text{Cu}(\text{TPMP-BA})_2]$

3.8.1. Molecular structure of complex 32

The molecular structure of the complex was determined from single crystal X-ray studies. ORTEP diagram of this complex with the atom numbering scheme is shown in Fig. 3.34. Crystallographic data of the complex are listed in Table 10. Important bond lengths and angles for the complex listed in Table 3.18. The packing arrangement of one of the complex molecules viewed down the a-axis is shown in Fig. 3.35.

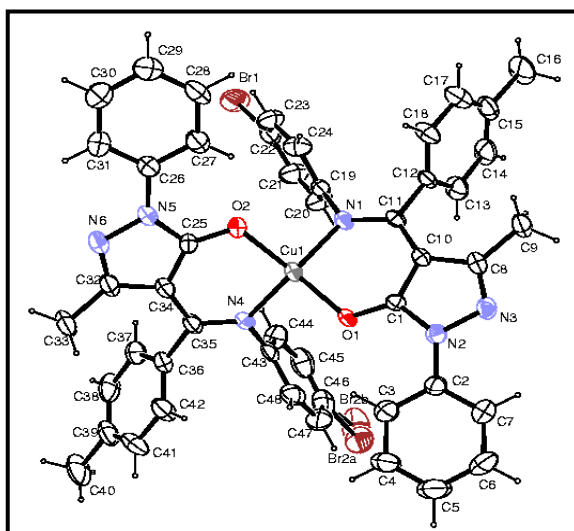


Fig. 3.34. Molecular structure of **32**, showing the atom labelling scheme. Displacement ellipsoids are drawn at the 50% probability level and H atoms are shown as small spheres of arbitrary radii

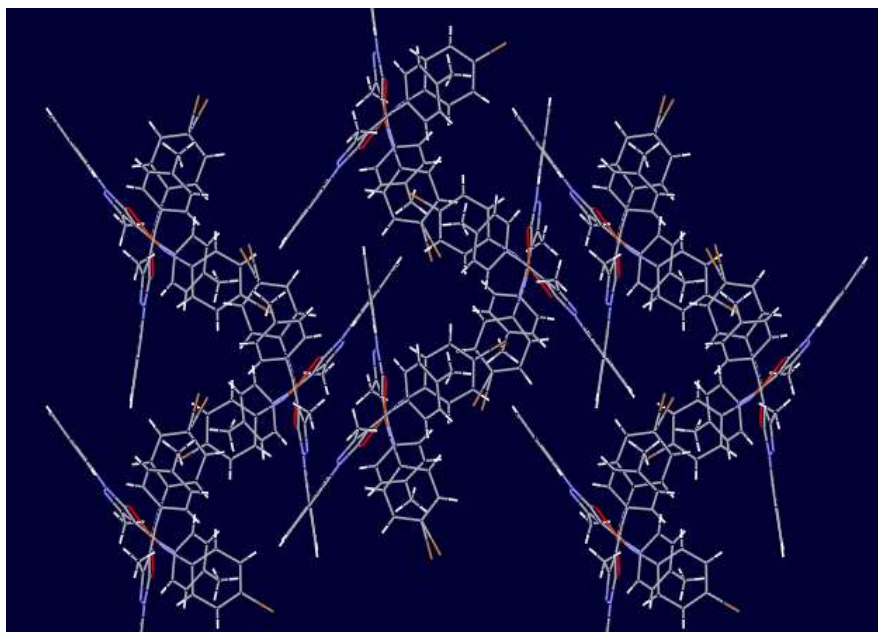


Fig. 3.35. The packing arrangement of **32** molecules viewed down the *a*-axis.

Table 3.18. Selected bond lengths and angles in the complex **32**

Bond distances (Å) with esd's in parentheses		Bond angles(Å) with esd's in parentheses	
C1 O1	1.286(6)	O1 C1 N2	121.4(5)
C1 N2	1.385(6)	O1 C1 C10	132.9(5)
C2 N2	1.406(7)	N2 C1 C10	105.7(5)
C8 N3	1.300(7)	C7 C2 N2	121.2(6)
C11 N1	1.320(6)	C3 C2 N2	121.0(6)
C19 N1	1.432(6)	N1 C11 C10	119.8(5)
C22 Br1	1.881(6)	N1 C11 C12	119.5(5)
C25 O2	1.287(6)	O2 C25 N5	122.0(6)
C25 N5	1.373(7)	O2 C25 C34	131.5(6)
C26 N5	1.422(8)	N4 C35 C34	119.8(6)
C32 N6	1.297(8)	N4 C35 C36	119.9(6)
C35 N4	1.326(6)	C11 N1 C19	120.7(4)
C43 N4	1.447(8)	C11 N1 Cu1	127.6(4)
C46 Br2A	1.895(12)	C19 N1 Cu1	110.4(3)
C46 Br2B	1.898(14)	C1 O1 Cu 1	119.2(3)
N1 Cu1	1.955(4)	C25 O2 Cu1	119.8(4)
N2 N3	1.410(6)	O1 Cu1 O2	147.74(16)
N4 Cu1	1.948(5)	O1 Cu1 N4	94.53(18)
N5 N6	1.391(6)	O2 Cu1 N4	94.07(19)
O1 Cu1	1.907(4)	O1 Cu1 N1	94.93(17)
O2 Cu1	1.917(4)	O2 Cu1 N1	93.89(19)
C2 C7	1.363(8)	N4 Cu1 N1	148.28(19)

In the complex, the four-coordinate copper atom is arranged in a distorted square-planar geometry where the two ligands acting as monoanionic bidentate N,O-chelators lie in the trans-conformation to create two stable delocalized six-membered chelate rings (Cu-O-C-C-C-N), with O–Cu–O and N–Cu–N angles 147.74(16) Å and 148.28(19) Å, respectively [72].

X-ray data indicates that the oxygen atom of both pyrazolone rings is oriented toward the metal center (Cu). However, the interatomic distances C=O1-----Cu and C=O2-----Cu of 1.907(4) Å and 1.917(4) Å, respectively [73], are little large to be considered a coordination bond (Fig. 34). Furthermore, the tetrahedral geometry is highly distorted, as evidenced by the 41 Å dihedral angle between the planes formed by the Cu(1)O(1)N(1) and Cu(1)O(2)N(4) planes, being more precisely an intermediate structure between a tetrahedral and a square planar arrangements. The magnetochemical data (Table 3.13) is in agreement with a system and is supports the idea of a mononuclear structure for complex.

Conclusions

A new set of eight bidentate heterocyclic Schiff base ligands, formed by the condensation of three different 4-toluoyl pyrazolones with various aromatic amines in ethanolic medium have been synthesized. All of these ligands have been characterized on the basis of elemental analysis, IR, NMR, and Mass spectral data. The molecular geometries of four of these ligands have been determined by single crystal X-ray study. It reveals that these ligands exist in amine-one tautomeric form in the solid state. The reaction of these ligands with Cu(II) and Ni(II) resulted in the formation of mononuclear complexes having the general composition $[ML_2(H_2O)_2]$ with two water molecules at axial positions. These complexes have been characterized on the basis of elemental analyses, Cu/Ni-estimation, molar conductivity, magnetic measurements, IR, UV-Visible, FAB-Mass, TG-DTA-DSC data and ESR spectral studies. ESR spectra and magnetic susceptibility measurements indicates distorted octahedral stereochemistry of metal(II) complexes, while non-electrolytic behaviour of complexes indicates the absence of counter ion. Attempts have been made to get the single crystal of this system, but it proved futile. Therefore, in order to get the single crystal, we have modified our synthesis procedure. After modification in procedure, we got the single crystal suitable for X-ray crystallography. The molecular geometry of this complex showed that the ligands are acting as bidentate O, N donor ligands and two ligands are coordinated per one M(II) atom.

Literature cited.

- [1] H. Schiff, *Ann. Chem. Pharm. Suppl.* (1864) 241.
- [2] A. Rauf, Bahauddin Zakariya University, 2005 “*Synthesis and biological studies of some Schiff base compounds and their transition metal complexes*”
- [3] J. S. Casas, M. S. Garcia-Tasende, A. Sanchez, J. Sordo, A. Touceda, *Coord. Chem. Reviews*, 251 (2007) 1561.
- [4] T. G. Takhirov, O. A. Diyachenko, D. B. Tagiev, A. L. Nivorozhkin, M. S. Korobov, R. Olekhovich, L. E. Nivorozhkin, V. I. Minkin, *Koord. Khim.*, 17 (1991) 711.
- [5] R. C. Maurya, D. D. Mishra, N. S. Rao, N. N. Rao, *Polyhedron*, 11 (1992) 2837.
- [6] F. Marchetti, C. Pettinari, A. Cingolani, D. Leonesi, *Polvhedron*, 15 (1996) 3835.
- [7] V. I. Sokol, V. V. Davydov, N. Y. Merkureva, O. A. Al-Saleh, M. A. Ryabov, V. S. Sergienko, Y. V. ShklyaeV, *Russ. J. Inorg. Chem.*, 47 (2002) 353.
- [8] J. -L. Wang, F. Ding, F. -M. Miao, *Acta Crystallogr. E*, 59 (2003) m128.
- [9] X. Q. Lue, F. Bao, Q. Wu, B. -S. Kang, S. W. Ng, *Acta Crystallogr. E*, 60 (2004) m362.
- [10] S. Parsons, L. Emeleus. P. Tasker, P. Wood, *Private Communication to CSD*, 2004.
- [11] A. -X. Li, Y. Yang, J. -L. Wang, *Yingyong Huaxue*, 21 (2004) 49.
- [12] S. -M. Zhang, P. -F. Li, M. Yu, J. -L. Wang, *Wuji Huaxue Xuebao*, 20 (2004) 439.
- [13] J. -L. Wang, A. -X. Li, Y. -J. Jia, S. -M. Zhang, *Huaxue Xuebao*, 62 (2004) 2329.
- [14] R. N. Jadeja , J. R. Shah, E. Suresh, P. Paul, *Polyhedron*, 23 (2004) 2465.
- [15] F. Bao, X. -Q. Lu, H. Gao, G. Gui, Q. Wu, *J. Polym. Sci., Part A: Polym. Chem.*, 43 (2005) 5535.
- [16] F. Bao, X. Lu, Y. Qiao, G. Gui, H. Gao, Q. Wu, *Appl. Organometal. Chem.*, 19 (2005) 957.
- [17] F. R. Perez, J. Belmar, C. Jimenez, Y. Moreno, P. Hermosilla, R. Baggio, *Acta Crystallogr. C*, 61 (2005) m318.
- [18] P. Tasker, A. Smith, S. Parsons, D. Messenger, *Private Communication to CSD*, 2005.

- [19] R. N. Jadeja, R. N. Shirsat, E. Suresh, *Struct. Chem.*, 16 (2005) 515.
- [20] F. Bao, J. Feng, S. W. Ng, *Acta Crystallogr. E*, 61 (2005) m2393.
- [21] P. Tasker, A. Parkin, A. Smith, S. Parsons, D. Messenger, *Private Communication to CSD*, 2005.
- [22] X. -Q. Lu, F. Bao, B. -Sh. Kang, Q. Wu, H. -Q. Liu, F. -M. Zhu, *J. Organomet. Chem.* 691 (2006) 821.
- [23] F. Bao, R. Ma, X. Lu, G. Gui, Q. Wu, *Appl. Organometal. Chem.* 20 (2006) 32.
- [24] R. N. Jadeja, J. R. Shah, *Polyhedron* 26 (2007) 1677.
- [25] B. T. Thaker, K. R. Surati, S. Oswal, R. N. Jadeja, V. K. Gupta, *Struct. Chem.*, 18 (2007) 295.
- [26] B. T. Thaker, R. S. Barvalia, *Spectrochim. Acta Part A*, 74 (2009) 1016.
- [27] R. C. Maurya, B. Shukla, J. Chourasia, S. Roy, P. Bohre, S. Sahu, M. H. Martin, *Arabian Journal of Chemistry*, (2011) (In press).
- [28] L. Liu, D. Jia, Y. Qiao, Y. Ji, K. Yu, *J. Chem. Crystallography*, 32 (2002) 255.
- [29] L. Zhang, L. Liu, D. Jia, G. Xu, K. Yu, *Inorg. Chem. Commun.*, 7 (2004) 1306.
- [30] L. Zhang, L. Liu, G. -F. Liu, D. -Z. Jia, K. -B. Yu, *Wuji Huaxue Xuebao*, 21 (2005) 291.
- [31] J. Li, L. Zhang, L. Liu, G. Liu, J. Guo, D. Jia, *Inorg. Chim. Acta*, 360 (2007) 3504.
- [32] L. Liu, Y. Li, D. Jia, G. Liu, K. Yu, *J. Inorg. Organomet. Poly. Mat.*, 17 (2007) 535.
- [33] J. Li, L. Zhang, L. Liu, G. Liu, D. Jia, G. Xu, *Inorg. Chim. Acta*, 360 (2007) 1995.
- [34] J. Lu, L. Zhang, L. Liu, G. Liu, D. Jia, D. Wu, G. Xu, *Spectrochim. Acta Part A*, 71 (2008) 1036.
- [35] S. Sawusch, N. Jager, U. Schilde, E. Uhlemann, *Struct. Chem.* 10 (1999) 105.
- [36] Z. -Y. Yang, R. -D. Yang, F. -S. Li, K. -B. Yu, *Polyhedron*, 19 (2000) 2599.
- [37] Y. -L. Ji, L. Liu, D. -Z. Jia, K. -B. Yu, *Wuji Huaxue Xuebao*, 19 (2003) 345.
- [38] L. Zhang, L. Liu, D. Jia, K. Yu, *Struct. Chem.*, 15 (2004) 327.
- [39] L. Zhang, L. Liu, G. -F. Liu, G. -C. Xu, D. -Z. Jia, J. -P. Lang, *J. Chem. Crystallogr.* 35 (2005) 583.

- [40] X. Hu, L. Zhang, L. Liu, G. Liu, D. Jia, G. Xu, *Inorg. Chim. Acta*, 359 (2006) 633.
- [41] F. R. Perez, J. Belmar, Y. Moreno, R. Baggio, O. Pena, *New J. Chem.*, 29 (2005) 283.
- [42] B. Adhikhari, O. P. Anderson, A. Cour, R. Hazell, S. M. Miller, C. E. Olsen, H. Toftlund, *J. Chem. Soc., Dalton Trans.*, (1997) 4539.
- [43] A. Cour, M. Findeisen, R. Hazell, L. Henning, C. E. Olsen, O. Simonsen, *J. Chem. Soc., Dalton Trans.*, (1996) 3437.
- [44] N. S. Rao, M. N. Jaiswal, D. D. Mishra, R. C. Maurya, N. N. Rao, *Polyhedron*, 12(1993) 2042.
- [45] M. Ying, R. Yuan, Z. -Q. Li, Y. -Q. Song, W. -X. Li, H. -G. Lin, G. -L. Shen, R. -Q. Yu, *Fresenius J. Anal. Chem.*, 361 (1998) 437.
- [46] R. N. Jadeja, N. J. Parmar, *Synth. React. Inorg. Met.-Org. Chem.*, 35 (2005) 111.
- [47] Y. Wang, Z. -Y. Yang, *J. Lumi.* 128 (2008) 373.
- [48] K. R. Surat, B. T. Thaker, G. R. Shah, *Synth. React. Inorg. Met.-Org. Chem.*, 38 (2008) 272.
- [49] H. Nazir, M. Yildiz, H. Yildiz, M. N. Tahir, D. Viku, *J. Mol. Struct.*, 524 (2000) 241.
- [50] S. R. Salman, J. C. Lindon, R. D. Farrant, T. A. Carpenter, *Magn. Reson. Chem.*, 31 (1993) 991.
- [51] G. O. Dodek, E. P. Dudelk, *J. Am. Chem. Soc.*, 88 (1966) 2407.
- [52] C. Ettling, *Ann. Chem. Pharm.*, 35 (1840) 241.
- [53] F. Basalo, R. C. Johnson, "Coordination Chemistry: The Chemistry of Metal Complexes". W. A. Benjamin, inc., P. 8 (1964).
- [54] W. L. F. Armarego, D. D. Perrin, *Purification of Laboratory Chemicals*, 4th edn., The Bath Press, Butterworth-Heinemann Publication, (1997).
- [55] A. R. Kartizky, R. A. Jones, *J. Chem. Soc.*, (1960) 2942.
- [56] G. -C. Xu, L. Zhang, L. Liu, G. -F. Liu, D. -Z. Jia, *Polyhedron*, 27 (2008) 12.
- [57] L. C. Emeleus, R. M. Swart, D. C. Cupertino, P. A. Tasker, S. G. Harris, D. J. White, *J. Chem. Soc., Dalton Trans.*, (2001) 1239.
- [58] W. Kemp, *NMR in chemistry, a multinuclear introduction*, (1986).

- [59] D. H. Williams, I. Fleming, *Spectroscopic methods in organic chemistry*, 4th ed. (1988).
- [60] R. J. Yadav, K. M. Vyas, R. N. Jadeja, *J. Coord. Chem.*, 63 (2010) 1820.
- [61] A. S. Amarasekara, O. S. Owereh, K. A. Lyssenko, T. V. Timofeeva, *Struct. Chem.*, 50 (2009) 1159.
- [62] W. J. Geary, *Coord. Chem. Rev.*, 7 (1971) 81.
- [63] (a) H. Temel, U. Cakir, B. Otludil, H. I. Ugras, *Synth. React. Inorg. Met.-Org. Chem.*, 31 (2001) 1323; (b) H. M. Parekh, P. K. Panchal, M. N. Patel, *J. Therm. Anal. Cal.* 86 (2006) 803; (c) M. S. Masoud, M. F. Amira, A. M. Ramadan, G. M. El-Ashry, *Spectrochim. Acta, Part A* 69 (2008) 230.
- [64] K. Nakamono, *Infrared and Raman Spectra of Inorganic and Coordination Compounds*, Wiley, New York, (1976).
- [65] A. B. P. Lever, *Inorganic Electronic Spectroscopy*, Elsevier, Amsterdam, (1984) pp. 355.
- [66] F. Yilmaz, V. T. Yilmaz, S. Topcu, *J. Coord. Chem.*, 57 (2004) 525.
- [67] S. A. Abdel-Latif, H. B. Hassib, *J. Therm. Anal. Calorimet.*, 68 (2002) 983.
- [68] F.A. Cotton, G. Wilkinson, *Advanced Inorganic Chemistry* 5th edi., John Wiley and Sons: Canada, (1989) pp. 625.
- [69] K. S. Bharathi, S. Sreedaran, R. A. Ayswarya, A. K. Rahiman, K. Rajesh, V. Narayanan, *J. Coord. Chem.*, 62 (2009) 600.
- [70] A. Syamal, R. L. Dutta, *Elementals of Magneto Chemistry*, East-West Press Pvt. Ltd., New Delhi, (1993).
- [71] A. W. Addison, *In Copper Coordination Chemistry: Biochemical and Inorganic Perspectives*, K.D. Karlin, J. Zubieta (Eds), Adenine, Guilderland, New York, (1983) pp. 109.
- [72] J. L. Wang, S. M. Zhang, A.X. Li, *Pol. J. Chem.*, 77 (2003) 1053
- [73] A.D. Garnovskii, A. S. Antsyshkina, E. L. Anpilova, O. Y. Korshunov, A. V. Bicherov, A. S. Burlov, G. G. Sadikov, V. S. Sergienko, I. E. Uflyand, *Zhurn. Neorg. Khim.*, 48 (2003) 1992.

CHAPTER

4



DNA binding, DNA cleavage, Protein binding and Anti cancer activities of many of the synthesized metal complexes

4.1. Introduction

Cancer is one of the most leading causes of death in developed countries, responsible for about 25% of all deaths. Cancer is a disease that has a high mortality rate worldwide [1]. On a yearly basis, 0.5% of the population is diagnosed with cancer. Several approaches are employed to treat cancer, such as surgery, radiotherapy and systemic therapies like chemotherapy, endocrine therapy and targeted agents or combination of these therapies. These targeted anti cancer therapies include monoclonal antibodies and small molecules, for example tyrosine kinase inhibitors. Conventional chemotherapeutic agents act by creating toxic effects on all dividing cells. This frequently results in severe damage of normal tissues leading to side effects like myelosuppression, alopecia, and gastrointestinal problems. The optimum goal is to find a treatment modality that specifically kills malignant cells and causes little or no side effects. The choice of the appropriate treatment depends on the nature of the tumor, the stage of the disease and the general state of the patient. The curing rate of chemotherapy has improved over the last decades, since new anti-cancer agents have been discovered, and significant advances in the different treatment protocols have been achieved [2]. Nowadays, cancer is almost always treated by a combination of several drugs (and/or applying different types of therapy).

Why to study only Lung cancer??????????

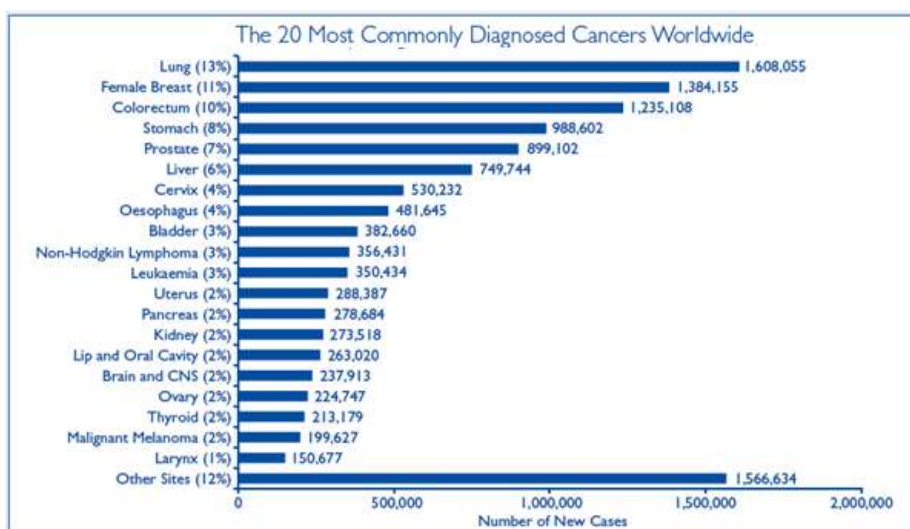


Fig. 4.1. The 20 most commonly diagnosed cancers worldwide

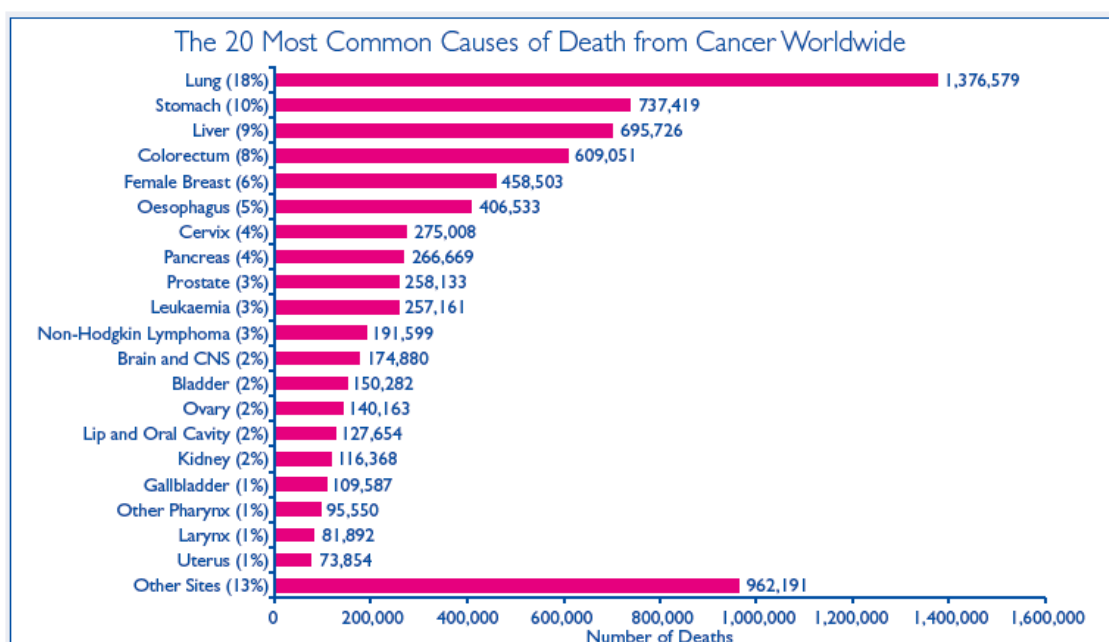


Fig. 4.2. The 20 most common causes of death from cancer worldwide

These reports (Figs. 4.1 & 4.2) describe the number of new cases and number of deaths due to cancer worldwide. The data are derived from the International Agency for Research on Cancer GLOBOCAN 2008 database (version 1.2), the World Health Organisation (WHO) Global Health Observatory and the United Nations World Population Prospects report [3-6].

China and India are by far the most populated countries in the world, accounting for 20% and 18% of the world's total population in 2008, respectively [4]. Between 2003 and 2008, approximately a one third (32%) of the world's population growth of around 400 million people occurred in India and China. India is expected to overtake China to become the world's most populated country by 2030. The UK accounted for less than 1% of the world's total population in 2008 [6].

The world population is ageing [6]. Between 1970 and 2010, the world median age increased from 22 years to 29 years, and it is projected to reach 38 years by 2050. The number of people in the world aged 60 and over is expected to almost triple to 2 billion by 2050 [6]. Since cancer is predominantly a disease of the elderly,

increases in the number of older people will inevitably lead to more cases of cancer, even if current incidence rates remain the same.

Lung cancer has been estimated as the most common cancer in the world for several decades (Figs. 4.1 & 4.2) [4, 7-11]. An estimated 1.61 million people across the world were diagnosed with lung cancer in 2008, accounting for 13% of the total [4]. More than half (55%) of the cases occurred in the developing world [4].

The link between tobacco and lung cancer was established more than fifty years ago [10] and incidence rates closely reflect past smoking prevalence with a time lag of approximately 20-30 years [4, 13, 14]. Manufactured cigarettes were first introduced at the end of the nineteenth century and since then the global consumption of tobacco has been rising steadily [14, 15]. There is estimated to be more than one billion smokers in the world, which is about a quarter of all adults. Smoking prevalence is higher in men than in women in most countries worldwide; the overall world estimates for 2006 were 41% of men and 9% of women smoking, though this varied considerably by country and age. In many developing countries the consumption of cigarettes is increasing rapidly in both sexes, due to both population growth and the increased targeting of tobacco marketing in these areas (especially to young people). Throughout most of Europe, smoking prevalence has now peaked among men but is increasing in women (particularly in the younger age groups, where teenage girls can be as likely to smoke as teenage boys). Worldwide, the number of smokers is continuing to rise, and without intervention this will lead to large increases in the incidence of lung cancer in the coming decades [14, 15].

Why to study the interaction with DNA first??????

DNA is a primary target for the discovery of anti-cancer drugs. Transcription and replication are vital to cell survival and proliferation as well as for smooth functioning of all body processes. DNA starts transcribing or replicating only when it receives a signal, which is often in the form of a regulatory protein binding to a particular region of the DNA. Thus, if the binding specificity and strength of this regulatory protein can be mimicked by a small molecule, then DNA function can be

artificially modulated, inhibited or activated by binding this molecule instead of the protein. Thus, this synthetic/natural small molecule can act as a drug when activation or inhibition of DNA function is required to cure or control a disease. DNA is the nucleic acid which contains the genetic 'blueprint' of all cellular life forms and of many viruses. It is responsible for two major roles: conducting its own replication during cell division and directing the transcription of complementary molecules of RNA.

DNA activation would produce more quantities of the required protein, or could induce DNA replication; depending on which site the drug is targeted. DNA inhibition would restrict protein synthesis or replication and could induce cell death. Though both these actions are possible, mostly DNA is targeted in an inhibitory mode, to destroy cells for antitumor and antibiotic action.

4.1.1. A structural introduction to DNA

Before embarking on our discussion of the binding and recognition of DNA, a brief description of the structure of DNA may be helpful.

DNA is a polymer of individual deoxyribonucleotides, each of which is composed of a heterocyclic base, a ribose sugar and a phosphate (Fig. 4.3). The most common form of DNA (and the form addressed almost exclusively in these pages) is the double-stranded, anti-parallel, right-handed double helix termed B-DNA [16, 17]. Within the polynucleotide assembly, the heterocyclic bases – adenine (A), guanine (G), cytosine (C), and thymine (T) – are bound to the sugars in an *anti* orientation with a disposition perpendicular to the helical axis. The base pairs collectively form a central π -stack that runs parallel to the helical axis between the two strands of the sugar-phosphate backbone. Each base forms hydrogen bonds with its complement on the opposite, anti-parallel strand, adenine with thymine and cytosine with guanine. The rise per base is 3.4 Å and there are ten base pairs per helical turn. Surrounding the central base stack, the polyanionic sugarphosphate backbone forms two distinct grooves, a wide major groove and a narrow minor groove (Fig. 4.3). All of these structural characteristics can and have been exploited for molecular recognition.

DNA, deoxyribonucleic acid, is the hereditary material in humans and almost all other organisms. In a person's body each cell has the same DNA. Most of the DNA molecules located in the cell nucleus are called DNA but a small amount of DNA can be found in the mitochondria as mtDNA. The information in DNA is stored as a code made up of four chemical bases: adenine (A), guanine (G), cytosine (C), and thymine (T). Human DNA consists of about 3 billion bases. More than 99 percent of these bases are the same in all people. The most widely accepted model for the structure of DNA molecule was proposed by Watson and Crick in 1953 for which he was awarded Nobel Prize for Medicine in 1962. According to him the DNA molecule is a double helix (Fig. 4.3). The molecule is formed by two antiparallel polynucleotide strands which are spirally coiled round each other in a right handed helix. The two strands are held together by hydrogen bonds. The double stranded helical molecule has alternated major and minor grooves. Each strand is a long polynucleotide of deoxyrebonucleotides. Two strands are complementary to each other with regards to the arrangement of the bases in the two strands. Thus, in a double helix, purines and pyrimidines exist in base pairs, i.e., (A and T) and (G and C). As a result, if the base sequence of one strand of DNA is known, the base sequence of its complementary strand can be easily deduced. The backbone of the strand is formed by alternately arranged deoxyribose sugar and phosphate molecules which are joined by the phosphodiester linkages.

The DNA molecule that Waton and Crick described was in B-form. However DNA can exist in other forms also. A and B forms have right handed helix, while Z form has left handed helix. B is the major form that is found in the cell.

The following Table 4.1 summarises the different forms of DNA and Fig. 4.4 shows the different forms of DNA.

Table 4.1. Some features of DNA forms

Geometry attribute	A-form	B-form	C-form
Helix sence	Right handed	Right handed	Left handed
Repeating unit	1 bp	1 bp	2 bp
Bp/turn	11	10.5	12
Pitch/turn of helix	28.2 Å (2.82 nm)	33.2 Å (3.32 nm)	45.6 Å (4.56 nm)
Diameter	23 Å (2.3 nm)	20 Å (2.0 nm)	18 Å (1.8 nm)

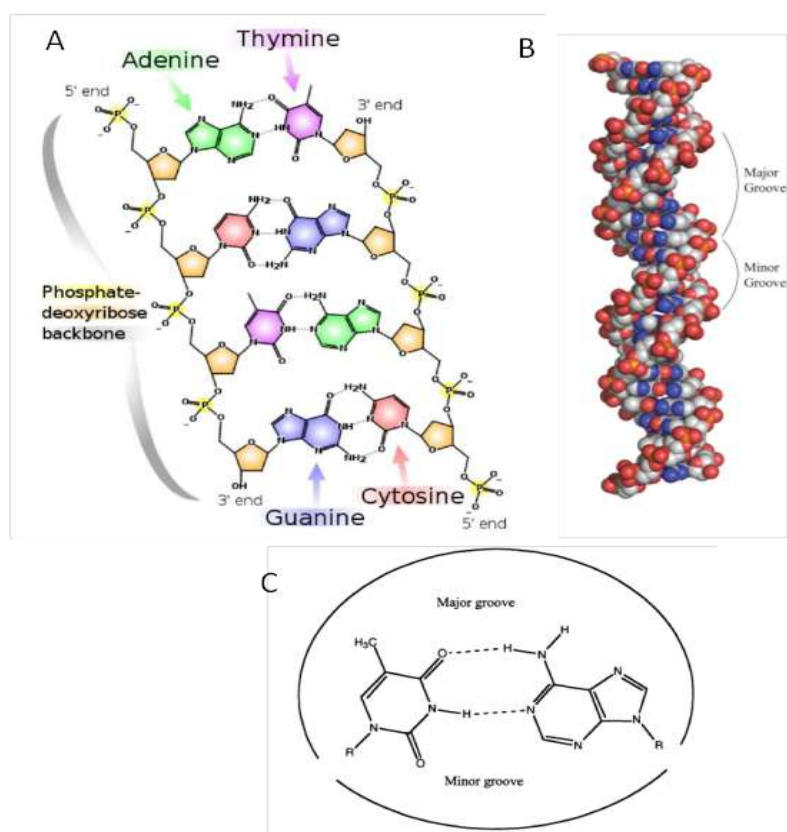


Fig. 4.3. Deoxyribonucleic Acid. (A) Structures of the 4 natural DNA bases attached to the sugar phosphate backbone. (B) The Watson-Crick base pairs with major and minor grooves illustrated. (C) Model of double-stranded, B-form DNA. The major and minor grooves are indicated. Carbon, oxygen, nitrogen, and phosphorus atoms are grey, red, blue, and orange, respectively [17]

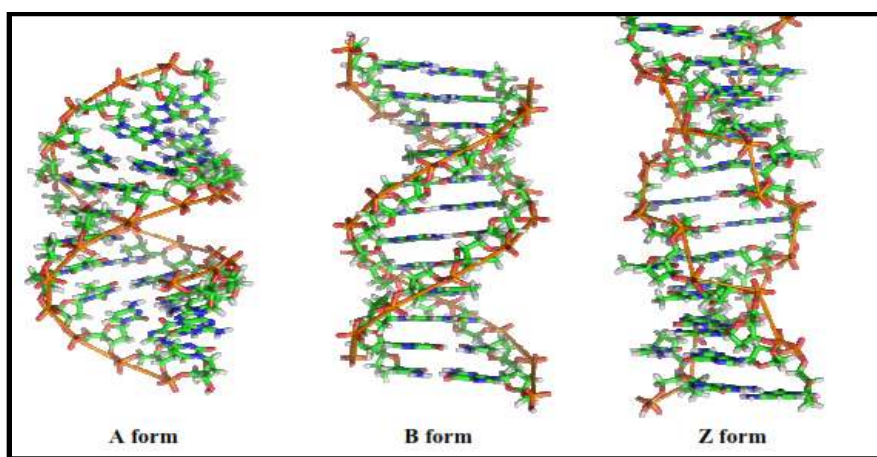


Fig. 4.4. Different forms of DNA [17]

4.1.2. Binding to DNA

Because of the features of their tertiary structure, the different forms of DNA do not interact in the same way with drugs. The hydrophobic part constituted by the bases is not accessible to the same extent in the three main cases of binding, depending on the size of the grooves. The interactions with the bases are favoured in the case where one of the grooves is wide enough to allow the molecule to bind to it. For each form of DNA the phosphate groups make up a polyanionic backbone on the outside surface allowing interaction with the aqueous medium. The edges of the bases have hydrogen bonding potential, which is only partially satisfied by the pairing and is therefore available for recognition by ligands [18].

4.1.3. Interest of binding drugs to DNA

DNA controls the genotype of each cell and so consists of a library where all the recipes' are stored. Without it, it would be impossible for cells to replicate themselves. This is the case not only for healthy cells but also for malignant cells. One approach to cancer therapy involves the use of cytotoxic agents, which reduce the proliferative drive to the tumour [18]. Many compounds with good tumour cell-killing activity have been discovered, but relatively few have found a clinical use because of the lack of discrimination between tumour and normal tissue.

The mode of action of cell-killing drugs is believed to involve the binding to DNA inside the cell, to stop the replication process. Replication is the process wherein the DNA is read base after base, translated into a codon, which codes for a particular amino acid [19]. If one base is missing or is the wrong one, the resulting nucleic acid chain or peptide, in the protein synthesis would be different; this is called *mutation* [20], and may lead to the death of the cell. There are two ways for the cytotoxic agents to act: the first is to bind covalently or noncovalently to the double strand and so block the RNA pathway to the replication, or more readily to cleave the strand directly.

4.1.4. DNA Binding Modes

DNA is an important genetic material in organisms and the basis of gene expression. Small molecules can interact with DNA [21-24] through intercalative binding, groove binding and electrostatic binding/external binding (Fig. 4.5).

4.1.4.1. Intercalative binding

Interactive binding results when small molecules or the drug intercalate into the nonpolar interior of the DNA helix. Aromatic group is stacked between the base pairs in this type of binding and this happens when ligands of an appropriate size and chemical nature fit themselves in between base pairs of DNA. The ligands suitable for intercalation are mostly polycyclic, aromatic and planar and therefore often make good nucleic acid stains. There is a current interest in designing and synthesizing DNA probes, as these molecules might function as chemotherapeutic agents.

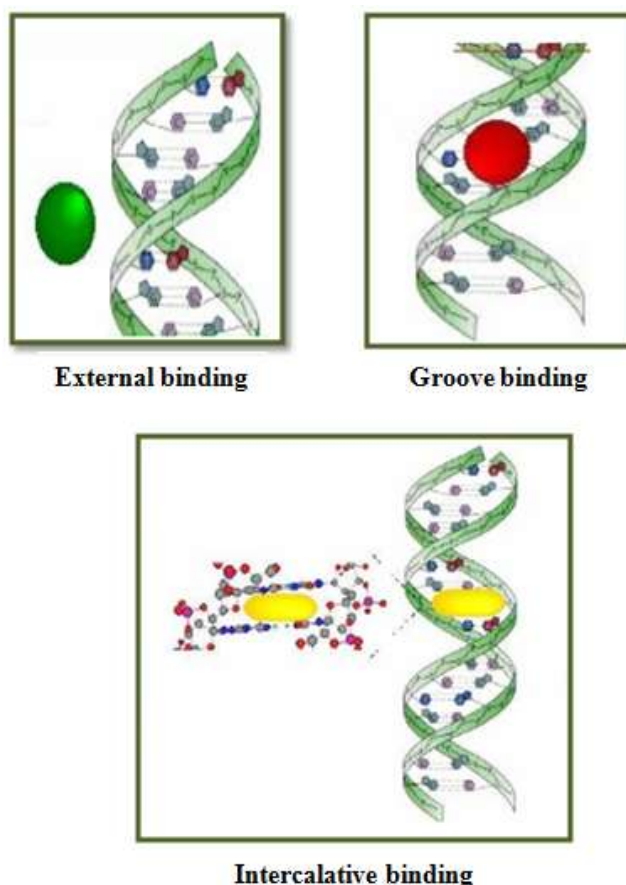


Fig. 4.5. Binding modes of small molecules with DNA [17]

4.1.4.2. Groove binding

Groove binding interactions involve direct interactions of the bound molecule with edges of base pairs in either major (G-C) or minor (A-T) grooves of the nucleic acids. The antibiotic netropsin is a model groove binder in which methyl groups prevents intercalation [25]. Binding within the major groove of the double helix is rare for small molecules.

4.1.4.3. External binding

Electrostatic interaction happens in the case of positively charged molecules. They electrostatically interact with the negatively charged phosphates backbone of DNA chain. Electrostatic attraction is generally weak under physiological conditions. Cations such as Mg^{+2} usually interact in this way [26].

The two most common binding modes are intercalation into the base pair stack at the core of the double helix and insertion into the minor groove. Intercalation is typically observed for cationic molecules having planar aromatic rings. The positive charge need not to be part of the ring system, but rather could be on a substituent. This binding mode requires two adjacent base pairs to separate from one another to create a binding pocket for the ligand [27]. Minor groove binders, on the other hand, usually have at least limited flexibility since this allows the molecule to adjust its structure to follow the groove as it twists around the central axis of the helix [28, 29].

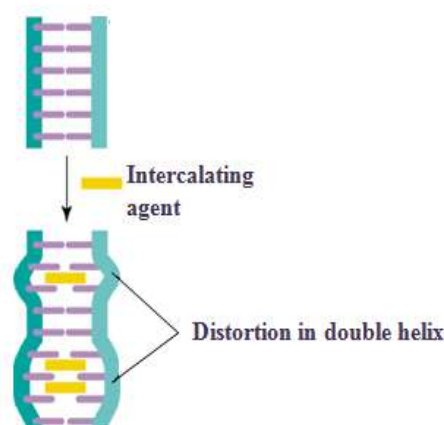


Fig. 4.6. Distortion in double helix after intercalation

Binding in the minor groove requires substantially less distortion of the DNA compared with intercalative binding (Fig. 4.6). The commonly used methods to provide insight into the binding modes of small molecules are UV-Visible spectroscopy, fluorescence spectroscopy, viscosity measurements, circular dichromism and linear dichromism.

4.1.5. Drugs which bind to DNA

Ethidium bromide is probably the best known intercalating agent [30]. Its planar aromatic unit is able to slide between the base pairs and form a strong complex (Fig. 4.7). Consequently the replication of the DNA is impossible and it is lethal for the cell [31]. A fluorimetric method for determining DNA and RNA concentrations using the fluorescence enhancement of ethidium bromide on binding to double strand nucleic-acids was proposed by LePecq and Paoletti in 1966 [32].

In the same family of intercalating drugs are acridine [33] and proflavine [34] (Fig. 4.7). They possess not only charged planar heteroaromatic rings but also amino groups able to form hydrogen bonds to acceptor sites on the DNA. Not all of the acridines are intercalative agents. The conditions of temperature and concentration can also affect the binding. At high concentration, the acridine dyes saturate the intercalative sites, after which they bind on the backbone surface [35].

The synthetic dye HOECHST 33258 (Fig. 4.7) is widely used as a fluorescent cytological stain for DNA, because it binds strongly to AT-rich sequences from the minor groove [36]. This binding is stabilized by Van der Waals interactions between the two benzimidazole rings and the sugar (O4'), and hydrogen bonds between benzimidazole NH groups and proximal Adenine (N3) and Thymine (O2). This groove binder is base-pair selective, by specific hydrogen bonding with the bases in the bottom of the groove and it is particularly selective for AT pairs in DNA.

As an example of these kinds of groove binders, Dervan *et al.* developed analogues of netropsin. The parent molecule contains a succession of pyrrole and imidazole rings interacting with the bases by specific hydrogen bonds, which targets specifically a sequence by formation of a third helix sitting in the minor groove [37].

These polyamides, because they have a higher affinity and specificity than naturally occurring DNA binding proteins, have the potential to control gene expression [38].

Actinomycin D is an intercalative antitumour drug which has also attached amino-acid side chains. It acts as a groove binder [39]. The peptide chains reside in the DNA groove, while the heterocyclic unit stacks between the base pairs. This is an example of an intercalator appended with a groove binding tail.

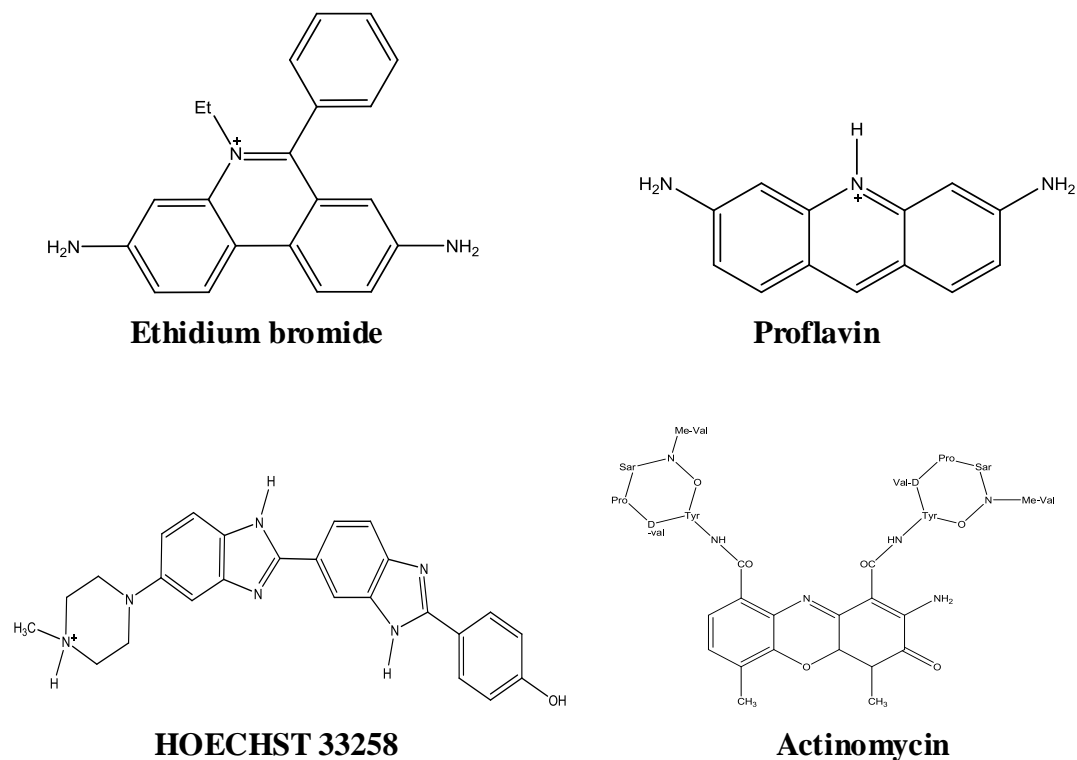


Fig. 4.7. Small molecules interacting with DNA

4.1.6. DNA Cleavage

DNA cleavage by metal complexes generally proceeds via two major pathways by oxidative pathway and hydrolytic pathway. The DNA cleavage activity of metal complexes can be targeted towards different constituents of DNA: the heterocyclic bases, deoxyribose sugar moiety and phosphodiester linkage. Oxidative cleavage of DNA takes place in the presence of additives or photo-induced DNA cleavage. Photo-cleavers requires the presence of a photo-sensitizer that can be activated on irradiation with UV or visible light.

Many metal complexes have been studied to understand their capability in the hydrolytic cleavage of DNA which involves hydrolysis of phosphodiester bond. Nucleophilic activation is required for hydrolytic cleavage of phosphodiester bond due to unusual stability of the diester bond in DNA. Among several types of DNA cleavage reactions, those occurring under photoactivation are of particular importance in highly targeted chemotherapeutic applications. The reagents showing photo induced DNA cleavage have major advantage over chemical nucleases, as the later requires a reducing agent and/or H₂O₂ for its activity.

4.1.7. Binding with Serum Albumins

Serum albumins, as the most abundant proteins in the circulatory system, act as transporter and disposer of many endogenous and exogenous compounds [40, 41]. The crystal structure analyses of human serum albumin (HSA) have revealed that the drug binding sites are located in subdomains IIA and IIIA [42]. A large hydrophobic cavity is present in IIA subdomain. Bovine serum albumin (BSA) is structurally homologous to human serum albumin (HSA) [43]. HSA has one tryptophan (Trp-214) in subdomain IIA, whereas BSA has two tryptophan moieties (Trp-134 and Trp-213) located in subdomains IB and IIA, respectively [44, 45]. The affinities of drugs to protein would directly influence the concentration of drugs in the blood and in the binding sites and the duration of the effectual drugs and consequently contribute to their magnitude of biological actions *in vivo*. Generally, the weak binding leads to a shorter lifetime or poor distribution, while strong binding decreases the concentration of free drug in plasma. Because of these, studies on this aspect can provide information on the structural feature that determines the therapeutic effectiveness of drugs and standardized screens for protein binding in new drug design and for fixing dose limits [46, 47]. Therefore, the binding of drugs to serum albumin *in vitro*, considered as a model in protein chemistry to study the binding behavior of proteins, has been an interesting research field in chemistry, life sciences, and clinical medicine [48].

4.1.8. Anti-cancer studies

4.1.8.1. Cell viability (MTT) assay

The MTT Cell Proliferation and Viability Assay is a safe, sensitive, *in vitro* assay for the measurement of cell proliferation or when metabolic events lead to apoptosis or necrosis, a reduction in cell viability. Cells are cultured in flat-bottomed, 96-well tissue culture plates. The cells are treated as per experimental design and incubation times are optimized for each cell type and system. The tetrazolium compound MTT (3-[4, 5-dimethylthiazol-2-yl]-2, 5-diphenyltetrazolium bromide) is added to the wells and the cells are incubated. MTT is reduced by metabolically active cells to insoluble purple formazan (Fig. 4.8) dye crystals. Detergent is then added to the wells, solubilizing the crystals so the absorbance can be read using a spectrophotometer. Samples are read directly in the wells. The optimal wavelength for absorbance is 570 nm, but any filter that absorbs between 550 and 600 nm may be used. The data is analyzed by plotting cell number versus absorbance, allowing quantitation of changes in cell proliferation. The rate of tetrazolium reduction is proportional to the rate of cell proliferation.

The **MTT assay** is a **colorimetric assay** for measuring the activity of cellular enzymes that reduce the tetrazolium dye, MTT, to its insoluble **formazan**, giving a purple color. A solubilization solution (usually either dimethyl sulfoxide, an acidified ethanol solution, or a solution of the detergent sodium dodecyl sulfate in diluted hydrochloric acid) is added to dissolve the insoluble purple formazan product into a colored solution. The absorbance of this colored solution can be quantified by measuring at a certain wavelength (usually between 500 and 600 nm) by a spectrophotometer. The absorption maximum is dependent on the solvent employed. These assays measure cellular metabolic activity *via* NAD(P)H-dependent cellular oxidoreductase enzymes and may, under defined conditions, reflect the number of viable cells (cell proliferation). Tetrazolium dye assays can also be used to measure cytotoxicity (loss of viable cells) or cytostatic activity (shift from proliferative to resting status) of potential medicinal agents and toxic materials. Using a spectrophotometric method to measure the absorption of the resulting colored solution, cell proliferation (and even cell viability) can now be accurately determined.

Even the slightest color changes that occur can be determined using the yellow tetrazole MTT – the process is thus called MTT assay.

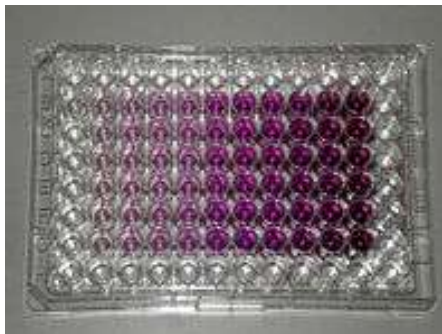


Fig. 4.8. A microtiter plate after an MTT assay. Increasing amounts of cells resulted in increased purple colouring [48]

4.1.8.1.1. Significance of MTT Assay

Tetrazolium dye reduction is dependent on NAD(P)H-dependent oxidoreductase enzymes largely in the cytosolic compartment of the cell. Therefore, reduction of MTT and other tetrazolium dyes increases with cellular metabolic activity due to elevated NAD(P)H flux. Resting cells such as thymocytes and splenocytes that are viable but metabolically quiet reduce very little MTT. In contrast, rapidly dividing cells exhibit high rates of MTT reduction. It is important to keep in mind that assay conditions can alter metabolic activity and thus tetrazolium dye reduction without affecting cell viability and that different tetrazolium dyes will give different results depending on whether they are reduced intracellularly (MTT).

The use of the MTT assay for many different applications is well documented. Because the MTT assay can accurately determine the cell count and cell proliferation it can be used for such applications as determining the cytotoxicity of various medicinal and toxic materials since these materials to be tested would either inhibit or stimulate cell growth and propagation.

MTT assays are far more superior to the Trypan blue staining method (which is less sensitive) and much safer than radiometric methods (which uses radio active materials). MTT assay makes use of a simple process and equipment that are already in most laboratories. The MTT assay is run using a 96-well plate. A microtitre plate

reader is then used to do the reading. MTT assay are readily available in kits for research purposes only. MTT assay kits are stable and can be kept in a dark refrigerated storage for up to 18 months.

4.1.8.2. LDH Release Assay

This assay is based on measurement of cytoplasmic enzyme activities released by damaged cells. Several enzyme-release assays have been described (*e.g.*, for alkaline and acid phosphatase); however, many of these assays are hampered by (i) the low amount of endogenous enzyme present in many types of cells, and (ii) the elaborate kinetic assays required to quantitate the enzyme activities. In contrast, lactate dehydrogenase (LDH) is a stable cytoplasmic enzyme that is present in all cells. LDH is rapidly released into the cell-culture supernatant when the plasma membrane is damaged and is simple to assay.

Cell death can occur either by apoptosis, a highly regulated pathway involving signal transduction cascades, or by necrosis. Necrosis is accompanied by mitochondrial swelling and increased plasma membrane permeability, while apoptosis involves an articulated breakdown of the cell into membrane-bound apoptotic bodies [49]. There are a number of screening techniques available that detect cytotoxicity and cell death, independent of mechanism. Most of these assays evaluate cell viability by measuring plasma membrane permeability [50].

Lactate dehydrogenase (LDH) is a soluble enzyme located in the cytosol. The enzyme is released into the surrounding culture medium upon cell damage or lysis, process that occur during both apoptosis and necrosis. LDH activity in the culture medium can, therefore, be used as an indicator of cell membrane integrity and thus a measurement of cytotoxicity. Since the activity of intracellular LDH corresponds to the number of cells in the culture, quantification of LDH in cell lysates can be used as a measurement of cell growth [50, 51].

4.1.8.3. Intracellular ROS generation (DCFDA staining)

CM-H₂DCFDA (chloromethyl-2',7'-dichlorofluorescein diacetate) is widely used to measure oxidative stress in cells. CM-H₂DCFDA is resistant to

oxidation, but when taken up by cells, is de-acetylated by intracellular esterases to form the more hydrophilic nonfluorescent reduced dye dichlorofluorescein DCFH, which then is rapidly oxidized to form a two-electron oxidation product, the highly fluorescent DCF in a reaction with the oxidizing species (H_2O_2).

Reactive oxygen species (ROS) assay uses the cell permeant reagent 2',7'-dichlorofluorescein diacetate (DCFDA), a fluorogenic dye that measures hydroxyl, peroxy and other ROS activity within the cell. After diffusion into the cell, DCFDA is deacetylated by cellular esterases to a non-fluorescent compound, which is later oxidized by ROS into 2',7'-dichlorofluorescein (DCF). DCF is a highly fluorescent compound which can be detected by fluorescence spectroscopy with maximum excitation and emission spectra of 495 nm and 529 nm, respectively.

The two major sources of cellular ROS are complex-I (NADH dehydrogenase ubiquinone-ubiquinol reductase) and complex-III (ubiquinol cytochrome c reductase), both part of the mitochondrial electron transport chain. These two complexes generate ROS particularly when electron transport is slowed by high mitochondrial membrane potential ($\Delta\psi_m$). The major product of ROS in mitochondria is in the form of superoxide and hydroperoxyl radical. Superoxide generated in complex-III occurs in the presence of slow electron transport which allows for the ubisemiquinone anion radical to react with oxygen dissolved in the membrane.

The exact source of superoxide generated by complex-I is less known and it is believed to be due to electron leakage from its iron-sulfur clusters. Low levels (or optimum levels) of ROS play an important role in signaling pathways. However when ROS production increases and overwhelms the cellular antioxidant capacity, it can induce macromolecular damage (by reacting with DNA, proteins and lipids) and disrupt thiol redox circuits. In the first instance, damage can lead to apoptosis or necrosis. Disruption of thiol redox circuits can lead to aberrant cell signaling and dysfunctional redox control.

4.1.8.4. Mitochondrial Membrane Potential

The Mitochondrial membrane potential detection assay uses a unique fluorescent cationic dye, JC-1 (5, 5', 6, 6'-tetrachloro-1, 1', 3, 3'-

tetraethylbenzimidazolylcarbocyanine iodide), to signal the loss of mitochondrial membrane potential. In healthy non-apoptotic cells, the dye stains the mitochondria bright red. The negative charge established by the intact mitochondrial membrane potential allows the lipophilic dye, bearing a delocalized positive charge, to enter the mitochondrial matrix where it accumulates.

When the critical concentration is exceeded, JC1-aggregates form and become fluorescent red. In apoptotic cells, the mitochondrial membrane potential collapses, and the JC-1 cannot accumulate within the mitochondria. In these cells JC-1 remains in the cytoplasm in a green fluorescent monomeric form. Apoptotic cells, showing primarily green fluorescence, are easily differentiated from healthy cells which show red and green fluorescence.

The aggregate red form has absorption/emission maxima of 585/590 nm. The green monomeric form has absorption/emission maxima of 510/527 nm. The JC-1 monomers and aggregates give strong positive signals, capable of yielding both qualitative and quantitative results. Detection methods include flow cytometry, fluorescence microscopy, and a fluorescent 96-well plate reader format.

4.1.8.5. Nuclear morphology assay (DAPI staining)

DAPI binds to the AT rich regions of DNA and is used to distinguish the compact chromatin of apoptotic nuclei from that of normal cells.

4.1.8.6. AO/EB staining

Acridine Orange stains live cells (green) whereas, Ethidium Bromide stains dead cells (red-to-orange) and hence this method of dual staining enables rapid and easy recognition/differentiation of live-dead cells when visualized under a fluorescence microscope [52].

4.1.8.7. Cell cycle analysis & FITC Annexin-V/PI Staining

Apoptosis is a common form of cell death in eukaryotes, playing a fundamental role during embryogenesis, in the homeostatic control of tissue integrity, tumor regression and immune response development [53]. On receiving specific

signals, a number of distinctive biochemical and morphological changes occur in the cell. A family of proteins known as caspases, and perhaps other proteases, are activated in the early stages of apoptosis. These proteins cleave key cellular substrates that are necessary for normal cellular function, including structural proteins in the cytoskeleton and nuclear proteins. The caspases can also activate other degradation enzymes such as DNases, which begin to cleave the DNA at the linker regions between oligonucleosomes [54]. The result of these biochemical events is the appearance of morphological changes in the cell and extensive DNA cleavage. The products of DNA degradation are nucleosomal and oligonucleosomal DNA fragments (180 bp and multiples of 180 bp), which generate a characteristic “ladder” pattern during agarose gel electrophoresis [55]. Because the DNA in apoptotic cells is partially degraded, the fraction of low-molecular-weight DNA can be extracted, whereas the non-degraded DNA remains in the cell nucleus [56]. Because DNA fragments are lost from apoptotic nuclei and nuclear DNA content can be easily measured by flow cytometry, after nucleic acid staining with specific fluorochromes [57], methods have been developed for a quantitative evaluation of apoptotic nuclei.

Basically, the method we describe uses PI for nuclear staining. PI is a fluorogenic compound that binds stoichiometrically to nucleic acids [58-60] so that fluorescence emission is proportional to the DNA (and RNA, which has to be removed if DNA is to be measured) content of a cell. When apoptotic cells are stained with PI and analyzed with a flow cytometer, they display a broad hypodiploid (sub-G1) peak, which can be easily discriminated from the narrow peak of cells with normal (diploid) DNA content in the red fluorescence channels.

This method appears to offer a number of advantages. It allows (i) a rapid, reliable and reproducible estimate of apoptosis, (ii) simultaneous analysis of cell-cycle parameters of surviving cells and (iii) when necessary, simultaneous analysis of cell surface antigens recognized by fluorescein isothiocyanate- or Alexa 488-conjugated monoclonal antibodies and the extent of apoptosis [61].

It should be stressed, however, that many types of apoptosis exist, and the extensive DNA fragmentation and loss of DNA fragments is not a universal finding in apoptotic death. Also, necrotic cells sometimes display some degrees of DNA

degradation that may result in hypodiploid nuclei. Furthermore, the 'sub-G1' peak can represent, in addition to apoptotic cells, nuclear fragments, clumps of chromosomes, micronuclei or nuclei with normal DNA content but different chromatin structure and diminished accessibility of fluorochrome to DNA (i.e., cells undergoing differentiation).

DNA peak is not a bonafide proof of apoptotic death. Morphological (microscopic observation of apoptotic bodies) [62], biochemical (DNA ladder in agarose gel) [55] or specific demonstration of DNA breaks (terminal deoxynucleotidyl transferase assay [63]) should be used to confirm apoptosis before quantitative analysis by flow cytometry.

Another important concern in quantitative evaluation of apoptotic cells by flow cytometry is the discrimination of true apoptotic nuclei from nuclear debris. A proper setting of acquisition parameters (volume of particles, usually measured as forward scatter (FSC)) and of diploid DNA peak by using a calibration standard (DNA check beads) and negative and positive cell controls is essential before using the method with a cell line that has never been analyzed before. It should also be remembered that apoptosis is a dynamic process and that there is a short "time window" during which apoptotic cells display their characteristic features. For this reason, different methods can produce different results depending on the time of the apoptosis process [64]. For example, in early phases of apoptosis, terminal deoxynucleotidyl transferase can be positive for DNA breaks, and the cell membrane can expose phosphatidylserine which is Annexin-V positive. However, morphological observation can be negative for apoptotic bodies and flow cytometric analysis can be negative for the sub-G1 peak, as DNA fragments are still maintained in the nucleus. Accordingly, the DNA ladder cannot be observed with agarose gel electrophoresis.

However, when used appropriately, the PI flow cytometric assay is a rapid and easily reproducible method that can be adapted for apoptosis evaluation in different kinds of cells.

4.1.9. Metal complexes against different diseases

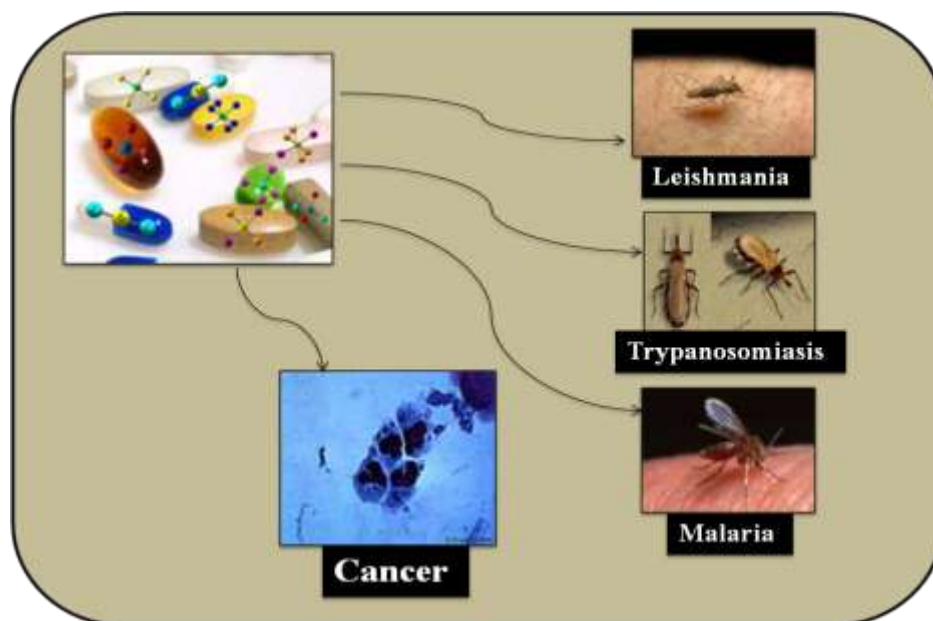


Fig. 4.9. Metal complexes against different diseases

4.2. Experimental

4.2.1. Materials

CT-DNA (Calf Thymus DNA) and BSA (Bovine Serum Albumin) were purchased from Sigma Aldrich. All the chemicals used were of AR grade. Solvents used in this study were purified following the standard procedures. Dulbecco's Modified Eagle Medium (DMEM), Trypsin Phosphate Versene Glucose (TPVG) solution Trypsin and methylthiazolyldiphenyl- tetrazolium bromide (MTT) were purchased from HiMedia Laboratories Pvt. Ltd. (Bombay, India). Fetal bovine serum (FBS) was purchased from Biosera (Ringmer, East Sussex UK) and dimethyl sulfoxide (DMSO) was purchased from the Sisco Research Laboratories Pvt. Ltd. (Mumbai, India). Rhodamine 123, 4',6-diamidino-2-phenylindole (DAPI) and 2',7'-dichlorofluorescein diacetate (CM-H₂-DCFDA) were purchased from Sigma (Delhi, India).

4.2.2. DNA binding studies

All of the experiments involving the binding of complexes with CT-DNA were carried out in double distilled water with trisodium citrate (Tris, 15 mM) and

sodium chloride (150 mM) and adjusted to pH 7.05 with hydrochloric acid. The DMF solution of the complexes was used throughout the study. The concentration of CT-DNA per nucleotide was estimated from its known extinction coefficient at 260 nm ($6600 \text{ M}^{-1} \text{ cm}^{-1}$) [65]. Solutions of CT-DNA in tris buffer gave a ratio of UV absorbance at 260 and 280 nm (A_{260}/A_{280}) 1.8-1.9 indicating that the DNA was sufficiently free of protein. Absorption titration experiments were performed by maintaining a constant metal complex concentration, while gradually increasing the concentration of DNA (μM). While measuring the absorption spectra, an equal amount of DNA was added to both the test solution and the reference solution to eliminate the absorbance of DNA itself.

The data were then fit to eq 1 [66] to obtain intrinsic binding constant K_b .

$$[\text{DNA}]/(\varepsilon_a - \varepsilon_f) = [\text{DNA}]/(\varepsilon_b - \varepsilon_f) + 1/K_b (\varepsilon_b - \varepsilon_f) \quad \dots\dots (1)$$

Where, $[\text{DNA}]$ is the concentration of DNA in base pairs, ε_a is the extinction coefficient observed for the MLCT absorption band at the given DNA concentration, ε_f is the extinction coefficient of the complex free in solution, and ε_b is the extinction coefficient of the complex when fully bound to DNA. A plot of $[\text{DNA}]/[\varepsilon_a - \varepsilon_f]$ versus $[\text{DNA}]$ gave a slope $1/[\varepsilon_b - \varepsilon_f]$ and Y intercept equal to $(1/K_b)[\varepsilon_b - \varepsilon_f]$, respectively. The intrinsic binding constant K_b is the ratio of the slope to the intercept [66].

Competitive studies of complexes as well as ligands with ethidium bromide (EB) have been investigated with fluorescence spectroscopy in order to examine whether the compound can displace EtBr from its CT DNA–EB complex. The CT DNA–EtBr complex was prepared by adding $3.3 \mu\text{M}$ EtBr and $4.2 \mu\text{M}$ CT-DNA in buffer (150 mM NaCl and 15 mM trisodium citrate at pH 7.05). The intercalating effect of the compound with the DNA–EtBr complex was studied by adding a certain amount of a solution of the compound step by step (μM) into the solution of the DNA–EtBr complex. The influence of the addition of each compound to the DNA–EtBr complex solution has been obtained by recording the variation of fluorescence emission spectra. The emission spectra were monitored by keeping the excitation of the test compound at 546 nm and the emission was monitored in the range of 550-750 nm. The emission was observed at 610 nm.

Commonly, fluorescence quenching can be described by the following Stern–Volmer equation (eq 2) [67].

$$F_0/F = 1 + K_{sv}[Q] = 1 + k_q \tau_0 [Q] \quad \dots\dots (2)$$

where F_0 and F are the steady-state fluorescence intensities in the absence and presence of quencher, respectively, K_{sv} is the Stern-Volmer quenching constant, obtained from the slope of the plot F_0/F versus $[Complex]$, $[Q]$ is the total concentration of quencher, k_q is the bimolecular quenching constant, and τ_0 is the average lifetime of protein in the absence of quencher, and its value is 10^{-8} s.

The apparent DNA binding constant (K_{app}) values of the complex was obtained from this fluorescence spectral measurement. The K_{app} values were obtained from the equation:

$$K_{app} \times [complex]_{50} = K_{EB} \times [EtBr] \quad \dots\dots (3)$$

where K_{app} is the apparent binding constant of the complex studied, $[compound]_{50}$ is the concentration of the complex at 50% quenching of DNA-bound ethidium bromide emission intensity, K_{EtBr} is the binding constant of ethidium bromide ($K_{EtBr} = 1.0 \times 10^7 \text{ M}^{-1}$), and $[EtBr]$ is the concentration of ethidium bromide ($3.3 \mu\text{M}$) [68].

For viscosity measurements, the flow time was measured with digital stopwatch using Ostwald's viscometer at $30 \pm 0.01 \text{ }^\circ\text{C}$. DNA samples were prepared in water by sonication in order to minimize complexities arising from DNA flexibility. The DNA solution ($50 \mu\text{M}$) was mixed with varied concentrations (mM) of complexes in DMF for flow time measurements. The flow time reported in the present study is an average of three readings for each sample. Data were shown as $(\eta/\eta_0)^{1/3}$ vs. $[Complex]/[DNA]$, where η_0 is the viscosity of DNA alone and η is the viscosity of DNA in the presence of the complex. The η_0 and η values were calculated from the observed flow time of DNA solution and DNA+metal complex solution, respectively and these values were corrected by subtracting the flow time observed for the DMF alone.

The cleavage of DNA by the Cu(II) complexes was monitored using agarose gel electrophoresis. Reactions using $3 \mu\text{M}$ DNA in water was treated with the Cu(II) complexes and $5 \mu\text{M}$ hydrogen peroxide. A loading buffer containing

0.25% bromophenol blue, 30% glycerol was added and the electrophoresis was performed at 100 V in Tris–acetate–EDTA (TAE) buffer using 1% agarose gel containing ethidium bromide. Agarose gel electrophoresis of plasmid DNA was visualized by photographing the fluorescence of intercalated ethidium bromide under a UV illuminator at 360 nm.

4.2.3. Tryptophan Quenching Studies

Similar experimental procedure was followed for tryptophan quenching study as DNA binding studies. Quenching of the tryptophan residues of BSA was performed using complexes and ligands as quencher. To the solutions of BSA in buffer, increments of the quencher were added and the emission signals at 343 nm (excitation wavelength at 296 nm) were recorded after each addition of the quencher [66].

The data were fitted in the stern-volmer eq 2 (section 4.2.2). The stern-volmer constant was obtained from the slope of the plot F_0/F versus [Compound].

4.2.4. Anticancer activity

4.2.4.1. Cell culture

Human lung carcinoma (A549) cells were obtained from National Centre for Cell Science, Pune, India and were seeded (1×10^5 cells/ T25 flask) and cultured in DMEM containing 10% FBS and 1% antibiotic-antimycotic solution at 37°C with 5% in water Jacketed CO₂ incubator (Thermo scientific, forma II). Cells were sub-cultured every third day by trypsinization with TPVG solution. Reagents used herein were filtered through 0.22 μ filter (Laxbro Bio-medical Aids Pvt. Ltd) prior to their use for the experiment. A549 cells were maintained for a period of 24 h in absence of presence of complexes at a cell density of 5.0×10^3 cells/well in 96 well plate for MTT and LDH assay and 1×10^5 cells/ well in 6 well plate for LDH release assay, mitochondrial membrane potential assay, DCFDA and AO-EB staining, cell cycle analysis and Annexin V-PI staining assays.

4.2.4.2. Cell viability (MTT) assay

A549 cells (7×10^3 cells/ well) were maintained in 96-well culture plates (Tarson India Pvt. Ltd.) for 24 h in absence and presence of complexes. At the end of incubation period 10 μ l of 3-(4,5-dimethylthiazol-2-yl)-2,5-diphenyl-tetrazolium bromide (MTT, 5 mg/ml) was added to the wells and plates were incubated at 37 °C for 4 h. Later, culture media were discarded and wells were washed with Phosphate Buffer Saline (Hi-media, India, Pvt. Ltd.), followed by addition of 150 μ l of DMSO and subsequent incubation for 30 min and absorbance was read at 540 nm in ELX800 Universal Microplate Reader [69].

4.2.4.3. Cellular integrity (LDH release) assay

A549 cells were maintained in 96 well plates for 24 h as mentioned above. Later supernatant from each well was collected and activity levels of LDH were assayed with commercially available kit (Reckon diagnostics Ltd., Mumbai, India) using Merck microlab L 300 semi-auto-analyzer and % cytotoxicity was calculated [69].

4.2.4.4. Intracellular ROS generation (DCFDA staining)

After 18 h of treatment with complexes, cells were incubated with 7.5 μ M chloromethyl-2, 7-dichlorodihydrofluorescein diacetate (CM-H₂-DCFDA) at 37°C for 30 min. Cells were observed in a Leica DMRB fluorescent microscope [70].

4.2.4.5. Mitochondrial Membrane Potential

The changes in mitochondrial membrane potential were measured using the fluorescent cationic dye Rhodamine 123 (RHO 123). After 24 h treatment with complexes, cells were incubated with 1 μ M RHO 123 for 10 min at 37 °C. The fluorescence was determined at excitation and emission wavelength of 485 and 530 nm, respectively using spectrofluorometer (Jasco FP-6300, Japan) and expressed as fluorescence intensity units (FIU) [71].

4.2.4.6. Nuclear morphology assay (DAPI staining)

Cells (5×10^4 cells/well) were plated into 6-well plate. After 80% confluence, the cells were treated with or without different concentrations of complexes at 37 °C for 24 h. Single-cell suspensions of treated cells were washed with PBS and fixed with 70% ethanol for 20 min at room temperature. Cells were washed again with PBS

and stained with DAPI (0.6 $\mu\text{g}/\text{mL}$ in PBS) incubated for 5 min. Nuclear morphology of apoptotic cells with condensed/fragmented nuclei was examined under a fluorescent microscope (Leica DMRB fluorescence microscope).

4.2.4.7. AO/EB staining

A549 cells (1×10^5 cells/well) were maintained in 6 well plates as described earlier for 24 h. At the end of experiment period, cells were collected using TPVG solution. 1 μl of dye mixture (1 mg/ml AO and 1 mg/ml EB in PBS) was mixed with 9 μl of cell suspension (0.5×10^6 cells/ml) on a clean microscope slide and examined and photographed under Leica DMRB fluorescence microscope. A minimum of 300 cells were counted in every sample to calculate percentage cell death.

4.2.4.8. Cell cycle analysis

Cells (1×10^6 cells/well) were cultured as mentioned earlier for 24 h. After incubation, the cells were washed once in ice-cold PBS and subjected to cell cycle analysis [72]. Briefly, 1×10^5 cells were fixed in 4.5 ml of 70% (v/v) cold ethanol for 30 min, centrifuged at 400g for 5 min. Supernatant was removed and cells were washed with 5 ml of PBS. Cells were then re-suspended in 0.5 ml of PBS and 0.5 ml of DNA extraction buffer (Mix 192 ml of 0.2 M Na_2HPO_4 with 8 ml of 0.1% Triton X-100 v/v) was added. The pH was adjusted to 7.8. Cells were incubated at room temperature for 5 min and then centrifuged at 400g for 5 min. Supernatant was discarded and cells were re-suspended in 1 ml of DNA staining solution (200 mg of PI in 10 ml of PBS + 2 mg of DNase free RNase). Cells are then incubated for at least 30 min at room temperature in the dark and the cell cycle distribution was then analyzed on a flow cytometer (BD FACS Aria III, USA) using FlowJo (Oregon, USA).

4.2.4.9. FITC Annexin-V/PI Staining

Annexin-V FITC/ Propidium iodide double staining assay was used to quantify apoptosis, according to the manufacturer's protocol (Invitrogen, UK). After incubation, cells were harvested using TPVG solution and washed with ice-cold PBS and suspended in 100 μl of $1 \times$ binding buffer (10 mM HEPES, 140 mM NaCl, and

2.5 mM CaCl_2 , pH 7.4). To this mixture, 5 μl of annexin V-FITC conjugate and 1 μl of propidium iodide solution were added to each cell suspension and incubated for 15 min at room temperature in the dark. Later, samples were analyzed on flow cytometer (BD FACSAria III, USA) using FlowJo (Oregon, USA). Double staining of cells with FITC Annexin-V and PI enables the discrimination of live cells (FITC⁻PI⁻), early apoptotic (FITC⁺PI⁻), late apoptotic (FITC⁺PI⁺) or necrotic cells (FITC⁻PI⁺).

4.2.4.10. Statistical analysis

Data was analyzed for statistical significance using one way analysis of variance (ANOVA) followed by Bonferroni's multiple comparison test and results were ex-pressed as mean \pm SEM using Graph Pad Prism version 3.0 for Windows, Graph Pad Software, San Diego, California, USA.

4.3. DNA binding activities of the compounds under investigation

Because DNA is the primary pharmacological target of many antitumor compounds, the interaction between DNA and metal complexes is of paramount importance in understanding the mechanism. Thus, the mode and propensity for binding of the complex to CT-DNA were studied with the aid of different techniques.

4.3.1. Electronic absorption titration

Absorption spectral titrations are the most common method to investigate the interactions of metal complexes with DNA [73]. The spectral changes reflect the corresponding changes in DNA in its conformation and structure after the complex bound to DNA. Monitoring the changes in absorption spectra of the metal complexes upon addition of increasing amounts of DNA is one of the most widely used methods for determining overall binding constants. In the UV spectra of the complex, the intense absorption bands observed are attributed to the intraligand transition of the characteristic groups of the coordinated ligand. Any interaction between complex and DNA could perturb the intraligand-centred spectral transitions as observed in the UV spectra of solution of the complexes upon addition of DNA at different concentrations. The binding of the metal complexes to DNA helix is often

characterized through absorption spectral titration, followed by the changes in the absorbance and shift in the wavelength. Hyperchromism and hypochromism are the spectral changes typical of a metal complex association with the DNA helix [74]. The extent of the hypochromism commonly parallels the intercalative binding strength. The hypochromicity, characteristic of intercalation has been usually attributed to the interaction between the electronic states of the compound chromophores and those of the DNA bases [75], while the red shift has been associated with the decrease in the energy gap between the highest and the lowest molecular orbitals (HOMO and LUMO) after binding of the complex to DNA [76]. The hypochromicity also suggests that the complex may bind to DNA by intercalation mode, due to a strong interaction between the electronic states of the intercalating chromophore and those of the DNA bases [77]. The hyperchromism observed may be a first evidence of possible external binding to CT DNA, while the existence of planar ligands may suggest stabilization upon binding to DNA; in such case, intercalation due to $\pi \rightarrow \pi^*$ stacking interactions between the base pairs of CT DNA may not be ruled out [78]. Nevertheless, the exact mode of binding cannot be merely proposed by UV spectroscopic titration studies.

4.3.1.1. Absorption spectral studies of 4-acyl pyrazolone based complexes

The complexes displayed intense absorption band at 250-300 nm in the UV region. Changes in the electronic absorption spectra of complexes were measured as a function of DNA concentration. There was a significant change in the absorption profile of complex on sequential addition of DNA, indicating a good binding propensity of the complex. An increase in molar absorptivity (hyperchromism) was shown by the complexes on the addition of increasing amounts of DNA. So, the above phenomena imply that the Cu(II) complexes interact with DNA by partial intercalating mode.

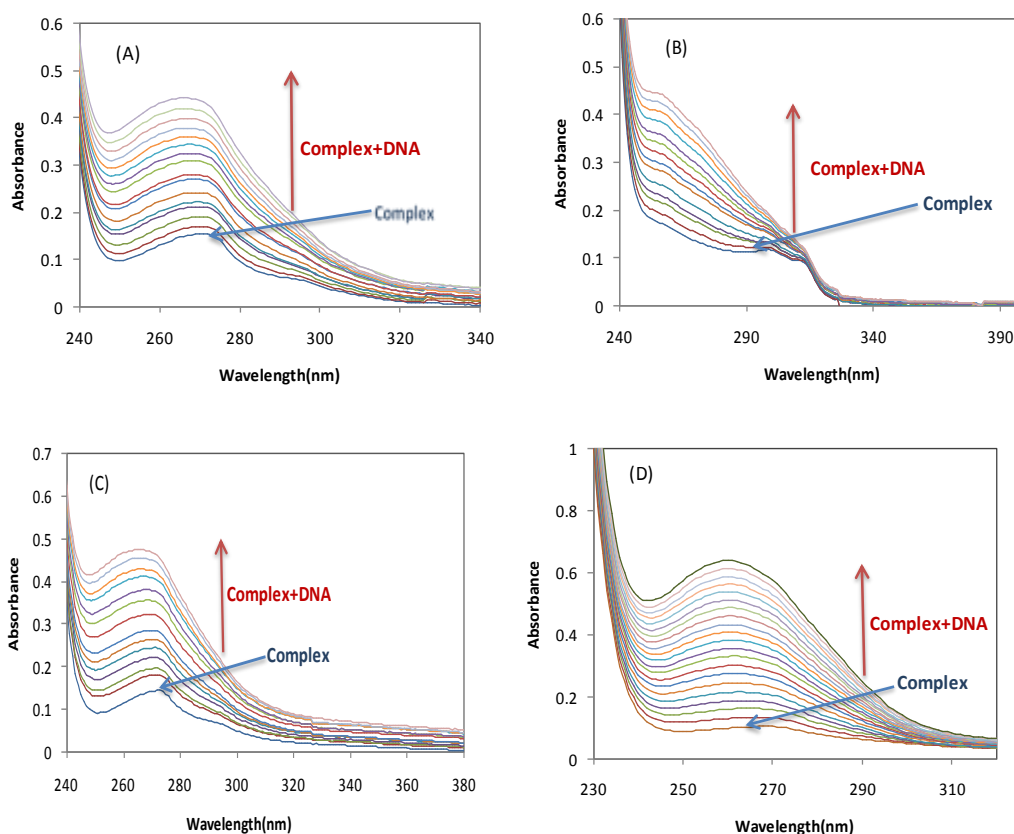


Fig. 4.10. Changes in the electronic absorption spectra of complex (A) **6** (B) **8**, (C) **12** and (D) **20** (10 μM) with increasing concentrations (0-100 μM) of CT-DNA (Tris, pH 7.04). The arrow shows the changes on addition of the CT-DNA

4.3.1.2. Absorption spectral studies of thiosemicarbazone based complexes

4.3.1.2.1. Simple complexes

Upon the addition of DNA, interesting changes in the absorbencies of the MLCT transition absorption bands of the complexes were observed. The observed hypochromism for both the complexes unambiguously revealed the active participation of pyrazolone moieties in association with the DNA. However, the lack of red shift suggests that the binding mode of both the complexes was not classical intercalation. Because of the bulky structure of the complexes, the aromatic rings cannot completely intercalate. Therefore, the observed spectral changes were rationalized in terms of partial intercalation.

4.3.1.2.2. Ternary complexes

In the UV region, complexes exhibited intense absorption bands around 270 nm, which was assigned to $\pi \rightarrow \pi^*$ transition of aromatic chromophore. With increasing CT-DNA (5-100 μM), the absorption bands of complex are affected, exhibiting hyperchromism in $\pi \rightarrow \pi^*$ transition of complex. A strong hyperchromic effect in $\pi \rightarrow \pi^*$ transition was observed for complexes, suggesting that these complexes possess higher propensity for DNA binding. The absorption spectra of few of the complexes in the absence and presence of CT-DNA (at a constant concentration of complex) are shown in Fig. 4.10.

To further illustrate the DNA binding strength, the intrinsic binding constant K_b was determined (**16** = 4.28×10^4 , **17** = 4.64×10^4 and **20** = 2.04×10^5). The binding constant of these complexes were lower in comparison to those observed for typical classical intercalators (ethidium-DNA, $1.4 \times 10^6 \text{ M}^{-1}$) [79]. The diminution of the intrinsic binding constants could be explained by the steric constraints imposed by the ligand framework and thus encouraging intercalation binding mode for the complexes. Our results are consistent with earlier reports on preferential binding to DNA in the Cu complexes [80, 81].

4.3.2. Ethidium Bromide Displacement Assay

In order to further investigate the interaction mode between the complexes and DNA, the fluorescence titration experiments are performed. The fluorescence titration experiments, especially the EtBr fluorescence displacement experiment, have been widely used to characterize the interaction of complexes with DNA by following the changes in fluorescence intensity of the complexes. The complexes showed no fluorescence either in DMF or in presence of DNA. So, the competitive DNA binding of complexes have been studied by monitoring changes in emission intensity of ethidium bromide (EtBr) bound to CT-DNA as a function of added complex concentration get final proof for the binding of the compounds to DNA *via* intercalation. Though the emission intensity of EtBr in buffer medium is quenched by the solvent molecules, [82] it is enhanced by its stacking interaction between adjacent DNA base pairs. When complexes were added to DNA pretreated with EtBr

{[DNA]/[EtBr]=1:1}, the DNA-induced emission intensity of EtBr was decreased (Fig. 4.11 (A, B, C & D)). Addition of a second DNA binding molecule would quench the EtBr emission by either replacing the DNA-bound EtBr (if it binds to DNA more strongly than EtBr) or accepting an excited state electron from EtBr. Because the complexes has planar ligands, they efficiently compete with strong intercalators like EtBr for intercalative binding sites on DNA by replacing EtBr, which is reflected in quenching of emission intensity of DNA-bound EtBr. The titrations were carried out also for the ligands (Fig. 4.11 (E & F)). The emission intensity was decreased in all the cases but it was much lower than that of the respective complexes. Ethidium bromide (EtBr) is a weak fluorophore, but its emission intensity in the presence of DNA can be greatly enhanced because of its strong intercalation between the adjacent DNA base pairs. EtBr, a planar aromatic heterocyclic dye intercalates non-specifically into the DNA which causes it to fluoresce strongly.

EtBr (weak fluorophore) + DNA (non-fluorophore) = EtBr-DNA (strong fluorophore)

In our experiments, as depicted in Fig. 4.11, the fluorescence intensity of EtBr show a remarkable decreasing trend with the increasing concentration of the complexes, indicating that some EtBr molecules are released from EtBr-DNA complex after an exchange with the complexes which results in the fluorescence quenching of EtBr. This may be due either to the metal complex competing with EtBr for the DNA-binding sites thus displacing the EtBr (whose fluorescence is enhanced upon DNA binding) or it should be a more direct quenching interaction on the DNA itself. We assume the reduction of the emission intensity of EtBr on increasing the complex concentration could be caused due to the displacement of the DNA bound EtBr by the Cu(II) complexes. Such a quenched fluorescence behavior of EtBr bound to DNA caused by the interaction between the binuclear Cu(II) complexes and DNA is also found in other copper complexes [83].

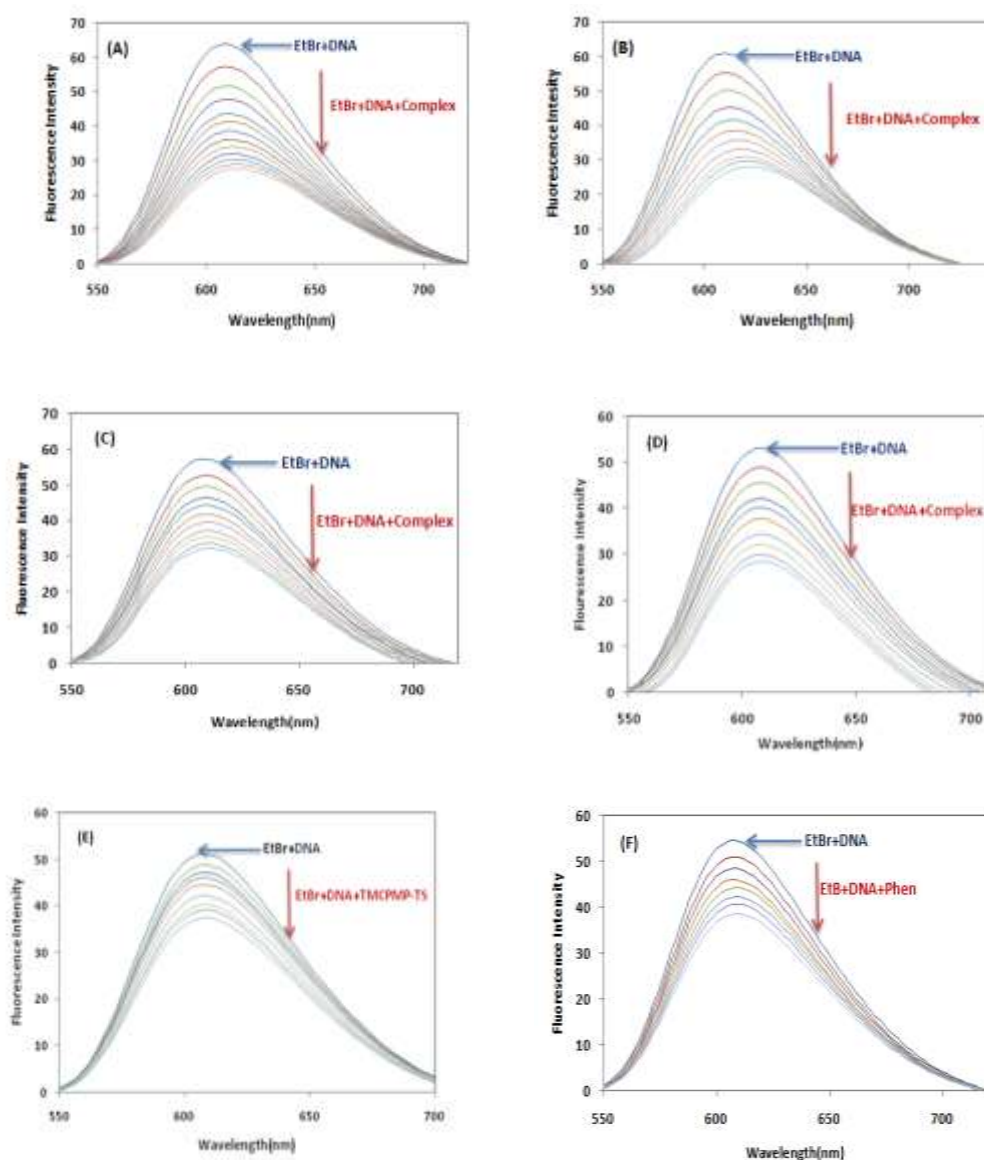
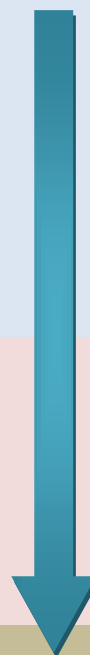


Fig. 4.11. Emission spectra ($\lambda_{em}=610$ nm) of DNA–EtBr complex in buffer solution in the absence and presence of the increasing amount of (A) **11**, (B) **13**, (C) **16**, (D) **20**, (D) TMCPMP-TS, and (D) Phen. The arrow shows the changes of intensity upon the increasing amount of compound.

Table 4.2. DNA binding parameters of the complexes

Complex	Apparent binding constant $K_{app} M^{-1}$	Stern-volmer constant $K_{sv} M^{-1}$	Bimolecular constant $K_q M^{-1} s^{-1}$
1	-	1.14×10^3	1.14×10^{11}
2	0.66×10^6	5.54×10^3	5.54×10^{11}
3	0.66×10^6	1.01×10^3	1.01×10^{11}
4	-	8.0×10^3	8.0×10^{11}
5	0.16×10^6	5.0×10^3	5.0×10^{11}
6	-	2.0×10^3	2.0×10^{11}
7	-	1.0×10^3	1.0×10^{11}
8	-	6.0×10^3	6.0×10^{11}
9	0.19×10^6	7.0×10^3	7.0×10^{11}
10	0.28×10^6	8.0×10^3	8.0×10^{11}
11	0.16×10^6	6.0×10^3	6.0×10^{11}
12	0.14×10^6	4.0×10^3	4.0×10^{11}
13	0.12×10^6	4.0×10^3	4.0×10^{11}
14	-	-	-
15	-	-	-
16	1.3×10^6	3.91×10^4	3.91×10^{12}
17	0.9×10^6	2.72×10^4	2.72×10^{12}
18	0.28×10^6	0.1×10^5	0.1×10^{13}
19	-	0.03×10^5	0.03×10^{13}
20	1.1×10^6	1.3×10^5	1.3×10^{13}
21	0.5×10^6	0.12×10^5	0.12×10^{13}
22	-	0.10×10^5	0.10×10^{13}
23	0.2×10^6	0.05×10^5	0.05×10^{13}
32	-	1.56×10^5	1.56×10^{13}

Progressively
Increase

Quenching data were analyzed according to the Stern-Volmer equation for the complex as well as for the ligands. The plot of F_0/F versus $[Q]$ for one of the complexes and its corresponding ligands is shown in Fig. 4.12. The values of stern-volmer constants were found to be $1.3 \times 10^5 M^{-1}$ (**20**), $0.6 \times 10^5 M^{-1}$ (TMCPMP-TS) and $0.8 \times 10^5 M^{-1}$ (1, 10, Phenanthroline). The values are in good agreement with the constants observed for typical classical intercalators (ethidium–DNA, $1 \times 10^7 M^{-1}$). The diminution of the intrinsic binding constants could be explained by the steric constraints imposed by the ligand framework and thus encouraging a partial intercalation binding mode for the complex. The figures also show that the ratio of quenching of the intensities in all complexes is different. Our results are consistent with earlier reports on preferential binding to DNA in the Cu complexes [80, 81, 84].

Further, the apparent binding constant (K_{app}) values obtained for the complex using the following eq 3 (section 4.2.2) and the data are listed in Table 4.2.

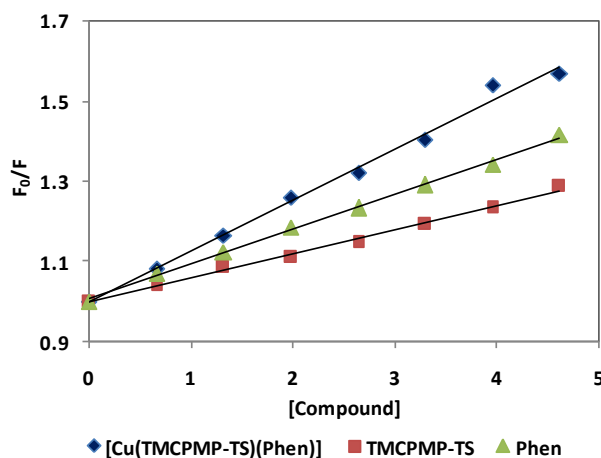


Fig. 4.12. Plot of F_0/F vs concentration for complex and ligands in buffer solution on increasing amount of DNA (150 mM NaCl and 15 mM trisodium citrate at pH 7.04) ($\lambda_{em}=610$ nm)

4.3.3. Viscosity measurements

Optical photophysical probes provide necessary, albeit not sufficient, insight to support a binding model. Hydrodynamic measurements, i.e. viscosity and sedimentation that are sensitive to length changes are regarded as the least ambiguous and most critical tests to a binding model in solution in the absence of crystallographic structural data [85]. A classical intercalation model usually results in lengthening of the DNA helix as base pairs are separated to accommodate the bound ligand, leading to an increase in the DNA viscosity. In contrast, semi-intercalation of a ligand could bend or kink the DNA helix, and thus reduce its effective length and, concomitantly, its viscosity. A classical intercalation mode causes a significant increase in viscosity of DNA due to an increase in separation of base pairs at intercalation sites and hence an increase in overall DNA length [86].

The viscosity measurements were studied for the binary complexes containing 4-toluoyl pyrazolones and also for simple complexes containing thiosemicarbazone based pyrazolones.

4.3.3.1. Viscosity measurements for binary complexes containing 4-toluoyl pyrazolones

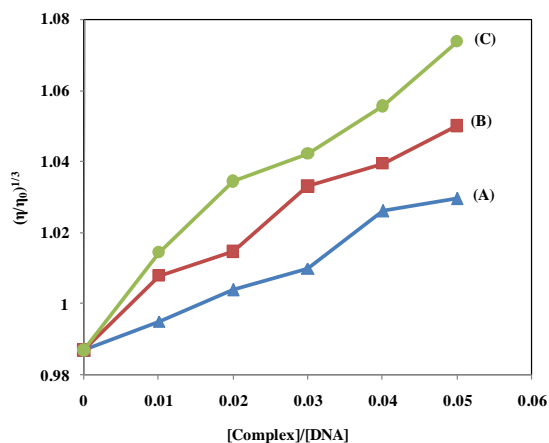


Fig. 4.13. Effect of increasing amounts of (A) **1**, (B) **2** and (C) **3** on the relative viscosities of DNA at 30.0 ± 0.1 °C. $[\text{DNA}] = 1$ mM, $[\text{Complex}]/[\text{DNA}] = 0, 0.01, 0.02, 0.03, 0.04, 0.05, 0.06$, respectively

The changes in the relative viscosity of rod-like DNA in the presence of these complexes are shown in Fig. 4.13. The viscosity of DNA increases greatly with increasing concentration of complex, which is similar to that of the proven intercalator EtBr [87]. This observation suggests that the principal mode of DNA binding by complexes involve base-pair intercalation, with one ligand intercalating into the base pairs and the other ligand being left outside the helix [88]. The intercalative interaction with DNA is related to the molecular structure, as in this complex there is a little distorted plane that may lead to the weak intercalative mode. This result also parallels the pronounced emission enhancement of both complexes and is comparable with the proven classical intercalator EtBr. On the basis of the viscosity results, the complexes bind with DNA through the intercalation mode. The increased degree of viscosity, which may depend on its affinity to DNA follows the order of EtBr > **3** > **2** > **1**, which is consistent with the results of Cu(II) complex proposes to be bound to DNA by intercalation [89].

4.3.3.2. Viscosity measurements for simple complexes containing pyrazolone based thiosemicarbazone

The changes in the relative viscosity of DNA in presence of increasing amount of the **16** and **17** are presented in Fig. 4.14. Ethidium bromide (EtBr), a known DNA classical intercalator, increases the relative specific viscosity of DNA double helix due to lengthening of helix axis owing to its intercalative binding mode. In presence of increasing amount of the complexes, the relative viscosity of DNA increases steadily [90]. However, this increase is rather less as compared to classical intercalators EtBr.

The increasing degree of viscosity follows the order EtBr > **16** > **17**. On the basis of viscosity results, at first glance, the increase in the viscosity of DNA appears to result from the intercalative interactions but the increase is quiet less than that for potential intercalator viz; EtBr with the same concentration ranges of DNA.

Thus, we conclude that, although the complexes exhibit affinity for the intercalative site on DNA but the binding affinity to a lower extent than EtBr. These results indicate that the complexes bring conformational changes in a manner, probably due to the steric matching of the DNA grooves and the complexes resulting in some partial intercalation of the complexes within the hydrophobic DNA pockets through the aromatic rings. This aggregation of the complexes into the groove of DNA helix inducing partial intercalative interactions causes an extension of the DNA helix with concomitant increase in its viscosity. Thus, the above results cumulatively indicate that the complexes bind to DNA in the groove regions [91]. Moreover, the increase in viscosity observed for complex **16** (Fig. 4.14 A) is more pronounced as compared to complex **17** (Fig. 4.14 B), indicating that complex **16** bind more strongly with DNA than complex **17**.

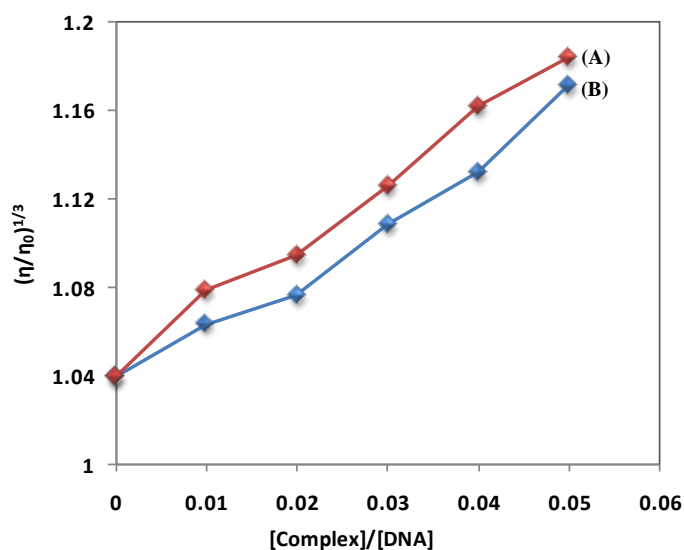


Fig. 4.14. Effect of increasing amounts of (A) **16** and (B) **17** on the relative viscosities of DNA at 30.0 ± 0.1 °C. [DNA] = 1 mM, [Complex]/[DNA] = 0, 0.01, 0.02, 0.03, 0.04, 0.05, 0.06, respectively

4.4. DNA cleavage activities of the compounds under investigation

It is well documented [92] that there are specific chemical compounds that can specifically recognize and cut DNA. The potential scope of utility of these compounds is enormous and range from the creation of synthetic restriction enzymes for use by molecular biologists to the development of chemotherapeutic agents that might be effective against a variety of diseases including cancer. More appropriately both the naturally occurring DNA cleavage agents and man-made compounds that can specifically recognize and cut DNA have been termed as chemical nucleases [93]. Since DNA cleavage is one of the important mechanism to arrest the growth of bacteria and viruses, in the control of diseases particularly cancer, there is considerable current interest in the development of reagents suitable for cleaving DNA. Further, most often the natural products prove to be toxic to the cells and hence great efforts are directed towards the design of synthetic analogs capable of cleaving DNA in a similar manner without exhibiting the associated toxicity.

Though many workers have reported several mechanisms for action of DNA cleavage such as (a) photolytic formation of phenyl cations [94], (b) alkylation of the

purines and (c) hydrolytic cleavage of double-stranded DNA involving a phosphodiester bond [92] and abstraction of a C-50 hydrogen from thymidylate and adenylate residues [95], the mechanism of action of Cu(II) complexes on DNA cleavage is underway. In order to assess the competence of the Cu(II) complexes for DNA strand scission, DNA was incubated with both Cu(II) complexes under identical reaction conditions. The cleavage reaction was monitored by gel electrophoresis. The delivery of high concentrations of metal ion to the helix, in locally generating oxygen or hydroxide radicals, leads to an efficient DNA cleavage reaction.

The characterization of DNA recognition by transition metal complexes has been aided by the DNA cleavage chemistry that is associated with redox-active or photoactivated metal complexes. DNA cleavage is controlled by relaxation of supercoiled circular form of DNA into nicked circular form and linear form. When circular plasmid DNA is conducted by electrophoresis, the fastest migration will be observed for the supercoiled form (Form I). If one strand is cleaved, the supercoiled will relax to produce a slower-moving open circular form (Form II). If both strands are cleaved, a linear form (Form III) will be generated that migrates in between. The cleavage studies have been carried out for few of the synthesized complexes.

4.4.1. Hydrolytic cleavage

Copper(II) complexes are able to cleave DNA through both oxidative and hydrolytic processes. The possibility of a hydrolytic mechanism for the DNA cleavage by the four complexes must be taken into account. Since complexes satisfy one of the primary criteria for catalyzing hydrolytic cleavage of DNA, i.e., coordination of the phosphate moiety of DNA to the copper(II) center of complex, its DNA cleaving ability has been investigated with various concentrations of the complexes. Interestingly, complexes are found to hydrolytically cleave DNA in the absence of any reducing agent or light. Figs. 4.15 & 4.16 show the results of the gel electrophoresis experiment carried out with supercoiled DNA in the absence and presence of complexes. Lane 1 in the figures (Figs. 4.15 & 4.16) shows the control DNA without any added complexes. In the absence of the complex, DNA remains in the supercoiled form while incubation of DNA with the complex leads to its

conversion to form II. Also in the presence of Cu-salt, no cleavage is observed (Lane 2 in Figs. 4.15 & 4.16).

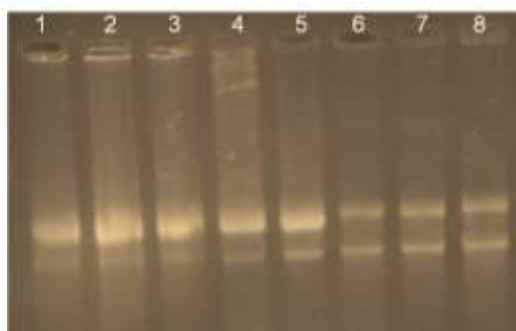


Fig. 4.15. Hydrolytic cleavage of DNA induced by **16** Lane 1, untreated DNA; lane 2, DNA + 60 μM Cu-acetate; lane 3, DNA + 10 μM complex; lane 4, DNA + 20 μM complex; lane 5, DNA + 30 μM complex; lane 6, DNA + 40 μM complex; lane 7, DNA + 50 μM complex; lane 8, DNA + 60 μM complex

Fig. 4.15 shows DNA cleavage in the presence of complex **16**. It was observed that the complex can cleave DNA with increase in the concentration. As shown in Fig. 4.15, with the increase of the concentrations of the complex, the supercoiled DNA decreases and nicked form gradually increases. The results indicate that the DNA cleavage activity of the complexes is obviously complex concentration dependent. It is also observed that the distance between two forms increases with the increase in the complex concentration. Fig. 4.16 shows the cleavage of DNA in the presence of **17**. It was observed that complex can cleave DNA effectively in a region of micromolar concentration, as evidenced by the disappearance of Form I and then disappearance of the Form II (lanes 3-8). The distance between two forms also increases. When the concentration of the complex reached to 50 μM , complete cleavage was observed. It is clear that the degradation of DNA is highly dependent on the concentration of the complex used.

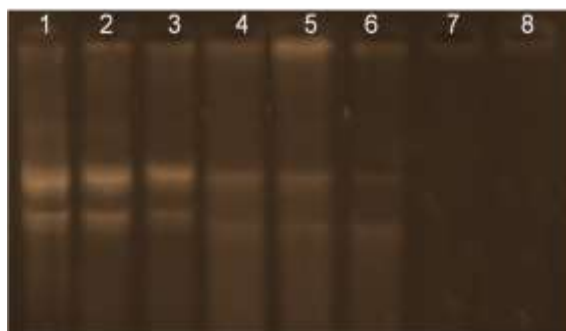


Fig. 4.16. Hydrolytic cleavage of DNA induced by **17** Lane 1, untreated DNA; lane 2, DNA + 60 μM Cu-acetate; lane 3, DNA + 10 μM complex; lane 4, DNA + 20 μM complex; lane 5, DNA + 30 μM complex; lane 6, DNA + 40 μM complex; lane 7, DNA + 50 μM complex; lane 8, DNA + 60 μM complex.

Based on our results and literature [96], the bonds between Cu(II) and labile carboxylate and/or phenolate oxygen of amino acid Schiff base could break under experimental conditions followed by simultaneous coordination of Cu(II) to the phosphate oxygen of DNA backbone by utilizing the strong Lewis acid property of Cu in +2 oxidation state which results in the breakage of the phosphodiester bond of DNA [97].

4.4.2. Oxidative cleavage

4.4.2.1. Oxidative cleavage by binary complexes of 4-toluoyl pyrazolones

The electrophoresis clearly revealed that all complexes act on DNA as there was molecular weight difference between the control and the treated DNA samples. The Cu(II) complexes in the presence of H_2O_2 as an oxidizing agent show high nuclease activity with DNA. As a sequel to find out whether any of these synthesized complexes would exhibit DNA cleavage activities *in vitro*, their effect at concentrations of 10-50 μM (lanes 4-8) was studied using DNA and the results are shown in Figs. 4.17, 4.18 & 4.19, respectively. In case of complexes **1** and **2**, we found similar results, while complex **3** gives different pattern. The difference between these two bands was also observed indicating the formation of linear DNA (form III).

As shown in Fig. 4.17, with the increase of the **1** concentration, the intensity of the nicked (Form II) band was found decrease and simultaneously, the circular super coiled DNA (Form I) band was also found decrease. When the complex

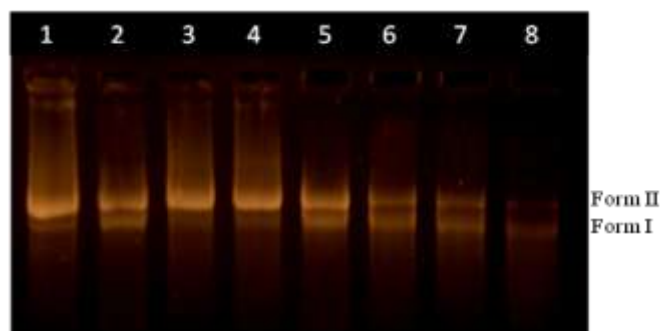


Fig. 4.17. Cleavage of DNA induced by **1** : Lane 1, untreated DNA; lane 2, DNA + 3 μ l H_2O_2 ; lane 3, DNA + 50 μ M complex; lane 4, DNA + 10 μ M complex + 3 μ l H_2O_2 ; lane 5, DNA + 20 μ M complex + 3 μ l H_2O_2 ; lane 6, DNA + 30 μ M complex + 3 μ l H_2O_2 ; lane 7, DNA + 40 μ M complex + 3 μ l H_2O_2 ; lane 8, DNA + 50 μ M complex + 3 μ l H_2O_2 .

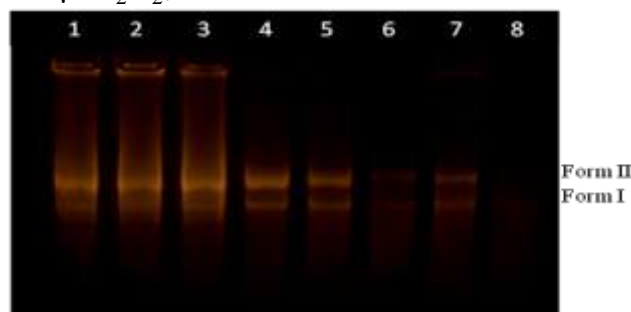


Fig. 4.18. Cleavage of DNA induced by **2**: Lane 1, untreated DNA; lane 2, plasmid DNA + 3 μ l H_2O_2 ; lane 3, DNA + 50 μ M complex; lane 4, DNA + 10 μ M complex + 3 μ l H_2O_2 ; lane 5, DNA + 20 μ M complex + 3 μ l H_2O_2 ; lane 6, DNA + 30 μ M complex + 3 μ l H_2O_2 ; lane 7, DNA + 40 μ M complex + 3 μ l H_2O_2 ; lane 8, DNA + 50 μ M complex + 3 μ l H_2O_2 .

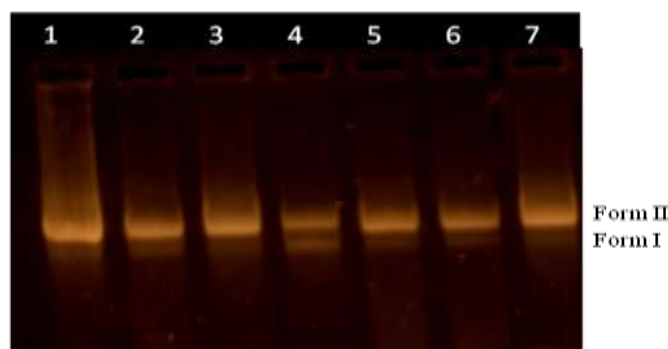


Fig. 4.19. Cleavage of DNA induced by **3**: Lane 1, untreated DNA; lane 2, plasmid DNA + 3 μ l H_2O_2 ; lane 3, DNA + 50 μ M complex; lane 4, DNA + 10 μ M complex + 3 μ l H_2O_2 ; lane 5, DNA + 20 μ M complex + 3 μ l H_2O_2 ; lane 6, DNA + 30 μ M complex + 3 μ l H_2O_2 ; lane 7, DNA + 40 μ M complex + 3 μ l H_2O_2 .

concentration was up to 50 μM (lane 8), the circular super coiled DNA (Form I) band was extremely faint, while the nicked (Form II) band was almost disappeared. Fig. 4.18 shows that on increasing the concentration of **2**, we found the result similar to **1**. But the difference was, when the complex concentration was up to 50 μM (lane 8), the circular super coiled DNA (Form I) and nicked (Form II) band were disappeared completely. **3** shows different cleavage than **1** and **2**. As shown in Fig. 4.19 with increase of **3** concentration, the super coiled DNA (Form I) apparently convert to nicked (Form II). These results are similar to that observed for some Cu-salen complexes as chemical nuclease [98]. It is likely the generation of hydroxyl radical and/or activated oxygen mediated by the copper complex results in DNA cleavage. Further studies are required to clarify the cleavage mechanism.

4.4.2.2. Oxidative cleavage by binary complexes of 4-toluoyl pyrazolones based thiosemicarbazone

The electrophoresis clearly revealed that both complexes act on DNA as there was molecular weight difference between the control and the treated DNA samples.

The Cu(II) complexes in the presence of H_2O_2 as an oxidizing agent show high nuclease activity with DNA. As a sequel to find out whether any of these synthesized compounds would exhibit DNA cleavage activities in vitro, their effect at concentrations of 10-50 μM (lanes 4-8) was studied using DNA and the results are shown in Figs. 4.20 & 4.21, respectively. Figures show the results of resolution of DNA on gel electrophoresis experiment carried out with DNA in the absence and presence of both complexes individually. Lane 1 in the figure shows the control DNA without any additives. However, the nature of reactive intermediates involved in DNA cleavage by the complexes is not clear. The results indicated the important role of metal in these isolated DNA cleavage reactions. Incubation of DNA with H_2O_2 (5 μM) or with complex (50 μM) alone does not bring about any apparent cleavage of DNA, as seen in lanes 2 & 3. Moreover, since the complex is not able to induce any effect on double stranded DNA (Lane 3), it appears that an oxidizing agent is required for producing cleavage. The DNA cleavage of complexes alone is inactive in the presence and absence of any external agents. The results indicate the importance of the metal in the complex for observing the chemical nuclease activity.

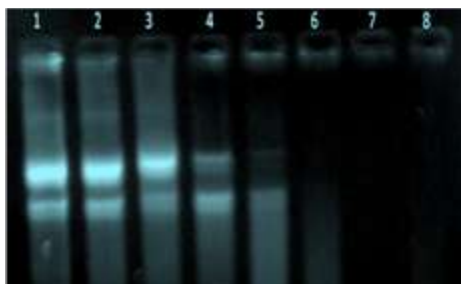


Fig. 4.20. Cleavage of DNA induced by **16** Lane 1, untreated DNA; lane 2, DNA + 5 μ l H_2O_2 ; lane 3, DNA + 50 μ M complex; lane 4, DNA + 10 μ M complex + 5 μ l H_2O_2 ; lane 5, DNA + 20 μ M complex + 5 μ l H_2O_2 ; lane 6, DNA + 30 μ M complex + 5 μ l H_2O_2 ; lane 7, DNA + 40 μ M complex + 5 μ l H_2O_2 ; lane 8, DNA + 50 μ M complex + 5 μ l H_2O_2 .



Fig. 4.21. Cleavage of DNA induced by **17** Lane 1, untreated DNA; lane 2, DNA + 5 μ l H_2O_2 ; lane 3, DNA + 50 μ M complex; lane 4, DNA + 10 μ M complex + 5 μ l H_2O_2 ; lane 5, DNA + 20 μ M complex + 5 μ l H_2O_2 ; lane 6, DNA + 30 μ M complex + 5 μ l H_2O_2 ; lane 7, DNA + 40 μ M complex + 5 μ l H_2O_2 ; lane 8, DNA + 50 μ M complex + 5 μ l H_2O_2 .

A decrease in intensity of DNA was observed by varying the concentration of the complexes in presence of DNA and H_2O_2 . While the complex is treated with DNA in presence of H_2O_2 , the disappearance of circular form takes place (lanes 4 & 5). After the disappearance of circular form, at last super coiled form disappears (lane 6). While at 40 & 50 μ M concentrations, the percent DNA cleavage activity occurred as evidenced by the total disappearance of DNA (lanes 7 & 8). However, as to the optimization of conditions like substrate concentration, concentration of the DNA, temperature, period of incubation, pH, etc., more detailed experiments are required to be carried out. A decrease in intensity of DNA (lanes 4 & 5) is a reflection of the mild DNA cleavage activity of the compound. The decrease in luminescence intensity in the presence of DNA by complex employed in the present study could be due to DNA

cleavage activity besides oxidation of guanine base. Thus the mono-copper complexes are promising candidates as chemical nucleases to cleave DNA with far reaching consequences.

4.5. Protein binding studies

Protein binding studies have been carried out for most of the complexes as well as their corresponding ligands. The data are listed in Table 4.3.

The tryptophan emission quenching experiments were carried out using bovine serum albumin (BSA) in the presence of complexes and ligands to investigate their interaction with proteins. Qualitative analysis of the binding of chemical compounds to BSA is usually detected by inspecting the fluorescence spectra. Generally, the fluorescence of BSA is caused by two intrinsic characteristics of the protein, namely tryptophan and tyrosine. Changes in the emission spectra of tryptophan are common in response to protein conformational transitions, subunit associations, substrate binding, or denaturation. Therefore, the intrinsic fluorescence of BSA can provide considerable information on their structure and dynamics and is often utilized in the study of protein folding and association reactions. The emission intensity depends on the degree of exposure of the two tryptophan side chains, 134 and 212, to polar solvent and also on its proximity to specific quenching groups, such as protonated carbonyl, protonated imidazole, deprotonated ϵ -amino groups, and tyrosinate anions. The quenching of emission intensity of BSA was observed in presence of complex because of possible changes in protein secondary structure leading to changes in tryptophan environment of BSA [64].

The interaction of BSA with complex was studied by fluorescence measurement at room temperature. A solution of BSA ($5 \mu\text{M}$) was titrated with various concentrations of the compounds (μM). The effects of one of the complexes and its respective ligands on the fluorescence emission spectrum of BSA are shown in Fig. 4.22. The addition of the compounds to the solution of BSA resulted in a significant decrease of the fluorescence intensity of BSA at 343 nm. This result suggested a definite interaction of the compounds with the BSA protein [78].

Table 4.3 (a). Protein binding parameters of the complexes

Complex	Stern-volmer constant $K_{sv} M^{-1}$	Bimolecular constant $K_q M^{-1} s^{-1}$
1	-	-
2	-	-
3	-	-
4	1.03×10^5	1.03×10^{13}
5	1.15×10^5	1.15×10^{13}
6	1.77×10^5	1.77×10^{13}
7	2.13×10^5	2.13×10^{13}
8	1.13×10^5	1.13×10^{13}
9	1.58×10^5	1.58×10^{13}
10	2.32×10^5	2.32×10^{13}
11	2.42×10^5	2.42×10^{13}
12	5.95×10^5	5.95×10^{13}
13	3.24×10^5	3.24×10^{13}
14	-	-
15	-	-
16	-	-
17	-	-
18	3.17×10^5	3.17×10^{13}
19	2.57×10^5	2.57×10^{13}
20	1.7×10^5	1.7×10^{13}
21	3.11×10^5	3.11×10^{13}
22	2.57×10^5	2.57×10^{13}
23	3.45×10^5	3.45×10^{13}

Table 4.3 (b). Protein binding parameters of the ligands

Ligand	Stern-volmer constant $K_{sv} M^{-1}$	Bimolecular constant $K_q M^{-1} s^{-1}$
TPMP	0.2×10^5	0.2×10^{13}
TMCPMP	0.4×10^5	0.4×10^{13}
TPTPMP	-	-
Phen	0.6×10^5	0.6×10^{13}
Bipy	0.12×10^5	0.12×10^{13}
PPMP	0.13×10^5	0.13×10^{13}
PMCPMP	0.15×10^5	0.15×10^{13}
PPTPMP	0.13×10^5	0.13×10^{13}
TMCPMP-TS	1×10^5	1×10^{13}
TPTPMP-TS	0.7×10^5	0.7×10^{13}
TPMP-TS	-	-

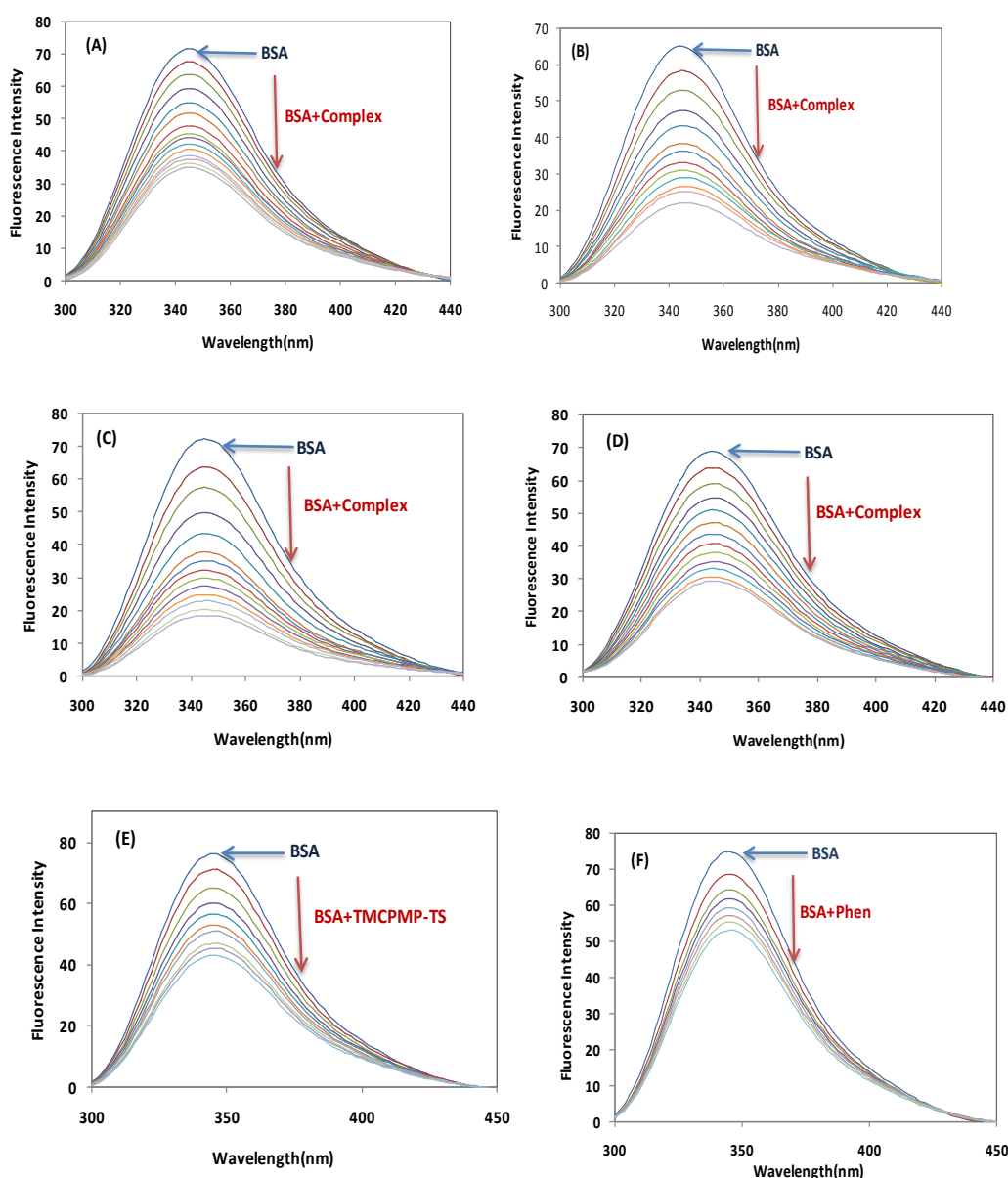


Fig. 4.22. Changes in the fluorescence spectra of BSA through its titration with (A) 5, (B) 10, (C) 12, (D) 20, (E) TMCPMP-TS and (F) Phen at RT. The concentration of protein is 5 μM , and complex concentration was varied from 0-20 μM ; pH 7.04 and λ_{ex} 296 nm.

Quenching can occur by different mechanisms, which are usually classified as dynamic quenching and static quenching; dynamic quenching refers to a process in which the fluorophore and the quencher come into contact during the transient existence of the excited state. Static quenching refers to fluorophore-quencher

complex formation in the ground state. The stern-volmer constants were calculated for this system and the values are listed in Table 4.3. These constants were calculated from the slope of the plot F_0/F versus [Compound]. (Fig. 4.23) The K_{sv} values suggest that the complexes have higher binding propensity than ligands. The bimolecular constants K_q were also calculated for the complexes and ligands and are presented in Table 4.3.

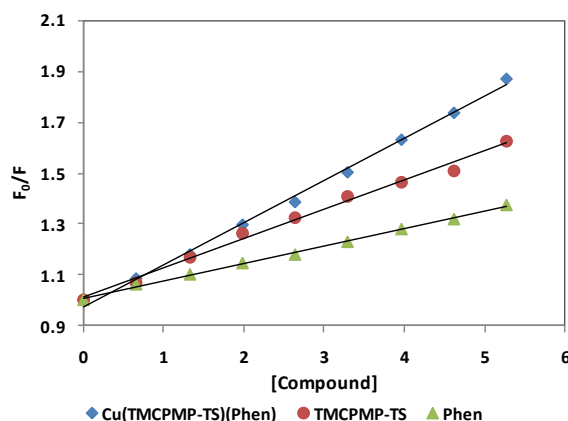


Fig. 4.23. Plot of F_0/F vs concentration of BSA in buffer solution on increasing amount of complex **20** and ligands (150 mM NaCl and 15 mM trisodium citrate at pH 7.04).

4.6. Anti cancer studies of the synthesized complexes

Some of the complexes have been screened for their anti cancer studies.

4.6.1. MTT Assay

The *in vitro* antiproliferative activity of complexes was estimated in human lung carcinoma cells (A549 cell line). The complexes were incubated with A549 cells at a wide range of concentrations (from 0 to 250 μ M) that inhibits the cell growth. It is known that the ability of cells to reduce MTT (methylthiazole tetrazolium) provides an indication of mitochondrial metabolic activity which, in turn, can be used as a measure of viability and/or cell number. As shown in Figs. 4.24, 4.25 & 4.26, complexes showed the antiproliferative activity in dose dependent manner, and it was highest at 150-300 μ M.

Similar cytotoxicity test (MTT assay) was also executed with rat cardiomyocytes (H9C2 cells) wherein, the cells were cultured in presence of

Cu(TMCPMP)(Phen). The rationale behind choosing H9C2 cells was to assess the possible cytotoxicity of complexes against a normal cell line as sensitive as rat cardiomyocytes. It was noted that complex treated cells revealed no significant cell death as evidenced by the results obtained that was comparable to that of control as shown in Figs. The same needs further investigation to probe into the underlying mechanism. Such selective inhibition on relevant cancer cells may be potentially useful in directing screen of effective anticancer agents in clinic applications. However, the anticancer activity of complexes is possibly attributable to its ability to bring about conformational changes and cleavage of cellular DNA and their ability to bind to the cellular proteins involved in inducing cancer.

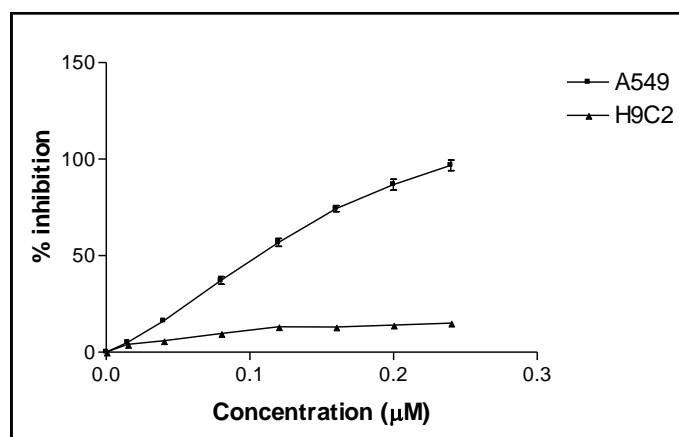


Fig. 4.24. Effect of **20** exposed to A549 cells on cell viability. Results are expressed as Mean \pm SEM for n = 3 (replicates)

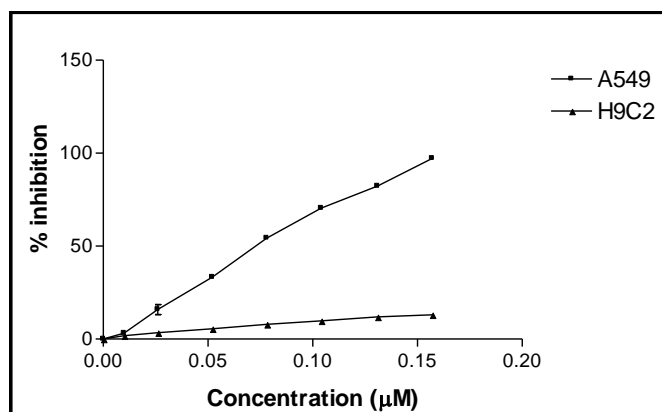


Fig. 4.25. Effect of **32** exposed to A549 cells on cell viability. Results are expressed as Mean \pm SEM for n = 3 (replicates)

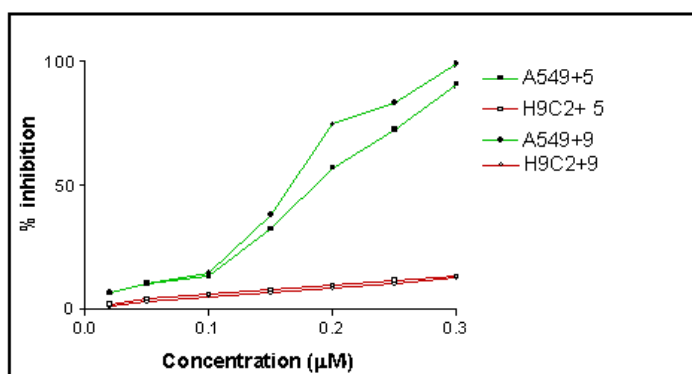


Fig. 4.26. Effect of complexes exposed to A549 cells on cell viability. Results are expressed as Mean \pm SEM for n = 3 (replicates)

4.6.2. LDH Release Assay

Further, the cytotoxic nature of complexes (Figs. 4.27, 4.28 & 4.29) was assessed by LDH release assay. The cytoplasmic enzyme LDH released from the cells and it can be correlated with cell death. LDH enzyme leaches out of dead cells and hence quantification of its content in culture media indirectly reveals extent of cell damage [99, 100]. The amount of LDH released from the cells increases with the exposure of complexes to the cells in dose dependent manner and it was highest in cells treated with complexes in the range of 150-300 μ M.

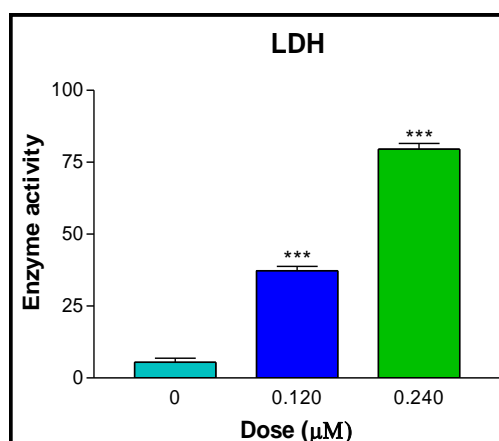


Fig. 4.27. Effect of **20** exposed to A549 cells on LDH release. Results are expressed as Mean \pm SEM for n = 3 (replicates). Where, ns $p > 0.05$, * $p < 0.05$, ** $p < 0.01$ and

*** $p < 0.001$ compared to 0 μ g/ml Cu(TMCPMP-TS)(Phen)

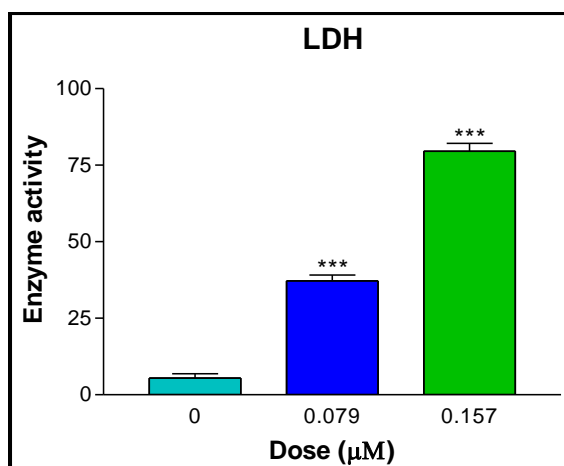


Fig. 4.28. Effect of **32** exposed to A549 cells on LDH release. Results are expressed as Mean \pm SEM for n = 3 (replicates). Where, ns p > 0.05, * p < 0.05, ** p < 0.01 and *** p < 0.001 compared to 0 $\mu\text{g/ml}$ Cu(TPMP-BA)₂

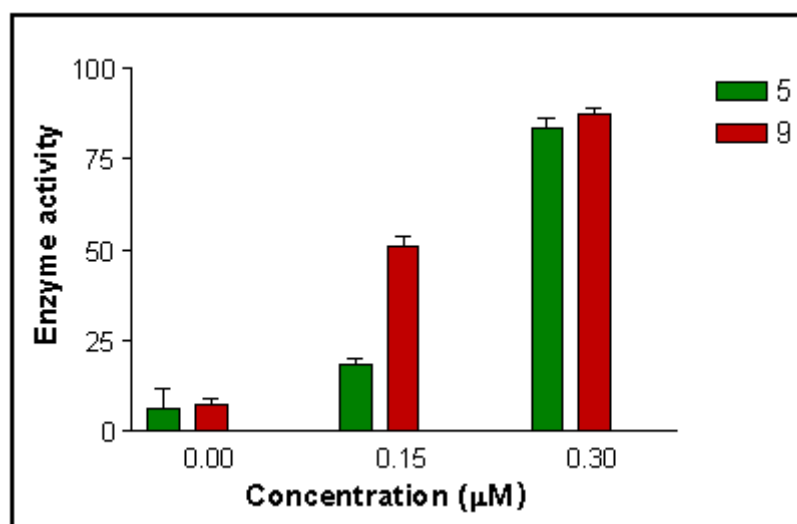


Fig. 4.29. Effect of complexes exposed to A549 cells on LDH release. Results are expressed as Mean \pm SEM for n = 3 (replicates). Where, ns p > 0.05, * p < 0.05, ** p < 0.01 and *** p < 0.001 compared to 0 μM complexes

4.6.3. Measurement of Mitochondrial Membrane Potential

A distinctive feature of the early stages of programmed cell death is the disruption of active mitochondria. This mitochondrial disruption includes changes in the membrane potential and alterations to the oxidation–reduction potential of the

mitochondria. Changes in the membrane potential are presumed to be due to the opening of the mitochondrial permeability transition pore (MPTP), allowing passage of ions and small molecules. The resulting equilibration of ions leads in turn to the decoupling of the respiratory chain and the release of cytochrome c into the cytosol. Rhodamine 123 is lipophilic cations used as indicator dye, which accumulates in mitochondria. The fluorescent intensity is in proportion to the energy state of the mitochondria. Treatment of A549 cells with complexes resulted in a dose dependent decrement as compared to the untreated cells (Figs. 4.30, 4.31 & 4.32). These results revealed that exposure of A549 cells to complexes inducing the drop of $\Delta\Psi_{mt}$ may be a possible cause for the apoptotic process.

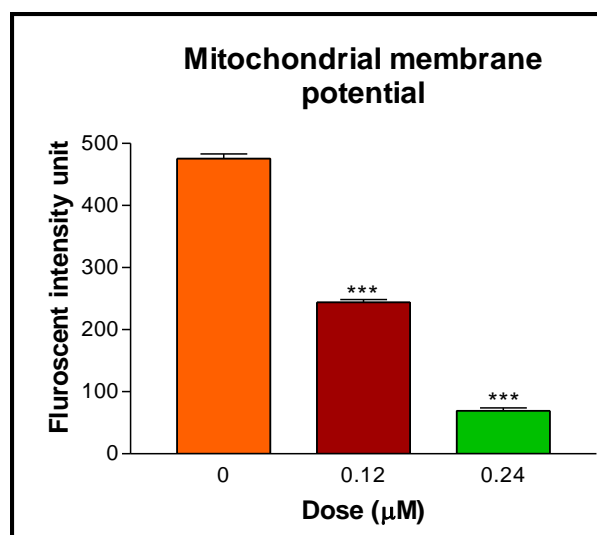


Fig. 4.30. Effect of **20** exposed to A549 cells on Mitochondrial membrane potential. Results are expressed as Mean \pm SEM for n = 3 (replicates). Where, ns p > 0.05, * p < 0.05, ** p < 0.01 and *** p < 0.001 compared to 0 μM Cu(TMCPMP-TS)(Phen)

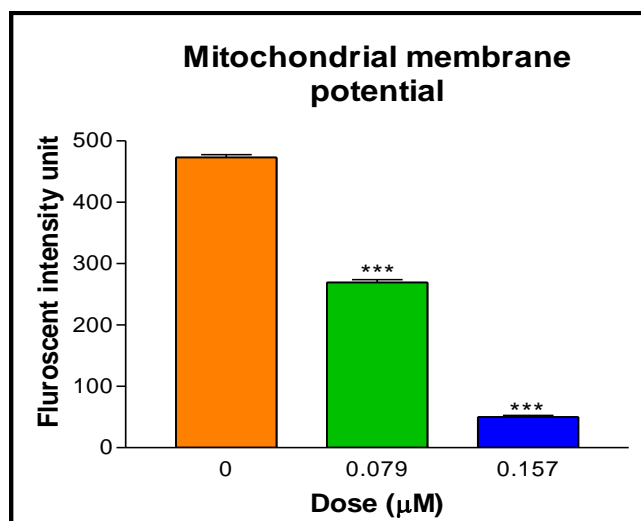


Fig. 4.31. Effect of **32** exposed to A549 cells on Mitochondrial membrane potential. Results are expressed as Mean \pm SEM for n = 3 (replicates). Where, ns p > 0.05, * p < 0.05, ** p < 0.01 and *** p < 0.001 compared to 0 μM Cu(TPMP-BA)₂

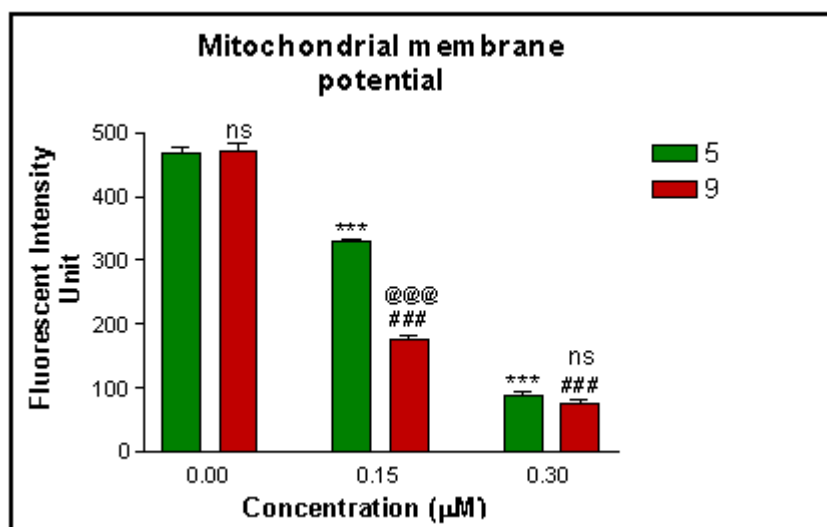
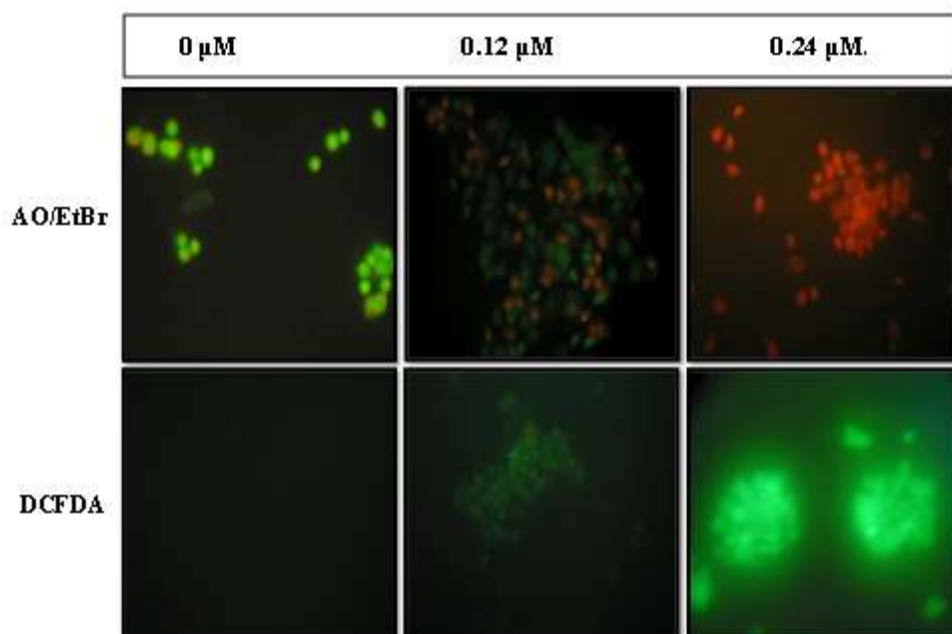
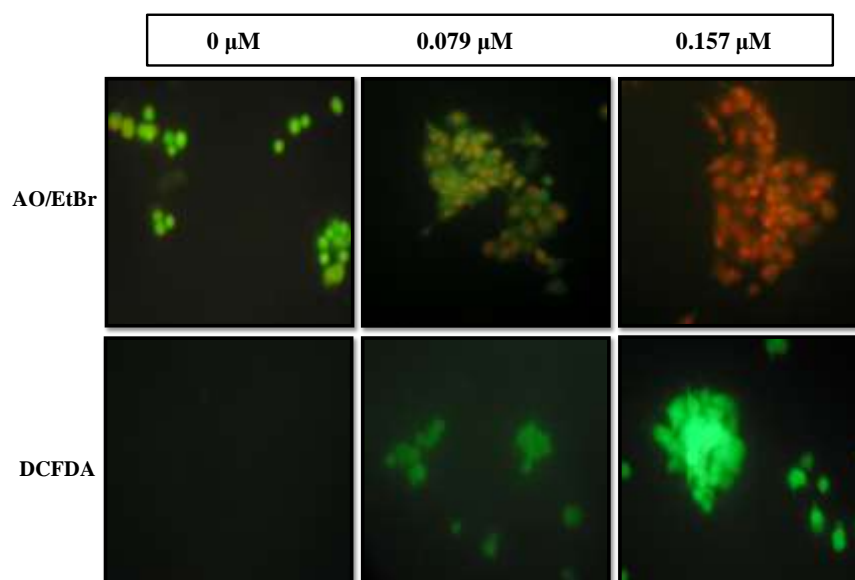


Fig. 4.32. Effect of complexes exposed to A549 cells on Mitochondrial membrane potential. Results are expressed as Mean \pm SEM for n = 3 (replicates). Where, ns p > 0.05, * p < 0.05, ** p < 0.01 and *** p < 0.001 compared to 0 μM complexes

4.6.4. Intracellular ROS generation (DCFDA staining)**Fig. 4.35.** Fluorescence photomicrographs of A549 cells exposed to **20****Fig. 4.36.** Fluorescence photomicrographs of A549 cells exposed to **32**

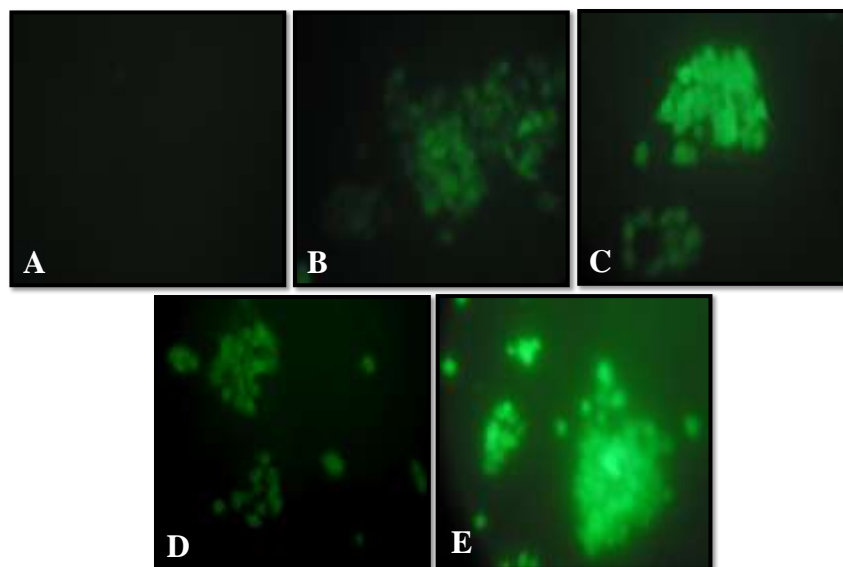


Fig. 4.37. Florescence photomicrographs of DCFDA staining of A549 cells exposed to (A) control, (B & C) **5** and (D & E) **9**

Intracellular ROS can trigger apoptosis *via* initiation of downstream signals in a cell cycle [101]. CM-H₂DCFDA is widely used to measure oxidative stress in cells. CM-H₂DCFDA is taken up by cells and de-acetylated by intracellular esterases to form the more hydrophilic nonfluorescent reduced dye dichlorofluorescein DCFH, which then is rapidly oxidized to form a two-electron oxidation product, the highly fluorescent DCF in a reaction with the oxidizing species (H₂O₂) [102, 103]. In the present study, complex treatment showed dose dependent increment in green fluorescence of A549 cells and there was most prominent fluorescence recorded in the range 0.150-130 μ M dose (Figs. 4.35, 4.36 & 4.37) which indicates that complexes elevate intracellular oxidative stress and are instrumental in generation of intracellular ROS in a dose dependent manner.

4.6.5. AO/EB staining

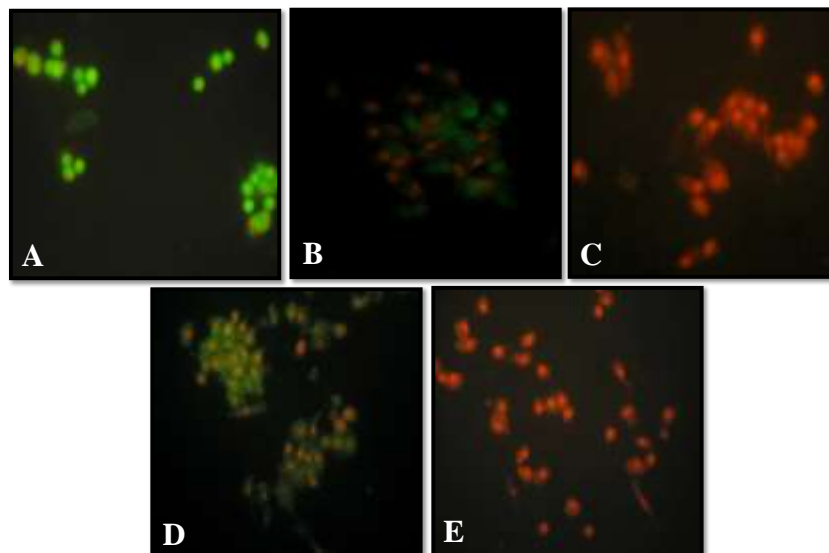


Fig. 4.38. Fluorescence photomicrographs of AO/EtBr staining of A549 cells exposed to (A) control, (B & C) 5 and (D & E) 9

Acridine Orange stains live cells (green) whereas, ethidium Bromide stains dead cells (red-to-orange) and hence this method of dual staining enables rapid and easy recognition/differentiation of live-dead cells when visualized under a fluorescence microscope [104]. The present study showed a dose dependent increment in EtBr positive cells following complex treatment as compared to untreated cells. Highest dose in the range of 0.150-250 μ M appeared to be the most potent in induction of cell death as evidenced by high EtBr positive and very less number of AO positive cells (Figs. 4.35, 4.36 & 4.38).

4.6.6. Nuclear morphology assay (DAPI staining)

It has been reported that cells undergoing apoptosis exhibit cytoplasmic blebbing, nuclear shrinkage, chromatin condensation, irregularity in shape and retraction of processes [105]. DAPI binds to the AT rich regions of DNA and used to

distinguish the compact compact chromatin of apoptotic nuclei from that of normal cells. As shown in Figs. 4.39, 4.40 & 4.41, exposure of A549 cell to complexes resulted in appearance of more number of cells with condensed nuclei compared with control cells.

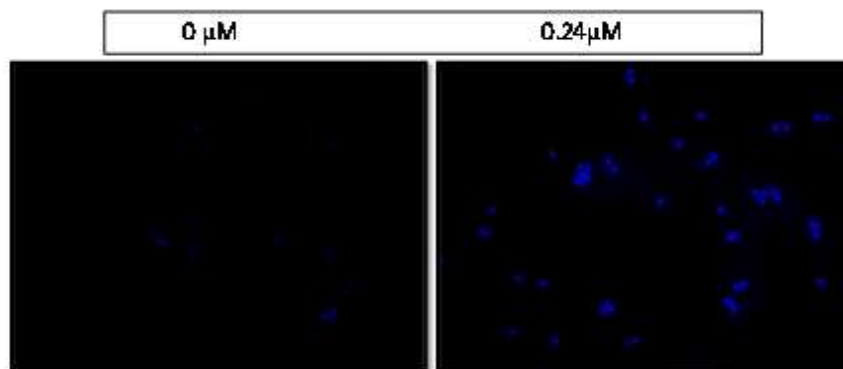


Fig. 4.39. Florescence photomicrographs of DAPI staining of A549 cells exposed to
20

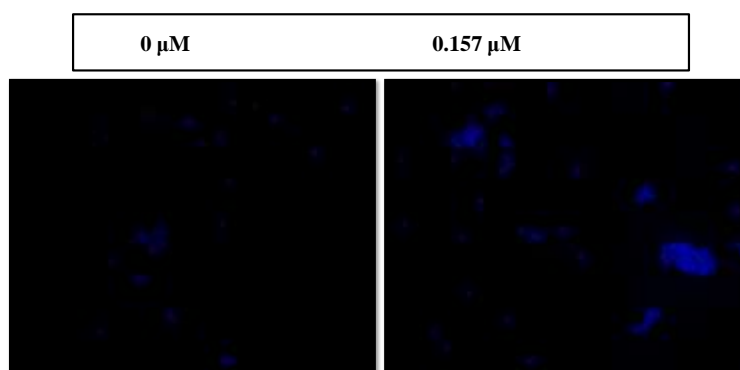


Fig. 4.40. Florescence photomicrographs of DAPI staining of A549 cells exposed to
32

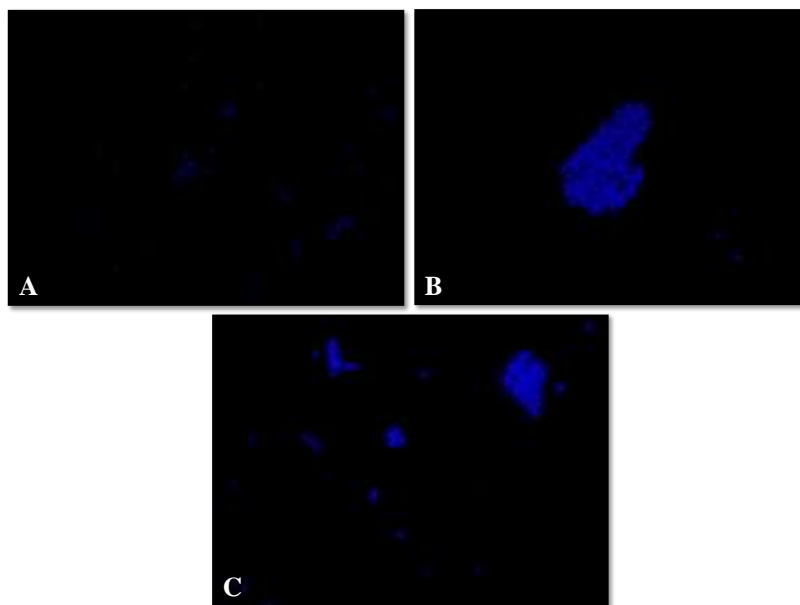


Fig. 4.41. Fluorescence photomicrographs of DAPI staining of A549 cells exposed to (A) control, (B) **5** and (C) **9**

4.6.7. Cell cycle analysis

The underlying mechanism involved in the inhibition of growth of A549 cells exposed to complexes was examined by assessment of cell cycle; a method that is based on evaluation of cellular DNA content [72]. It showed that cells having a hypodiploid DNA content (sub-G1 material) that is characteristic of apoptosis and reflects fragmented DNA as shown in Figs. 4.42, 4.43 & 4.44. The majority of control cells were in Sub G0/G1 phase around 3 %, G0/G1 phase around 93%, S phase around (2%) and G2+M around (1.5) whereas, in the range of 150-250 μ M complexes treated cells were increased in Sub G0/G1 and decreased in G0/G1 phase. Increased Sub G0/G1 phase suggested DNA fragmentation and the G2-M and S phases were slightly decreased after the treatment, indicating that it may induce the G0/G1 growth arrest A549 cells. These results indicate that complexes induced apoptosis is likely to involve the modulation of cell cycle progression.

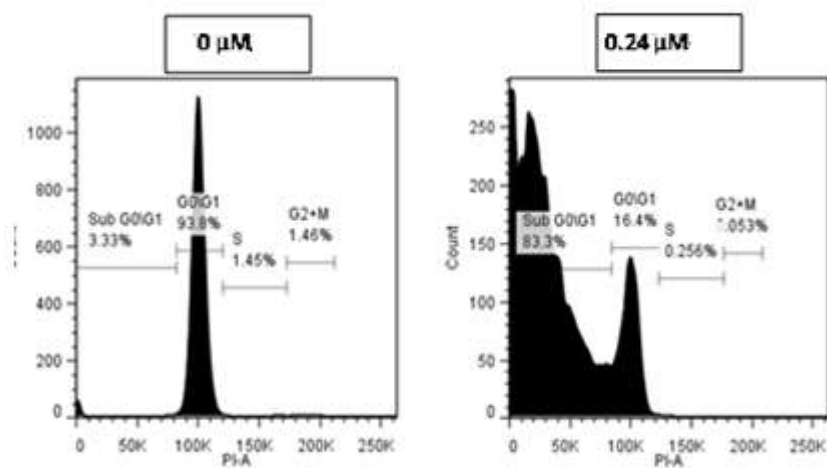


Fig. 4.42. Cell cycle analysis of A549 cells exposed to 20

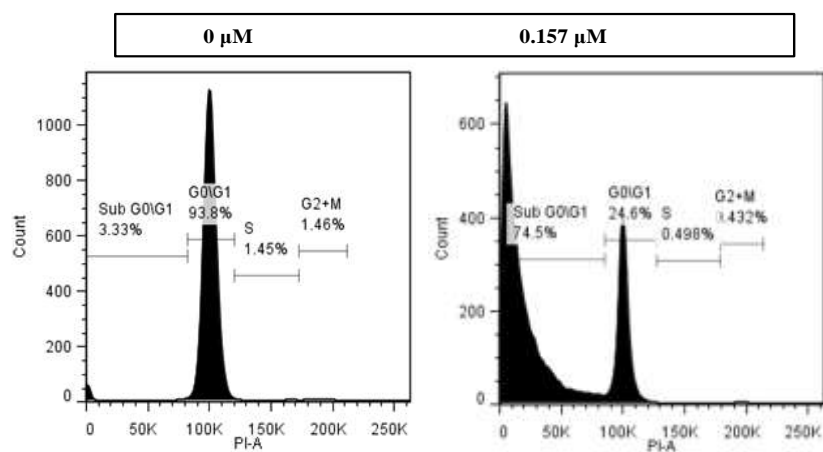


Fig. 4.43. Cell cycle analysis of A549 cells exposed to 32

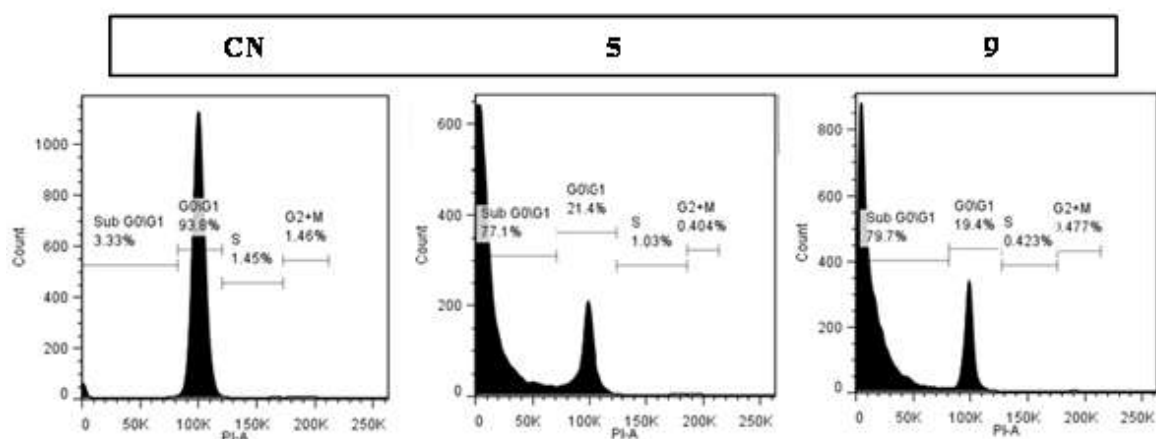


Fig. 4.44. Cell cycle analysis of A549 cells exposed to complexes

4.6.8. FITC Annexin-V/PI Staining

Apoptosis is a process of cell death characterized by various morphological and biochemical alteration leading to cell disruption and formation of apoptotic bodies. One of the hallmarks of apoptosis is that membrane phospholipid such as phosphatidylserine rearrange from inner to outside surface of the plasma membrane and gets exposed on cell surface. The same can be detected due to its high affinity for annexin V. This assay is based on the ability of the protein annexin V to bind to phosphatidylserine (PS) exposed on the outer membrane leaflet in apoptotic cells (PS also appears on the necrotic cell surface). In viable cells, PS is located in the inner membrane leaflet, but upon induction of apoptosis it is translocated to the outer membrane leaflet and becomes available for annexin V binding. The addition of PI enabled viable ($\text{AnnV}^{\text{neg}}/\text{PI}^{\text{neg}}$), early apoptotic ($\text{AnnV}^{\text{poz}}/\text{PI}^{\text{neg}}$), late apoptotic ($\text{AnnV}^{\text{poz}}/\text{PI}^{\text{poz}}$) and necrotic ($\text{AnnV}^{\text{neg}}/\text{PI}^{\text{poz}}$) cells to be distinguished. Flow cytometric assay with Annexin V/PI double staining of control and complexes treated cells showed that apoptosis rate was increased with complex treatment wherein, the treated cells recorded higher % annexin V positive (early apoptotic) and lower % PI positive cells (late apoptotic) (Figs. 4.45 & 4.46).

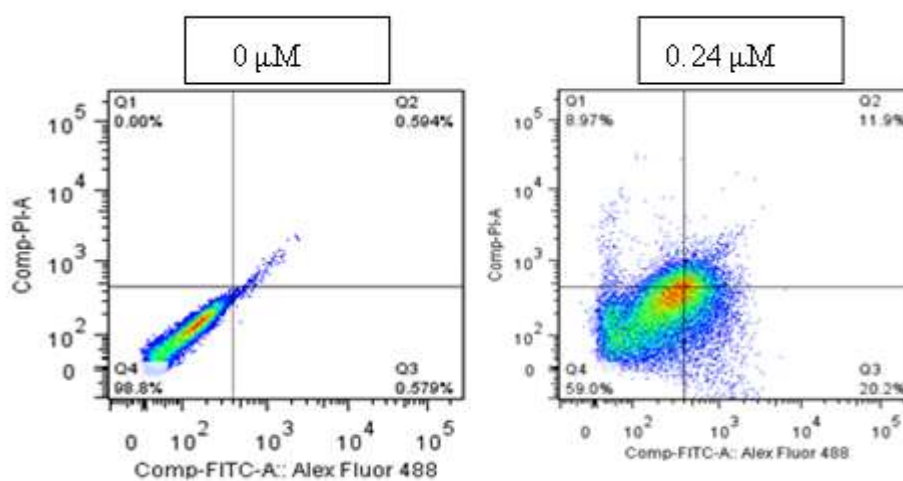


Fig. 4.45. Annexin V-Alexa fluoro 488/PI staining of A549 cells exposed to 20

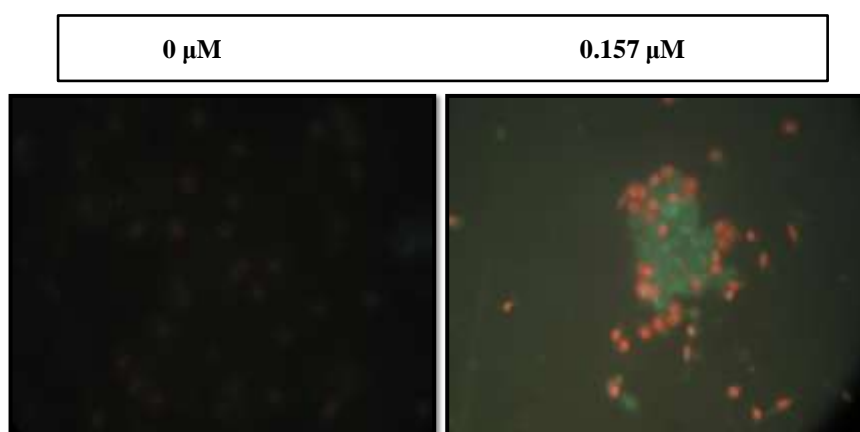


Fig. 4.46. Annexin V-Alexa fluoro 488/PI staining of A549 cells exposed to 32

Conclusions

One of the most rapidly developing areas of pharmaceutical research is discovery of drugs for cancer therapy. Lung cancer has been estimated as the most common cancer in the world for several decades. In this view, we have synthesized different types of Cu(II) complexes. These complexes have bio-active ligands and so we considered that these can be a series of good anti-cancer drugs. DNA is a primary target molecule for any drug discovery. In this regards, the interaction of our complexes with CT-DNA have been studied by absorption titration, ethidium bromide displacement study and viscosity measurements. It suggested that the complexes have good binding capacity with CT-DNA. Artificial nuclease activity has been ascertained by gel electrophoretic mobility assay; the complexes display efficient cleavage activity of DNA converting the Form I to Form II and ultimately to leading to the formation of linearized Form III with increasing concentrations of the complex. The DNA cleavage activity of some of the complexes has been studied by both hydrolytic and oxidative pathways. We found that the complexes can cleave the DNA even in the absence of any external indicator and the cleavage. This work presents a good overall correlation between DNA binding and DNA cleavage activity of the complexes. The results are of importance towards further designing and developing Cu(II) based complexes and systematic assessment of DNA binding, cleavage activity for their potential applications as therapeutic agents. Further, the interaction of these complexes with bovine serum albumin (protein) has also been studied by tryptophan quenching assay. It suggested the higher binding of the complexes with this protein. Generally, the weak binding leads to a shorter lifetime or poor distribution, while strong binding decreases the concentration of free drug in plasma. Because of these, studies on this aspect can provide information on the structural feature that determines the therapeutic effectiveness of drugs and standardized screens for protein binding in new drug design and for fixing dose limits. The anticancer activity of the complexes on A549 (human lung cancer) cell line has been studied. Anticancer study also revealed high grade of cytotoxicity and cell cycle arrest in sub G0/G1 phase implying to the potency of complexes as an anticancer agents against A549 lung carcinoma

cells. Results envisaged herein indicate that complexes hold sufficient merit to develop it as a therapeutic agent against cancer.

The presence of copper with a daily intake not exceeding 4-7 mg is safe and can minimize the above diseases. Therefore, it is appropriate to design anticancer drugs based on copper, which is anticipated to cause lower toxic effects. In this context, we have started to develop ternary complexes of Cu(II) that are expected to be less toxic but highly potent in smaller dosage compared to cisplatin and analogous compounds.

Literature cited.

- [1] www.who.int, *World Health Organization*, 2005.
- [2] B. A. Chabner, T. G. Roberts, *Nat. Rev. Cancer* 5 (2005) 65.
- [3] J. Ferlay, H. R. Shin, F. Bray, D. Forman, C. Mathers, D. M. Parkin, *Int. J. Cancer*, 127(12) (2010) 2893.
- [4] J. Ferlay, H. R. Shin, F. Bray, D. Forman, C. Mathers, D. M. Parkin, *GLOBOCAN 2008 v1.2, Cancer Incidence and Mortality Worldwide: IARC CancerBase No. 10 [Internet]. Lyon, France: International Agency for Research on Cancer, 2010.* Available from: <http://globocan.iarc.fr>. Accessed May 2011.
- [5] WHO. WHO Global Health Observatory. World Health Organisation, (2010).
- [6] UN. World Population Prospects: The 2008 Revision. United Nations, Department of Economic and Social Affairs, Population Division (2009).
- [7] D. M. Parkin, J. Stjernsward, C. S. Muir, *Bull. World Health Organ.* 62(2) (1984) 163.
- [8] D. M. Parkin, E. Laara, C. S. Muir, *Int. J. Cancer* 41(2) (1988) 184.
- [9] D. M. Parkin, P. Pisani, J. Ferlay, *Int. J. Cancer* 54(4) (1993) 594.
- [10] D. M. Parkin, P. Pisani, J. Ferlay, *Int. J. Cancer* 80(6) (1999) 827.
- [11] D. M. Parkin, F. Bray, J. Ferlay, P. Pisani, *Int. J. Cancer* 94(2) (2001) 153.
- [12] R. Doll, A. B. Hill, *Br. Med. J.* 2 (1950) 739.
- [13] IARC. World Cancer Report 2008: IARC, (2008).
- [14] WHO. WHO report on the Global Tobacco Epidemic, 2009: implementing smoke-free environments. Geneva: World Health Organisation, (2009).
- [15] WHO. WHO report on the Global Tobacco Epidemic, 2008: the MPOWER package. Geneva: World Health Organisation, (2008).
- [16] J. D. Watson, F. H. C. Crick, *Nature* 171 (1953) 737.
- [17] (a) V. A. Bloomfield, D. M. Crothers, I. Tinoco, *Nucleic Acids: Structure, Properties, and Functions*. University Science Books: Sausalito, California, 2000; (b) T. Wang, DNA recognition and cleavage by phenyl-benzimidazole modified gly-glyhis-derived metalloptides, M. Sc. Thesis submitted to the Purdue University, Indianapolis, Indiana, May 2010; (c) Leeju P, DNA interaction and catalytic activity studies of some new transition metal complexes of Schiff bases derived from

Quinoxaline, Ph. D. Thesis submitted to Cochin University of Science and Technology, April 2012.

[18] (a) C. E. Mathieu, Chiral lanthanide complexes as probe of nucleic acids, Ph. D. Thesis submitted to Durham University, Available at Durham E-Theses Online: <http://etheses.dur.ac.uk/3812/> (2001); (b) F. T. Boyle, G. F. Costello, *Chemical Society Reviews*, 27 (1998) 251.

[19] R. S. Hawley, C. A Mori, *The Human Genome*, 1999, Ed. Academic Press, 21-44.

[20] U. Diederichsen, *Angew. Chem. Int. Ed.*, 37 (1998) 1655.

[21] W. D. Wilson In: G. M. Blackburn, M. J. Gait (eds) *Nucleic acids in chemistry and biology*. Oxford University Press, Oxford (1996) 329.

[22] J. A. Mountzouris, L. H. Hurely In: S. M. Hecht Ed, *Bioorganic chemistry: nucleic acids*. OXFORD University Press, New York, (1996) 288

[23] J. A. Cowan, *Curr. Opin. Chem. Biol.* 5 (2001) 634.

[24] L. N. Ji, X. H. Zou, J. G. Liu, *Coord. Chem. Rev.* 216 (2001) 513.

[25] H. Mei, J. Barton, *J Am Chem Soc.*, 108 (1986) 7414.

[26] J. Kelly, A. Tossi, D. McComell, *Nucl. Acids. Res.*, 13 (1985) 6017.

[27] L. S. Lerman, *J. Mol. Biol.* 3 (1961) 18.

[28] B. H. Geierstanger, D. E. Wemmer, R. Annu, *Biophys. Biomol. Struct.* 24 (1995) 463.

[29] B. A. Armitage, *Top Curr. Chem.* 253 (2005) 55.

[30] T.-C. Tang, H.-J. Huang, *Electroanalysis*, 11 (1999) 1185.

[31] H. W. Zimmermann, *Angew. Chem. Int. Ed.*, 25 (1986) 115.

[32] (a) Le Pecq, C. Paoletti, *Anal. Biochem*, 17 (1966) 100; (b) K. G. Strothkamp, R. E. Strothkamp, *J. Chem. Educ.* 71 (1990) 77.

[33] (a) E. Fredericq, C. Houssier, *Biopolymers*, 11 (1972) 2281; (b) B. Gardner, S. Mason, *Biopolymers*, 5 (1967) 79.

[34] (a) J. M. Rosenberg, N. C. Seeman, R. O. Day, A Rich, *J. Mol. Biol.*, 104 (1976) 145; (b) H. M. Berman, W. Stallings, H. L. Carrell, J. P. Glusker, S. Neidle, G. Taylor, A Achari, *Biopolymers*, 18 (1979) 2405.

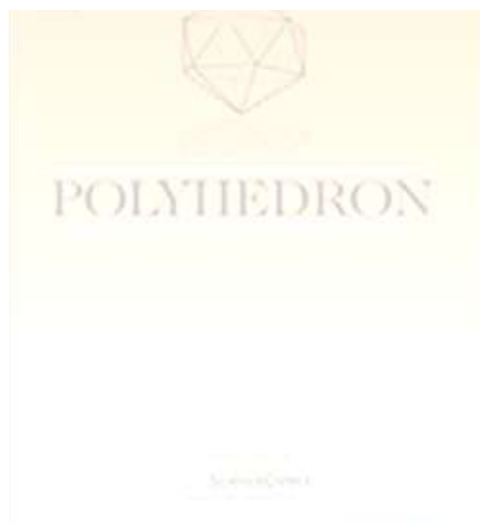
[35] G. Felsenfeld, D. R. Davies, A Rich, *J. Am. Chem. Soc.*, 79 (1957) 2023.

- [36] (a) M. Teng, N. Usman, C. A. Frederick, A. H. J. Wang, *Nucleic Acids Res.* 16 (1988) 2671; (b) N. Spink, D. G. Brown, J. V. Skelly, S. Neidle, *Nucleic Acids Res.*, 22 (1994) 1607;
- (c) A. A. Wood, C. M. Nunn, A. Czamy, D. W. Boykin, S. Neidle, *Nucleic Acids Res.*, 23 (1995) 3678.
- [37] D. M. Hermann, E. E. Baird, P. B. Dervan, *Chem. Eur. J.*, 5 (1999) 975.
- [38] a) J. M. Gottesfeld, L. Nealy, J. W. Trauger, E. E. Baird, P. B. Dervan, *Nature*, 387 (1997) 202. b) L. A. Dickinson, R. J. Gulizia, J. W. Trauger, E. E. Baird, D. E. Mosier, J. M. Gottesfeld, P. B. Dervan, *Proc. Natl. Acad. Sci. USA*, 95 (1998) 12890.
- [39] a) S. Kamitori, F. Takusagawa, *Journal of Mol. Biol.* 225 (1992) 445. b) S. Kamitori, F. Takusagawa, *J. Am. Chem. Soc.*, 116 (1994) 4154.
- [40] D. C. Carter, J. X. Ho, *Adv. Protein Chem.* 45 (1994) 153.
- [41] Y.-Z. Zhang, J. Dai, X. Xiang, W.-W. Li, Y. Liu, *Mol. Biol. Rep.* 37 (2010) 1541.
- [42] A. Sulkowska, *J. Mol. Struct.*, 614 (2002) 227.
- [43] K. Hirayama, S. Akashi, M. Furuya, K. Fukuhara, *Biochim. Biophys. Res. Commun.* 173 (1990) 639.
- [44] T. J. Peters, *Adv. Protein Chem.*, 37 (1985) 161.
- [45] U. Kragh-Hansen, *Pharmacol. Rev.*, 33 (1981) 17.
- [46] B. Sandhya, A. H. Hegde, S. S. Kalanur, U. Katrahalli, J. Seetharamappa, *J. Pharm. Biomed. Anal.*, 54 (2011) 1180.
- [47] J. Tian, Y. Zhao, X. Liu, S. Zhao, *Luminescence*, 24 (2009) 386.
- [48] (a) Y.-Z. Zhang, B. Zhou, Y.-X. Liu, C.-X. Zhou, X.-L. Ding, Y. Liu, *J. Fluoresc.*, 18 (2008) 109; (b) Available at http://en.wikipedia.org/wiki/MTT_assay.
- [49] E. Bonfoco, D. Krainc, M. Ankarcona, *Proc. Natl. Acad. Sci. USA* 92 (1995) 7162.
- [50] G. Haslam, D. Wyatt, P. A. Kitos, *Cytotechnology*, 32 (2000) 63.
- [51] H. T. Wolterbeek, J. G. M. Van der Meer, *ASSAY and Drug Development Technologies*, 3(6) (2005) 675.
- [52] D. L. Spector, R. D. Goldman, L. A. Leinwand, *Cell: a laboratory manual: culture and biochemical analysis of cells*, Cold Spring Harbor Laboratory Press, New York, 1998, 1, 34.1–34.9.

- [53] A. H. Wyllie, Apoptosis: an overview. *Br. Med. Bull.* 53 (1997) 451.
- [54] M. J. Arends, R. G. Morris, A. H. Wyllie, *Am. J. Pathol.*, 136 (1990) 593.
- [55] K. S. Sellins, J. J. Cohen, *J. Immunol.* 139 (1987) 3199.
- [56] J. Gong, F. Traganos, Z. Darzynkiewicz, *Anal. Biochem.* 218 (1994) 314.
- [57] R. Nunez, *Curr. Issues Mol. Biol.* 3 (2001) 67.
- [58] C. A. Wallen, R. Higashikubo, L. A. Dethlefsen, *Cytometry* 3 (1982) 155.
- [59] A. Pollack, G. Ciancio, *Cell. Biol.* 33 (1990) 19.
- [60] M. G. Ormerod, M. K. Collins, G. Rodriguez-Tarduchy, D. Robertson, *J. Immunol. Methods* 153 (1992) 57.
- [61] I. Schmid, C. H. Uittenbogaart, B. Keld, J. V. Giorgi, *J. Immunol. Methods* 170 (1994) 145.
- [62] A. H. Wyllie, R. G. Morris, A. L. Smith, D. Dunlop, *J. Pathol.* 142 (1984) 67.
- [63] Y. Gavrieli, Y. Sherman, S. A. Ben-Sasson, *J. Cell Biol.* 119 (1992) 493.
- [64] W.G. Telford, A. Komoriya, B. Z. Packard, *Cytometry* 47 (2002) 81.
- [65] M. E. Reichmann, S. A. Rice, C. A. Thomas, P. Doty, *J. Am. Chem. Soc.*, 76 (1954) 3047.
- [66] S. S. Bhat, A. A. Kumbhar, H. Heptullah, A. A. Khan, V. V. Gobre, S. P. Gejji, V. G. Puranik, *Inorg. Chem.* 50 (2011) 545.
- [67] J. R. Lakowicz, *Principles of Fluorescence Spectroscopy*; 3rd ed.; Springer Science+Business Media: New York, 2006.
- [68] M. Lee, A. L. Rhodes, M. D. Wyatt, S. Forrow, J. A. Hartley, *Biochemistry* 32 (1993) 4237.
- [69] M. C. Thounaojam, R. N. Jadeja, D. S. Dandekar, R. V. Devkar, A. V. Ramachandran, *Exp. Toxicol. Pathol.* 64 (2010) 217.
- [70] M. C. Thounaojam, R. N. Jadeja, R. V. Devkar, A. V. Ramachandran, *Cardiovasc Toxicol.* 11 (2011) 168.
- [71] R. N. Jadeja, M. C. Thounaojam, R. V. Devkar, A. V. Ramachandran, *Food Chem Toxicol.* 49 (2011) 1195
- [72] R. Carlo, N. Ildo, *Nature Protocols*, 1 (2006) 1458.
- [73] Q. Wang, Z.-Y. Yang, G.-F. Qi, D.-D. Qin, *Eur. J. Med. Chem.* 44 (2009) 2425.
- [74] C. S. Chow, J. K. Barton, *Methods Enzymol.* 212 (1992) 219.

- [75] B. D. Wang, Z. Y. Yang, P. Crewdson, D. Q. Wang, *J. Inorg. Biochem.* 101 (2007) 1492.
- [76] J. H. Tan, Y. Lu, Z. S. Huang, L. Q. Gu, J. Y. Wu, *Eur. J. Inorg. Chem.* 42 (2007) 1169.
- [77] J. Tan, B. Wang, L. Zhu, *Bioorg. Med. Chem.* 17 (2009) 614.
- [78] E. S. Koumoussi, M. Zampakou, C. P. Raptopoulou, V. Psycharis, C. M. Beavers, S. J. Teat, G. Psomas, T. C. Stamatatos, *Inorg. Chem.* 51 (2012) 7699.
- [79] J. B. Le Pecq, C. Paoletti, *J. Mol. Biol.* 27 (1967) 87.
- [80] F. Arjmand, M. Aziz, *Eur. J. Med. Chem.* 44 (2009) 834.
- [81] N. Raman, R. Jeyamurugan, A. Sakthivel, L. Mitu, *Spectrochim. Acta. Part A* 75 (2010) 88.
- [82] D. S. Raja, N. S. P. Bhuvanesh, K. Natarajan, *Inorg. Chem.* 50 (2011) 12852.
- [83] U. McDonnell, M.R. Hicks, M.J. Hannon, A. Rodger, *J. Inorg. Biochem.* 102 (2008) 2052.
- [84] S. Ramakrishnan, D. Shakthipriya, E. Suresh, V. S. Periasamy, M. A. Akbarsha, M. Palaniandavar, *Inorg. Chem.* 50 (2011) 6458.
- [85] S. Satyanarayana, J. C. Dabrowiak, J. B. Chaires, *Biochemistry* 32 (1993) 2573.
- [86] X. H. Zou, B. H. Ye, H. Li, Q. L. Zhang, H. Chao, J. G. Liu, L. N. Ji, X. Y. Li, *J. Biol. Inorg. Chem.* 6 (2001) 143.
- [87] Q.-L. Zhang, J.-G. Liu, H. Chao, G.-Q. Xue, L.-N. Ji, *J. Inorg. Biochem.* 83 (2001) 49.
- [88] P. Xi, Z. Xu, F. Chen, Z. Zeng, X. Zhang, *J. Inorg. Biochem.* 103 (2009) 210.
- [89] B. Peng, X. Chen, K.J. Du, B. LeYu, H. Chao, L. NianJi, *Spectrochim. Acta Part A* 74 (2009) 896.
- [90] Y. Li, Y. Wu, J. Zhao, P. Yang, *J. Inorg. Biochem.* 101 (2007) 283.
- [91] M. Roy, T. Bowmick, R. Santhanagopal, S. Ramakumar, A. R. Chakravarty, *Dalton Trans.*, (2009) 4671.
- [92] S. Dhar, P.A.N. Reddy, A. R. Chakravarty, *Dalton Trans.*, (2004)697-698.
- [93] A. Chin, M. H. Hung, L. M. Stock, *J. Org. Chem.* 46 (1981) 2203.
- [94] J. R. Hwu, C. C. Lin, S. H. Chuang, K. Y. King, T. Su, S. Tsay, *Bioorg. Med. Chem.* 12 (2004) 2509.

-
- [95] A. G. Myers, M. E. Kort, M. Hammond, *J. Am. Chem. Soc.* 119 (1997) 2967.
- [96] P. A. N. Reddy, M. Nethaji, A. R. Chakravarty, *Eur. J. Inorg. Chem.* (2004) 1440.
- [97] B. Selvakumar, V. Rajendiran, P. Uma Maheswari, H. Stoeckli-Evans, M. Palaniandavar, *J. Inorg. Biochem.* 100 (2006) 316.
- [98] D. Li, R. Cle'rac, O. Roubeau, *J. Am. Chem. Soc.* 130 (2008) 252.
- [99] G. Travis, B. W. Vicki, M. Roy, *Infect Immun.* 67 (1999) 4367.
- [100] M. Valodkar, R. N. Jadeja, M. C. Thounaojam, R. V. Devkar, S. Thakore, *Mat. Sci. Eng.* 31 (2011) 1723.
- [101] M. D. Evans, M. Dizdaroglu, M. S. Cooke, *Mutat Res* 567 (2004)1.
- [102] D. A. Bass, J. W. Parce, L. R. DeChatelet, P. Szejda, M. C. Seeds, M. Thomas, *J. Immunol.*, 130 (1983) 1910.
- [90, 103] W. O. Carter, P. K. Narayanan, J. P. Robinson, *J. Leukoc. Biol.* 55 (1994) 253.
- [104] Spector, D. L.; Goldman, R. D.; Leinwand, L. A. *Cell: a laboratory manual: culture and biochemical analysis of cells*, Cold Spring Harbor Laboratory Press, New York, **1998**, 1, 34.1–34.9.
- [105] G. M. Cohen, *Biochem. J.* 326 (1997) 1.



Publications



(I)



- [1] R. J. Yadav, **K. M. Vyas**, R. N. Jadeja, "Synthesis and spectral characterization of Cu(II) complexes of some Thio-Schiff bases of acyl pyrazolone analogues" **J. Coord. Chem.** 63 (2010) 1820–1831.
- [2] N. P. Moorjani, **K. M. Vyas**, R. N. Jadeja, "Synthesis & Characterization of Cu(II) complexes derived from acyl pyrazolones & 2-amino phenol" **PRAJÑĀ - Journal of Pure and Applied Sciences**, 18 (2010) 68-72 .
- [3] **K. M. Vyas**, V. K. Shah, R. N. Jadeja, "Synthesis and Characterization of Ni(II) complexes of some O,N donor Schiff bases derived from acyl pyrazolone analogues" **J. Coord. Chem.** 64 (2011) 1069–1081.
- [4] **K. M. Vyas**, R. N. Jadeja, V. K. Gupta, K. R. Surati, "Synthesis, characterization and crystal structure of some bidentate heterocyclic Schiff base ligands of 4-toluoyl pyrazolones and its mononuclear Cu(II) complexes" **J. Mol. Struct.** 990 (2011) 110–120.
- [5] **K. M. Vyas**, R. G. Joshi, R. N. Jadeja, C. Ratna Prabha, V. K. Gupta, "Synthesis, spectroscopic characterization and DNA nuclease activity of Cu(II) complexes derived from pyrazolone based NSO-donor Schiff base ligands, **Spectrochim. Acta A.**, 84 (2011) 256-268.
- [6] R. N. Jadeja, **K. M. Vyas**, V. K. Gupta, R.G. Joshi, C. Ratna Prabha Syntheses, characterization and molecular structures of calcium(II) and copper(II) complexes bearing O2-chelate ligands: DNA binding, DNA cleavage and anti-microbial study **Polyhedron** 31 (2012) 767-778.
- [7] R. N. Jadeja, S. Parihar, **K. Vyas**, V. K. Gupta, Synthesis and crystal structure of a series of pyrazolone based Schiff base ligands and DNA binding studies of their Copper complexes, **J. Mol. Struct.**, 1013 (2012) 86–94
- [8] N. Sharma, **K. M. Vyas**, R. N. Jadeja, Rajni Kant, V. K. Gupta, "2-Amino-7,7-dimethyl-5-oxo-4-(p-tolyl)-5,6,7,8-tetrahydro-4H-chromene-3-carbonitrile" **Acta Cryst. E.**, 68 (2012) o3036.

- [9] S. I. Thakore, J. Y. Soni, **K. Vyas**, R. N. Jadeja, R. V. Devkar, P. Rathore, "Synthesis and cytotoxicity evaluation of novel acylated starch nanoparticles" **Bioorg. Chem.** 46 (2013) 26-30.
- [10] Joseph V. A., **K. M. Vyas**, R. N. Jadeja, V. K. Gupta "Studies on DNA binding behavior of biologically active Cu(II) complexes of Schiff bases containing acyl pyrazolones and 2-ethanolamine" **J Coord. Chem.** (Accepted, GCOO-2012-0649).
- [11] **K. M. Vyas**, R. N. Jadeja, D. Patel, S. Desai, R. V. Devkar, V. K. Gupta, *Novel pyrazolone based ternary Cu(II) complex: Synthesis, characterization, crystal structure, DNA binding, protein binding and anti-cancer activity towards A549 human lung carcinoma cells with a minimum cytotoxicity to non-cancer cells* " **Eur. J. Med. Chem.**, (Communicated, EJMECH-D-12-02020).



Syntheses, characterization and molecular structures of calcium(II) and copper(II) complexes bearing O₂-chelate ligands: DNA binding, DNA cleavage and anti-microbial study

R.N. Jadeja^{a,*}, Komal M. Vyas^a, Vivek K. Gupta^b, Rushikesh G. Joshi^c, C. Ratna Prabha^c

^a Department of Chemistry, Faculty of Science, The M. S. University of Baroda, Vadodara 390 002, India

^b Post-Graduate Department of Physics, Jammu University, Jammutawi 180 006, India

^c Department of Biochemistry, Faculty of Science, The M. S. University of Baroda, Vadodara 390 002, India

ARTICLE INFO

Article history:

Received 16 September 2011

Accepted 2 November 2011

Available online 10 November 2011

Keywords:

O₂-donor ligands

Ca(II) and Cu(II) complexes

Crystal structures

DNA studies

Anti-microbial activity

ABSTRACT

A new set of supramolecular complexes, [Cu(PMP)₂] [1], [Cu(MCPMP)₂] [2] and [Cu(PTPMP)₂] [3] (PMP = 5-methyl-4-(4-methyl-benzoyl)-2-phenyl-2,4-dihydro-pyrazol-3-one, MCPMP = 2-(3-chloro-phenyl)-5-methyl-4-(4-methyl-benzoyl)-2,4-dihydro-pyrazol-3-one and PTPMP = 5-methyl-4-(4-methyl-benzoyl)-2-p-tolyl-2,4-dihydro-pyrazol-3-one) have been synthesized and characterized by elemental analysis, metal estimation, molar conductivity, IR, UV–Vis and TG-DTA. The molecular geometry of one of these complexes has been determined by single crystal X-ray study. The X-ray diffraction analyses of the complexes show that the Cu(II) ion center is four-coordinated. The interaction of Cu(II) complexes with pET30a plasmid DNA was investigated by viscosity and fluorescence spectroscopy. Results suggest that the copper complexes bind to DNA via an intercalative mode and can quench the fluorescence intensity of EB bound to DNA. The interaction between the complexes and DNA has also been investigated by agarose gel electrophoresis, interestingly, we found that the Cu(II) complexes can cleave circular plasmid DNA to nicked and super coiled forms. The complexes were screened for their anti microbial activity against Gram positive (*Bacillus subtilis*) and Gram negative (*Escherichia coli*). In the preparation of these complexes the acyl pyrazolone ligands are used and prepared by method suggested by Jensen. In contrast to conventional Claisen condensations, this method produces acyl derivative of the pyrazolone in good yield and is relatively easy to prepare. In these synthesis, condensations of acid chlorides with pyrazolones in dioxane, catalyzed by suspended calcium hydroxide results Ca(II) intermediate complex and then decomposition in 2 M hydrochloric acid to give acyl pyrazolone ligands. The intermediate Ca(II) complex, [Ca(PMP)₂(EtOH)₂], was isolated for the first time and its crystal structure is reported. The crystal structure of Ca(II) complex is stabilized by O–H...N, C–H...π and π–π stacking interactions.

© 2011 Elsevier Ltd. All rights reserved.

1. Introduction

DNA plays a fundamental role in the storage and expression of genetic information in a cell. DNA is not only an important biological material with a unique double helical rod like structure, but also an interesting anionic polyelectrolyte. DNA is a particularly good target for metal complexes as its base-pairs owns rich electrons. Therefore, transition metal complexes can bind to DNA in many modes such as electrostatic, groove and intercalative binding, etc. Among them, the intercalative mode is the most important mode in which transition metal complexes can intercalate between the pair-bases of double helix DNA, forming π–π overlapping interaction. It is this interaction that greatly affects and/or damages

DNA conventional behavior and so that these transition metal complexes possess a very broad application background in the field of bio-inorganic chemistry [1–3].

Studies pertaining to DNA cleavage by synthetic reagents are of considerable interest because of their utility tools in molecular biology. This has resulted in the development of both sequence specific DNA cleavers [4] and DNA foot printing agents [5]. In most of the cases, the cleavage of DNA was carried out by metal complexes or organic dyes. Transition metal complexes with their varied coordination environments and versatile redox and spectral properties are multi-utility model nucleases that are capable of cleaving DNA by both oxidative and hydrolytic cleavage pathways [5,6].

Pyrazolones constitute a group of organic compounds that have been extensively studied due to their properties and applications. Furthermore, 4-acyl-pyrazolone derivatives have the potential to form different types of coordination compounds due to the several

* Corresponding author. Tel.: +91 265 2795552.

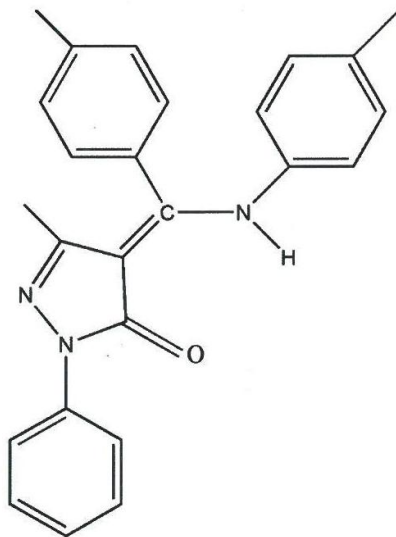
E-mail address: rajendra_jadeja@yahoo.com (R.N. Jadeja).

(Z)-3-Methyl-1-phenyl-4-[(p-tolyl)(p-tolylamino)methylidene]-1H-pyrazol-5(4H)-oneNaresh Sharma,^a Komal M. Vyas,^b R. N. Jadeja,^b Rajni Kant^a and Vivek K. Gupta^{a*}^aPost-Graduate Department of Physics & Electronics, University of Jammu, Jammu Tawi 180 006, India, and ^bDepartment of Chemistry, Faculty of Science, The M. S. University of Baroda, Vadodara 390 002, India
Correspondence e-mail: vivek_gupta2k2@hotmail.com

Received 17 September 2012; accepted 24 September 2012

Key indicators: single-crystal X-ray study; $T = 293$ K; mean $\sigma(\text{C}-\text{C}) = 0.003$ Å; R factor = 0.052; wR factor = 0.132; data-to-parameter ratio = 15.1.

In the title molecule, $\text{C}_{25}\text{H}_{23}\text{N}_3\text{O}_2$, the pyrazole ring forms dihedral angles of 28.56 (7), 80.35 (7) and 31.99 (7)° with the phenyl ring, the *p*-tolyl ring and the *p*-tolylamino ring, respectively. The N–H group attached to the exocyclic C=C bond is in a *syn* arrangement with respect to the C=O bond of the pyrazolone group and an intramolecular N–H...O hydrogen bond is observed. In the crystal, weak C–H... π interactions link molecules along [100].

Related literatureFor related structures, see: Vyas *et al.* (2011); Ma *et al.* (2006); Sun *et al.* (2007).**Experimental***Crystal data*

$\text{C}_{25}\text{H}_{23}\text{N}_3\text{O}$	$V = 2076.80$ (17) Å ³
$M_r = 381.46$	$Z = 4$
Monoclinic, $P2_1/n$	Mo $K\alpha$ radiation
$a = 9.2694$ (4) Å	$\mu = 0.08$ mm ⁻¹
$b = 18.3156$ (8) Å	$T = 293$ K
$c = 12.6716$ (7) Å	$0.30 \times 0.30 \times 0.20$ mm
$\beta = 105.124$ (5)°	

Data collection

Oxford Diffraction Xcalibur	9542 measured reflections
Sapphire3 diffractometer	4077 independent reflections
Absorption correction: multi-scan	2343 reflections with $I > 2\sigma(I)$
(<i>CrysAlis PRO</i> ; Oxford	$R_{\text{int}} = 0.039$
Diffraction, 2010)	
$T_{\text{min}} = 0.914$, $T_{\text{max}} = 1.000$	

Refinement

$R[F^2 > 2\sigma(F^2)] = 0.052$	H atoms treated by a mixture of independent and constrained refinement
$wR(F^2) = 0.132$	$\Delta\rho_{\text{max}} = 0.17$ e Å ⁻³
$S = 1.01$	$\Delta\rho_{\text{min}} = -0.14$ e Å ⁻³
4077 reflections	
270 parameters	

Table 1

Hydrogen-bond geometry (Å, °).

Cg is the centroid of the C7–C12 ring

$D-H\cdots A$	$D-H$	$H\cdots A$	$D\cdots A$	$D-H\cdots A$
$\text{N21}-\text{H21}\cdots\text{O5}$	0.99 (2)	1.82 (2)	2.702 (2)	146.4 (17)
$\text{C15}-\text{H15}\cdots\text{Cg}^i$	0.93	2.63	3.470 (2)	152

Symmetry code: (i) $x - 1, y, z$.

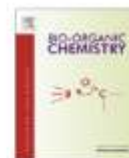
Data collection: *CrysAlis PRO* (Oxford Diffraction, 2010); cell refinement: *CrysAlis PRO*; data reduction: *CrysAlis PRO*; program(s) used to solve structure: *SHELXS97* (Sheldrick, 2008); program(s) used to refine structure: *SHELXL97* (Sheldrick, 2008); molecular graphics: *ORTEP-3* (Farrugia, 1997); software used to prepare material for publication: *PLATON* (Spek, 2009).

RK acknowledges the Department of Science & Technology for the single-crystal X-ray diffractometer sanctioned as a National Facility under project No. SR/S2/CMP-47/2003. VKG is thankful to the University of Jammu, Jammu, for financial support.

Supplementary data and figures for this paper are available from the IUCr electronic archives (Reference: LH5535).

References

- Farrugia, L. J. (1997). *J. Appl. Cryst.* **30**, 565.
 Ma, R.-M., Sun, S.-F. & Ng, S. W. (2006). *Acta Cryst.* **E62**, o4679–o4680.
 Oxford Diffraction (2010). *CrysAlis PRO*. Oxford Diffraction Ltd, Yarnton, England.
 Sheldrick, G. M. (2008). *Acta Cryst.* **A64**, 112–122.
 Spek, A. L. (2009). *Acta Cryst.* **D65**, 148–155.
 Sun, Y.-F., Li, J.-K., Wu, R.-T. & Zheng, Z.-B. (2007). *Acta Cryst.* **E63**, o2176–o2177.
 Vyas, K. M., Jadeja, R. N., Gupta, V. K. & Surati, K. R. (2011). *J. Mol. Struct.* **990**, 110–120.



Synthesis and cytotoxicity evaluation of novel acylated starch nanoparticles

Sonal Thakore^{a,*}, Mayur Valodkar^a, Jigar Y. Soni^a, Komal Vyas^a, Rajendrasinh N. Jadeja^a, Ranjitsinh V. Devkar^b, Puran Singh Rathore^a

^a Department of Chemistry, Faculty of Science, The Maharaja Sayajirao University of Baroda, Vadodra 390 002, Gujarat, India

^b Department of Zoology, Faculty of Science, The Maharaja Sayajirao University of Baroda, Vadodra 390 002, Gujarat, India

ARTICLE INFO

Article history:
Received 7 June 2012
Available online 13 October 2012

Keywords:
Acylated starch nanoparticles
Cytotoxicity
DNA binding

ABSTRACT

Starch nanoparticles (StNPs) were acylated under ambient conditions to obtain various nanosized derivatives formed stable suspension in water and soluble in organic solvents. The degree of substitution (DS) was determined using ¹H NMR technique. The cytotoxicity potential of the derivatised StNPs was evaluated in mouse embryonic fibroblast (3T3L1) cells and A549 tumor cell line using MTT cell viability assay. Other parameters that determine the oxidative stress viz., reactive oxygen species (ROS) generation, intracellular reduced glutathione (GSH), superoxide generation and acridine orange/ethidium bromide staining were also investigated. The present study led to the conclusion that cytotoxic activity of acylated starch nanoparticles was dependent on their dosage, DS and type of substitution. The non-toxic nature in non-cancerous cells reveals that the nanoparticles (NPs) can be used for cancer therapy and drug delivery. The nanoparticles also offered reasonable binding propensity with CT-DNA.

© 2012 Elsevier Inc. All rights reserved.

1. Introduction

Cytotoxic drugs continue to play a major role in cancer therapy but often produce side effects, especially through the destruction of lymphoid and bone marrow cells [1]. Therefore, strategic improvements in cancer therapy are needed to improve efficacy while decreasing side effects. Over the past decades, nanoparticles (NPs) have been of great interest in applications for biological fields such as drug delivery systems [2,3] and anticancer applications [4]. The antitumor activities of natural biopolymer chitosan and its NPs are well reported [5]. Another abundant polysaccharide starch, is relatively, more competent than chitosan due to its low cost, easy availability and better solubility but suffers from drawback of hydrophilic nature. The synthesis of starch nanoparticles (StNPs) reported by Dufresne et al. [6] paved the way for the development of novel nanosized starch derivatives which can offer great potential for use in diverse medicinal applications. The evaluation of the *in vitro* cytotoxicity of a biomaterial is the initial step of biocompatibility study. Hence we investigated the cytotoxic potential of hydrophobic, nanosized, starch derivatives for two different applications viz. potential anticancer agents and promising biocompatible drug carriers. In the past our group has extensively studied the cytotoxicity evaluation of metal nanoparticles [4,7] as well as starch metal nanoconjugates [8] with prokaryotic as well as eukaryotic cells. In this paper we have reported the interesting interaction of nanosized acyl derivatives of starch with A549

human lung carcinoma cells as well as mouse embryonic fibroblast (3T3L1) cells and CT-DNA.

2. Experimental

Starch nanocrystals (StNPs) were prepared according to the procedure described elsewhere [6]. Acylation of StNPs was carried out by dispersion in aqueous alkali followed by room temperature reaction with various acid chloride or anhydride [9]. Attempts were made to carry out the synthesis under ambient conditions so as to preserve the nanosize. Four type of derivatives were synthesized viz. St-palmitate, St-benzoate, St-phthalate and St-cinnamate. The product was collected by centrifugation and purified (Supporting information).

3. Results and discussion

The acylation was confirmed by spectroscopic analysis. The characteristic peaks in the FT-IR spectra (Supporting information) of all the starch nanoparticles are the stretching and bending vibrations of hydrogen bonded –OH groups observed at 3400 and 1650 cm⁻¹. The FT-IR spectra after acylation, showed a carbonyl absorption band at 1736, 1740, 1742 and 1750 cm⁻¹ for palmitate, benzoate, cinnamate and phthalate starch nanoparticles respectively. In case of aromatic derivatives the peaks due to stretching and bending of aromatic –C–H appear around 3000 and 800 cm⁻¹ respectively.

The ¹H NMR data of the starch nanoparticles is given below.

* Corresponding author. Fax: +91 0265 2581102.

E-mail address: chemistry2797@yahoo.com (S. Thakore).



Synthesis, spectroscopic characterization and DNA nuclease activity of Cu(II) complexes derived from pyrazolone based NSO-donor Schiff base ligands

Komal M. Vyas^a, Rushikesh G. Joshi^b, R.N. Jadeja^{a,*}, C. Ratna Prabha^b, Vivek K. Gupta^c

^a Department of Chemistry, Faculty of Science, The M.S. University of Baroda, Vadodara 390002, India

^b Department of Biochemistry, Faculty of Science, The M.S. University of Baroda, Vadodara 390002, India

^c Post-Graduate Department of Physics, Jammu University, Jammuwat 180006, India

ARTICLE INFO

Article history:

Received 12 July 2011

Received in revised form 2 September 2011

Accepted 14 September 2011

Keywords:

Schiff base ligands

Crystal structure

Cu(II) complexes

DNA binding

DNA cleavage

ABSTRACT

Two neutral mononuclear Cu(II) complexes have been prepared in EtOH using Schiff bases derived from 4-toluoyl pyrazolone and thiosemicarbazide. Both the ligands have been characterized on the basis of elemental analysis, IR, ¹H NMR, ¹³C NMR and mass spectral data. The molecular geometry of one of these ligands has been determined by single crystal X-ray study. It reveals that these ligands exist in amine-one tautomeric form in the solid state. Microanalytical data, Cu-estimation, molar conductivity, magnetic measurements, IR, UV–Visible, FAB–Mass, TG–DTA data and ESR spectral studies were used to confirm the structures of the complexes. Electronic absorption and IR spectra of the complexes suggest a square-planar geometry around the central metal ion. The interaction of complexes with pET30a plasmid DNA was investigated by spectroscopic measurements. Results suggest that the copper complexes bind to DNA via an intercalative mode and can quench the fluorescence intensity of EB bound to DNA. The interaction between the complexes and DNA has also been investigated by agarose gel electrophoresis, interestingly, we found that the copper(II) complexes can cleave circular plasmid DNA to nicked and linear forms.

© 2011 Elsevier B.V. All rights reserved.

1. Introduction

Biomaterial science has expanded rapidly in the past few decades, nurtured by bioengineers in the field of basic and medical professionals. Coordination chemists are also contributing to the development of biomaterials [1] and biomaterial science. The biological activities have made synthesis of the pyrazolone ring system attractive over the years. Synthesis of pyrazolone provides many compounds with various biological activities, therefore, the molecular design and synthesis of novel pyrazolone derivatives is still an active research area. Recent years have witnessed a great deal of interest in the synthesis and characterization of transition metal chelates of pyrazolone derivatives.

Schiff bases of thiosemicarbazones with 4-acyl pyrazolone have aroused with significant interest in the field of chemistry and biology due to their different biological activities [2]. The biological activities of thiosemicarbazones are considered to be related to their ability to form chelates with metals. The biological activities of metal complexes differ from those of either the free ligands or the metal ions and increased or decreased activities in relation to the

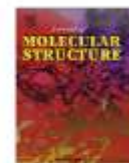
non-complexed thiosemicarbazones have been reported for several transition metal complexes [3].

Coordination metal complexes are gaining increasing importance in recent years particularly in the design of repository, slow release long acting drugs in nutrition and in the study of metabolism. A number of metal chelates are of current interest due to their important applications in nucleic acid chemistry as DNA probes of DNA structure in solutions, reagents for the mediation of strand scission of duplex DNA under physicochemical conditions, and as chemotherapeutic agents and in the genomic research [4]. The interaction between DNA and transition metal complexes is an important fundamental issue in life sciences. These complexes can bind to DNA in non covalent modes such as electrostatic, intercalative, and groove binding. The above applications require that the complex binds to DNA through an intercalative mode wherein the planar aromatic heterocyclic group is inserted and stacked between the base pairs of DNA [5], which is related to the *in vivo* replication and transcription of DNA, mutation of genes, variations of species in their character, and to the action mechanism of some synthetic chemical nucleases [4].

Deoxyribonucleic acid (DNA) is the primary target molecule for most anticancer and antiviral therapies according to cell biology [6]. Investigations of the interactions of DNA with transition metal complexes containing multidentate ligands are basic work to design new types of the pharmaceutical molecules, to elucidate

* Corresponding author. Tel.: +91 265 2795552.

E-mail address: rajendra.jadeja@yahoo.com (R.N. Jadeja).



Synthesis and crystal structure of a series of pyrazolone based Schiff base ligands and DNA binding studies of their copper complexes

R.N. Jadeja^{a,*}, Sanjay Parihar^a, Komal Vyas^a, Vivek K. Gupta^b

^aDepartment of Chemistry, Faculty of Science, The M.S. University of Baroda, Vadodra 390 002, India

^bDepartment of Physics, University of Jammu, Jammu Tawi 180 006, India

ARTICLE INFO

Article history:
Received 22 November 2011
Accepted 6 January 2012
Available online 28 January 2012

Keywords:
Schiff base
Pyrazolone
Crystal structure
DNA binding
Cu(II) complex

ABSTRACT

PMP (5-methyl-4-(4-methyl-benzoyl)-2-phenyl-2,4-dihydro-pyrazol-3-one), PTPMP (5-methyl-4-(4-methyl-benzoyl)-2-p-tolyl-2,4-dihydro-pyrazol-3-one) and MCPMP (2-(3-Chloro-phenyl)-5-methyl-4-(4-methyl-benzoyl)-2,4-dihydro-pyrazol-3-one) were synthesized and used for the synthesis of Schiff base ligands. Schiff base ligands were characterized by FT-IR, ¹H NMR, Mass and single crystal X-ray analysis. Cu(II) complexes of synthesized ligands were prepared and characterized by elemental analysis, FT-IR, TGA-DTA, UV-Visible, ESI mass and ESR spectroscopy. On the basis of analytical and spectroscopic techniques, distorted octahedral geometry of the complexes was proposed. The interaction of Cu(II) complexes with CT-DNA was investigated by Absorption titration, Viscosity and fluorescence spectroscopy. Results suggest that the synthesized complexes bind to DNA via an intercalative mode and can quench the fluorescence intensity of EB bound to DNA.

© 2012 Elsevier B.V. All rights reserved.

1. Introduction

Pyrazolone and its derivatives form an important class of compounds and have attracted considerable scientific and applied interest. Pyrazolones especially, Acylpyrazolones are an interesting class of β -diketone compounds which are widely used as solvent extractions of metal ions, laser working materials and NMR shift-reagents [1–3]. The 4-acyl-pyrazolone derivatives are broadly used in many fields, especially in biological, clinical and analytical applications [4–7].

The interest in the coordination chemistry of pyrazolones has increased greatly in the last decade [8]. Due to the presence of two oxygen donor atoms and facile keto–enol tautomerism, they easily coordinate with metal ions after deprotonation of the enolic hydrogen and provide stable metal complexes with six-membered chelate rings. Pyrazolones are used in analytical chemistry for the determination and isolation of almost all metal ions due to their high extracting ability, intense color of the complex extracts and low solubility of the complex in some solvents [9].

The well-known Cu(II) ion forms a series of coordination compounds with well defined structures. It plays an important role in the numerous biological processes that involve electron transfer reactions or the activation of some anti-tumor substances [10]. In addition, 4-acyl pyrazolones can form a variety of Schiff bases and are reported to be superior reagents in biological, clinical

and analytical applications [11,12]. Investigations on copper complexes to probe nucleic acids are becoming more prominent in the research area of bioinorganic chemistry [13–15]. Studies pertaining to DNA cleavage by synthetic reagents are of considerable interest because of their utility tools in molecular biology. This has resulted in the development of both sequence specific DNA cleavers [16] and DNA foot printing agents [17].

In our previous work, a series of Schiff base of 4-acylpyrazolone derivatives and their transition metal complexes have been reported [18,19]. In this paper, our group has focused much on synthesizing new Schiff bases of 4-acyl pyrazolone derivatives (see Scheme 1), studying on their crystal structures, synthesis of their transition metal complexes and also studying their DNA binding activities. In this present paper we are reporting the binding studies of Cu(II) complexes with CT-DNA by UV-Visible, fluorescence spectroscopy and viscosity measurements.

2. Experimental

2.1. Materials and physical measurements

All reagents and solvents were purchased from commercial sources and were further purified by the standard methods, if necessary [20]. Pyrazolones were obtained from Nutan Dye Chem. Sachin, Surat. Copper acetate and naphthylamine were purchased from Loba Chem., Mumbai. Disodium salt of calf thymus DNA (highly polymerized), purchased from Sigma, was stored at 4 °C and used as received. The stock solution of DNA was prepared by

* Corresponding author. Tel.: +91 265 2795552.

E-mail address: rajendra_jadeja@yahoo.com (R.N. Jadeja).



Synthesis, characterization and crystal structure of some bidentate heterocyclic Schiff base ligands of 4-toluoyl pyrazolones and its mononuclear Cu(II) complexes

Komal M. Vyas^a, R.N. Jadeja^{a,*}, Vivek K. Gupta^b, K.R. Surati^c

^aDepartment of Chemistry, Faculty of Science, The MS University of Baroda, Vadodra 390 002, India

^bDepartment of Physics, Jammu University, Jammutawi 180 006, India

^cDepartment of Chemistry, Sardar Patel University, Vallabhvidyanagar 388 120, India

ARTICLE INFO

Article history:

Received 1 December 2010

Received in revised form 1 January 2011

Accepted 3 January 2011

Available online 22 January 2011

Keywords:

Bidentate Schiff base ligands

Cu(II) complexes

Acyl pyrazolone

Crystal structures

ABSTRACT

We depict the synthesis of a new set of six bidentate heterocyclic Schiff base ligands, formed by the condensation of three different 4-toluoyl pyrazolones with various aromatic amines in ethanolic medium. All of these ligands have been characterized on the basis of elemental analysis, IR, ¹H NMR, ¹³C NMR and Mass spectral data. The molecular geometries of three of these ligands have been determined by single crystal X-ray study. It reveals that these ligands exist in amine-one tautomeric form in the solid state. The reaction of these ligands with copper(II) resulted in the formation of mononuclear complexes having the general composition [CuL₂(H₂O)₂] with two water molecules at axial positions. These complexes have been characterized on the basis of elemental analysis, Cu-estimation, molar conductivity, magnetic measurements, IR, UV-Visible, FAB-Mass, TG-DTA-DSC data, cyclic voltametric measurements and ESR spectral studies. ESR spectra and magnetic susceptibility measurements indicates distorted octahedral stereochemistry of Cu(II) complexes, while non-electrolytic behaviour of complexes indicates the absence of counter ion.

© 2011 Elsevier B.V. All rights reserved.

1. Introduction

The design of new coordination supramolecules and polymers based on transition metal compounds and multidentate organic ligands has attracted much interest in recent years [1]. Current interest in the coordination chemistry of β-diketones toward several metal ions [2] particularly in the development of the relatively new class of 4-acyl, 5-pyrazolones [3], having a pyrazole ring fused to a chelating carbonyl, has emerged from several points of view.

Acylation is one of the fundamental reactions in organic chemistry and can be carried out by wide variety of reagents. Pyrazolone-5 derivatives, especially 4-acyl pyrazolone form an important class of organic compounds and their derivatives represent a big scientific and applied interest in analytical applications, catalysis, dye and extraction metallurgy, etc. [4–6] because they display several different coordination modes, with respect to classical β-diketone. Furthermore, 4-acyl pyrazolone derivatives have the potential to form different types of coordination compounds due to the several electron-rich donor centers [7,8] and tautomeric effect of the enol form and keto form [9]. Complexes containing these ligands are known for almost every transition and main group metal [10]. Dependent on the nature of the metal and the coordination behaviour of the ligand

one can develop synthetic strategies to influence the one, two or three-dimensional arrangement in the crystal in a more directed way [11].

They are also known to show extensive solid state tautomerism and the insertion of substituents with special conjugated system to them leads to formation of compounds with intense stable colour [12]. Schiff bases are important ligands in coordination chemistry and find extensive application in different fields [13]. Among them, the Schiff base derivatives of 1-phenyl 3-methyl 5-pyrazolone and their metal complexes have been widely studied because of the high pharmaceutical activities [14].

As a part of our continuing interest in pyrazolones chemistry, we synthesized a number of such compounds [15–18]. Now we report on the successful synthesis of a series of Cu(II) complexes containing pyrazolone based Schiff base ligands.

2. Experimental

2.1. Materials

The compounds 5-methyl-2-phenyl-2, 4-dihydro-pyrazol-3-one; 5-methyl-2-m-tolyl-2,4-dihydro-pyrazol-3-one and 2-(3-chloro-phenyl)-5-methyl-2,4-dihydro-pyrazol-3-one were obtained from Nutan Dye Chem Pvt. Ltd., Sachin, Surat and were used after recrystallization. Para toluidine, para bromo aniline and dioxane were obtained from

* Corresponding author. Tel.: +91 265 2795552.

E-mail address: rajendra_jadeja@yahoo.com (R.N. Jadeja).

Synthesis and characterization of Ni(II) complexes of O,N-donor Schiff bases derived from acyl pyrazolone analogues

KOMAL M. VYAS, VRUNDA K. SHAH and R.N. JADEJA*

Department of Chemistry, Faculty of Science, The Maharaja Sayajirao University of Baroda, Vadodara-390 002, Gujarat, India

(Received 19 July 2010; in final form 23 December 2010)

Two bidentate Schiff bases, 5-methyl-2-*p*-tolyl-4-(1-*p*-tolylimino-propyl)-2H-pyrazol-3-ol (L1) and 2-(3-chloro-phenyl)-5-methyl-4-(1-*p*-tolylimino-propyl)-2H-pyrazol-3-ol (L2), were synthesized by condensation of 4-acyl pyrazolones with *p*-toluidine in ethanol. These ligands have been characterized by elemental analysis, infrared (IR), ¹H NMR, and mass spectra. A single crystal molecular structure of ligand L2 was also solved. Nickel(II) complexes of these ligands with general formula [ML₂·2H₂O] have been prepared by the interaction of aqueous solution of Ni-acetate with ethanolic solution of the appropriate ligand. The complexes were separated, analyzed, and their structures were elucidated on the basis of elemental analysis, Ni(II) determination, IR, UV-Vis, conductance, mass, and TGA-DTA data. Octahedral structure was proposed for the synthesized complexes.

Keywords: Acyl pyrazolone; Schiff bases; Ni(II) complexes; Pyrazolone derivatives

1. Introduction

Pyrazolones have been extensively studied due to their properties and applications. Pyrazolone sometimes refers to nonsteroidal anti-inflammatory agents. Pyrazolone derivatives, such as lactam-structure-related compounds, are also widely used in preparing dyes and pigments [1]. Acylated derivatives of pyrazolones (acyl pyrazolones), as heterocyclic β-diketones, have special characteristics such as extractability, colors suitable for photometric analyses, and intense biological activity [2]. These compounds display the majority of their properties as ligands in transition metal complexes. They are active as a pharmaceutical ingredient, especially in nonsteroidal anti-inflammatory agents used in the treatment of arthritis and other musculoskeletal and joint disorders. There are a number of reports in which the acyl pyrazolones bind with various metal ions resulting in structurally interesting coordination compounds [3, 4].

The chemistry of Schiff-base derivatives of 4-acylpyrazolones are less explored, even though these ligands also show appealing complexation properties [5–8]. Furthermore, Schiff-base formation extends the scope of the classical β-diketone

*Corresponding author. Email: rajendra_jadeja@yahoo.com

Synthesis and spectral characterization of Cu(II) complexes of some thio-Schiff bases of acyl pyrazolone analogues

RAVINDRA J. YADAV, KOMAL M. VYAS and R.N. JADEJA*

Department of Chemistry, Faculty of Science, The Maharaja Sayajirao University of Baroda, Vadodara – 390002, Gujarat, India

(Received 22 April 2009; in final form 3 February 2010)

A series of tridentate pyrazolone-based thio-Schiff bases were synthesized by the interaction of 4-acyl/aroyle pyrazolones with thiosemicarbazide in an ethanolic medium. All of these ligands were characterized on the basis of elemental analysis, infrared (IR), ¹H- and ¹³C-NMR data. Nuclear magnetic resonance (NMR) suggests the amine-one form of ligand in solution at room temperature. Copper Schiff-base complexes, [Cu(L)(H₂O)], have been prepared by the interaction of the aqueous solution of copper sulfate pentahydrate with hot ethanolic solution of the appropriate ligand. The resulting complexes have been characterized by elemental analysis, metal content determination, molar conductance, fast atom bombardment mass spectra, magnetic measurements, thermogravimetric analysis (TGA), IR, and electronic spectral studies. Thermal stability, heat capacity, and activation energy of thermal degradation for these complexes were determined by TGA, differential thermal analysis, and differential scanning calorimetry. Suitable structures are proposed for these complexes.

Keywords: Acyl pyrazolone; Copper complexes; Thio-Schiff base; Thiosemicarbazone

1. Introduction

The interest in sulfur donor chelating agents has grown very rapidly. Most of the early investigations on these systems were centered on their use as analytical reagents. Interest in complexes of these ligands now covers a full gamut of areas ranging from general metal–sulfur bonding and electron delocalization in transition metal complexes to potential biological activity and practical application in fields as diverse as rubber technology and agriculture. Complexes of transition metals containing ligands with N, S or N, S, and O donors are known to exhibit interesting stereochemical, electrochemical, and electronic properties [1, 2]. Derivatives of semicarbazones and thiosemicarbazones are among the most widely studied nitrogen and oxygen/sulfur donors [3, 4]. Particularly, thiosemicarbazones have emerged as an important class of sulfur ligand for transition metal ions. The real impetus toward developing their coordination chemistry was their physicochemical properties and significant biological activities [5, 6]. Compounds containing a thiosemicarbazone component have shown broad spectrum chemotherapeutic properties, including antimalarial [7],

*Corresponding author. Email: rajendra_jadeja@yahoo.com



SYNTHESIS & CHARACTERIZATION OF Cu(II) COMPLEXES DERIVED FROM ACYL PYRAZOLONE & 2-AMINO PHENOL

N. P. Moorjani, K. M. Vyas and R. N. Jadeja*

Department of Chemistry, Faculty of Science, The Maharaja Sayajirao University of Baroda,
Vadodra-390 002, Gujarat, India

ABSTRACT

A series of tridentate pyrazolone-based Schiff bases were synthesized by the interaction of 4-acyl/aroyl pyrazolones with 2-Amino Phenol in an ethanolic medium. All of these ligands were characterized on the basis of elemental analysis, infrared (IR) and ¹H-NMR data. Nuclear magnetic resonance (NMR) suggests the amine-one form of ligand in solution at room temperature. Copper Schiff-base complexes [Cu₂(L)₂], have been prepared by the interaction of the aqueous solution of copper acetate monohydrate with hot ethanolic solution of the appropriate ligand. The resulting complexes have been characterized by elemental analysis, metal content determination, molar conductance, fast atom bombardment mass spectra, magnetic measurements, thermogravimetric analysis (TGA), IR and electronic spectral studies. Suitable square planar structure is proposed for these complexes.

Key words: Acyl pyrazolones, Copper complexes, Schiff bases, Spectral studies

INTRODUCTION

The chemistry of pyrazolone derivatives has attracted much attention because of their interesting structural properties and applications in diverse areas [1-4]. They are useful reagents for the extraction and separation of various metal ions [5, 6]. They can also be used in laser materials, as ¹H NMR shift reagents, in chromatographic study and in the petrochemical industry [7, 8]. Many of these ligands exhibit keto enol tautomerism and because of this they show interesting structural and spectroscopic properties which have been the subject matter of many reports [9]. β-diketones have played and continue to play a key role in coordination compounds that have found wide application in several fields, from new materials to catalysts [10], as precursors for CVD in the microelectronic industry and as potential antitumourals [11]. Even the simplest pyrazolone-5 derivatives for instance, antipyrine and amidopyrine are well-known analgesics and widely used in medicine. Pyrazolone derivatives are also used as starting materials for the synthesis of biologically active compounds and for the construction of condensed heterocyclic systems [12]. Among these ligands, acyl pyrazolones have been studied extensively owing to their effective properties with respect to extracting metal ions [13]. On the other hand pyrazolone-based Schiff base chemistry is less extensive.

Pyrazolyl and pyrazolyl-derived ligands can form relevant coordination compounds with different metal ions. Copper complexes have been extensively studied, especially dinuclear and polynuclear species, as mimics of the proteins hemocyanin and tyrosinase or as compounds with interesting catalytic and magnetic properties [14]. In most of these complexes, copper ions are linked by N, N'-bridging pyrazolato anions, or coordinated by one nitrogen atom of the pyrazole ring. However, recently an unusual coordination mode of this type of ligand was described, where nitrogen atoms of the pyrazole rings are not bound to copper, but involved in strong intramolecular hydrogen bonds.

Recently, some Schiff bases from 3-methyl-1-(4'-methylphenyl)-2-pyrazoline-5-one and aromatic amines were

prepared and their molecular structures were determined. These ligands can exist in three tautomeric forms: keto-imine, imine-ol and keto-amine, although the ketoamine form is predominant in the solid state. Their corresponding mononuclear copper(II) complexes were also prepared and characterized by spectroscopic techniques, indicating a tetragonal geometry around the copper(II) ion, N,O coordinated [15].

We were interested to synthesis a new series of pyrazolone-based Schiff base ligands, which can form stable neutral complexes with Cu(II) metal ions and may find some application in solvent extraction chemistry. With this view we have synthesized a series of ligands by condensation of acyl pyrazolones with 2-amino phenol. The reaction of these ligands in alcoholic medium with copper acetate resulted the novel square planar complexes, which were then characterized by various spectral techniques.

MATERIALS AND METHODS

All the chemicals used in the present study were of best quality. Dioxane was obtained from Sisco Chem. Pvt Ltd, Mumbai and used after purification. Calcium hydroxide and acetyl chlorides were supplied by Suvidhinath Labs, Baroda. 2-aminophenol was obtained from LOBA Chem. Pvt. Ltd., Mumbai. Ethanol was obtained from Baroda Chemicals Industry Ltd., Baroda and Benzoyl chloride was obtained from Gayatri Mineral and Chemicals, Baroda. In preparation of metal complexes of Cu(II), copper acetate was used.

Physical measurements

Elemental analyses (C, H, and N) were performed on a model 2400 Perkin-Elmer elemental analyzer. Infrared (IR) spectra were recorded on a Perkin Elmer FT-IR spectrum RX 1 spectrometer as KBr pellets. NMR was recorded on a model 400 Bruker FT NMR. The electronic spectra were recorded on a model Perkin Elmer Lambda 35 UV-VIS spectrometer. A simultaneous TG/DTA was recorded on EXSTAR6000 TG/DTA6300 model. A FAB mass spectrum was recorded on a Jeol SX 102/Da-600 mass spectrometer at room temperature using m-nitro benzyl alcohol as a matrix and Argon/Xenon as the FAB gas. Specific conductivity of the complexes was

*Corresponding author: rajendra_jadeja@yahoo.com

PARTICIPATION IN SEMINARS/CONFERENCES

- 1) "Synthesis and Characterization of Ni(II) complexes of some O, N donor Schiff bases" presented at the "Sixth All Gujarat Research Scholars Meet" held at the Dept. of Chemistry, M. S. University of Baroda on January 31, 2010.
- 2) National Symposium on Emerging Horizons in Catalysis held at Department of Chemistry, Baroda Chapter during September 25-26, 2009.
- 3) National Workshop on Radiochemistry and Applications of Radioisotopes held at the Department of Chemistry, M. S. University of Baroda during January 4-12, 2010.
- 4) A 5 Day School of Bioinorganic Chemistry held at the Department of Chemistry, M. S. University of Baroda during March 8-12, 2010.
- 5) National Conference on Chirality 2011 held at the Department of Chemistry, M. S. University of Baroda during December 2-3, 2010.
- 6) One Day Seminar on Innovations in Collegiate Science Education and Research held at VP & RPTP Science College, V. V. Nagar on January 8, 2011.
- 7) "*Schiff bases derived from acylpyrazolone and DNA nuclease of their copper complexes*" presented at National Conference on Chemical Sciences in New Millennium held at the Department of Chemistry, Pacific College of Basic & Applied Sciences, Pacific University, Udaipur on 8th January 2012.
- 8) "*Synthesis, characterization, crystal structure, DNA interaction and DNA cleavage activities of copper(II) thiocyanato complex with 4-tolouyl pyrazolone and phenanthroline base*" presented at the XXVI Gujarat Science

Congress 2012 held at the Department of Chemistry, M. S. University of Baroda, Vadodara on February 26, 2012.

- 9) *“Novel efficient anti-cancer ternary Cu(II) complex containing pyrazolone based thiosemicarbazone and polypyridyl ligands: Synthesis, characterization, crystal structure, DNA binding, protein binding and anti-cancer activity towards A549 human lung carcinoma cells”* presented at the Regional Science Congress 2012 held at the Department of Chemistry M. S. University of Baroda, Vadodara on September 15-16, 2012.